

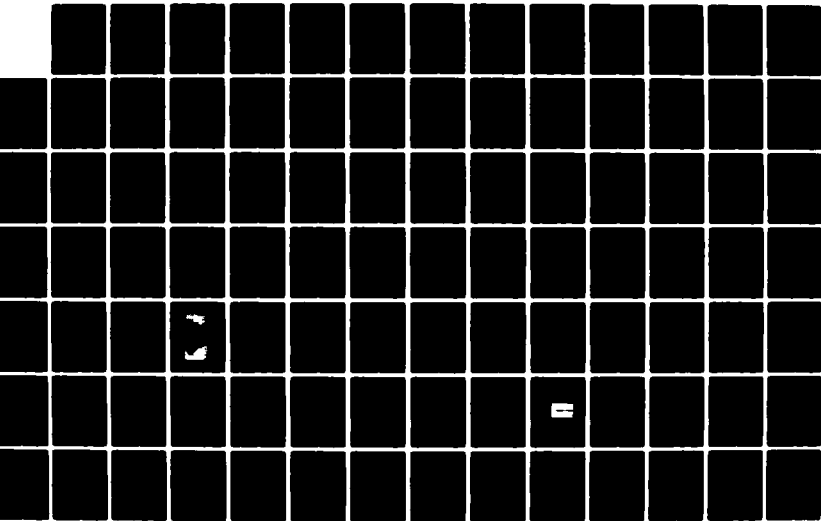
AD-A132 688 WORKSHOP ON REPETITIVE SPARK GAP OPERATION HELD AT  
TAMARRON COLORADO ON JANUARY 17-19 1983(U) BATTELLE  
COLUMBUS LABS DURHAM NC M O HAGLER ET AL. 20 MAY 83

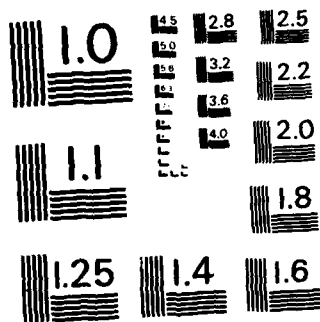
UNCLASSIFIED

F/G 9/1

1/4

NL





MICROCOPY RESOLUTION TEST CHART  
NATIONAL BUREAU OF STANDARDS - 1963 - A

(0)

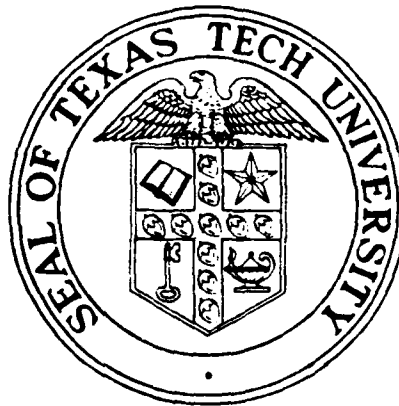
WORKSHOP  
ON

# REPETITIVE SPARK GAP OPERATION

(January 17-19, 1983)

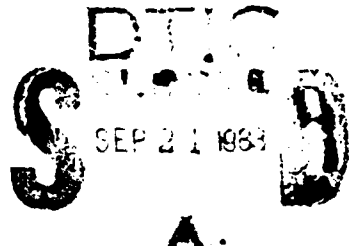
M. O. Hagler and M. Kristiansen  
Workshop Co-Chairmen

A/32688



Sponsored by  
Battelle Columbus Laboratories

May 20, 1983



DTIC FILE COPY

PLASMA AND SWITCHING LABORATORY  
LASER LABORATORY

Department of Electrical Engineering  
TEXAS TECH UNIVERSITY

Lubbock, Texas 79409

83 09 20 173

This document has been approved  
for public release and sale; its  
distribution is unlimited.

Unclassified

SECURITY CLASSIFICATION OF THIS PAGE (When Data Entered)

REPORT DOCUMENTATION PAGE			READ INSTRUCTIONS BEFORE COMPLETING FORM
1. REPORT NUMBER	2. GOVT ACQUISITION NO.	3. RECIPIENT'S CATALOG NUMBER	A132688
4. TITLE (and Subtitle)  Workshop on Repetitive Spark Gap Operation	5. TYPE OF REPORT & PERIOD COVERED  Final		
7. AUTHOR(s)  M. O. Hagler (Workshop Co-Chairmen) M. Kristiansen	8. CONTRACT OR GRANT NUMBER(s)  DAAG29 81 D 0100		
9. PERFORMING ORGANIZATION NAME AND ADDRESS  Texas Tech University Lubbock, TX 79409	10. PROGRAM ELEMENT, PROJECT, TASK AREA & WORK UNIT NUMBERS		
11. CONTROLLING OFFICE NAME AND ADDRESS  U. S. Army Research Office Post Office Box 12211 Research Triangle Park, NC 27709	12. REPORT DATE  May 20, 1983		
14. MONITORING AGENCY NAME & ADDRESS (if different from Controlling Office)	13. NUMBER OF PAGES  363		
15. SECURITY CLASS. (of this report)  Unclassified			
16. DISTRIBUTION STATEMENT (of this Report)  Approved for public release; distribution unlimited.			
RE: Copyright -- DTIC and NTIS HAS PERMISSION TO REPRODUCE AND SELL THIS REPORT			
17. DISTRIBUTION STATEMENT (of the abstract entered in Block 20, if different from Report)  <i>B. D. Guenther</i>			
18. SUPPLEMENTARY NOTES  The view, opinions, and/or findings contained in this report are those of the author(s) and should not be construed as an official Department of the Army position, policy, or decision, unless so designated by other documentation			
19. KEY WORDS (Continue on reverse side if necessary and identify by block number)			
20. ABSTRACT (Continue on reverse side if necessary and identify by block number)  A workshop on Repetitive Spark Gap Operation was conducted by Texas Tech University for the Department of Defense. The workshop objectives were to summarize the present state-of-the-art and knowledge about repetitive spark gap operation and to make recommendations about needed research in this important pulsed power area. A group of invited papers provided background information for the participants who were experts in various important scientific and engineering subdisciplines but who did not necessarily have any direct experience with spark gaps. The workshop participants were divided into various working groups which provided summary			

FILE COPY

UNCLASSIFIED

SECURITY CLASSIFICATION OF THIS PAGE(When Data Entered)

Abstract cont.

reports about their deliberations and recommendations. These papers and group reports are included in this report together with a summary of the workshop recommendations.

UNCLASSIFIED

SECURITY CLASSIFICATION OF THIS PAGE(When Data Entered)

Scientific Services Program  
U.S. Army Research Office\*

Final Report on  
WORKSHOP ON REPETITIVE SPARK GAP OPERATION

Sponsored by  
Battelle Columbus Laboratories  
Delivery Order No 0441  
200 Park Drive  
P.O. Box 12297  
Research Triangle Park, NC 79409

Conducted by  
Plasma and Switching Laboratory  
Department of Electrical Engineering  
Texas Tech University  
Lubbock, Texas 79409

at  
Tamarron, Colorado  
January 17-19, 1983

Submitted by  
M.O. Hagler                            M. Kristiansen  
Workshop Co-Chairman                 Workshop Co-Chairman

May 20, 1983

The views, opinions, and/or findings contained in this report are those of the author(s) and should not be construed as an official Department of Defense position, policy, or decision, unless so designated by other documentation.

---

\* Support from the Air Force Office of Scientific Research and the Naval Surface Weapons Center is also acknowledged.

## TABLE OF CONTENTS

I.	Workshop Advisory Board.....	iii
II.	Abstract.....	1
III.	Working Groups.....	2
IV.	Introduction.....	6
V.	Workshop Summary.....	12
VI.	Invited Background Papers.....	18
	1. An Introduction to Gas Filled Spark Gaps..... (M. Kristiansen)	19
	2. Electrode Processes in High Intensity Arcs..... (E. Pfender)	36
	3. Survey of Gas Flow and Heat Transfer Effects on Performance of Gas Spark Gaps..... (J. Kuhlman)	85
	4. Surface Phenomena in Spark Gaps..... (L. Murr)	154
VIII.	Group Reports.....	216
	1. Thermal and Gas Dynamic Effects..... (M. Molen)	217
	2. Engineering Implications..... (M. Buttram)	263
	3. Materials and Chemistry..... (L. Hatfield)	283
	4. Electrical Characteristics and Breakdown Processes..... (J. Proud)	302
VIII.	Appendices.....	336
	A. Summary of the Capabilities of Repetitive Spark Gap Switches..... (I. Smith, T. Burkes, A. Guenther, M. Kristiansen, G. Lauer, and W. Portnoy)	337
	B. List of Participants.....	358

## WORKSHOP ADVISORY BOARD

M. Hagler	Texas Tech University (Co-Chairman)
M. Kristiansen	Texas Tech University (Co-Chairman)
M. Buttram	Sandia National Laboratories
A. Guenther	Air Force Weapons Laboratory
A. Hyder	Auburn University
M. Molen	Old Dominion University
J. Naff	Physics International Company
W. Nunnally	Los Alamos National Laboratory
J. Proud	GTE Laboratories
A. Ramrus	Maxwell Laboratories, Inc.
F. Rose	Naval Surface Weapons Center
J. Thompson	University of South Carolina

## EX-OFFICIO MEMBERS OF ADVISORY BOARD

B. Guenther	Army Research Office
L. Luessen	Naval Surface Weapons Center
H. Pugh	Air Force Office of Scientific Research

REF ID: A6544

Accession For	
NTIS GRA&I	
P&IC TAB	
Undisseminated	
Justification	
By	
Distribution/	
Availability Codes	
Avail and/or	
Dist	Special
A	

**ABSTRACT**

A workshop on Repetitive Spark Gap Operation was conducted by Texas Tech University for the Department of Defense. The workshop objectives were to summarize the present state-of-the-art and knowledge about repetitive spark gap operation and to make recommendations about needed research in this important pulsed power area. A group of invited papers provided background information for the participants who were experts in various important scientific and engineering subdisciplines but who did not necessarily have any direct experience with spark gaps. The workshop participants were divided into various working groups which provided summary reports about their deliberations and recommendations. These papers and group reports are included in this report together with a summary of the workshop recommendations.

## WORKING GROUPS

1. Thermal Group

Marshall Molen (Chairman)	Old Dominion University
Herbert Carper (Co-chairman)	Texas Tech University
Tommy Burkes	T.R. Burkes, Inc.
Stanley Byron	Mathematical Sciences N.W., Inc.
Marion Hagler	Texas Tech University
John Kuhlman	Old Dominion Universtiy
William Moeny	Tetra Corporation
Gerald Rohwein	Sandia National Laboratories
Karl Schoenbach	Texas Tech University
Bill Wright	U.S. Army ERADCOM

2. Engineering Implications Group

Malcolm Buttram (Chairman)	Sandia National Laboratories
Barry Ballard	Foreign Technology Division Wright-Patterson Air Force Base
Art Guenther	Air Force Weapons Laboratory
A. Hyder	Auburn University
M. Kristiansen	Texas Tech University
Larry Luessen	Naval Surface Weapons Center
H.G. Hammond	Physics International
Henry Pugh	Air Force Office of Scientific Research
Ian Smith	Pulsed Sciences, Inc.
Jim Thompson	University of South Carolina
Larry Turner	U.S. Army Foreign Science & Technology Center

3. Materials and Chemistry

Lynn Hatfield (Chairman)	Texas Tech University
Lloyd Gordon (Co-chairman)	Lawrence Livermore National Laboratory
Fred Biondi	University of Pittsburgh
Lucas Christophorou	Oak Ridge National Laboratory
J. Ewing	Mathematical Sciences N.W., Inc.
John Gustafson	GTE Laboratories, Inc.
Erich Kunhardt	Texas Tech University
John Marx	Texas Tech University
James Mote	University of Denver
Larry Murr	Oregon Graduate Center
Emil Pfender	University of Minnesota
Paul Predecki	University of Denver

**4. Electrical Characteristics and Breakdown Processes**

Joe Proud (Chairman)	GTE Laboratories
Ron Gripshover (Co-chairman)	Naval Surface Weapons Center
Norman Bardsley	University of Pittsburgh
Robert DeWitt	Naval Surface Weapons Center
Anthony Donaldson	Texas Tech University
David Fenneman	Naval Surface Weapons Center
Karl Freytag	Lawrence Livermore National Laboratory
Alan Hill	Plasmtronics
Bob Junker	Office of Naval Research
Gene Lauer	Lawrence Livermore National Laboratory
William Nunnally	Los Alamos National Laboratory
Gerhard Schaefer	Texas Tech University
Frazer Williams	Texas Tech University

## INTRODUCTION

A workshop on "Repetitive Spark Gap Operation" was conducted for the Department of Defense (Army Research Office, Air Force Office of Scientific Research, and Naval Surface Weapons Center/Dahlgren Laboratory) by Texas Tech University at Tamarron, Colorado on January 17-19, 1983. The workshop objectives were to summarize the present state-of-the art and knowledge concerning repetitive spark gap operation and to make recommendations about the most critical research issues in this important pulsed power, research area. The workshop was the fourth in a series held over the past three years to study key issues relating to high average power switching.

Spark gaps have been the "work horses" of pulsed power switching and in many parameter ranges they have no peers. This is especially true for single shot, high peak power, operation. Many recent application interests, however, are related to high average power repetitive switching operation. In the past, spark gap work has been largely empirical in nature and there has been relatively little physical understanding or sound engineering design tools upon which to base extrapolations of current practices to the rep-rated operating regimes of interest.

The situation is further complicated by its extremely diverse nature - involving physics, chemistry, and several engineering disciplines. Numerous national, university, and industrial laboratories have worked on developing or studying the properties of long life, reliable (low jitter and prefire),

repetitive spark gaps over the past several years. It was, therefore, judged important and timely to bring together representatives from the main research groups in this field as well as experts from the various key subdisciplines needed for making significant spark gap advances. Researchers with backgrounds in pulsed power and spark gap research as well as those with expertise in plasma chemistry, arc and discharge physics, material science, heat transfer and fluid flow, etc., were, therefore, invited to attend the workshop. Representatives from various government agencies with potential interest in high power, repetitive switching were also invited in order to bring focus to realistic background scenarios and requirements.

The 44 invited participants came from universities, industry, national laboratories, and government agencies. A series of invited papers presented the first day provided background information and set the tone for the subsequent working group discussions. Each working group had an appointed discussion leader. The groups' conclusions and recommendations were presented in a plenary meeting on the last day. The Advisory Committee met the following day to further refine and integrate some of these conclusions.

A preliminary meeting, involving some 18 of the workshop participants, was held at Texas Tech University in September, 1982. That meeting defined many of the workshop goals and identified some of the important areas which needed to be covered. It also identified some of the people with backgrounds and expertise appropriate for contributing to the successful achievement of the workshop goals.

We, the workshop coordinators, feel that the workshop was most successful. The unusual amount of intense, scientific discussion resulted in significant information exchange. The participants seemed genuinely interested in the problems posed and many (certainly we) learned a great deal about an exciting, current and increasingly important problem. The workshop generated many new ideas for future work.

The main goals for the workshop were:

- 1) To identify the limitations of high power spark gaps with regard to repetition rate, lifetime, and reliability.
- 2) To identify the main, limiting, unresolved research problems and to define the basic research issues which must be supported in order to resolve these problems.
- 3) To establish avenues for exchange of information about this important research field.
- 4) To establish research goals.

The repetition rate question was addressed mainly by the working groups on thermal problems and engineering implications, while the lifetime and reliability questions were discussed primarily in the groups on materials and chemistry, and electrical characteristics and breakdown processes. There was considerable overlap between the groups and each group had "floating representatives" in the other groups to ensure that each group discussed the same general objectives and parameter ranges.

9

There are some fairly significant points of agreement to be found in the various group reports, evidently due to a clear consensus and understanding of the key issues involved rather than from a direct information exchange between the groups. Several references were made to possible competitive switch concepts, such as thyratrons, solid state switches, and magnetic switches. A small subgroup was, therefore, formed to summarize the capabilities of repetitive spark gaps in comparison with some of these other switch concepts. A report from this subgroup is enclosed as an Appendix to the main report.

The question of research issues and priorities centered, as expected, around gas flow and heat transfer, materials selections and compatibility, plasma chemistry, testing and evaluation criteria and methods, and electrical discharge characteristics. The fascinating topic of diffuse discharges (a topic of the second Tamarron workshop in 1982) was brought up as a possible approach to decreased electrode and insulator damage (increased life time) and to increased repetition rate. This topic was probably given too much attention (for this particular workshop) by the working group on electrical characteristics and breakdown processes since it was not considered in any great extent by the other working groups and hence was not scrutinized from a heat transfer and materials view point in the same way arc discharges were. It is clear, however, that successful development of high current density, diffuse discharges with low forward (conducting) voltage drop and high hold-off strength in the open (non-conducting) state is of extreme interest to both opening and closing switches, as well as to the area of gas discharge lasers.

The third goal of the workshop, that of establishing avenues of information exchange between researchers in the field was not achieved in any formal sense. Certainly there is a new awareness among the participants with regard to whom is doing what and where it is being done. Also, several of the participants established excellent working relationships for the future at several levels of formality, including joint proposal preparations. There was much talk in the informal gatherings in the afternoons and late at night about the need for a data bank and a central depository for spark gap data. Most of the participants appreciated the value of such a bank in view of the enormous parameter space under consideration. The general concensus, however, was that it would be extremely difficult, although not necessarily very expensive, to obtain long term support and commitments from any sponsoring agency for such an undertaking.

The questions of testing facilities and standardized testing methods were also raised. Most high power switch test data are user generated and focused on the specific users needs and interests. The need for a general testing facility with high power (~ 10 MW), high repetition rate (~ 10 kpps), and high voltage (~ 1 MV) capability was identified. Because of the associated diagnostics requirements, heat transfer capability, etc., such a facility is beyond the financial capability of most laboratories and most probably would require a multi-government agency undertaking. Discussions of such a facility and the required, standardized, testing procedures were somewhat outside the scope of the workshop and, therefore, not addressed in detail during the meeting.

The last workshop goal, that of setting research goals was, as usual, extremely difficult. The research topics listed in the next section are primarily due to the Workshop Co-Directors, with some input from the Advisory Committee. Most of the suggested topics were gleaned from the various group reports. Because of time limitations the Advisory Committee members were not given sufficient time for careful comments and rebuttals to our draft. Each of them received a copy before we went to print, however, with a request for verbal comments in case of violent disagreements.

#### SUMMARY AND RESEARCH RECOMMENDATIONS

There was reasonable agreement among the conclusions and recommendations of the four working groups, indicating a general consensus about some of the most important research issues. It was also generally agreed that spark gaps are still the most important, flexible, and utilitarian of all high power switches. Other switches have certain advantages in limited operating regions and some of the newer switch concepts, such as magnetic switches and solid state switches, benefit from less understanding and experience in using them.

Magnetic and solid state switches were mentioned as being able to replace spark gaps in certain repetitive operations. A subgroup was therefore formed to discuss some of the advantages and disadvantages of spark gaps and some of their nearest competitors. The results of these deliberations are summarized in Appendix A to this report. Solid state switches were also considered at another ARO sponsored workshop the week before this one and the deliberations of that workshop are summarized in a separate report\*.

---

\* Proceedings of ARO sponsored Workshop on Solid State Pulsed Power Switching, Tamarron, Colorado, January 12-14, 1983, (W.M. Portnoy and M. Kristiansen, Texas Tech University, Editors)

The Working Group on Electrical Characteristics and Breakdown Processes pointed out the desirability of finding methods for reliable multichanneling or low loss diffuse discharge operation since this should reduce electrode erosion and perhaps allow for increasing the repetition rate. The diffuse discharge operating regime was, however, not considered in detail by any of the other working groups. The need to determine the time-varying resistance of an arc in order to make estimates of electrode heat deposition became clear. It was also pointed out that methods for enhancing the repetition rate, other than gas flow, should be investigated. This point was also mentioned by other working groups. Suggestions included several basic phenomena, such as recombination effects in electrode metal vapors, quenching of metastables, recombination rates in injected attaching gases, recovery of gases at elevated temperatures, etc. This is an area where novel ideas may have high pay-off.

The need for spark gap model development and scaling laws was also discussed by the Working Group on Engineering Implications. It is particularly important, from an engineering viewpoint, to understand the gas flow-rate requirement scaling as functions of repetition rate, voltage, spark gap size, etc. This implies an improved basic physics understanding of some of the phenomena discussed in the next paragraph. The importance of measuring the self breakdown voltage distribution function to

determine spark gap performance was discussed at length. This method provides measures of the performance of spark gaps as various parameters are varied and thus constitutes one of the most direct and important diagnostic techniques available. Standardized experiments at appropriate power levels, gas flow, trigger capabilities, etc. that demonstrate the true spark gap limitations rather than testing facility limitations are needed. Current test facilities are insufficient and many spark gap data do not represent the true limits of the gap in question but rather the capability and limitations of the test facility. It should be appreciated that the needed testing capabilities involve multi-megawatt, high repetition rate facilities with a wide range of currents and voltages, large gas handling, cooling, and recycling systems, fast trigger systems, and sophisticated diagnostics equipment.

The Working Group on Thermal and Gas Dynamic Effects discussed the importance of determining electrode erosion as a function of gas flow rate and geometry. The relative importance of various gas and liquid electrode cooling schemes should be evaluated. Most of the basic considerations were concerned with the details of gas flow effects, including shock waves, the fractional gas volume replacement between discharges needed to achieve the requisite voltage recovery (studies of gas dynamics and density distributions and their effects on breakdown voltage),

boundary layer phenomena, and upstream and downstream methods for improving recovery (turbulent mixing, attacher and mist injection effects, etc.). Recovery experiments with gas mixtures which have a high breakdown strength and high acoustic speed should be evaluated.

In the Working Group on Materials and Chemistry, the needs for a data base and for figures of merit (implying modeling) to compare various materials combinations was emphasized. These are needed to be able to make system extrapolations to other parameter regimes. Experiments to study the effectiveness of gas attacher injection were proposed in this group also, as well as a study of the insulating properties of gas decomposition products. Electrode erosion and insulator damage as a function of various switch operating parameters ( $I_p$ ,  $di/dt$ ,  $\int idt$ ,  $\int i^2dt$ , gas type and pressure, etc.) need to be evaluated. An understanding of any synergism between gases, electrodes, and insulation materials is a general goal.

The main research recommendations of the various working groups are summarized in Table 1. The ordering in the table is non-prioritized. These recommendations are reformulated in terms of the basic science issues in Table 2.

## SUMMARY OF RESEARCH RECOMMENDATIONS

1. Spark Gap Model Development
  - a) Breakdown initiation
  - b) Arc channel development
  - c) Erosion
  - d) Scaling relations and parameter interactions
2. Gas Flow Effects and Heat Transport
  - a) Clearing factors (e.g. as a function of input power)
  - b) Flow effects on erosion
  - c) Turbulent vs laminar flow effects
  - d) Boundary layer effects
  - e) Gas vs liquid cooling
3. Alternatives to Gas Purging for Voltage Recovery
  - a) Metal vapor-plasma interactions
  - b) Injection of gas attachers or mists
  - c) Operating at elevated temperatures
  - d) Quenching of long-lived metastables
  - e) Gas-insulator interactions
  - f) Others
4. Data File and Standardized Testing Under Conditions Which are not Limited by the Test Equipment Capabilities
5. Triggering and Discharge Conditions
  - a) Reliable triggering of under-volted gaps at high repetition rate
  - b) Multichannel initiation at high repetition rate
  - c) Diffuse discharge operation (with high current density and conductivity) at high repetition rate

Table 2

## BASIC RESEARCH ISSUES

- 1) Arc initiation and channel formation for fast rising voltage pulses (high dv/dt) for various electrode materials, gas types and pressures.
- 2) Electrode erosion as a function of various electrical and gas parameters ( $di/dt$ ,  $I_p$ ,  $\int i dt$ ,  $\int i^2 dt$ ; gas pressure, type and flow rate; repetition rate; etc.).
- 3) Boundary layer effects on voltage breakdown in gas flow systems.
- 4) Turbulent vs laminar gas flow effects on voltage breakdown.
- 5) Mechanisms of free recovery (no gas flow) in gases.
- 6) Physics of precise discharge initiation (low jitter triggering) for various gases and electrode materials.

INVITED BACKGROUND PAPERS

## AN INTRODUCTION TO GAS FILLED SPARK GAPS

M. Kristiansen  
Texas Tech University  
Lubbock, Texas 79409 USA

## ABSTRACT

A brief introduction to the operation of gas filled spark gaps is presented. The level is aimed at those who are not experts in the field. The basic spark gap configurations, trigger methods, and present performance levels are outlined. Parameter dependencies, past spark gap research, and needs for future research are also described briefly.

## A. INTRODUCTION

Spark gaps have been the work horses of pulsed power switching technology for years. They cover an extremely wide parameter range and are relatively easy and cheap to construct. Single shot or very slow repetition rate spark gap technology has been developed to a high level by empirical methods. Recent requirements for high repetition rates while retaining the proven single shot performance of high voltage, current, and Coulomb transfer with extremely precise triggering has made past,

empirical methods and design extensions impractical. The new requirements for several orders of magnitude increase in repetition rate and life time make it necessary to obtain a solid understanding of the basic physics and chemistry principles involved in high power spark gap operation.

The purpose of this workshop is to address these issues and to determine the most important research issues. Because of the wide range of science and engineering disciplines required to solve this extremely difficult problem, several of the participants invited to this workshop had little prior experience with spark gaps. The following brief description of spark gaps and their operation is, therefore, aimed at the non-expert with the purpose of providing some common background and terminology for these participants.

Several other switches, besides spark gaps, also have the potential of being operated in a repetitive mode. Some of these switches and their apparent problems are summarized in Fig. 1. The issues concerning high pressure spark gaps are addressed below.

#### B. BASIC SPARK GAP ISSUES

A generalized spark gap is shown in Fig. 2. Several trigger methods, including laser, UV, x-ray, and electron-beam induced breakdown, field distortion, plasma injection, etc. can be used to initiate the arc between the two electrodes. For repetitive

operation it is necessary to equalize the gas pressure between the electrodes before reapplying the inter-electrode voltage. Figure 3 shows a generalized breakdown condition, known as the Paschen Law. It demonstrates that the breakdown field in a spark gap is determined by the product of gas density and gap distance. Since the gap distance is fixed and since high pressure spark gaps operate on the right hand side of the Paschen minimum it is clear that density differentials, such as induced by a high intensity spark discharge will affect the subsequent voltage hold-off capability. Other factors that affect the voltage hold-off include residual ionization and long lived metastables. In most cases these effects are of shorter duration than the density gradient effects at the pressures of interest here.

The reasons for using high pressure in spark gaps are two-fold; it provides high voltage hold-offs and hence relatively low discharge inductances (short discharge distances) and it is relatively easy to initiate the discharges with extreme accuracy (ns and sub-ns). The hot discharge gases must be flushed out of the gap in order to achieve rapid recovery. In order to keep the hot, often highly reactive, gas away from the insulator surfaces, it is usually found advantageous to flow the gas radially inward and out through holes in the electrodes. The choice of gas, gas flow, and gas flow geometry are current research topics of high importance.

Usually the spark gap lifetime depends upon electrode erosion and/or insulator damage. Auxiliary trigger electrodes often have low mass and may also affect the lifetime through their erosion. Figure 4 shows a block diagram of the pertinent spark gap issues and Figs. 5-7 show some repetitive spark gap geometries. Figure 8 shows a different geometry (with different problems) where the discharge is initiated along a dielectric surface, between two rail electrodes. The rail electrode geometry is also of considerable interest in regular gas spark gap operation.

Electrode erosion is affected by many factors, some of which are summarized in Fig. 9. Repetitive spark gap operation is similarly affected by many parameters, as outlined in Fig. 10. In the past, spark gap research has primarily been empirical in nature and data have been generated with little attention paid to scaling laws or physical understanding of the phenomena involved. This is summarized in Fig. 11. The needed switch improvements which constitute the main topic of this workshop are summarized in Fig. 12 and some of the needed research issues are listed in Fig. 13.

Additional information about spark gap operation can be found in "A Critical Analysis and Assessment of High Power Switches," Naval Surface Weapons Center (Dahlgren Laboratory), Report No. NP 30/78 (Co-authored by T.R. Burkes, J.P. Craig, M.O. Hagler, M. Kristiansen, E. Kunhardt, and W.M. Portnoy, Texas Tech University).

## SWITCHES WITH REP-RATE POTENTIAL AND THEIR PROBLEMS

- 1) Spark Gaps:
  - a) Gas Filled: Recovery, Life
  - b) Vacuum: Jitter, Voltage Hold-off
- 2) Thyratrons:  $I_{max}$ ,  $dI/dt$ , Efficiency, Voltage
- 3) Magnetic Switches: Energy/pulse, Efficiency, Engineering, Triggering, Weight
- 4) Solid State Switches: Energy/pulse, Scaling, Fundamental Understanding,  
 $I_{MAX}$

Fig. 1 Switches with Rep-rate Potential and Their Problems

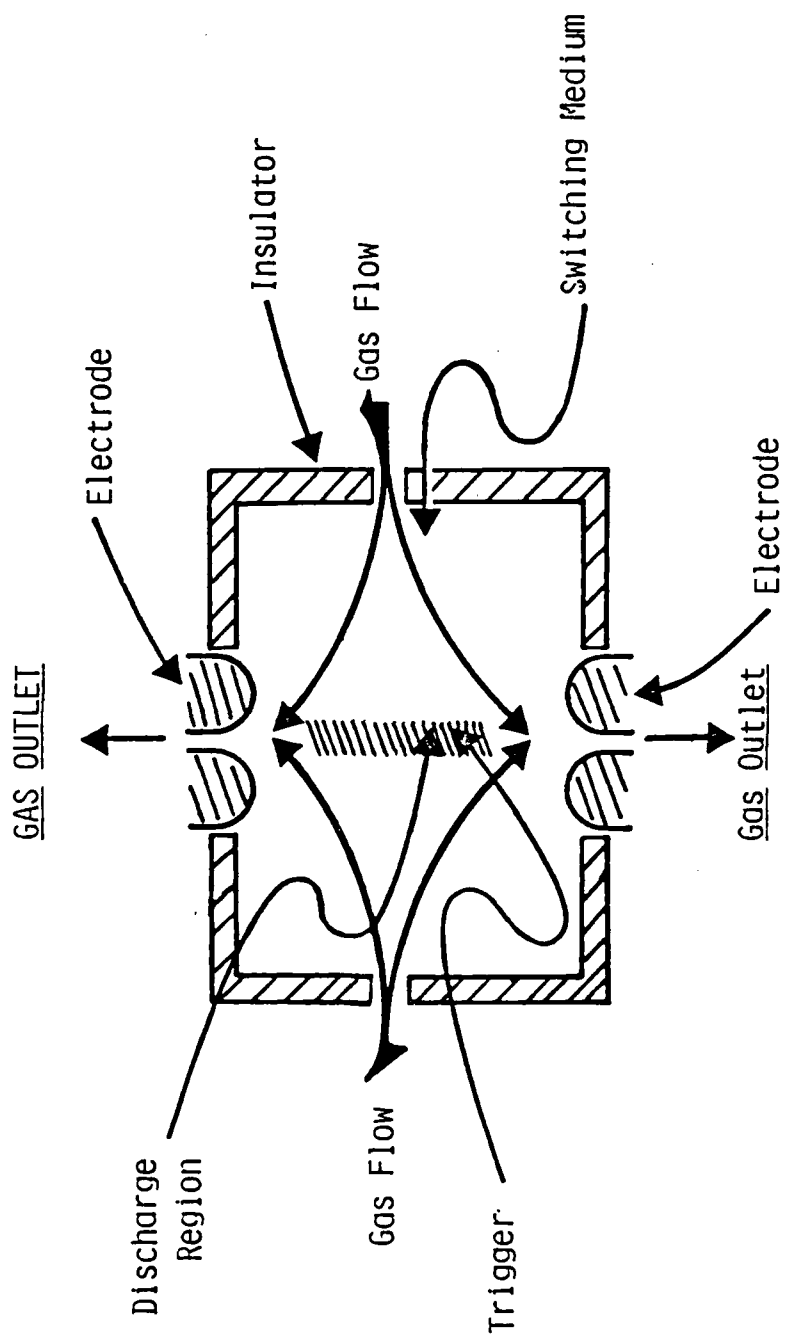


Fig. 2 Generalized Gas Spark Gap

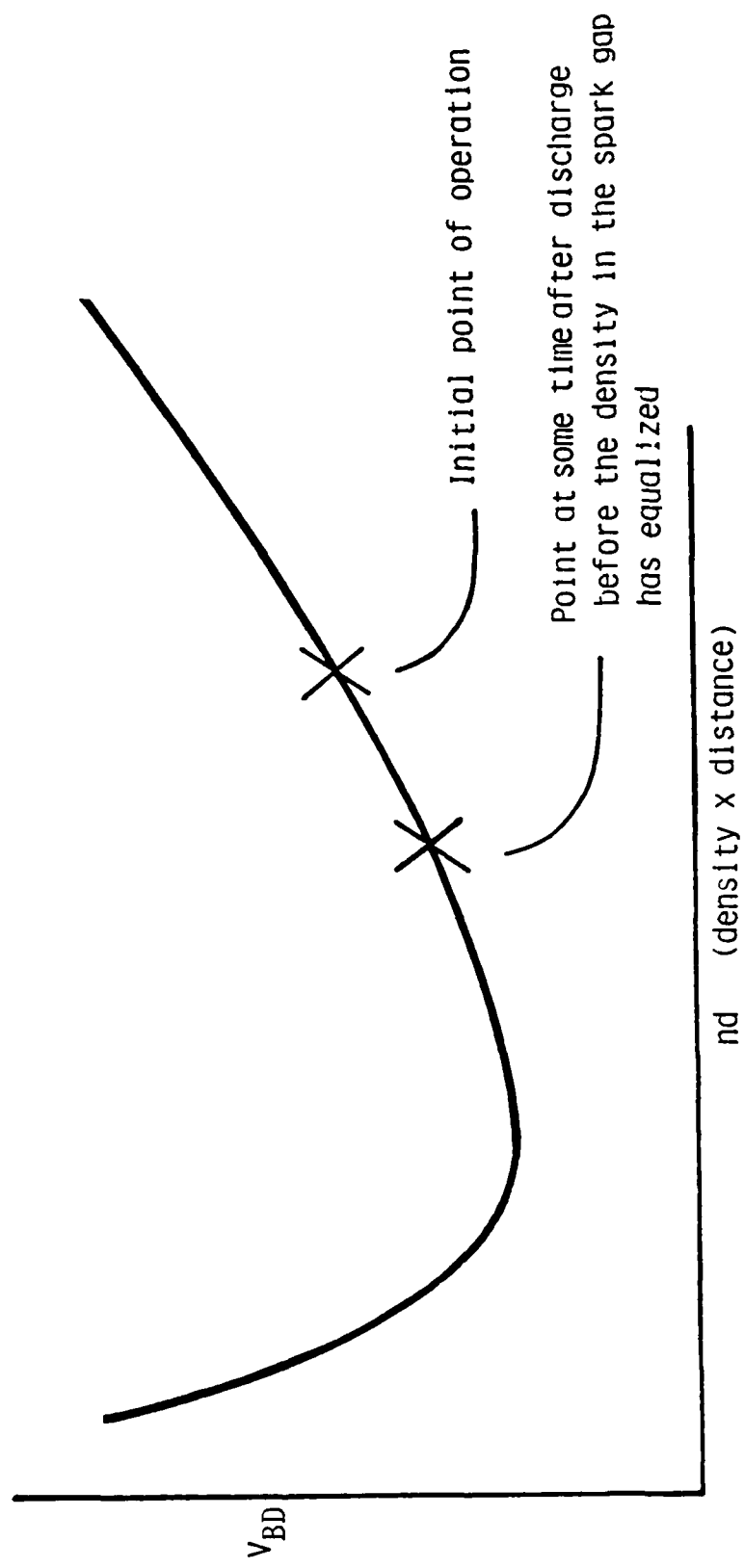


Fig. 3 Generalized Paschen Curve

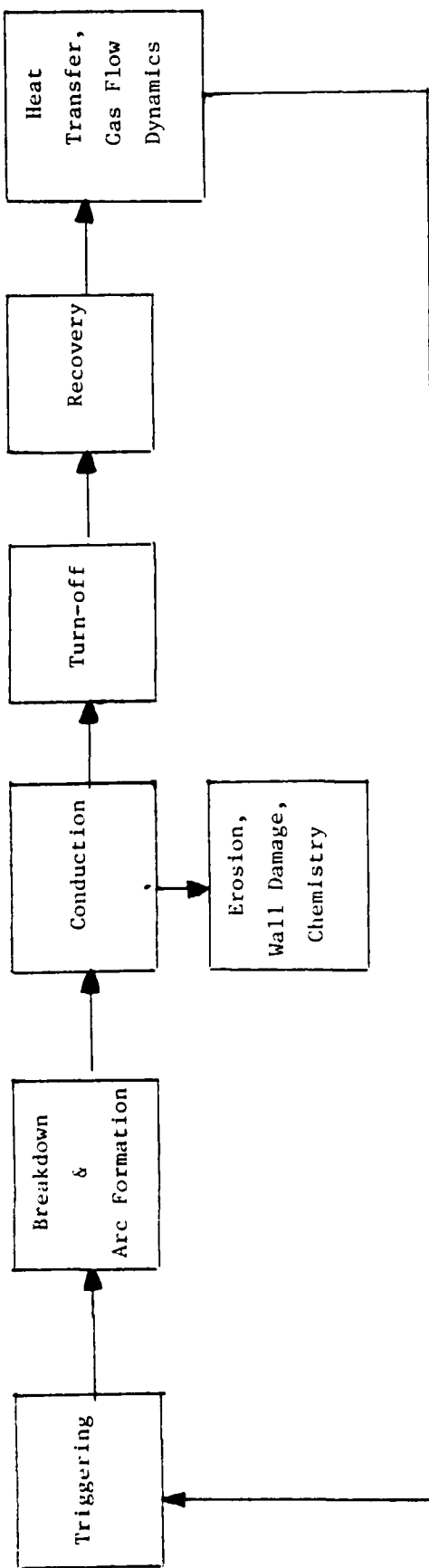


Fig. 4 Flow Diagram of Repetitively Operated Gas Filled Switch in Closing or Opening Mode

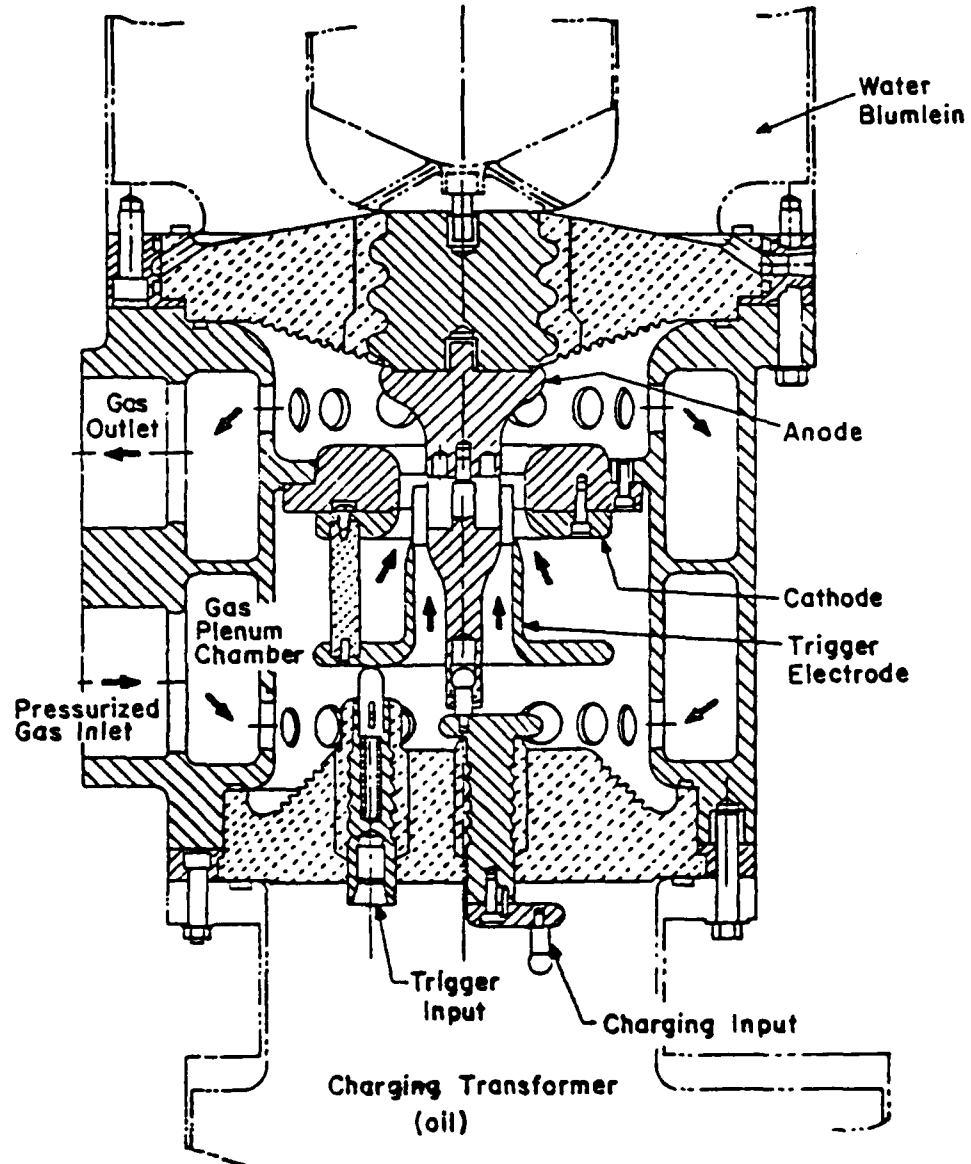


Fig. 5 ATA Spark Gap  
(Lawrence Livermore National Laboratory)

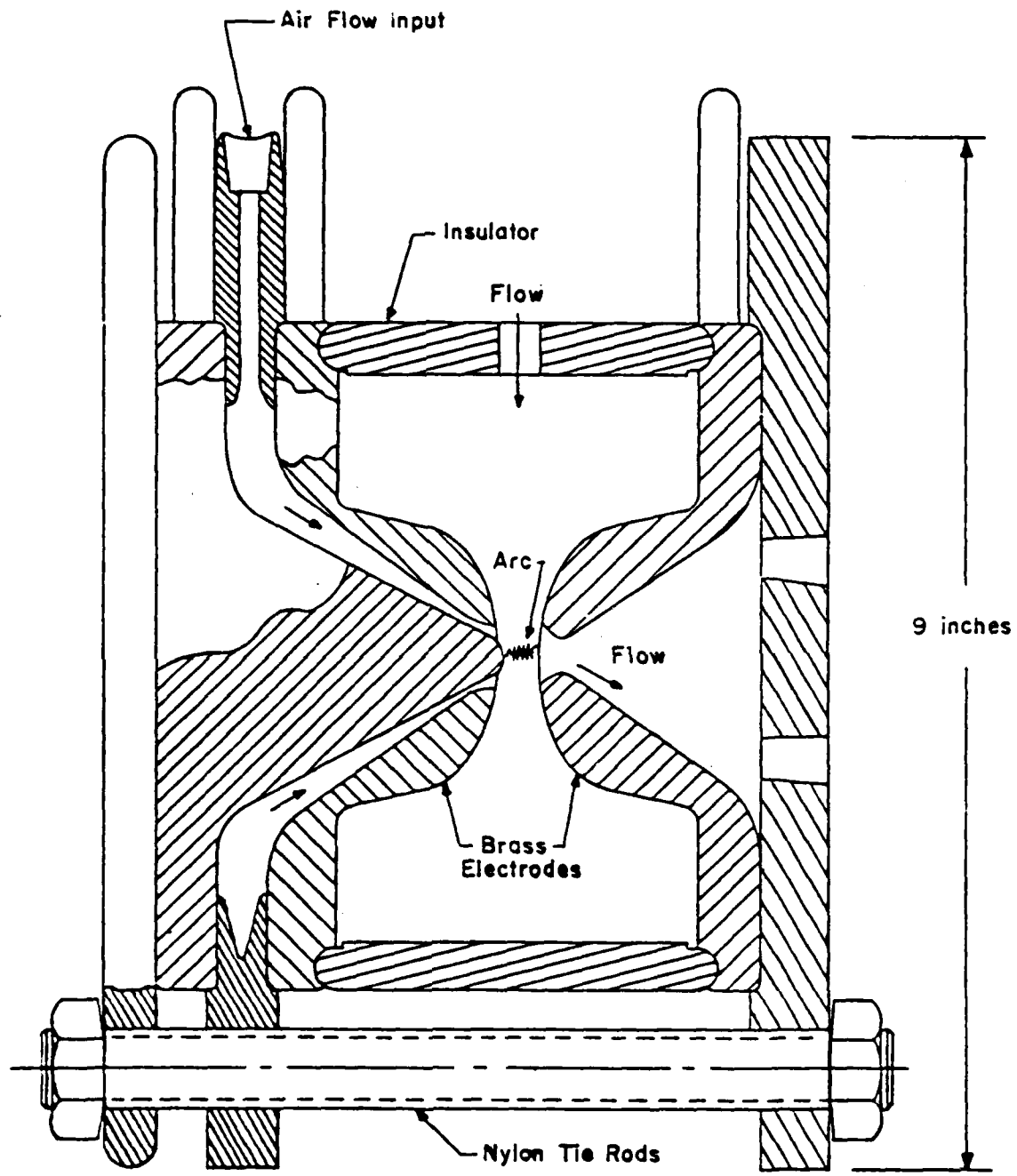


Fig. 6 Rep Rate Spark Gap Switch Assembly  
(Maxwell Laboratory, Inc.)

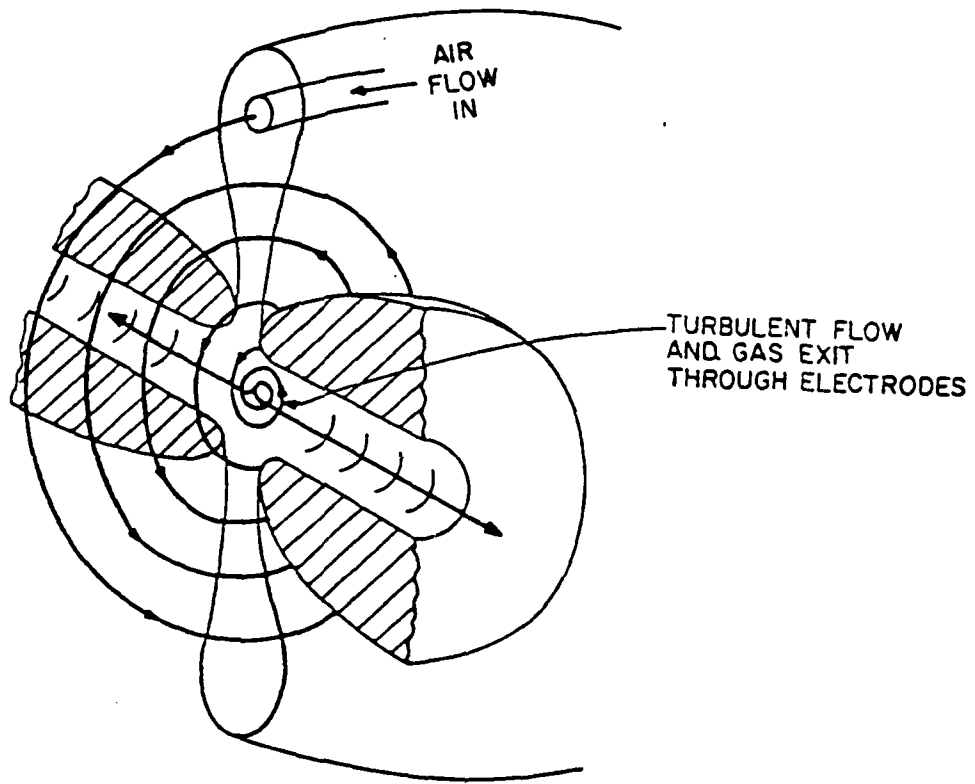


Fig. 7 Turbulent Flow Switch

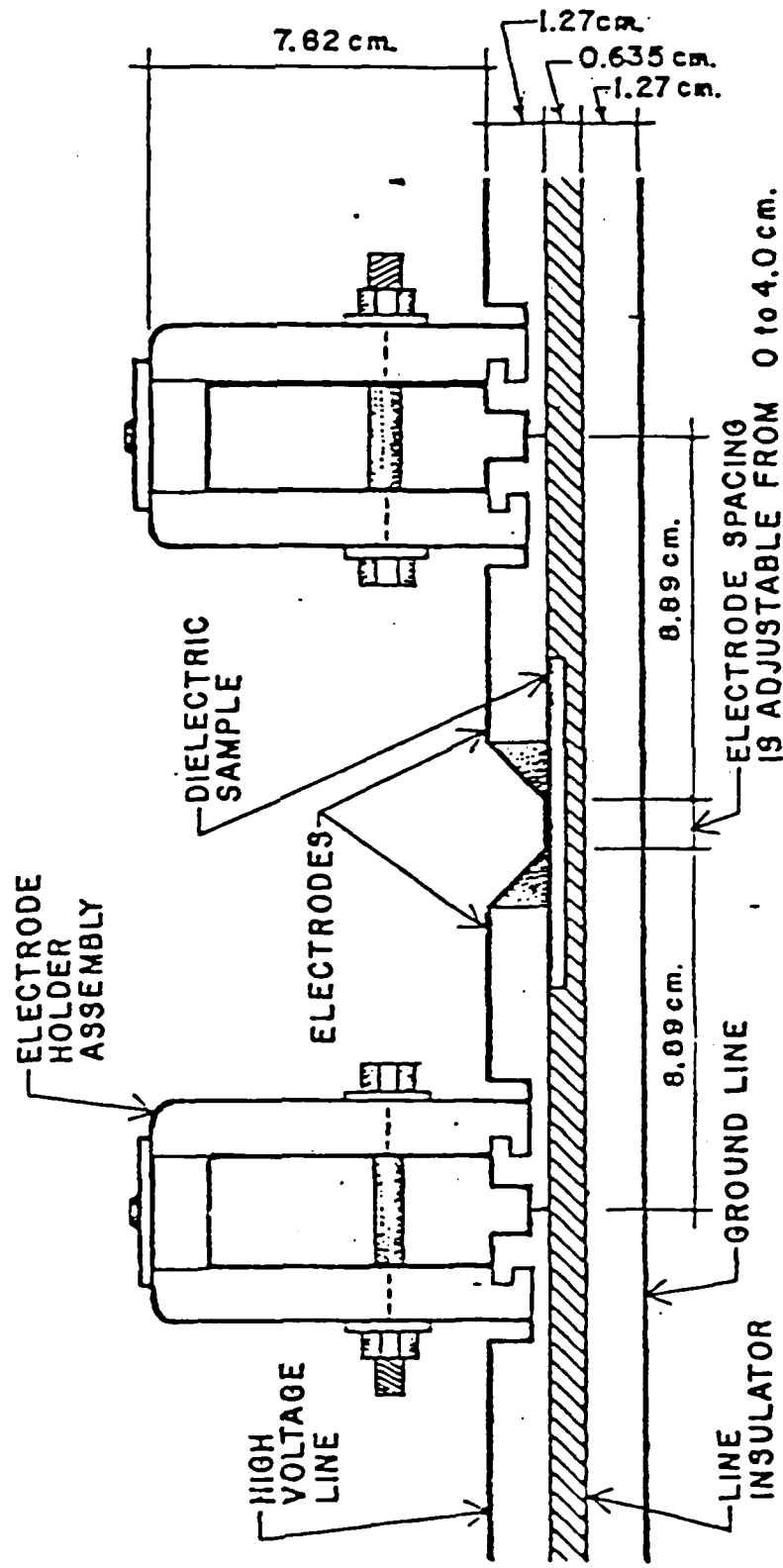


Fig. 8 Surface Discharge Spark Gap

- 1)  $\frac{dI}{dT}$
- 2)  $I_p$
- 3)  $\int I \frac{dI}{dT}$
- 4)  $\int I^2 \frac{dI}{dT}$
- 5) ELECTRODE MATERIAL AND FABRICATION
- 6) GAS TYPE
- 7) GEOMETRY
- 8) POLARITY
- 9) TRIGGER METHOD
- 10) ELECTRODE COOLING
- 11) GAS FLOW
- 12) REP-RATE

FIG. 9 SOME ELECTRODE EROSION FACTORS

GAS FLOW RATE	GAP SPACING
GAS TYPE	ELECTRODE SHAPE
GAS PRESSURE	ELECTRODE MATERIAL
CURRENT	GRACE PERIOD
VOLTAGE	RECHARGE TIME
CHARGE TRANSFER	REP-RATE

FIG. 10 SOME FACTORS AFFECTING REP-RATED OPERATION

- SINGLE SHOT APPLICATIONS
- LIMITED LIFE TIME REQUIREMENTS
- NO TEST STANDARDS
- LIMITED TEST FACILITIES FOR REPETITIVE OPERATION
- USER GENERATED TEST DATA (OVER VERY LIMITED RANGE)
- EMPIRICAL DESIGN EQUATIONS AND PRACTICES, LITTLE PHYSICS BACKGROUND  
ON WHICH TO BASE THE LARGE EXTRAPOLATIONS NEEDED

FIG. 11 SPARK GAP RESEARCH HISTORY

NEED ORDERS OF MAGNITUDE INCREASE IN:

REPETITION RATE

LIFE

WHILE

RETAINING SINGLE SHOT PERFORMANCE OF:

LOW JITTER

LOW PREFIRE

HIGH VOLTAGE STANDOFF

HIGH PEAK CURRENT

HIGH DI/dT

CONCLUSION: EMPIRICAL ENGINEERING PRACTICES OF THE PAST ARE INSUFFICIENT  
AND THE PHYSICS MUST BE MUCH BETTER UNDERSTOOD

FIG. 12 NEEDED SWITCH IMPROVEMENTS

EROSION PARAMETERS

REPETITIVE OPERATION

STREAMER AND ARC CHANNEL FORMATION

TESTING METHODS (LIFE, EROSION, PREFIRE)

TRIGGERING

INSULATOR DAMAGE

GAS FLOW DYNAMICS

FIG. 13 NEEDED GAS SPARK GAP RESEARCH

Electrode Processes in High Intensity Arcs

contributed by

E. Pfender

Dept. of Mechanical Engineering  
University of Minnesota  
Minneapolis, MN 55455

to the

DOD Sponsored Workshop

on

"Repetitive Spark Gap Operation"

Tamarron, Col.  
Jan. 17-19, 1983

Organized by

M. Hagler and M. Kristiansen  
Texas Tech University

1983

### I. Introduction

This contribution is restricted to a discussion of electrode phenomena in high intensity arcs with a few selected examples of recent results obtained in the author's laboratory. In spite of the fact that high intensity arcs have been known for almost 200 years, their electrode regions are still poorly understood. This lack of understanding is primarily due to the strong interaction of electrical, magnetic, thermal, and fluid dynamic effects in the electrode regions, further magnified by electrode melting and/or evaporation. In contrast to low intensity arcs, high intensity arcs are, to a large extent, dominated by fluid dynamic effects induced by the arc itself, a feature which serves as a criterion for distinguishing high and low intensity arcs. Typically, high intensity arcs are operated at current levels from approximately 50A to  $10^4$  A or even higher and pressures around 1 atm or above. Plasmas produced by such arcs are known as thermal plasmas because the thermodynamic state of the plasma approaches thermodynamic equilibrium or at least local thermodynamic equilibrium (LTE).

Many previous investigations of high intensity arcs excluded the electrode regions entirely. There is, for example, no consistent quantitative theory of the anode region available which permits a complete interpretation of the observed anode phenomena.

The cathode or anode region of a high intensity arc is defined as that portion of the discharge path which contains the

electrode, the zone of the net positive or negative space charge immediately in front of the electrode (sheath or fall zone), followed by a zone over which the presence of the electrode is felt and which is characterized by strong gradients of temperature and particle densities (see Fig. 1). It is customary to designate such a zone as a boundary layer. The final link between this boundary layer and the arc column consists of a transition zone which may be classified as a flow-effected zone. Frequently, this zone is more or less constricted due to the action of self-induced flow fields at the electrode.

The thickness of the various zones differs by several orders of magnitude. The sheath overlying the electrode surface has a thickness in the order of a Debye length (typically in the range of  $10^{-6}$  cm for a high intensity arc), which is substantially less than the free path length of electrons and ions. The thickness of the previously mentioned boundary layer is in the range from 0.01 to 0.1 cm, approximately an order of magnitude smaller than the adjacent flow-effected zone. As an example Fig. 2 shows an anode boundary layer.

The space charge zone which may be treated as an electrical boundary layer located at the bottom of the thermal boundary layer provides the transition from gaseous to metallic conduction.

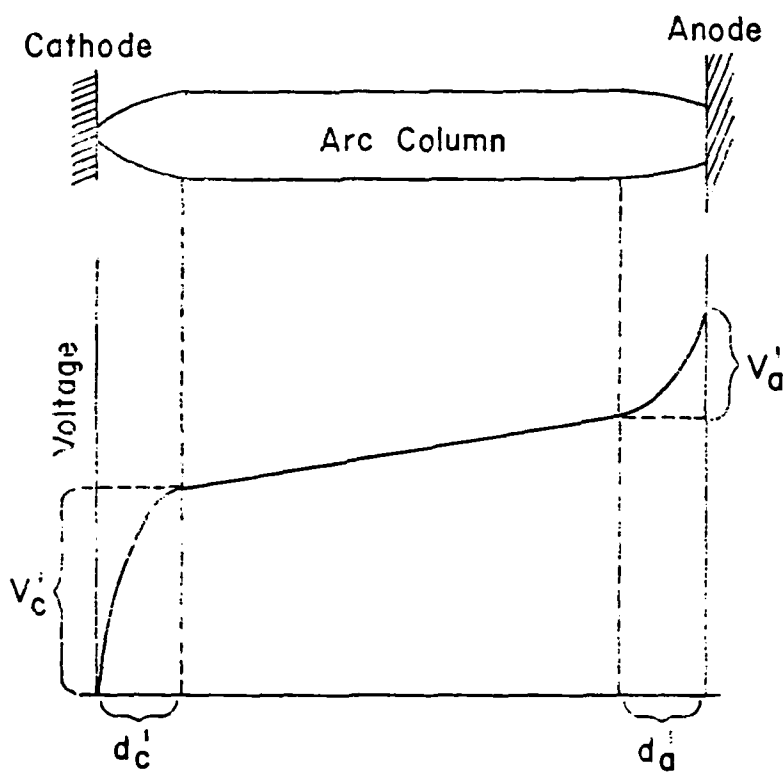


Fig. 1: Schematic of an arc with electrode regions (not to scale)

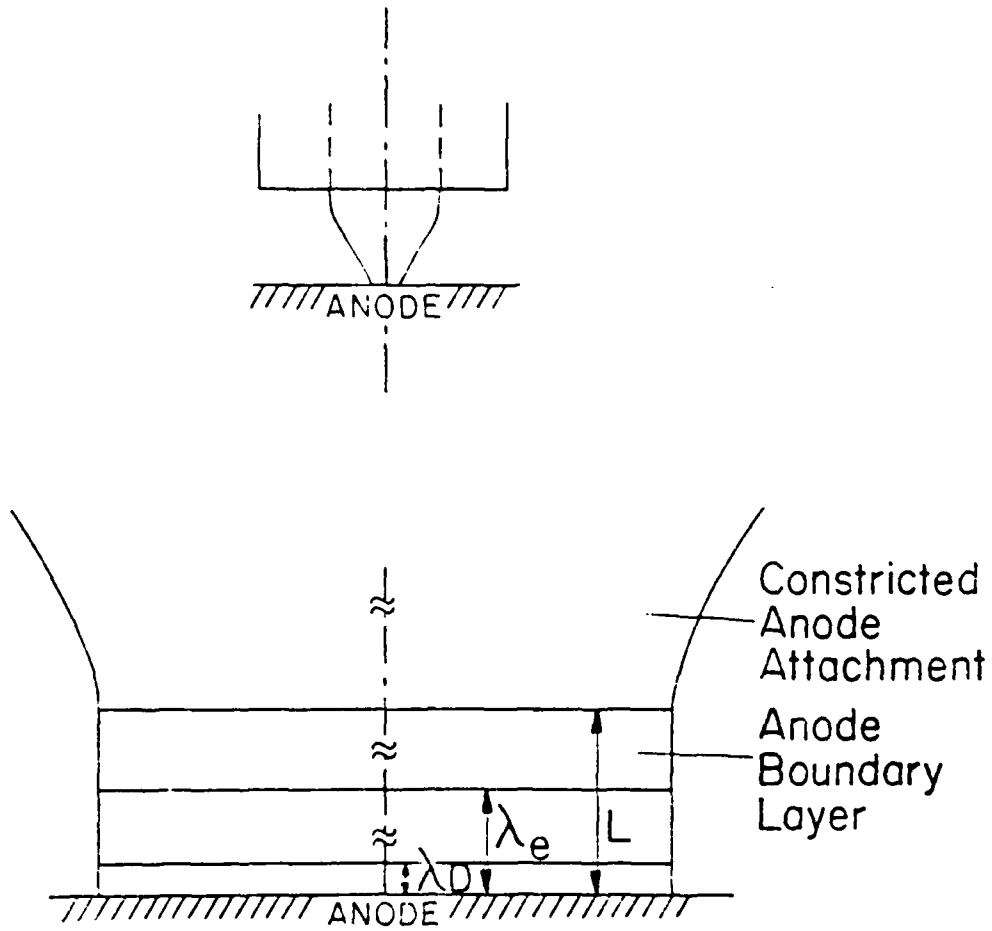


Fig. 2: Schematic of an anode boundary layer  
 $\lambda_e$  = mean free path length of the electrons  
 $\lambda_D$  = Debye length

The electrode regions, as any other part of the arc, are governed by the conservation equations, including the current equation. Any attempt to solve these equations for the electrode regions excluding the sheath faces two major problems. First of all, the application of the conservation equation requires that the plasma is in local thermodynamic equilibrium (LTE) or at least that its thermodynamic state is known. Previous results indicate that there are severe deviations from LTE in the anode boundary layer (1) which also extend into the flow-effected zones (2-4). These deviations from LTE must be considered in a realistic model for the electrode regions.

The second problem is associated with the formulation of realistic boundary conditions in the electrode regions. Consider, for example, an anode attachment in the form of a so-called anode spot which may move around on the anode surface in spite of the steady nature of the bulk of the plasma. The formation of such an anode spot is frequently accompanied by melting and evaporation of anode material. The described phenomena make the formulation of well-defined boundary conditions extremely difficult. In such a situation, recourse is frequently taken to experimental data. Unfortunately, the available data base is rather limited and not consistent. The physical dimensions of and the experimental conditions in the electrode regions of high intensity arcs

prohibit the application of many conventional diagnostic tools as, for example, potential probes, magnetic probes, etc. Many findings are more or less only concerned with phenomenological observations.

According to the described complexity of the electrode regions and the associated difficulties with which analytical and experimental investigations are faced, it is not surprising that these regions did not receive as much attention as, for example, the arc column.

An additional dimension of complexity is introduced by the appearance of electrode vapors in the arc. Metal vapors which have in general a substantially lower ionization potential than permanent gases have a dominant effect on the electrical conductivity (seeding of MHD plasmas), especially in regions of lower plasma temperatures. Therefore, the electrode regions in which arc fringe effects play an important role are strongly affected by metal vapors.

### III. The Electrode Regions of High Intensity Arcs

In this paragraph previous pertinent work associated with the cathode and anode region of high intensity arcs including modeling work will be briefly summarized. Recent results obtained in this laboratory dealing primarily with the anode region of high intensity arcs will be reported in the next section.

1.) The cathode region.

Phenomenologically, the current attachment at the cathode of arcs may be divided into two broad categories:

- a. "Diffuse attachment" without evidence of single or multiple cathode spots.
- b. Attachment in the form of one or several distinct spots.

The term "diffuse attachment" characterizing the first mode requires further explanation because this mode is frequently referred to in the literature as "spot attachment." The arc may indeed reveal in this mode an appreciable constriction in front of the cathode so that the actual current transition zone appears as a "spot" with current densities in the range from  $10^3$  to  $10^4$  A/cm<sup>2</sup>, at least one order of magnitude higher than in the arc column. This mode, however, may be clearly distinguished from the second mode for which the constriction is much more severe, with current densities in the range from  $10^6$  to  $10^8$  A/cm<sup>2</sup>. In addition to the entirely different cathode electron emission mechanisms for these two modes, the cathode attachment in the first mode is stationary or slowly moving in contrast to the second mode which frequently shows one or several spots moving with high velocities and randomly over the cathode surface.

In the first mode thermionic emission of electrons is the governing mechanism for liberation of electrons from the cathode.

This mode is, however, restricted to cathode materials with very high boiling points (carbon and refractory metals).

From an energy balance at the cathode one finds that more than 15% of the current is carried by ions which are primarily responsible for heating of the cathode to temperatures required for thermionic emission. The cathode fall is typically around 10V for high intensity arcs revealing some minor variation with current (5).

A comprehensive treatment of the cathode region of arcs has been reported by Ecker (6). In this treatment the cathode region is subdivided into 3 model zones - the contraction, space charge, and cathode surface zone. By specifying matching boundary conditions between the zones, he establishes a self-consistent model. The contraction of the arc is confined to the contraction zone in which quasi-equilibrium without space charges is prescribed. Solutions of the conservation equations yield the shape of the arc in the cathode region.

Although the magnetic pinch effect as such is negligible for typical high intensity arcs, the cathode jet induced by the interaction of the arc current with the self-magnetic field, however, may have a strong effect on the constriction of the arc. Convective heat transfer due to the induced flow represents an important term in the energy balance. This convective term has

been taken into account by Lee and Greenwood (7) and by Lee et al. (8,9). In this case the cathode region is divided into a number of zones which allow the calculation of the fraction of the ion current to the total current over the entire thickness of the cathode region.

Guile (10) summarizes in a comprehensive review many observations and measurements in the cathode region of arcs. He stresses the fact that secondary effects, such as vapor and plasma jets originating in the cathode region or on the cathode itself may exert a strong influence on the cathode regions and sometimes on the entire arc.

Cathode jets have been observed in thermionic as well as in nonthermionic arcs, particularly at higher current levels. These cathode jets may be attributed to four different sources.

- a.) Electromagnetically induced jets.
- b.) Vaporization of cathode material and/or surface impurities.
- c.) Ablation and explosive release of cathode material.
- d.) Chemical reactions on the cathode surface producing gases.

Electromagnetically induced jets which have been first described by Maecker (11) are of particular interest because they may be induced in the cathode as well as in the anode region. The

maximum velocity of the cathode jet depends on the arc constriction in the cathode region which may be influenced by the cathode shape (12) in the case of thermionically emitting cathodes.

The cathode effects impose serious problems on attempts to model the entire arc. Several analytical models (13-15) have been proposed for analyzing the behavior of a free-burning arc column. Since a number of severe simplifications and assumptions have been introduced, the corresponding solutions are restricted to the indication of trends; they cannot describe the actual arc behavior, especially near the electrode regions. Realistic predictions can only be obtained from numerical solutions of the set of conservation equations combined with proper boundary conditions.

Lee and Greenwood (9) considered the transition zone in front of a plane cathode by making certain assumptions about the flow fields and solving the energy equations only. Fink (16) simulated the transition zone of a cathode nozzle with a sharp-tipped cathode under forced convective conditions. In spite of the knowledge gained from these studies, a number of phenomena observed in the cathode region and on the cathode itself remain unexplained.

## 2.) The anode region

There are a number of similarities and common features of cathode and anode region in high intensity arcs. In contrast to the cathode region, the anode region plays a more passive role which is reflected in a comparatively small number of investigations and available data.

For an analysis of the anode region, the conservation equations including the current equations must be solved. Unfortunately, any attempt to solve these equations faces three major problems. First of all, the conventional conservation equations apply only as long as the continuum approach is valid. Since the anode fall spacing is smaller than one mean free path length of the electrons, the continuum approach is no longer valid for that part of the anode region. Secondly, the application of the conservation equations requires that the plasma is in LTE or at least that its thermodynamic state is known. There is evidence (3) that LTE does not exist for the entire anode region. Close to and in the anode boundary layer deviations from LTE occur due to differences in electron and heavy particle temperatures and due to deviation from chemical composition equilibrium (3). Finally, the specification of realistic boundary conditions faces similar problems as in the cathode region.

Results of previous work concerned with the anode region of high intensity arcs have been summarized in a number of reviews (2,5,6,10) and will not be reiterated here. Some of the more recent results will be discussed in the following section.

### III. Selected Results of Studies of the Anode Region

#### 1.) Studies of anode arc roots.

An experimental arrangement has been developed which allows simulation of short, as well as of long, high intensity arcs. This arrangement is particularly useful for studying the arc behavior in the anode region. Two stable anode arc roots have been observed depending on the flow situation in the anode region. There is a diffuse anode arc root governed by the cathode jet (Cathode Jet Dominated mode shown in Fig. 3) and/or the additional flow induced in the anode region. This flow impinges on the anode surface producing the well-known bell shape of the arc. The second mode shows a more or less constricted anode arc root governed by the flow induced in the anode region (Anode Jet Dominated mode shown in Fig. 4) and accelerated away from the anode (anode jet). Using a fast scanning spectrometric system which has been described elsewhere (17), temperature distributions of the arc in the anode region have been measured for both anode arc roots assuming LTE in the plasma. The maximum temperatures in

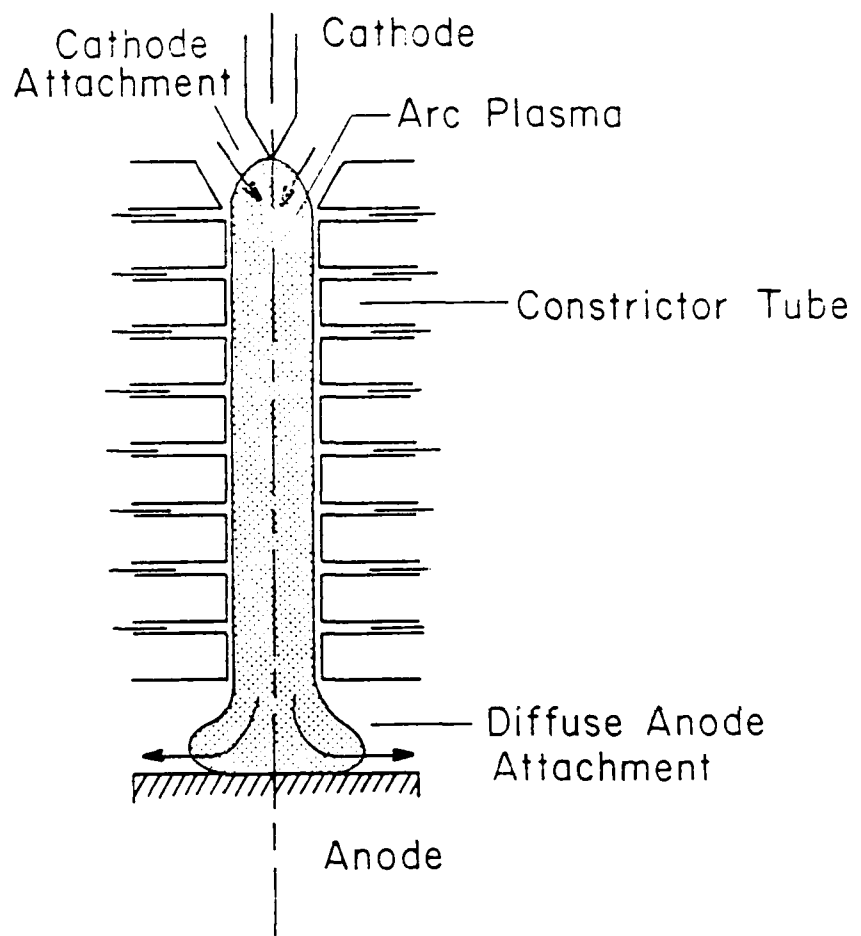


Fig. 3: Diffuse anode arc root [Cathode Jet Dominated mode (CJD)]

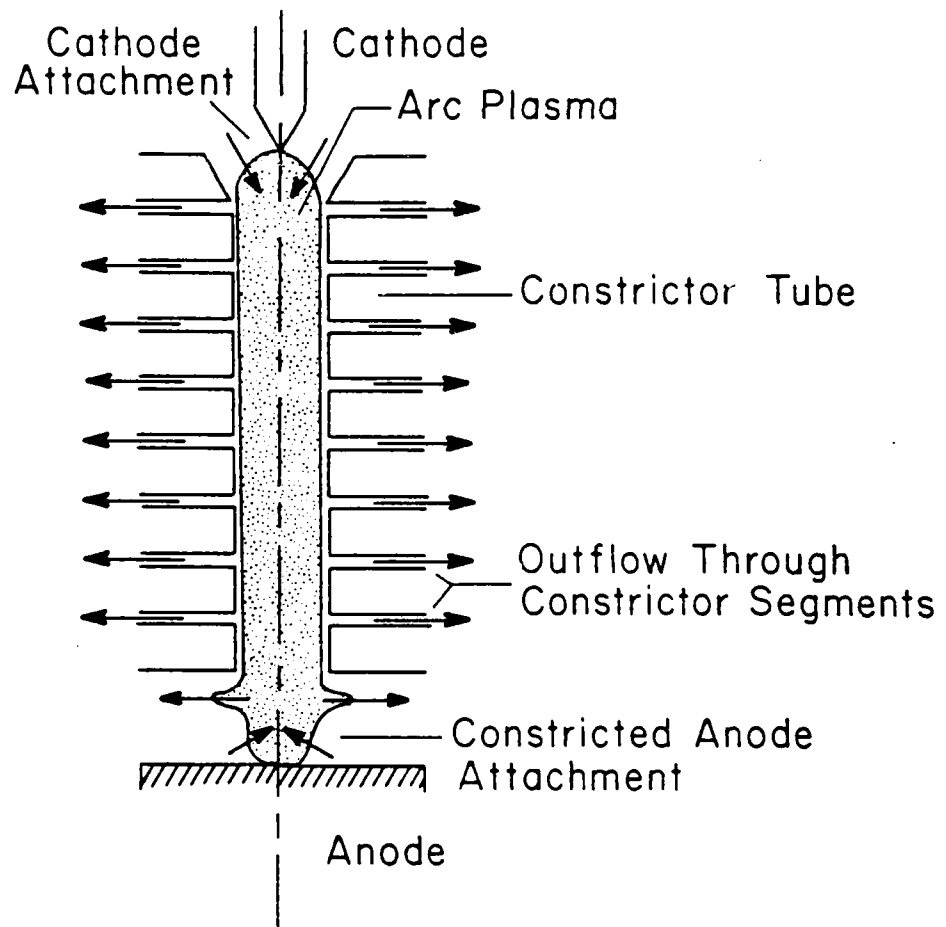


Fig. 4 : Constricted anode arc root [Anode Jet Dominated mode (AJD)]

the arc core compare favorably with calculated temperatures in the AJD mode. The calculated isotherms, however, show a substantial shift with respect to measured isotherms which is probably due to the chosen boundary conditions at the end of the constrictor tube (Figs. 5 and 6).

The results of this work clearly demonstrate that the "natural" anode attachment (without the effect of the cathode jet) will be constricted, i.e. in arcs where the effect of the cathode jet is no longer felt at the anode, the anode arc root will be more or less constricted. In contrast, in arcs in which the cathode jet impinges on the anode surface, the arc root tends to be diffuse.

Additional details of this work are described in a recent paper (18).

## 2.) Investigation of the anode boundary layer.

Previous analytical studies in this laboratory predicted negative anode falls on plane, unrestricted anode surfaces based on a one-dimensional analysis of the anode boundary layer (1). Fig. 2 shows a sketch of the anode boundary layer. This sketch refers to a constricted anode arc root, but the analysis holds also for diffuse anode arc roots. The steep gradients of particle densities and temperatures in front of the anode induce

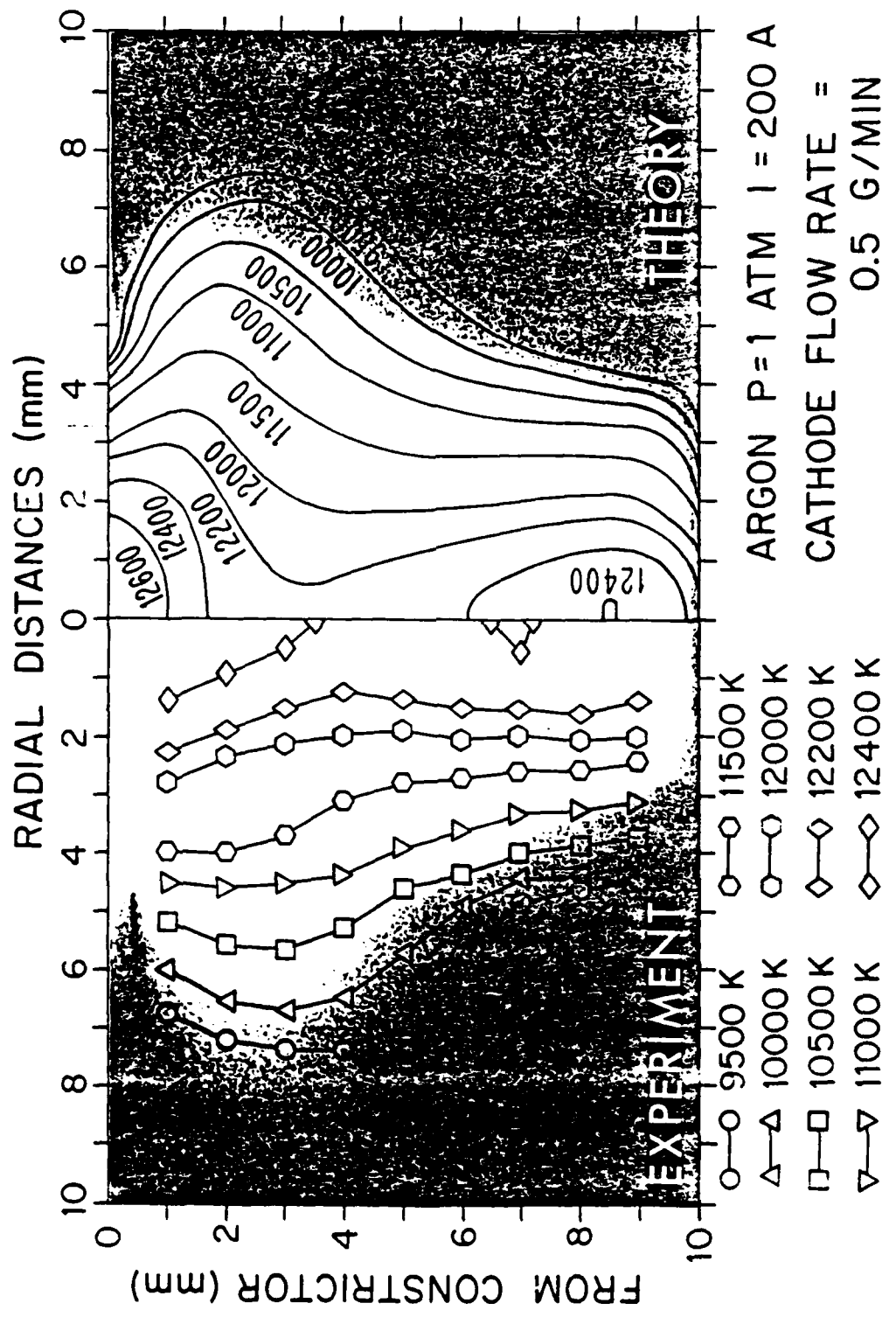


Fig. 5: Measured and calculated isotherms of the anode region (arc operated in the AJD mode)

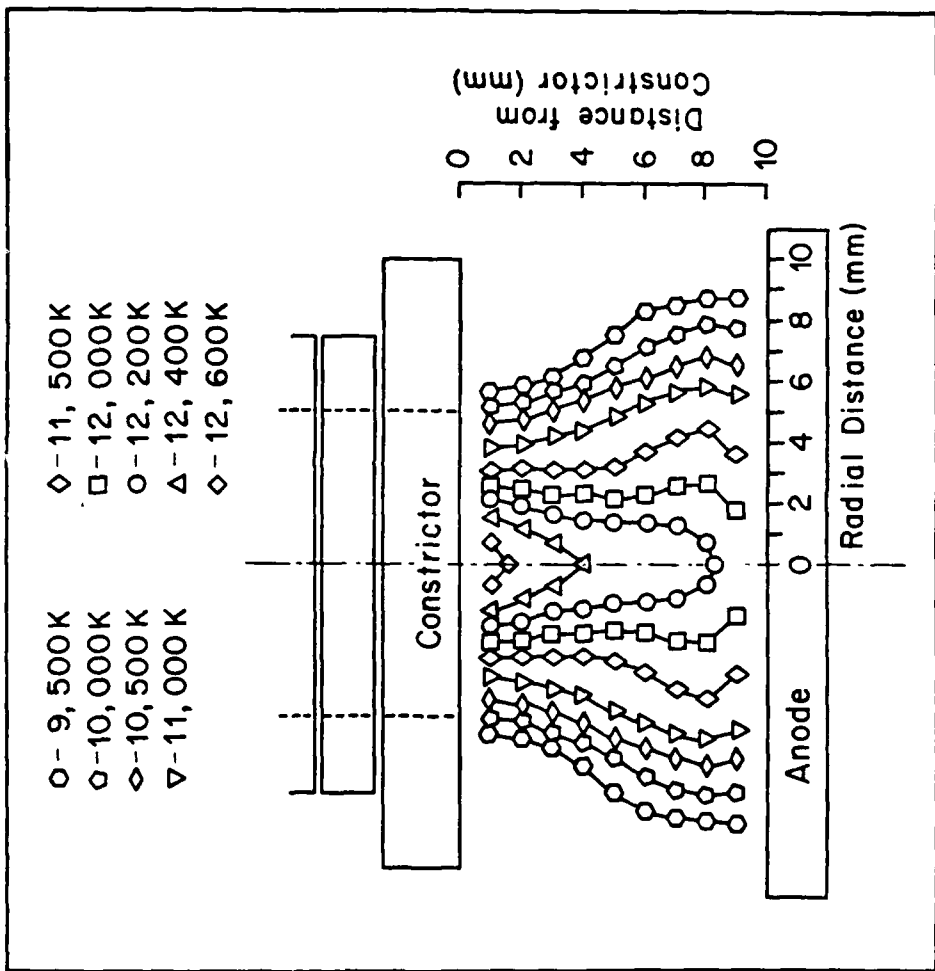


Fig. 6x Measured isotherms of the anode region (arc operated in the CJD mode)

additional driving forces for the electron current, i.e. the current equation assumes the form

$$j = \sigma(E + \frac{1}{en_e} \frac{dp_e}{dx}) + \frac{dT_e}{dx} \quad (1)$$

The second and third term in this equation (ordinary diffusion and thermal diffusion of the electrons, respectively) are so strong that negative electric fields become necessary for balancing the current equation, i.e. the anode fall becomes negative. Typical values for the calculated anode falls are given in Table I as a function of the electron current density at the anode. Also included in this table are values of the thickness of the anode boundary layer.

$J_a (\text{A/cm}^2)$	L (mm)	$\phi_a$ (v)
600	0.53	-2.2
900	0.34	-1.8
1,000	0.32	-1.9
2,000	0.20	-1.5
3,000	0.12	-2.7

Table I: Predicted thickness of anode boundary layer and anode falls for different current densities at the anode.

These predictions have been confirmed by the results of recent measurements and, to this author's knowledge, this is the first time that negative anode falls have been measured in such arcs. These findings are crucial for modeling of anode heat fluxes in a number of arc applications including arc switches.

Since the results of this work are not yet published (a publication is in preparation), the most important findings of this study will be briefly discussed. Figs. 7 and 8 show the arc arrangement including the electric probe used for measuring electron temperatures and floating potentials in front of the anode. The arc arrangement shown in Fig. 7 allows operation of the arc either in the CJD or in the AJD mode, whereas Fig. 8 refers to the free-burning arc arrangement. In this case, an auxiliary anode is required in order to avoid destruction of the probe during starting of the arc.

The electron temperatures at and at several locations above, the anode surface are obtained with the probe shown in Fig. 7 and 8. A typical example of measurements is shown in Fig. 9.

These measurements indicate a deviation from the Maxwellian distribution for high energy electrons. The reason for the deviation may be due to a depletion of the number density of high energy electrons caused by ionizing collisions in the boundary layer. Electrons making such collisions close to the anode may not have a chance to equilibrate before they are collected at the anode.

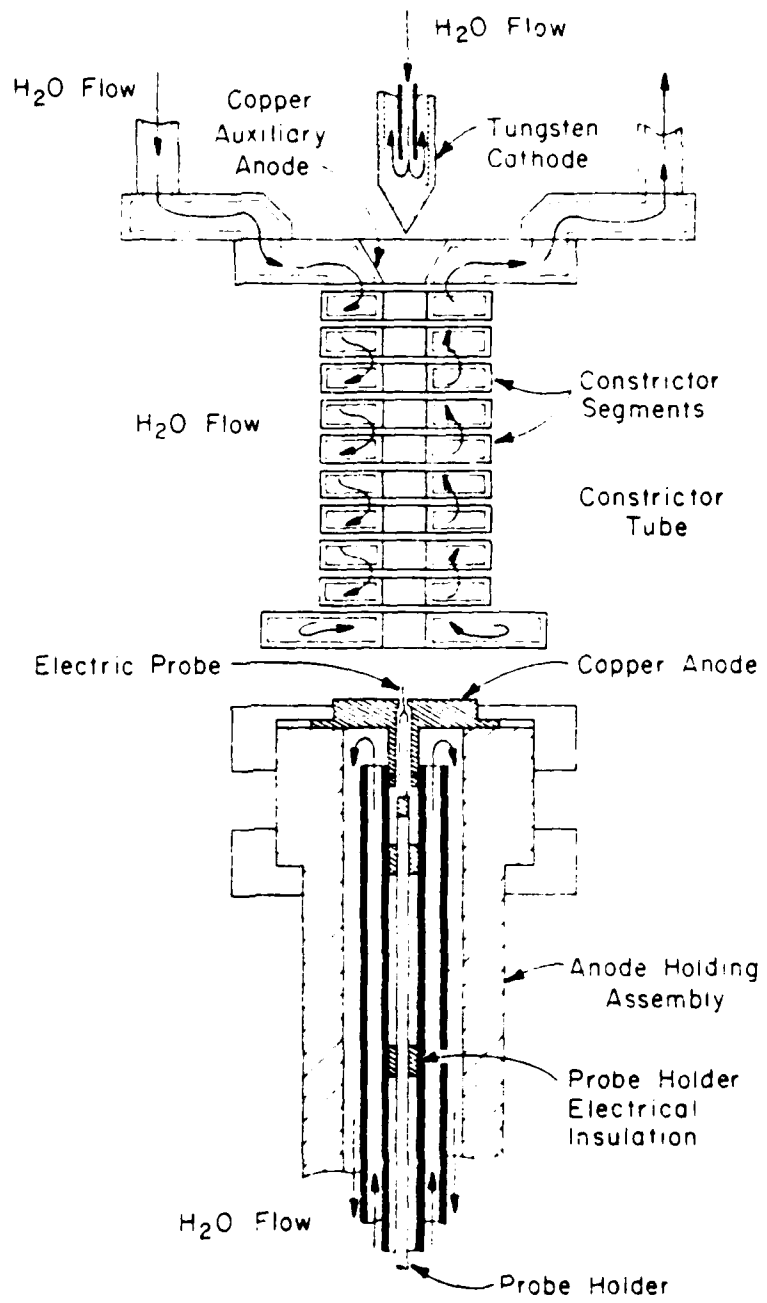


Fig. 7: Arc arrangement for measuring anode falls (CJD and AJD mode)

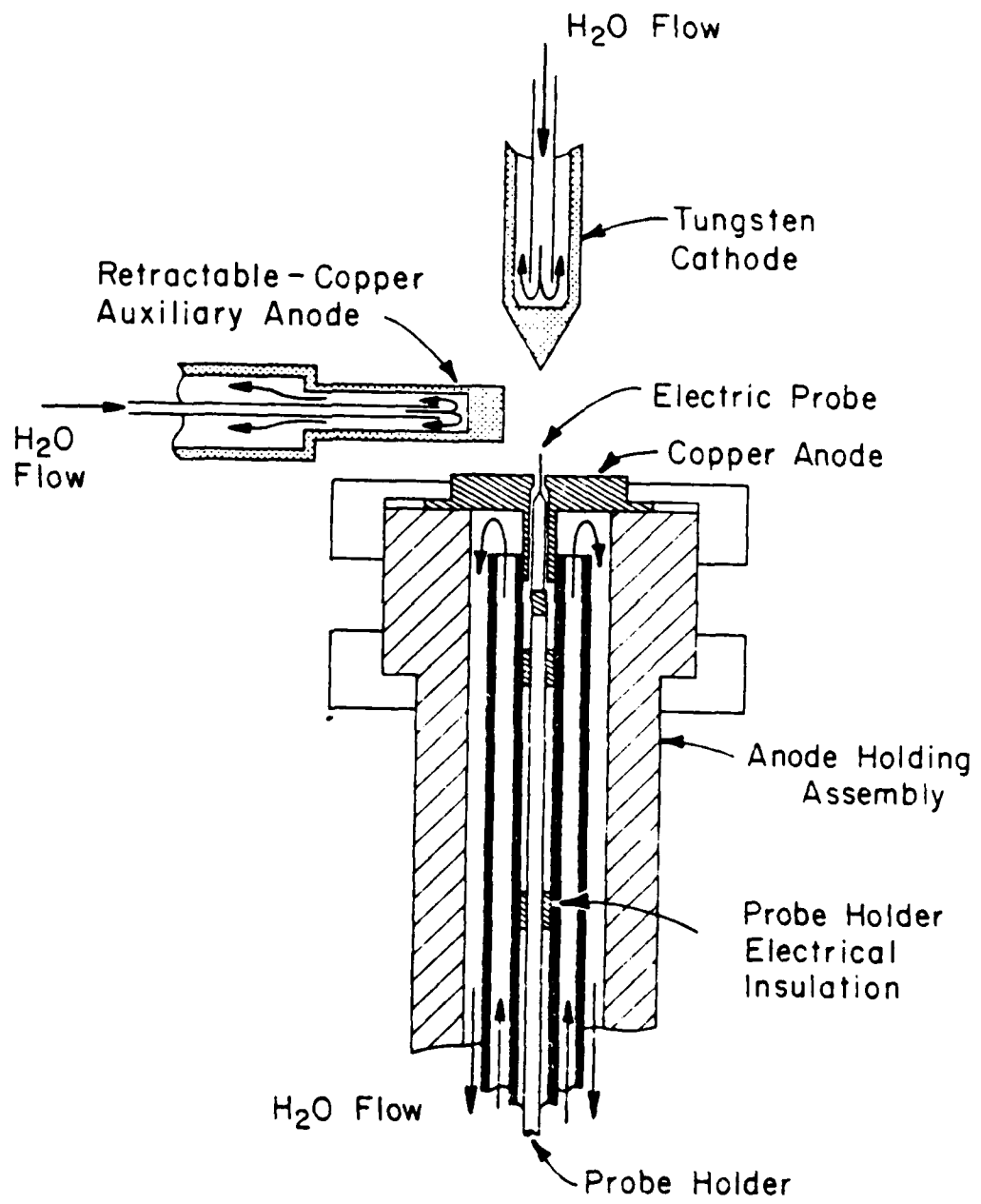


Fig. 8: Free-burning arc arrangement for measuring anode falls

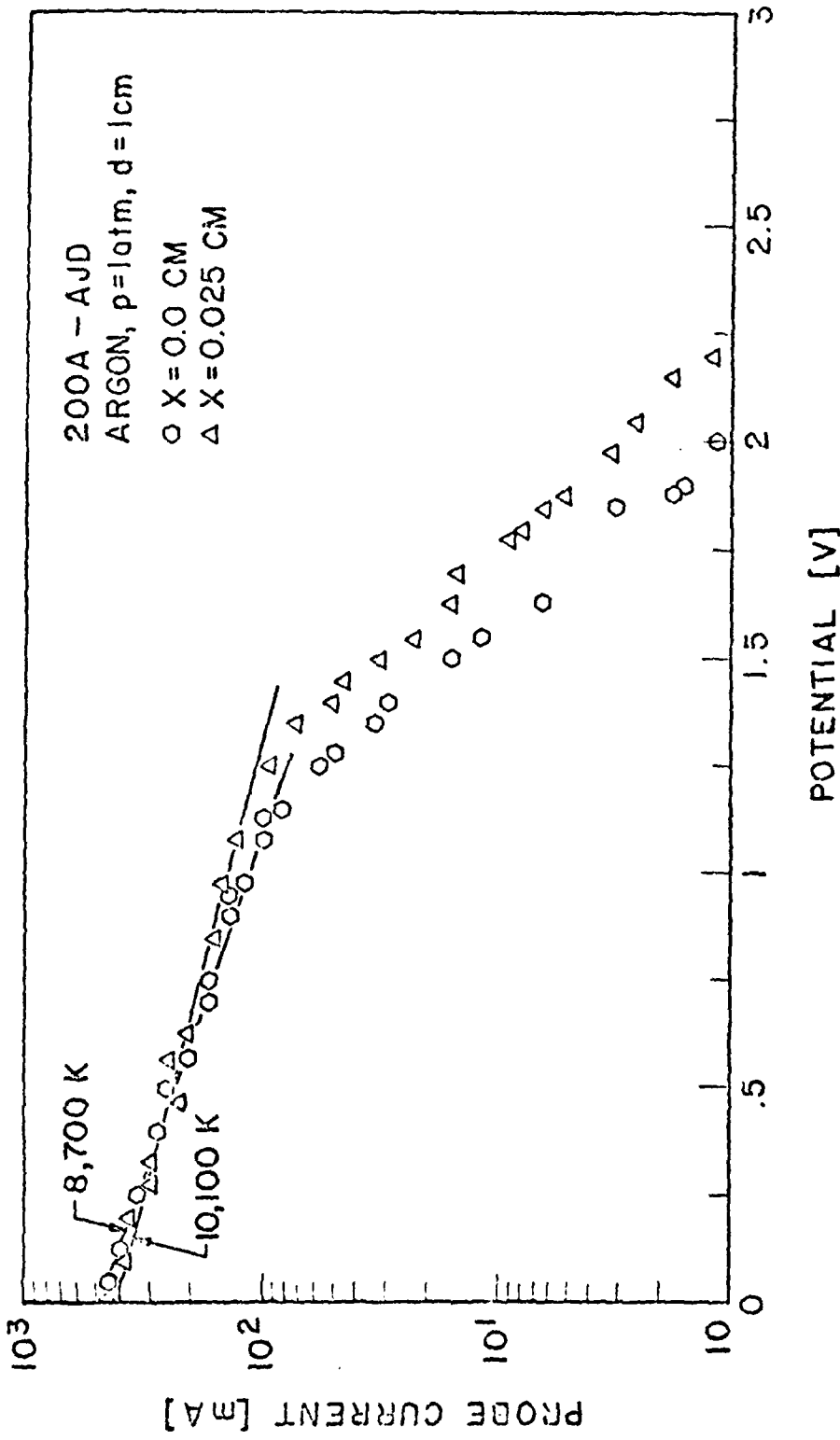


Fig. 9 Logarithmic plot of the electric probe characteristics.

The results for both anode arc attachments (AJD and CJD mode) and for different arc currents are summarized in the table of Fig. 10. The last column in this table refers to results of spectrometric measurements taken 0.1 cm above the anode surface. Unfortunately, the probe can not be extended beyond  $x=0.025$  cm above the anode surface because of over heating problems. Fig. 11 shows as an example the distribution of electron temperatures in front of the anode and, for comparison, analytical predictions which are in good agreement with experimental data.

From floating potential measurements at and above the anode surface combined with corresponding electron temperatures, the true space potential distribution above the anode surface may be determined. As an example, Fig. 12 shows such data. In all cases covered in this study, the anode falls are negative with values varying from -2.4 to -1.6V. Again, these values are in good agreement with analytical predictions (1).

The results of calorimetric measurements of anode heat transfer are shown in Fig. 13 for both modes of anode arc attachment and average percentage values of the various modes of anode heat transfer are shown in the table of Fig. 14.

ATTACHMENT MODE	ARC CURRENT [A]	$(Te)_{Pr}$ $X = 0$	$(Te)_{Pr}$ $X = 0.0125 \text{ cm}$	$(Te)_{Pr}$ $X = 0.025 \text{ cm}$	$(Te)_{Sp}$ $X = 0.1 \text{ cm}$
AJD	100	9,200	9,700	10,100	11,700
	150	8,800	9,700	10,100	12,000
	200	8,700	9,600	10,100	12,300
CJD	150	9,100	10,400	11,050	11,800
	200	9,840	10,600	12,100	12,200
	250	9,600	11,250		12,500

$(Te)_{Pr}$  - ELECTRON TEMPERATURE OBTAINED FROM PROBE MEASUREMENTS

$(Te)_{Sp}$  - ELECTRON TEMPERATURE OBTAINED SPECTROMETRICALLY

$X$  - DISTANCE FROM ANODE SURFACE

Fig. 10 Measured electron temperatures in front of the anode.

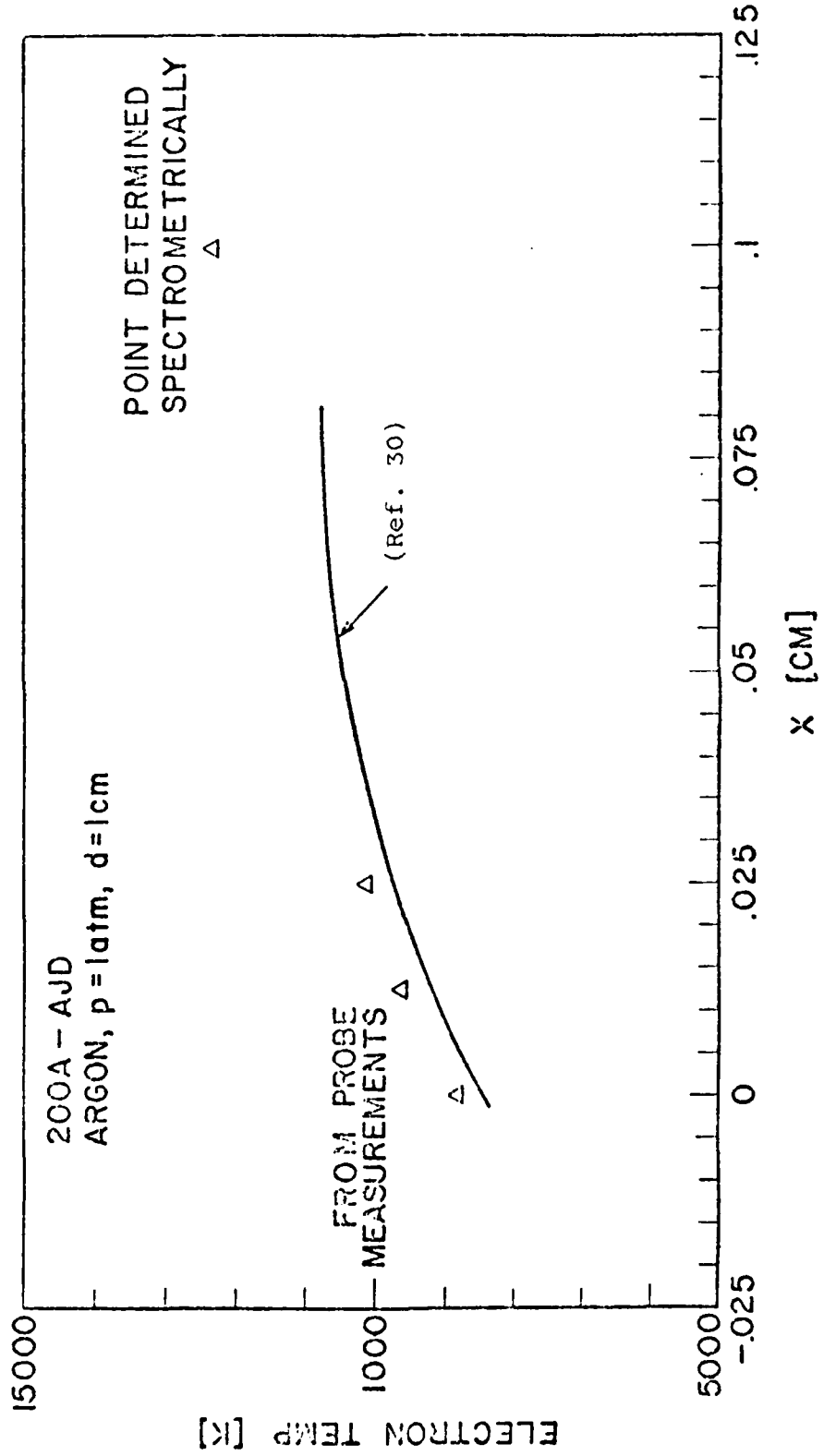


Fig. 11 Electron temperatures in front of the anode.

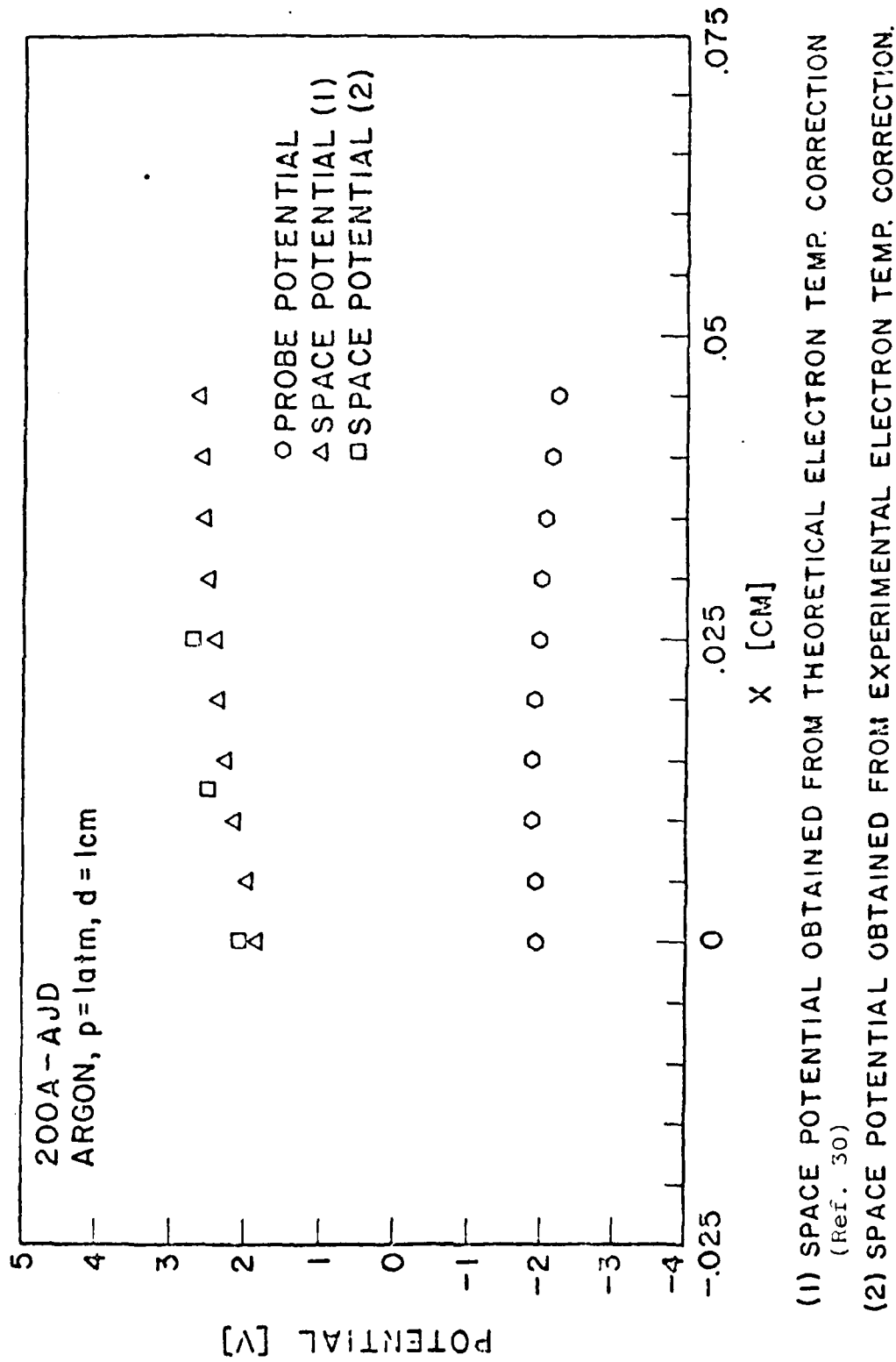


Fig. 12 Floating and space potentials in front of the anode.

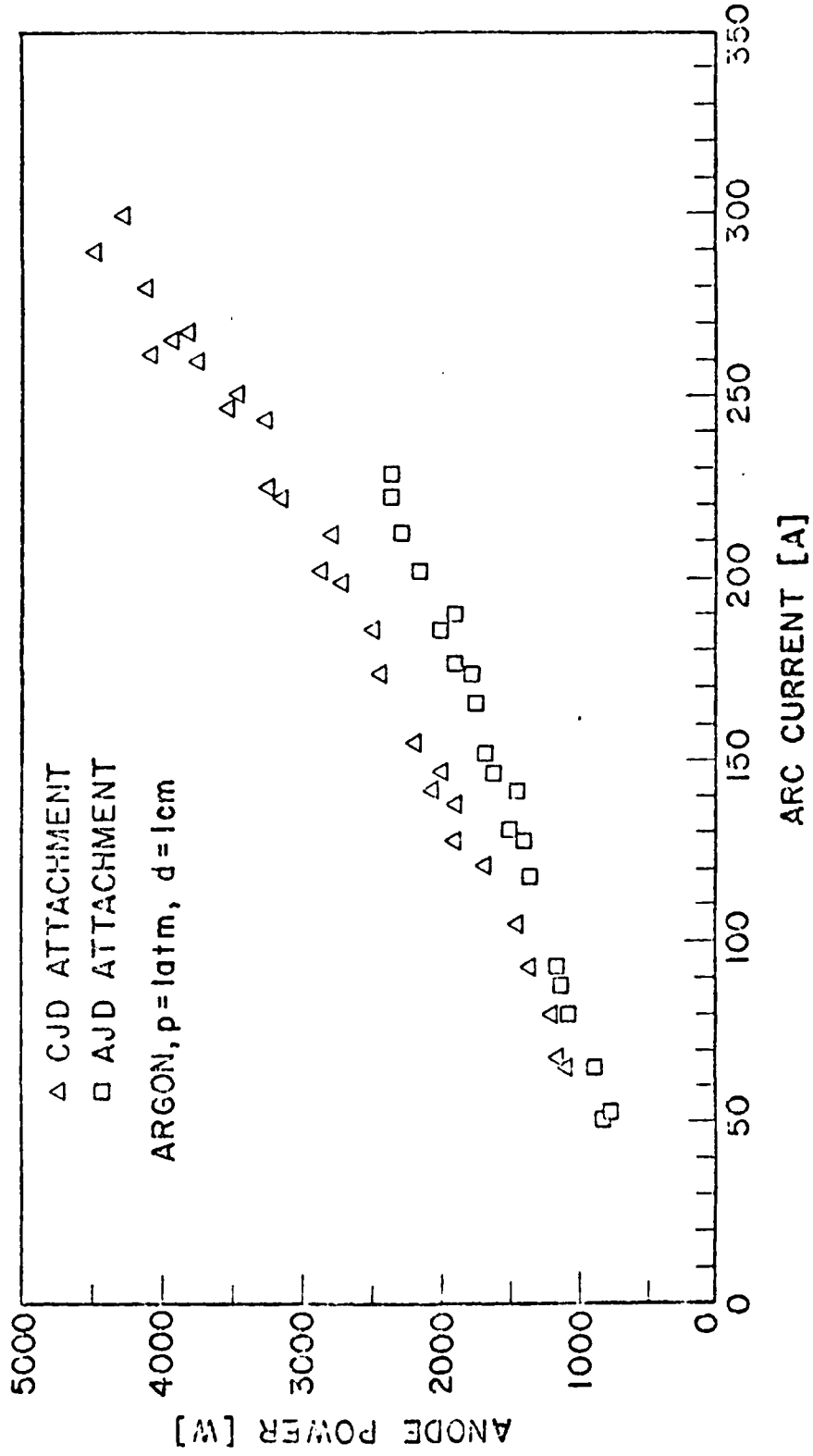


Fig. 13 Anode heat transfer (calorimetric).

ATTACHMENT MODE	$\frac{\bar{Q}_{elac}}{Q_a}$ %	$\frac{\bar{Q}_{conv}}{Q_a}$ %	$\frac{\bar{Q}_{cond}}{Q_a}$ %	$\frac{\bar{Q}_{rad}}{Q_a}$ %
AJD	83	0	12	5
CJD	51	33	11	5

Fig. 14 Average distribution of anode heat fluxes for an argon arc  
(p = 1 atm, 50 < I < 300 A)

If the anode fall is assumed to be positive, the energy carried by the electrons may be expressed by

$$Q_{\text{elec}} = I \left( \frac{5}{2} \frac{kT_e}{e} + U_a + \phi_a \right) \quad (2)$$

where  $I$  is the arc current,  $k$  the Boltzmann constant,  $e$  the elementary charge,  $U_a$  the anode fall and  $\phi_a$  the work function of the anode material. The results of calorimetric and probe measurements are incompatible with this equation. It seems that previous work which claimed positive anode falls underestimated convective heat transfer when the arc attaches in the CJD mode at the anode. Such an underestimate pretends a positive anode fall according to an overall energy balance. The fact that negative values of the anode fall ( $U_a$ ) have been measured and the obvious incompatibility of Eq. (2) with experimental data suggests another electron energy term (1)

$$Q_{\text{elec}} = I \left( 3.2 \frac{kT_e}{e} + \phi_a \right) \quad (3)$$

The factor of 3.2 applies for the conditions of this study and contains contributions due to diffusion (1); but this equation does not contain the anode fall. Therefore, there is no possibility of measuring anode falls indirectly (calorimetrically)

if the anode fall is negative. All experimental data obtained in this study are compatible with the electron heat transfer model of Eq. (3).

Overall heat fluxes to the anode may be expressed by

$$q_a = q_{\text{conv}} + q_{\text{cond}} + q_{\text{rad}} + j_e \left\{ \frac{5}{2} + \frac{e}{k} \frac{\phi}{\sigma} \right\} \frac{kT_e}{e} + \phi_a \quad (4)$$

with  $q_{\text{conv}} = 0$  for AJD mode

$q_{\text{conv}} \neq 0$  for CJD mode

In this equation  $q_{\text{conv}}$  represents convective heat transfer,  $q_{\text{cond}}$  conductive heat transfer,  $q_{\text{rad}}$  heat transfer by radiation;  $j_e$  is the current density at the anode,  $\phi$  is the thermal diffusion coefficient, and  $\sigma$  is the electrical conductivity. For the conditions of this study  $\frac{e\phi}{k\sigma} \approx 0.7$  as mentioned previously.

In general, conduction and convection cannot be separated. In this study, however, such a separation is useful because in the case of the AJD mode, convective heat transfer to the anode is negligible, but conduction is still present.

### 3.) Anode heat flux measurements in pulsed arcs

Most of the available data for anode heat transfer are based on steady arcs. Only a few investigators report anode heat flux measurements in transient arcs. Anode heat fluxes of  $10^8$  to  $10^9$   $\text{W/m}^2$  have been reported (19) using a technique based on

measurements of the time required for incipient melting of the anode surface.

Over the past years a powerful diagnostic method has been developed in this laboratory (20-23) for measuring local heat fluxes at the anode of high intensity arcs. Although the duration of an individual current pulse is only 200  $\mu$ s, the arc reaches after approximately 100  $\mu$ s a quasi-steady state, i.e., the results of these measurements will also apply to steady state arcs at the same current level.

The electrode configuration used for these measurements is illustrated in Fig. 15. The electrodes are housed in an environmental chamber permitting control of the operating gas atmosphere. A circular anode consisting of 0.025 or 0.051 mm thick metal foil is clamped in a rotationally symmetric holder. The cathode consists of a 0.47 cm diameter tungsten rod perpendicular to the plane anode with a 60 degree conical tip. The tip of the cathode is positioned 1 cm above the anode. The cathode tip is refinished and a new anode foil is used for each experiment.

The arc is operated as a short pulse. A capacitor bank power supply coupled to a lumped parameter network generates a square wave current pulse (5-10 kA) of 200  $\mu$ s duration. The rise time required to reach the full current is approximately 10  $\mu$ s.

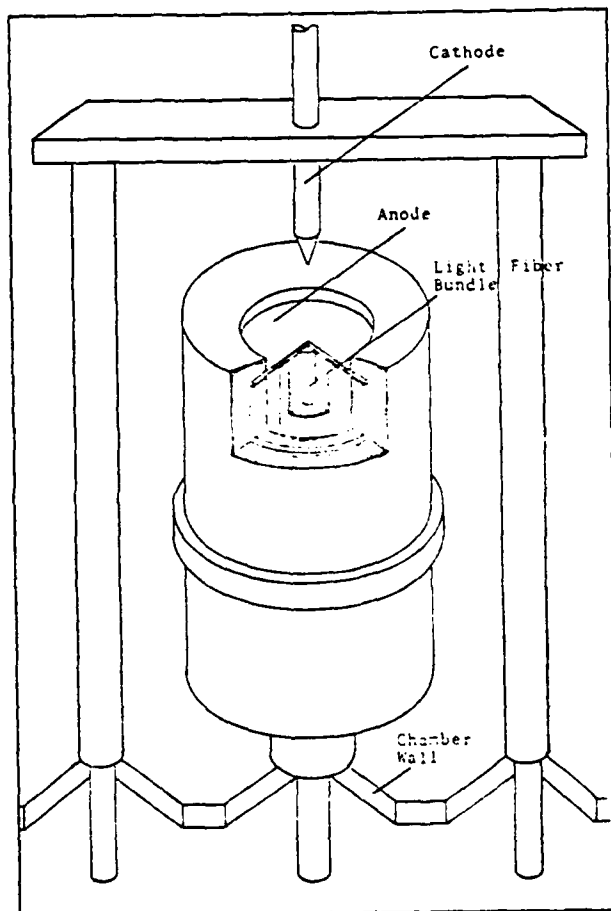


Fig. 15: Electrode Configuration for a pulsed arc.

Breakdown of the arc is accomplished by an overvoltage of approximately 12 kV applied to the electrode gap when the charged capacitor bank is connected to the network by an ignitron switch.

The method used for modeling the anode heat flux requires measurement of the anode rear face temperature history. This history is measured by using an optical technique developed in this laboratory (21,22). Infrared radiation emitted by the rear face of the anode is collected at the center of the anode during the discharge using a 3.2 mm diameter light fiber bundle transmissive to infrared light. The light fiber optics terminate at the photocathode of a RCA 7201 infrared sensitive photomultiplier tube. The voltage output of the photomultiplier tube is related to the infrared radiation intensity measured at the rear face of the anode. The voltage history of the photomultiplier tube, translated by a calibration into the anode rear face temperature history, is recorded during operation of the arc by a Biomation digital waveform recorder. Calibration is accomplished using materials and conditions identical to those during arc operation (21,22). The temperature history of the anode rear face is calculated and plotted by a resident microcomputer system using the corresponding calibration curve. Figure 16 shows an example of typical rear face temperature history measurement.

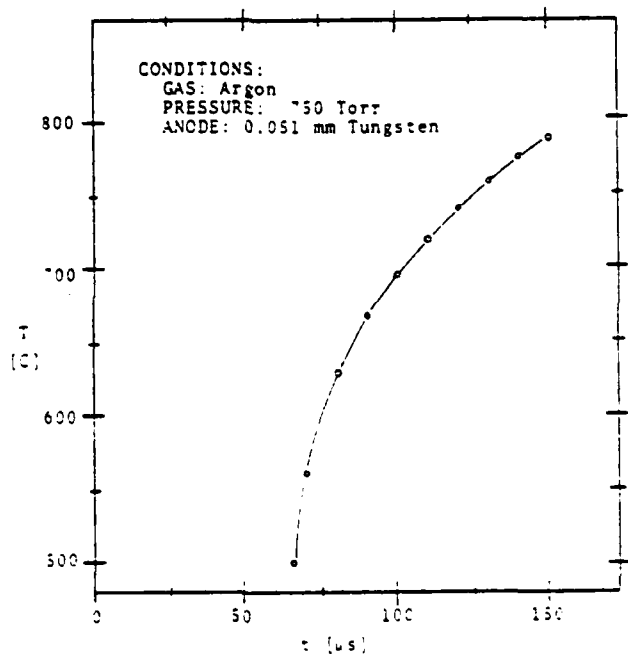


Fig. 16: Typical Measured, On-Axis, Anode Rear Face Temperature History

A high speed streak camera independently records the radius and the integrated radiation intensity of the arc as a function of time. The camera views the arc through a 0.051 mm slit oriented in a plane parallel to the anode and at a distance of approximately 2 mm above the anode. The image viewed through the slit is swept across the film during arc operation. A typical streak photograph of the anode attachment region is shown in Figure 17.

A finite difference method is used for calculating heat conduction through the anode and for determination of rear face temperature histories based on arbitrary anode front face heat fluxes. The input heat fluxes to the program are systematically modified until calculated and measured rear face temperature histories match. The input heat flux model required to match the experimentally measured rear face temperature history represents the desired anode heat flux to the anode surface facing the arc. The input heat flux which is used for the finite difference scheme consists of connected segments of linearly varying heat fluxes with respect to time. Development of the anode heat flux model requires correlation of information obtained from the high speed streak photographs and the rear face temperature history measurements.

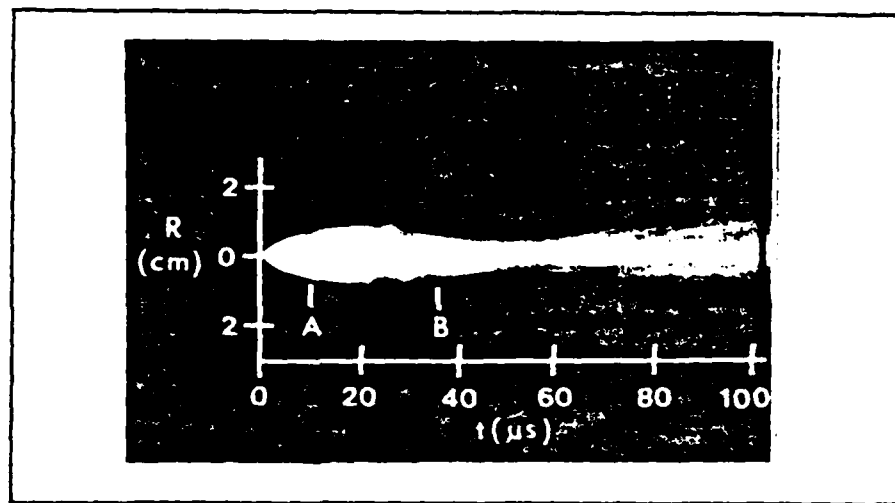


Fig. 17: Streak Photograph of the Anode Arc Attachment Region

Several simplifications are used to facilitate the modeling process. Only the region of the anode viewed by the light fiber bundle is considered. Radial heat conduction is neglected since the central region of the anode is heated rather uniformly over a radius large compared to the radius of the light fiber bundle. Rotational symmetry of the arc attachment is assumed and verified with the streak photograph data. These simplifications reduce the heat transfer situation at the anode to a one-dimensional problem. Estimates show that the ohmic heating of the material in the central region caused by the current is small and, therefore, this contribution is neglected. Only radiation heat transfer from the anode rear face is considered since convection losses through the surrounding gas are minimal during the 200  $\mu$ s run time of the arc. The rate of change of the input heat flux is sufficiently slow so that the second term of Fourier's heat conduction law may be neglected (24,25).

The solution of the heat conduction problem of the anode is impaired by the fact that the information at the anode rear face is smeared by heat transport through the anode material. In addition, information concerning the early part of the temperature history is lost due to poor response of the photomultiplier system at low anode surface temperatures. The high speed streak photograph data are used to provide the additional information

necessary to develop the model, in particular for the early stages of the arc.

The pulsed arc heat flux model has two distinct regimes. A transient heat flux regime dominates the first 100  $\mu$ s of arc operation, followed by a quasi-steady state heat flux for the remainder of the arc operating time. The heat flux at the anode is dominated by the energy transported by the electrons and consequently the model will be described in terms of current density.

During the first 10  $\mu$ s after arc initiation, the current increases rapidly as governed by the rise time characteristic of the power supply system. The streak photographs indicate that a highly luminous rapidly expanding plasma shell is formed during this period. Initial breakdown of the gap takes place along the electrode axis followed by a rapid increase in the radius of the hot plasma. The high luminosity of the region in the streak photographs indicates that a shell of plasma must be formed since the total energy dissipated in the arc during this time is insufficient to heat the entire volume to such high temperatures. The arc current is carried primarily by the highly ionized shell and the heat flux at the center of the anode is quite small. The shell expands rapidly until steady state current conditions are reached.

Further evidence of the relatively cool interior of the shell can be inferred from the input heat flux model required to match experimental data. The rear face temperature history indicates a very low heat flux at the center of the anode during this time. The peak heat fluxes occur at a radius large compared to the radius of the measurement area. The primary heat transport mechanism within the anode is relatively slow radial conduction. Conditions at the anode during the first 10-15  $\mu$ s are sketched in Figure 18.

The postulated plasma shell formation is consistent with the findings of Shih (26). Infrared photographs taken after interruption of an arc operating under similar conditions show circumferential hot rings formed during the early period of arc attachment. The photographs suggest an annular shaped attachment region of high current density.

After 10 to 15  $\mu$ s, the current reaches a steady state value and a transition takes place in the plasma current density distribution. The shell continues to expand slowly and reaches a maximum diameter 25-30  $\mu$ s after initiation of the arc. At the end of the shell formation period, the current density is relatively high within a thin annular region of approximately 1 cm radius at the anode surface. As the current becomes steady, the current density rises in the central portion of the arc and the shell

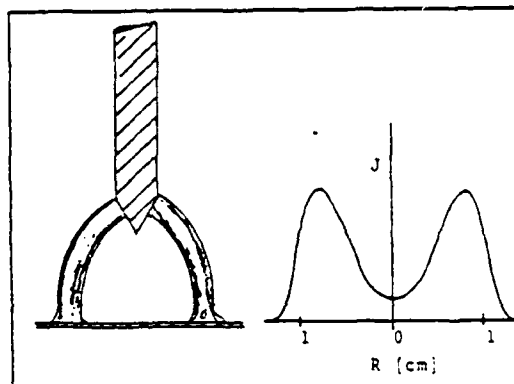


Fig. 18: Plasma Shell Formation and Current Density Distribution During the Initial 10-15  $\mu$ s of the Arc

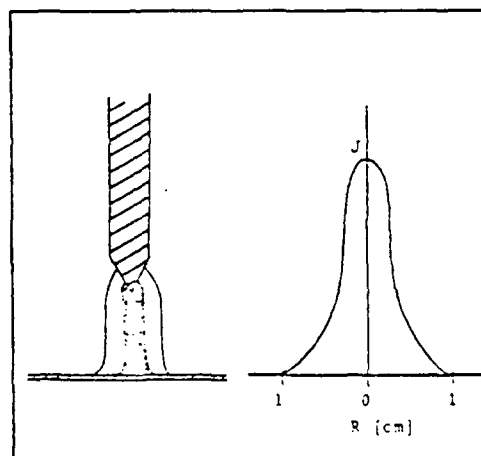


Fig. 19: Current Density Distribution Prior to arrival of the Cathode Jet at the Anode Surface

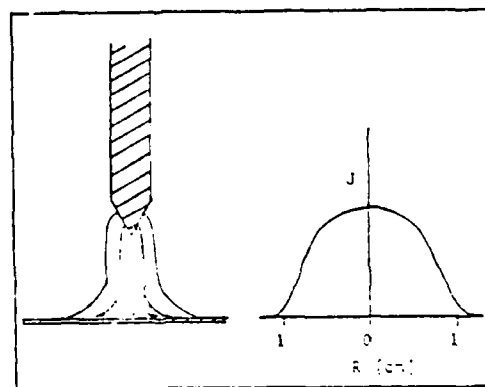


Fig. 20: Arc Attachment and Current Density Distribution During Quasi-steady Regime

region of the arc cools as the region of high current density shifts toward the center. The streak photographs show a decreasing diameter and decreasing light intensity of the shell region and an increase in intensity of the central region of the plasma. The shift of the luminous hot plasma region from the shell region to the central core of the discharge requires 10-20  $\mu$ s. The rear face temperature history also indicates a rapidly rising heat flux during the transition period.

After 35 to 40  $\mu$ s, the internal heat dissipation in the shell region has diminished and the cooled outer portion of the shell no longer appears on the streak photograph. A high intensity core of constant diameter, corresponding to the region of high current density, is formed and remains steady for 10-15  $\mu$ s. During this time the peak heat flux occurs at the anode center, as indicated by the rear face temperature history.

Strong MHD pumping forces acting at the cathode form a high velocity jet of plasma as soon as the arc current reaches appreciable levels (11). Calculations indicate that the jet velocity at the axis of the discharge may approach 700 m/s. A maximum of 15-20  $\mu$ s is required to traverse the gap at these velocities. It is suspected that arrival of the cathode jet contributes to the peak heat flux. The formation process and arrival time of the cathode jet is not yet well understood and is

the subject of continuing investigation. However, the high speed streak photographs show that rapid expansion of the anode attachment begins 50 to 60  $\mu$ s after initiation of the arc, suggesting that formation and traverse time for the jet together is approximately 50 to 60  $\mu$ s at 750 Torr. Conditions for the discharge during this time period are sketched in Figure 19.

Arrival of the cathode jet at the anode surface is followed by formation of a stagnation flow regime at the anode surface. The highly ionized jet spreads on the anode surface and the current density distribution changes rapidly. The streak photographs indicate an increase of the plasma radius with time and a reduction in intensity of the hot central core. The anode attachment region increases in diameter by a factor of 2 or 3 during the initial 25  $\mu$ s of jet impingement. The hot core region expands into a larger portion of the attachment area during this time period. The rear face temperature history also indicates a rapid reduction in the anode heat flux corresponding to the spreading of the jet on the anode surface. The heat flux at the center decreases rapidly in spite of convective heat transfer induced by the cathode jet. The energy transport by the electrons carrying the arc current represents the dominating heat transfer mechanisms; the rapid reduction of current density at the center results in decreasing heat flux at the central region.

A quasi-steady state regime exists after the flow induced by the cathode jet becomes fully developed. A slow decrease in the heat flux is characteristic for the remaining 100  $\mu$ s of arc operation. The heat flux diminishes slowly as the anode surface temperature rises and the anode attachment area increases. However, changes in the heat flux during this time are small compared to the earlier transient regime and consequently this regime is referred to as a quasi-steady state. Heat fluxes experienced during this period should be comparable to a steady state arc operating under similar conditions. Quasi-steady state attachment conditions are sketched in Figure 20.

A typical match between calculated and measured rear face temperature histories is illustrated in Figure 21. The solid line represents the finite difference scheme calculated rear face temperature history. In this case, three representative sets of data collected at 750 Torr in argon have been matched.

The heat flux model for 750 Torr pressure in argon is shown in Figure 22. The heat flux model is applicable only at the center region of the anode. An initial period of low heat flux corresponds to the shell formation time when the current density is high at a radius large with respect to the measurement area. A steeply rising heat flux follows as the current density increases to its maximum value along the centerline of the arc. Peak heat

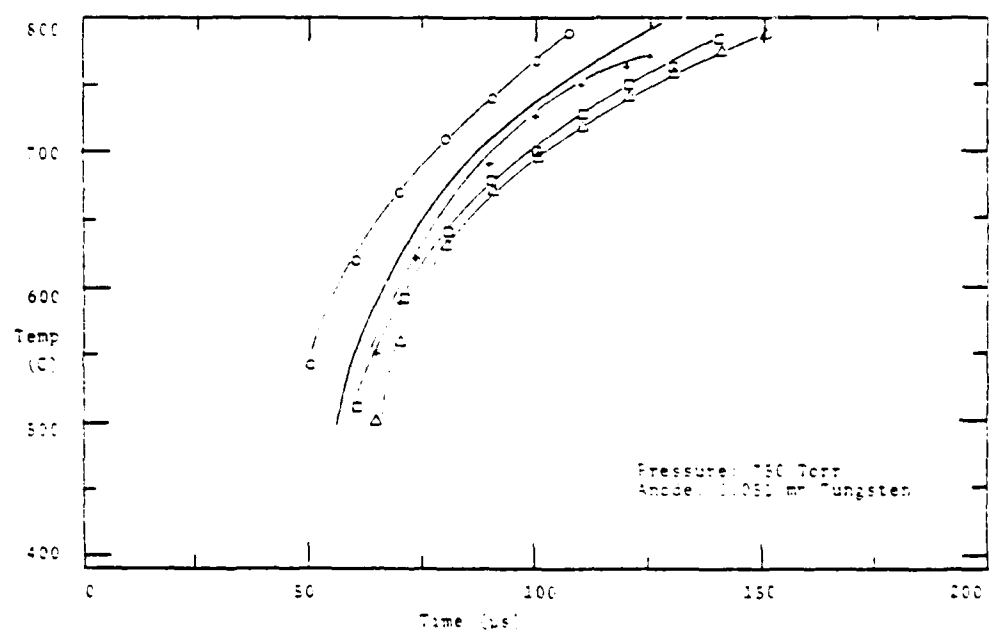


Fig. 21: Measured and Calculated Rear Face Temperature Histories in Argon Gas at 750 Torr Pressure

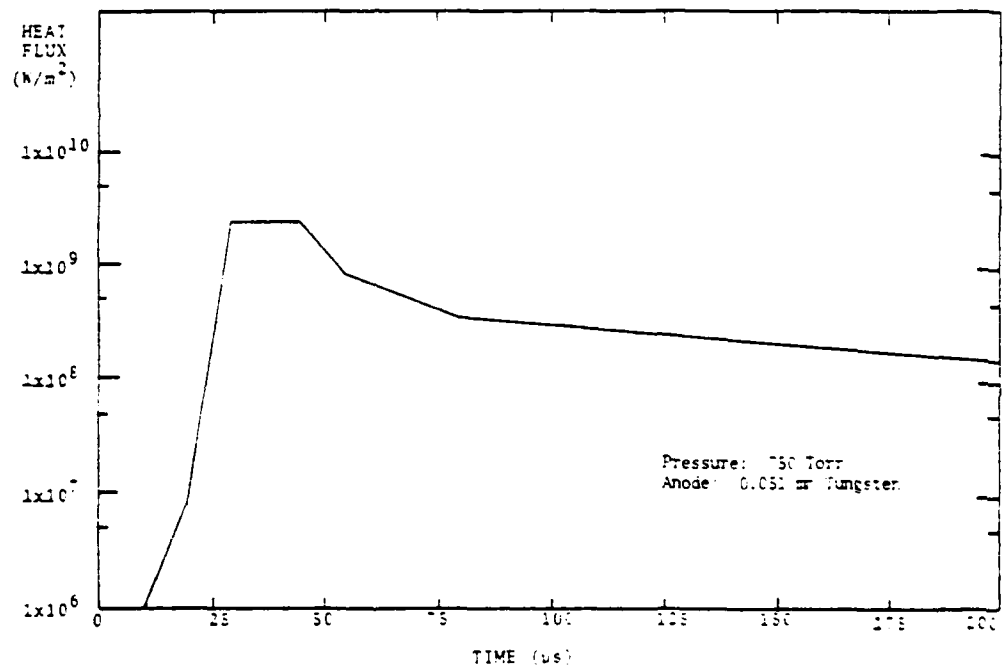


Fig. 22: Anode Heat Flux Model for Argon Gas at 750 Torr  
Operating Pressure

fluxes of  $2 \times 10^9 \text{ W/m}^2$  are typical at 1 atm pressure in argon. The heat flux decreases as the cathode jet causes an enlargement of the anode arc attachment area, simultaneously reducing the peak current density and, therefore, the peak heat flux. A relatively flat region of quasi-steady state heat flux follows, as the stagnation flow of the cathode jet becomes fully developed and, at the same time, the anode surface temperature increases slowly. Steady state heat fluxes from  $9 \times 10^7$  to  $1.5 \times 10^8 \text{ W/m}^2$  have been measured at 1 atm pressure in argon as working fluid.

IV. References

1. H. A. Dinulescu and E. Pfender, J. Appl. Phys. 51(6), 3149 (1980).
2. E. Pfender, "Electric Arcs and Arc Gas Heaters," Gaseous Electronics, Vol. 1, 291 (1978); Academic Press, Inc.
3. D. M. Chen and E. Pfender, IEEE Transact. in Plasma Sci., Vol. PS-9, No. 4, 265 (1981).
4. D. M. Chen, K. C. Hsu, and E. Pfender, Plasma Chemistry and Plasma Processing, Vol. 1, No. 3, 295 (1981).
5. W. Finkelnburg and H. Maecker, "Elektrische Bögen und thermisches Plasma," Encyclopedia of Physics, ed. S. Flügge, Vol. XXII, 254 (1956); Springer-Verlag, Germany.
6. G. Ecker, "Electrode Components of the Arc Discharge," Ergebnisse der exakten Naturwiss., Bd. 33, 1 (1961); Springer-Verlag, Germany.
7. T. H. Lee and A. Greenwood, ARL report 63-163 (1963).
8. T. H. Lee, A. Greenwood, W. D. Breingan, and H. P. Fullerton, ARL report 64-152 (1964).
9. T. H. Lee, A. Greenwood, and W. D. Breingan, Proc. of the 7th Internat'l. Conf. on Phenomena in Ionized Gases, Vol. I, Part I 670; Part II 675 (1966); Građevinska Knjiga Publishing House, Beograd.
10. A. E. Guile, IEE Reviews, Vol. 118, 1131 (1971).
11. H. Maecker, J. Phys. 141, 198 (1955).
12. T. W. Petrie and E. Pfender, Weld. J., Res. Suppl, Vol. 49, 588-S (1970).
13. C. J. Allum, "Gas Flow in the Column of a TIG Welding Arc", J. Phys. D., 14, 1041 (1981).

14. S. Ramakrishnan and B. Nuon, "Prediction of Properties of Free-Burning Welding Arc Columns", *J. Phys. D*, 13, 1845 (1980).
15. J. J. Lowke, "Simple Theory of Free-Burning Arcs", *J. Phys. D.*, 12, 1873 (1979).
16. J. E. Fink, "Theory and Computation of the Characteristics of the Thermal Electric Plasma Arc for Chemical Engineering Applications", *Chem. Eng. Commun.* 5, 37 (1980).
17. K. Etemadi and E. Pfender, *Rev. Sci. Instrum.* 53, 255 (1982).
18. N. Sanders, K. Etemadi, K. C. Hsu, and E. Pfender, *J. Appl. Phys.* 53(6), 4136 (1982).
19. K. T. Shih and R. Dethlefsen, "Anode Heat Flux Density of High Current Arcs", *J. Heat Transfer* 93 (Series C), 1, 119, 1971.
20. D. Johnson and E. Pfender, IEEE, TPS, Vol. PS-7, No. 1, 44 (1979).
21. J. L. Smith, "Anode Heat Flux in High Current Arcs," Ph.D. Thesis, University of Minnesota, August 1974.
22. J. L. Smith and E. Pfender, IEEE Transactions on Power Apparatus and Systems, Vol. PAS-95, No. 2, 704 (1976).
23. J. L. Smith and E. Pfender, *Rev. Sci. Instrum.*, Vol. 47, No. 9, 1056 (1976).
24. M. H. Sadd and J. E. Didlake, "Non-Fourier Melting of a Semi-Infinite Solid", *J. Heat Transfer* 99 (Series C) 1, 25, 1977.
25. D. C. Wiggert, "Analysis of Early Time Transient Heat Conduction by Method of Characteristics". *J. Heat Transfer* 99, (Series C), 1, 35, 1977.
26. K. T. Shih, "Investigation of Electrode Erosion in High Current Electric Arcs", Report from March 1 to March 31, 1969, ARL Contract F33615-67-1386.

SURVEY OF GAS FLOW AND HEAT TRANSFER EFFECTS ON  
PERFORMANCE OF GAS SPARK GAPS\*

by

John M. Kuhlman  
Dept. of Mechanical Engineering and Mechanics  
Old Dominion University, Norfolk, VA 23508

Abstract

A survey is given of typical previous high power repetitive gas flow spark gaps, as to their geometries, performance and flow diagnostic methods. Also, examples are given of more detailed flow diagnostic studies made in other, previous spark gap studies. The types of related theoretical models are briefly summarized, as are the general, known effects of flow upon spark gap performance. Recommendations for future efforts to relate flow phenomena to spark gap performance are made.

Introduction

It is known that use of gas flow between the electrodes of a high power, repetitively switched gas spark gap can lead to dramatic performance gains in terms of switch recovery and rep rate. Also, electrode cooling is enhanced, while electrode erosion may also be enhanced. However, presently, theoretical modeling and experimental measurements of detailed, time-dependent flow physics in gas flow spark gaps are both difficult and few in numbers. Certainly it appears that a great deal remains to be learned about the physics of gas flow spark gaps before any type of simple design criteria or guidelines can be established to meet specific rep rate or lifetime performance goals.

---

\*For presentation at "Repetitive Spark Gap Operation" workshop, Jan. 17-19, 1983 at Tamarron, Colorado. Sponsored by DoD.

The purpose of this paper, then, is to survey several previously developed representative gas flow spark gaps. Their geometries will be described, as well as gas type, pressure, voltage and current levels, waveform shape, and triggering mechanism. Also, the types of flow diagnostics used in these previous rep-rated spark gap investigations will be described, along with rep rate performance results and any erosion or switch efficiency measurements.

Related to these specific spark gap hardware examples, examples of previous spark gap studies where more detailed flow measurements were made will be given, and a brief survey of the status of theoretical modeling of flow phenomena in gas flow spark gaps will be given. Most of these previous studies where more detailed experimental measurements or theoretical models have been obtained will not be specifically for the type of high rep rate gas blown spark gaps surveyed in the first portion of the paper, but instead will primarily consist of various arc phenomena in shock tubes, current interrupting switches, or laser triggered sparks in a stationary gas. Finally, the paper concludes by listing several known, general effects of flow upon gas spark gap performance, and by listing several suggested areas for more detailed study. An introduction to compressible fluid flow is given in the Appendix.

#### Examples of Previous High Rep Rate Gas Spark Gaps-Geometry and Performance

In this section several previous types of repetitive gas spark gaps will briefly be described, primarily as to their geometry, electrical and flow characteristics, and maximum rep rate achieved. Further details of the types of flow measurements made for each spark gap will be given in the following section of the paper. A summary of the performance data to be discussed in this section has been given in Table 1; where these previous flowing gas spark gaps have been listed in chronological order. Performance data listed in

Table 1 are those given in the references, and may not be representative of more recent efforts.

Baranov et. al. (1976)<sup>(1)</sup> describe using a two-dimensional converging-diverging nozzle to establish a supersonic flow of a mixture of CO<sub>2</sub>, N<sub>2</sub> and He at Mach 2 between a pair of electrodes embedded in the flow channel walls, as shown schematically in Fig. 1, taken from their paper. The flow channel between the electrodes was 1.5 cm high by 25 cm wide. The cathode consisted of 45 thin plates mounted on 0.5 cm centers which were 4 cm in length along the flow axis. The anode was 8 cm long by 22 cm wide. This flow channel was mounted between a gold coated spherical mirror and a plane germanium plate which formed the resonator for a CO<sub>2</sub> laser; the resonator axis could be moved along the flow axis. Laser pulses of duration 20-40  $\mu$ sec and energy of 0.1 Joule/pulse were obtained at a repetition frequency of 4-5 kHz at a voltage of 30 kV. It was noted that laser pulse duration depended upon the position of the resonator axis along the flow channel, where this pulse duration was approximately equal to the transit time of the plasma across the resonator. No details were given of gas pressures used, while the gas temperature was specified as between 200-300°C. The flow channel emptied into an evacuated receiver chamber.

Rebe (1976)<sup>(2)</sup>, in an invention disclosure document, describes a supersonic spark gap switch of a cylindrical geometry, as shown schematically in Fig. 2. Two hollow cylindrical electrodes are utilized, and the airflow is brought radially inwards from outside of the cylindrical electrodes, flows between the two electrodes, and exits axially through the hollow electrodes. The tips of the electrodes are contoured so as to form an annular converging-diverging nozzle, the outer section of which is made of an insulating material. Arcing is designed to occur in the supersonic flow region between

the pair of electrode inserts. A supply pressure of 54 psia is necessary to establish this supersonic flow, assuming that the flow exhausts to the atmosphere. A rep rate of 500 Hz is claimed at a voltage of 20 kV. No details are given of the current magnitude or pulse shape.

A second coaxial geometry has been described by Faltens et. al. (1978)<sup>(3)</sup> of the Lawrence Livermore Laboratory. As shown in Fig. 3, this spark gap mounts to a water Blumlein and consists of an annular cathode surrounding a cylindrical anode. Gas flows from an annular plenum chamber between the electrodes and exits via a second annular plenum. Note the third, hollow trigger electrode mounted upstream of the anode and cathode. A gas mixture of 6-8% SF<sub>6</sub> in nitrogen has been used, supplied from a pressure tank by a blower. Gas velocity between electrodes was estimated to be 50 m/s. A rep rate of 1 kHz was observed at 220 kV, 42 kA with a gas pressure of 150 psi. The pulse width was 50 ns, with a 12 ns risetime and 2 ns jitter. Jitter was observed to increase as the voltage was decreased. A rep rate of 1.8 kHz was obtained at 150 kV. Lifetime tests at full voltage but reduced rep rate for 10<sup>5</sup> shots showed very little wear on anode or cathode. However, some noticeable wear was observed on the trigger electrode. Some deposition of arc debris could be seen on the insulator material. A projected lifetime was estimated to be in excess of 10<sup>7</sup> shots.

A third coaxial geometry developed by Malyuta and Mezhevov (1979)<sup>(4)</sup> is shown schematically in Fig. 4. In this spark gap, flow of N<sub>2</sub> is fed axially around the first electrode, through a small hole in a ceramic diaphragm, and exits axially over the second electrode. Triggering is achieved through use of a small third electrode which penetrates the spark gap from the side. Electrode separation is about 2 cm, while the hole in the diaphragm is of 4-8 mm diameter. This leads to a cross sectional area for flow that is one tenth

the flow area around the electrodes, and results in a high (but unspecified) flow velocity. This switch was used to switch energy stored in capacitor banks to a supersonic CO<sub>2</sub> laser. Sustained operation at voltages of 40 kV and currents of 1-10 kA were observed at repetition rates of 4 kHz. The pulse width was 100 ns, and the observed spread in triggering was 0.5  $\mu$ s. Two pulse tests of the switch gave a recovery time of only 75  $\mu$ s, so it was concluded that the switch should be capable of rep rates up to approximately 10 kHz.

Ramrus and Shannon (1980)<sup>(5)</sup> of Maxwell Laboratories describe a fourth coaxial geometry spark gap shown in Fig. 5. Flow of dried air is fed through the nested-pair electrode, and radially inward between the two electrodes, and exits axially through a hole in the center of the second electrode. Triggering was achieved by a UV source mounted along the flow axis downstream of the two electrodes. Rep rates of up to 250 Hz were achieved at 100 kV with a peak current of 10 kA. Flow rates of 35 SCFM at a supply pressure of 40 psig were necessary, leading to air velocities of approximately 3 m/s in the discharge pipe; it is anticipated that significantly higher gas velocities were achieved between the electrodes. Switch jitter was observed to be minimized when the nested-pair electrode was charged negatively, and when the UV trigger was used.

A fifth coaxial geometry is shown in Fig. 6, taken from Naff et. al. (1980)<sup>(6)</sup>, of Physics International. This spark gap uses a vortex swirl airflow concept to improve heat transfer and arc thermal recovery by increasing turbulence levels between the electrodes. The switch consists of a pair of annular electrodes, and a 3/4 inch thick annular midplane trigger electrode. Air flow is injected tangentially around the electrodes, swirls radially inwards, and exits axially through holes in the centers of the electrodes. This switch was tested at a rep rate of 1 kHz for  $11 \times 10^6$  shots,

at a holdoff voltage of 52 kV and peak current of 20 kA. The pulse width was 98 ns and the jitter was 5 ns. The switch was operated successfully at rep rates up to 1850 Hz, the upper limit of the trigger circuitry. Inlet air pressure was maintained constant at 65 psig for the first 7 million shots, and then was reduced thereafter to maintain a negligible misfire rate. Air flowrate was maintained between 77-115 SCFM, yielding an interelectrode flushing time of 0.25 ms. Detailed erosion profiles were obtained for all three electrodes after 7 and 11 million shots, and switch energy dissipation was measured as approximately 25 percent.

Watson (1980)<sup>(7)</sup> of Air Research Mfg. Co. described a second spark gap, shown in Fig. 7, which does not use a coaxial geometry. The application envisioned for this switch is to furnish pulsed power to a KrF laser. This switch consists of three spherical electrodes (Fig. 7), mounted transversely to the airflow between the electrodes. The middle electrode is mounted to a midplane plate, and is fitted with a hole to provide a cooling airflow. Observed performance of this switch at a voltage of 30 kV was a rep rate in excess of 1 kHz for 100 ns pulses with 20 ns risetime and 4 ns jitter. Airflow was supplied at 100 psia, and air velocities between electrodes were measured to be approximately 35 m/s. Peak current was relative low, at 0.5 kA. A total of 39 million shots were fired, and erosion rates were determined, along with switch losses. Maximum firing frequency was observed to be 1700 Hz at 27 kV.

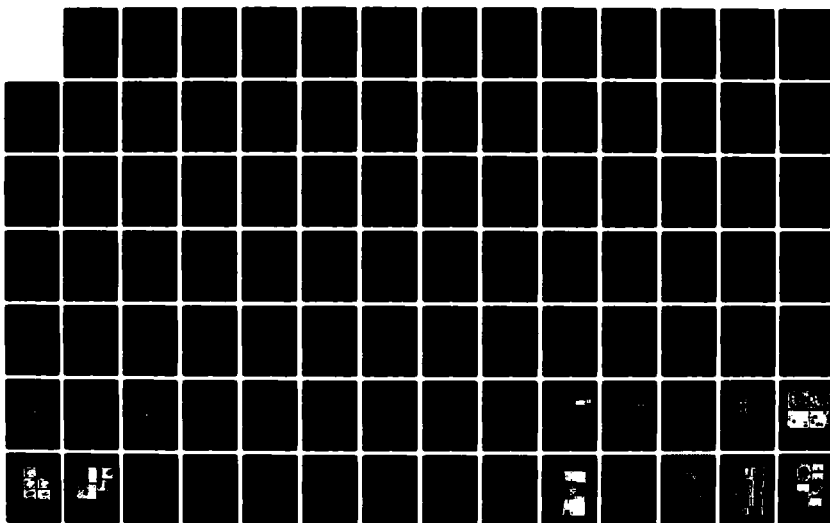
Finally, Molen et. al. (1982)<sup>(8)</sup> have recently presented results for a gas blown spark gap shown in Fig. 8. This spark gap consisted of a two-dimensional converging-diverging nozzle made of plexiglas fed through a pressure regulating valve from two large storage tanks and an air compressor. Two brass electrodes were mounted flush with the flow channel walls in the

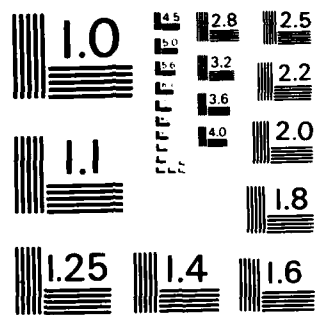
AD-A132 688 WORKSHOP ON REPETITIVE SPARK GAP OPERATION HELD AT  
TAMARRON COLORADO ON JANUARY 17-19 1983(U) BATTELLE  
COLUMBUS LABS DURHAM NC M O HAGLER ET AL. 20 MAY 83  
UNCLASSIFIED DAAG29-81-D-0100

2/4

NL

F/G 9/1





MICROCOPY RESOLUTION TEST CHART  
NATIONAL BUREAU OF STANDARDS - 1963 - A

viscosity of the flow channel throat. The flow channel was fitted with static pressure taps to determine the pressure distribution, and indirectly the velocity distribution, in the flow channel. This gap was not operated in a continuously repetitive mode, but instead was tested in a two-pulse mode to determine the recovery time for the gap as a function of air pressure and the resulting air velocity. At a breakdown voltage of nominally 10 kV, with a peak current of about 1 kA, a minimum total recovery time of approximately 0.2 ms was obtained with a supply air pressure of 8.05 psig. This pressure led to approximately sonic air velocities between the electrodes. The measured recovery times indicate a maximum possible rep rate of approximately 5000 Hz. Voltage risetime was 10  $\mu$ s. Further performance and flow diagnostic results for this spark gap will be presented below.

In comparing these eight previous spark gap switches, it is interesting to note that while there is a surprising range of geometries used, a majority of these geometries are cylindrically symmetrical, with only three gaps being of a two dimensional geometry. Two of these 2-D spark gaps had electrodes which were mounted flush to the flow channel walls, while one (Watson, 1980) utilized spherical electrodes which protruded into the flow channel. From the performance data summarized in Table 1, it is not clear which geometry is indeed to be preferred for maximum rep rate. Also, note that one of the 2-D switches which achieved a rep rate of 4-5 kHz (Baranov et. al, 1976) was at a very low current level. All of the spark gaps that were successfully operated in a repetitive mode used some sort of third trigger electrode. Finally, the use of tangential, swirling gas injection (Naff et. al. 1980) to generate turbulence and enhance electrode heat transfer is an interesting concept, but it appears unclear as to whether this flow mechanism is beneficial or not.

Previous High Rep Rate Gas Spark Gaps--Flow Diagnostics

The types of flow and heat transfer related measurements which have been made in the repetitive spark gap investigations which have been summarized in the previous section will now be described. This will in turn be followed by a brief description of the types of more detailed flow diagnostics which have been made in other spark gap studies, primarily without any gas flow between the electrodes. It is felt that use of these more detailed diagnostic methods will be necessary to better relate the effects of flow to performance of a high power gas flow spark gap.

Baranov et. al. (1976) and Rebe (1976) mention no flow or heat transfer diagnostic measurements other than to measure (and control) the supply pressure and exit pressure. Faltens et. al. (1978) measured supply pressure, pressure drop across their spark gap, and volumetric gas flow rate of their N<sub>2</sub>-SF<sub>6</sub> mixture. Results were presented for the observed switch rep rate as a function of gas pressure and applied voltage, reproduced in Fig. 9. At fixed gas pressure, higher voltage led to decreased rep rate, while higher gas pressure increased the rep rates achieved at fixed voltage. Malyuta and Mezhevov (1980) measured, and varied, their N<sub>2</sub> supply pressure. Ramrus and Shannon (1980) measured and varied their air supply pressures and flow rates. Naff et. al. (1980) presented measured pressure drops across their spark gap as a function of air supply pressure and flow rate, but no measurements were made of the spark gap recovery characteristics as a function of air pressure or flow rate. Also measured were air inlet and outlet temperatures, from which switch losses were determined to be approximately 25 percent. In summary, these first six investigations did not make any detailed flow measurements inside the actual spark gap, and certainly did not investigate the details of the time history of the flow and thermal characteristics of the

gap while the arc existed.

Watson (1980) measured air supply pressure, temperature and volume flow rates, but also measured a detailed average velocity distribution in the flow channel between the electrodes. Also presented was a picture of the spark gap in operation, showing the arc location. However, again no time-dependent, quantitative measurements were made of flow characteristics in the gap.

Molen, Kirby and Kuhlman (1982) again measured air inlet pressure and temperature and exit pressure, but also measured the axial static pressure distribution along the flow channel, both upstream and downstream of the electrodes. From these measured static pressure data the average flow Mach number and velocity could be computed; these results indicated the flow over the downstream ends of the electrodes to have been supersonic for higher supply pressures. Schlieren flow visualization was utilized to observe the steady-state position of shocks which occurred at the higher supply pressures, downstream of the point of minimum electrode separation. Photographs taken of the shock location were of very poor quality, due to the poor optical quality of the plexiglas sides of the flow channel, and hence will not be presented herein. Finally, video records of the flow between the electrodes were utilized to determine the locations of the arcs formed during the two-pulse testing of the spark gap. These optical records showed that the second arc often occurred downstream of the first, away from the location of the steady-state minimum value of pressure times electrode separation,  $pd$ , as will be shown below.

The two-dimensional converging-diverging nozzle geometry used by Molen et. al. (1982) has been shown in Fig. 8. Minimum electrode separation was 0.125 inches; the brass electrodes were one inch wide by nominally three inches along the flow direction, while the flow channel was four inches wide.

Pairs of voltage pulses (10-30 kV), separated by a variable delay, were applied to the gap by using a 0-30 kV DC power supply to charge a pair of 0.167  $\mu$ F capacitors which were discharged using a pair of thyratrons. No triggering electrode was used for these experiments; instead an overvoltage was applied to initiate self-breakdown of the gap. For various air velocities, and various time delays between the first and second voltage pulses, as shown in Fig. 10, the two voltage amplitudes were recorded using a storage oscilloscope.

Twenty-five to fifty two-pulse bursts, repeated at five second intervals, were recorded and analyzed manually at each air velocity and time delay to determine gap recovery as the ratio of the average breakdown voltage for the second pulse, divided by the average breakdown voltage for the first pulse. Also recorded separately, using the video camera, were the physical locations of first and second pulses.

Examples of the measured axial static pressure distributions for air supply pressures of 2 and 8 psig are shown in Fig. 11. Axial distance has been normalized by the minimum electrode separation, or nozzle throat,  $d_{throat}$ , and pressures have been normalized by the supply, or stagnation pressure. The pressure falls to a minimum value just downstream of the nozzle throat and then rises slightly. These pressure distributions match well those obtained using isentropic, one dimensional gas dynamics, up to the nozzle throat. Poor agreement between theory and experiment downstream of the throat is indicative of flow separation in the diffuser section. Velocities calculated from the pressure data have been shown in Fig. 12; note that the flow was nearly sonic (approximately 950 ft/s) at the throat for the higher stagnation pressure (8 psig), while the air velocity at the throat was approximately 500 ft/s at a stagnation pressure of 2 psig. Similar data were

obtained at higher stagnation pressures; these data indicated a region of supersonic flow downstream of the nozzle throat which was terminated by a shock. The length of this supersonic flow region increased as the stagnation pressure was increased. Figure 13 displays the steady-state pd product distribution along the axis of the gap. For these two stagnation pressures (2 and 8 psig) the minimum pd value was found to be just downstream of the nozzle throat, or the axial position of minimum electrode separation. For higher stagnation pressure values, the establishment of a region of supersonic flow downstream of the nozzle throat resulted in dramatic pressure decreases downstream of the throat, such that the pd minimum was moved appreciably downstream of the throat. It was determined through analysis of the video records of arc location along the gap that the arc for the first pulse consistently was located at this axial position of minimum pd product. However, as will be shown, this was not the case for the second arc.

Recovery data for this gap at stagnation pressures of 2 psig (Fig. 14) and 8 psig (Fig. 15), labelled slow speed and medium speed respectively, have been compared with gap recovery data with no flow in Fig. 16, where a percent recovery has been plotted versus the time delay between first and second pulses. Note that while complete recovery of the gap took about 5 ms with no flow, the gap was found to recover completely in about 0.2 ms for the slow speed case. Initially, recovery was even more rapid for the medium flow speed, but for some unknown reason complete recovery was not obtained at this flow velocity until the time delay approached 10 ms. It was believed that this may have been due to contamination of the electrodes by oil from the air compressor used to charge the air supply tanks. Comparison of recovery results with no flow and at low speed ( $p_{stag} = 2$  psig), however, does clearly indicate an order of magnitude decrease in the recovery time for this spark

gap when an air flow is used.

Finally, through analysis of the video records of arc locations, it was determined that for some interpulse time delays, the second arc consistently occurred downstream of the first. Average separation distances between the first and second arcs are shown in Fig. 17 for the slow speed case ( $p_{stag} = 2$  psig), and in Fig. 18 for  $p_{stag} = 8$  psig. As the delay was increased, the interpulse spacing increased, until a value of the time delay was reached where the second arc was observed to jump back upstream to the location of the first arc; ie, the point of minimum pd. Also shown on Figs. 17 and 18 are solid curves of the convection distance of the debris from the first arc, obtained using the velocity data presented in Fig. 12. These curves match the data quite well, indicating that the second arc was occurring at the axial location of the debris from the first pulse. Also, the maximum interpulse separation distance observed was approximately equal to the distance from the location of the first arc to the downstream ends of the electrodes. Thus, once the first arc products had convected past the downstream ends of the electrodes, the location of the second arc was the same as that of the first arc. Comparison between Fig. 16 and Figs. 17 and 18 further reveals that this time for the first pulse debris to leave the interelectrode region is a good measure of the recovery time for this spark gap. These results, then, indicate that a key spark gap performance flow parameter relating to rep rate is the gas transit time between electrodes, assuming that recovery times smaller than the relaxation time of the arc plasma are desired.

#### Examples of Flow Diagnostic Measurements in Other Spark Gap Studies

In summary, while this last study (Molen et. al., 1982) has begun to go inside the spark gap to make detailed flow diagnostic measurements, none of the eight examples of gas flow spark gap studies described above have made any

attempts at documenting the time history of arc location and expansion, or gas temperature, electrode temperatures, or of propagation of arc-generated shock waves, or of the generation of and effects of turbulence on spark gap performances. Several of these flow phenomena have been studied previously in other spark gap work, primarily for gaps with no mean gas flow, or for gaps with flow which were not intended for fast, repetitive switching applications, as will now be described.

Scholz and Anderson (1970)<sup>(9)</sup> describe use of a simple T shock tube shown in Fig. 19 to study propagation of arc-generated shock waves. Two tungsten electrodes in the top of the T-shaped glass tube were energized via a capacitor bank, to generate an arc in the tube. This arc generated a shock wave which propagated down the vertical leg of the tube. A pair of moveable, enclosed photomultiplier tubes fitted with slits were used to determine the propagation speed of the luminous arc front along the tube, as shown in Fig. 20, as taken from Scholz and Anderson. An initial, accelerating phase of front propagation may be seen, which occurred during the time of energy addition to the front. This was followed by a phase of blast wave expansion, after the capacitors had been discharged, where the shock speed decreases proportional to the negative one half power of position along the tube (Taylor, 1950)<sup>(10)</sup>. Thus, the propagation of the shock, or heat wave, generated by the arc, and the flow of the plasma behind it, was observed to be accelerated during the time of energy input, and decelerated thereafter. Also, a Paschen curve was determined for this geometry, and the average plasma conductivity was measured.

Stabnikov and Tombak (1972)<sup>(11)</sup> utilized a Q-switched ruby laser to record holograms of the formation of an arc between a pair of electrodes with no initial gas flow, as shown schematically in Figs. 21 and 22. Pulsewidth

was less than 150 ns, with a risetime of nominally 10 ns. The initial spark discharge location and arc channel expansion were clearly recorded (Fig. 21), while at later times laser shadowgraphs (Fig. 22) indicated a separation between the inner arc channel and the outwardly propagating shock. Initially this shock was of cylindrical geometry and propagated at a Mach number of 3 to 4, while at later times the shock shape gradually became spherical, and propagation speed approached the sound speed. Turbulence was visible in the vicinity of the arc channel.

Although not a study of a gap spark gap, Boxman (1975)<sup>(12)</sup> describes measurements of time-dependent anode surface temperature in a vacuum spark gap using nickel electrodes 9 mm apart. Discharge duration was 7.2 ms and peak current was 3.8 kA. A silicon photovoltaic detector was used to measure anode temperature through use of the Planck radiation law and assumed emissivity values. Before transition of the discharge from a diffuse plasma to a constricted arc occurred, at a current of 2.7 kA, the anode surface temperature was below 1500°K, while after high voltage arcing, surface temperature rose rapidly ( $10^7$ °K/s) to approximately 2900°K. Such time-dependent temperature measurements could be useful for gas spark gaps as well, as an aid in electrode material selection.

The above measurements were all made in spark gaps having no initial gas flow, with no rapid, repetitive switching. Three studies where detailed flow diagnostics have been obtained for spark gaps with a mean gas flow are those due to Howatson and Rowe (1972)<sup>(13)</sup>, Klingenberg (1968)<sup>(14)</sup>, and recently by Schade and Ragaller (1982)<sup>(15)</sup>. While none of these experiments were conducted on repetitively switched spark gaps, detailed two pulse recovery data were obtained for the gas flow spark gap studied by Schade and Ragaller. Also, some studies were made of the effects of turbulence upon recovery.

Howatson and Rowe (1972)<sup>(13)</sup> investigated the effects of a shock wave and flow travelling axially along a DC arc, upon arc extinction. Low voltages and currents (300V, 150A) were used. Tungsten electrodes were supported axially in a rectangular shock tube fitted with viewing ports (Fig. 23). An image converter camera was utilized to record the arc, and was used in conjunction with a Q-switched ruby laser to visualize flow phenomena. An instability was observed to develop in the arc; as shown schematically in Fig. 24. Passage of the shock front also caused arc voltage oscillations which were due to the unsteadiness of the arc as it moved from side to side and was elongated. Shadowgraph pictures also indicated a transition from laminar to turbulent flow along the arc. Finally, a semi-empirical heat transfer model for the arc was developed which correlated well the experimental arc voltage-current characteristics, assuming a constant value of gas density times axial velocity squared. A balance between radiation and radial conduction was assumed in the arc core, while turbulent convection was assumed to be the dominant heat transfer mechanism outside of the arc.

In an interesting study of the effects of magnetic fields upon the propagation of an arc-generated plasma, Klingenbergs (1968)<sup>(14)</sup> utilized two image converter cameras operated in the streak mode to visualize shock propagation in the plasma. A plasma was generated in a diaphragm shock tube behind a shock wave. This plasma moved supersonically along the shock tube and came under the influence of a transverse magnetic field (6.8 kG), at the same time it passed between viewing ports and pairs of electrodes. A current passed through the moving plasma while the interaction of this current with the magnetic field slowed down the plasma. If the magnetic field was strong enough, a reflected planar shock was generated which propagated upstream,

until it reached the contact front and subsonic flow, as shown schematically in Fig. 25, taken from Klingenberg.

Finally, the most detailed experimental study to date of recovery characteristics of a gas blown arc switch, and the effects of flow physics upon switched performance, has recently been described by Schade and Ragaller (1982) for an axial geometry model experiment designed to be representative of a high-voltage current interrupting circuit breaker. The switch geometry, taken from Schade and Ragaller, appears in Fig. 26. Also shown is the turbulence grid which was used to study the effects of turbulence upon switch recovery. Flow of SF<sub>6</sub> was directed under pressure radially inward between the two electrodes to a stagnation region, and then exited axially along both electrodes. The nozzle contour was designed so that a continuous expansion to the exhaust pressure occurred in the nozzle. A 1.2 kA current pulse at 300 kV of 5 ms duration was generated using an exploding wire, and the time history of the decaying arc after current zero was studied using pulsed Argon laser interferometry for laminar flow, or Schlieren visualization for turbulent flow. The arc channel size, shock generation by the arc, and turbulence all could be visualized. If the flow was laminar, the interferometric measurements of refractive index allowed computation of radial gas density distributions, which yielded radial temperature distributions, if the pressure was assumed constant within the arc column. Turbulence could be seen inside the decaying arc for later times, while the use of a turbulence grid increased the size of the flow region in and around the arc, which was turbulent, especially for short times after current zero. Recovery data for this study (Fig. 27) showed the switch to have recovered in about 250  $\mu$ s when no turbulence grid was present. These data were obtained by applying a 320 kV voltage pulse with a 5  $\mu$ s risetime between the two metal nozzles, after a variable time delay

after current zero. When a turbulence grid was inserted, recovery time showed considerable scatter, between 150-500  $\mu$ s (Fig. 28). Comparison between the laminar case (Fig. 27) and the turbulent case (Fig. 28) showed that a greater percent recovery was obtained with the turbulence grid for delays less than 100  $\mu$ s, but that a smaller percent recovery was obtained for delays over 200  $\mu$ s. These conflicting trends for small and large delay times were not explained, and appear surprising.

These examples of flow measurements made using holography, interferometry, or Schlieren and shadowgraph techniques, using pulsed lasers as light sources, filters, and image converter cameras, demonstrate methods which enable a detailed documentation of the time history of transient arc-generated flow phenomena. Alternately, photodetectors and slit systems may be used to determine shock propagation velocities. However, careful experiment design appears necessary to allow successful use of these flow visualization techniques. A two-dimensional flow geometry appears ideally suited for such flow visualization, while the coaxial and cylindrical geometries appear less well suited for use of such flow diagnostic methods. Use of these flow diagnostic techniques may be necessary to clearly relate flow physics to the performance of high voltage repetitive gas flow spark gaps.

#### Examples of Theoretical Modeling of Arc Flow and Heat Transfer Phenomena

Although there has to date not been a great deal of development of theoretical models of the flow and heat transfer phenomena which occur in gas flow repetitive spark gaps, there have been theoretical analyses of other related spark or arc phenomena, including the shock propagation due to a spark generated by a focused, pulsed laser, the steady flow in chemical lasers, shock generation by an arc channel between two electrodes with no mean flow, and recently of the extinguishing of the arc in a current interrupting gas

flow switch used as a circuit breaker. Examples of these analyses will now be briefly surveyed.

Reviews of the phenomena occurring during and after breakdown of a gas due to a focused, high power laser have been given by Raizer (1966)<sup>(16)</sup>, DeMichelis (1969)<sup>(17)</sup>, and Shkarofsky (1974)<sup>(18)</sup>. Ramsden and Davies (1964)<sup>(19)</sup> were among the early workers to describe gas breakdown due to a focused laser beam, showing a streak photograph of the spark's motion and expansion towards the focusing lens. They also found a frequency shift of radiation scattered by the spark plasma, which they interpreted as a Doppler shift due to motion of the plasma. Initial velocities of the luminous shock front obtained from the image converter camera, of  $10^7$  cm/s, agreed well with the observed Doppler shift. Velocity of the luminous front decreased for later times. In a second paper, Ramsden and Savic (1964)<sup>(20)</sup> developed a radiatively driven detonation wave model for the propagation of the luminous plasma front during the laser pulse, while the spherical blast wave theory of Taylor (1950)<sup>(10)</sup> modeled front propagation well for the later times. Daiber and Thompson (1967)<sup>(21)</sup> refined the radiative detonation model to include the time-varying power input from the laser to the gas, and the gas breakdown time in their solution; this solution matched front propagation data for a range of laser powers, lenses, and gas species. However, their shock propagation results for large times were not in agreement with the blast wave theory of Taylor (1950), and the reason for this discrepancy was not explained. Ahlborn and Strachan (1973)<sup>(22)</sup> developed a one dimensional gas dynamical model for the effects of concentrated energy input to a gas, where energy absorption in a narrow region behind a step change in gas pressure and temperature, called a heat wave, both causes and maintains the steadily propagation front. They distinguished between three possible types of heat waves; a subsonic wave

(relative to the gas) for small energy inputs, a supersonic wave for large energy inputs, and a critical or sonic wave.

Recently, much more sophisticated numerical models of the fluid mechanics and heat transfer phenomena which occur in chemical lasers have been developed, in which finite difference forms of the continuum conservation equations are solved by computer. Presently such models are limited to two-dimensional or axisymmetric geometries. Ramshaw and Dukowicz (1979)<sup>(23)</sup>, for example, describe in detail a finite difference model for multicomponent, reacting, radiating gas flows, which includes a turbulence model, which may be used for either axisymmetric or two-dimensional geometries, and which includes time-dependent behavior. An example of a more limited fluid mechanical model is that developed by Srivastava et. al. (1981)<sup>(24)</sup> to study density exponentiation and thermal instability in the cavity of a pulsed CO<sub>2</sub> laser. Quan et. al. (1982)<sup>(25)</sup> describe a numerical model having capabilities similar to those of the model described by Ramshaw and Dukowicz (1979), but limited to steady state flows. These types of numerical models appear to have the capability to predict many of the physical phenomena occurring in a repetitive gas flow spark gap, but are presently limited to relatively simple axisymmetric or two-dimensional geometries and therefore are not suited to a complete analysis of such a flowing spark gap. However, one successful application of numerical modeling to describe the detailed flow and heat transfer phenomena which occur in a gas flow spark gap has recently be described by Ragaller et. al. (1982)<sup>(26)</sup>, for the axisymmetric geometry arc interrupting switch studied experimentally by Schade and Ragaller (1982), as was shown in Fig. 26. A time-dependent three-dimensional axisymmetric finite difference, flow model was developed which included simple, jet-like, turbulent eddy viscosity and eddy conductivity models. These conservation equations were solved, assuming the

pressure to be constant in the radial direction and assuming local thermal equilibrium, for assumed initial axial pressure and temperature distributions, to obtain the time evolution of the temperature distribution both axially and radially in the arc as it recovered, assuming either laminar or turbulent flow. Using these temperature solutions, a simplified recombination model was used to show the recombination of SF<sub>n</sub> to form SF<sub>6</sub> at the stagnation point. In a separate paper, Brand et. al. (1982)<sup>(27)</sup> compare this theoretical model with the experimental recovery results of Schade and Ragaller (1982), both for laminar and turbulent flows. Good agreement was achieved between calculated and measured dielectric-recovery characteristics in both instances. Thus, use of complicated fluid mechanical models of flow and heat transfer phenomena in repetitive gas flow spark gaps appears to be very promising, if slightly more complicated geometries can be modeled.

#### Discussion and Summary

In this section of the paper a general discussion of the state of present knowledge of fluid and heat transfer phenomena in gas flow, repetitively switched spark gaps will be given, followed by some suggestions for future work.

First, it is certain that while detailed experimental flow measurements or sophisticated theoretical flow models of gas flow spark gaps are lacking, many of the same physical processes modeled or measured previously in other arc phenomena will occur in a rep rated gas flow switch. For example, arc formation in a gas flow spark gap will generate shock or heat waves which will propagate through the flowing gas away from the arc channel. Propagation speeds of such fronts will decay as they expand, and probably different propagation speeds will be observed during and after the arc phase. These shock waves will increase nonuniformities of the electric fields between

electrodes, and will generate shock waves which will travel through the electrode and insulator materials. All of these events occur in a gas spark gap without a flowing gas medium.

However, the addition of a flowing gas greatly complicates the flow and heat transfer phenomena except for geometries where the flow is along the arc, such as that studied by Schade and Ragaller (1982), since this mean gas flow destroys any symmetry in the problem. For example, the arc-generated heat waves and shocks will initially be strong enough to propagate upstream ahead of the electrodes, but eventually will weaken sufficiently to be swept back downstream between the electrodes. Such events should contribute to either switch jitter, or in extreme cases, switch misfire. All of these phenomena are also likely to be highly dependent upon the particular geometry of interest; for example, the problem of reflected shocks propagating back between the electrodes would be greatly influenced by the proximity of any confining flow channel side walls. Indeed, the entire steady-state gas flowfield would in effect be determined by switch geometry. It is also clear that the presence of turbulence in the mean flowfield should alter switch performance measurably. It would be expected that a turbulent flow should aid in electrode cooling, but at the same time decrease switch lifetime due to increased erosion. However, these effects have not been well documented to date. The interesting results shown by Schade and Ragaller (1982), where turbulence initially aided dielectric recovery of their switch for small times, but degraded such recovery for large times is not well understood and indicates that quantifying the effects of turbulence upon gas flow switch performance may be a complicated task. It appears, however, that one simple flow parameter which is of critical importance in determining recovery times for a gas flow switch is the convection or transit time for the undisturbed gas to

pass between the electrodes, and future high power gas spark gaps designed for repetitive switching should be designed to minimize this fluid transit time.

Future efforts at understanding flow and heat transfer phenomena in gas flow spark gaps should investigate the limitations of the importance of this fluid transit time on rep rated switch performance. Effects of turbulent versus laminar mean flow should be studied in more detail for a number of switch geometries. Coupling of the arc-generated gas flow shock waves with shock waves travelling through the electrodes and insulator materials should be investigated to determine whether or not such phenomena could lead to fatigue of the insulator materials.

While the majority of previous gas flow repetitive spark gaps have utilized some type of axisymmetric geometry, it is not at present clear that such geometries lead to any real performance gains relative to a 2-D geometry, and if so, why. Both types of switches should be developed further until this can be clearly determined. Further, since flow visualization is not easily interpreted in cylindrical geometries, it is recommended that a carefully designed two-dimensional model experiment be undertaken to carefully document the effects of various flow parameters upon the performance of a two-dimensional spark gap at high power. Good quality flow visualization using image converter cameras should be undertaken to determine quantitatively the effects of mean gas flow upon arc channel development and shock propagation. Such a model experiment could also determine if reflection or downstream convection of arc-generated shocks affect switch jitter or misfire. These studies of a two-dimensional spark gap should be conducted at various gas pressures and using various gas species, and the average gas velocity should be varied.

The overall aim of such studies would be to increase our understanding of

flow and heat transfer phenomena as related to performance of high power, repetitive gas flow switches, and to develop the capability of determining values of switch design parameters necessary to achieve a desired rep rate performance with maximum lifetime and minimum associated switch hardware. This is quite an ambitious goal, but it appears that the time is ripe both for more detailed experimental documentation and theoretical modeling of gas flow spark gap flow physics and its influence on the performance of such switches, such as is embodied by the studies done at Brown Boveri Research Center. (15,26,27)

#### References

1. Baranov, V. Yu., Malyuta, D. D., Mezhevov, V. S., and Napartovich, A. P., "Pulse-Periodic CO<sub>2</sub> Laser with Supersonic Gas Flow," Soviet Journal of Quantum Electronics, Vol. 6, No. 3, pp 356-357, March 1976.
2. Rebe, D. C., "Supersonic Spark Gap Switch," Invention Disclosure AF Inv 11535, AD-D002 626, 1976.
3. Faltens, A., Reginato, L., Hester, R., Chesterman, A., Cook, E., Yokota, T., and Dexter, W., "High Repetition Rate Burst-Mode Spark Gap," Lawrence Livermore Laboratory Preprint UCRL-80634, Presented at 13th Pulse Power Symposium, Buffalo, NY, June 19-22, 1978.
4. Malyuta, D. D. and Mezhevov, V. S., "Discharger with High Pulse Repetition Frequency," Pribory i Tekhnika Eksperimenta, Vol. No. 4, pp. 89-90, July-Aug., 1980.
5. Ramrus, A., and Shannon, J., "Testing of a 100 kV, 100 Hz Rep Rate Gas Switch," IEEE Transactions on Plasma Science, Vol. PS-8, No. 3, pp. 160-162, Sept. 1980.
6. Naff, J. T., Sojka, R. J., and Zeehandelaar, E. P., "Design and Performance of a High Repetition Rate Spark Gap Switch at 50-kW Power Levels," 14th Pulse Power Modulator Symposium, Baltimore, MD, 1980.
7. Watson, H., "Long-Life High-Repetition-Rate Triggered Spark Gap," IEEE Transactions on Plasma Science, Vol. PS-8, No. 3. pp. 154-159, Sept. 1980.
8. Molen, G. M., Kirbie, H. C., and Kuhlman, J. M., "High Power Gas-Flow Spark Gaps," presented at Workshop on Gaseous Breakdown Phenomena, Naval Surface Weapons Center, Dahlgren, VA, Sept. 15, 1982.

9. Scholz, P. D. and Anderson, T. P., "Four Electromagnetic Shock Tube Experiments to Demonstrate Some High-Temperature High-Speed Flow Phenomena," American Journal of Physics, Vol. 38, No. 3, March 1970, pp. 279-290.
10. Taylor, G. I., "The Formation of a Blast Wave by a Very Intense Explosion I. Theoretical Discussion," Proc. Royal Society of London, Series A. Vol. 201, pp. 159-174, 1950.
11. Stabnikov, M. V. and Tombak, M. Sh., "Holograms of Spark Discharges Produced by Nanosecond Electrical Pulses," Soviet Physics--Technical Physics, Vol. 17, No. 5, Nov. 1972, pp. 852-854.
12. Boxman, R. L., "Measurements of Anode Surface Temperature During a High-Current Vacuum Arc," Journal of Applied Physics, Vol. 46, No. 11, Nov. 1975, pp. 4701-4704.
13. Howatson, A. M. and Rowe, R. D., "An Arc Column in Forced Axial Convection," Journal of Physics D: Applied Physics, Vol. 5, 1972, pp. 104-118.
14. Klingenberg, H., "Arc Phenomena and Gasdynamic Effects due to Interaction of Shock Waves with Magnetic Fields," Zeitschrift für Naturforsch, Vol. 23A, pp. 1929-1939, 1968.
15. Schade, E. and Ragaller, K., "Dielectric Recovery of an Axially Blown SF<sub>6</sub>-Arc After Current Zero: Part 1--Experimental Investigations," IEEE Transactions on Plasma Science, Vol. PS-10, No. 3, Sept. 1982, pp. 141-153.
16. Raizer, Yu. P., "Breakdown and Heating of Gases under the Influence of a Laser Beam," Soviet Physics Uspekhi, Vol. 8, No. 5, March-April 1966, pp. 650-673.
17. DeMichelis, C., "Laser Induced Gas Breakdown: A Bibliographical Review," IEEE Journal of Quantum Electronics, Vol. QE-5, No. 4, April 1969, pp. 188-202.
18. Shkarofsky, I. P., "Review of Gas-Breakdown Phenomena Induced by High-Power Lasers--I," RCA Review, Vol. 35, March 1974, pp. 48-78.
19. Ramsden, S. A. and Davies, W. E. R., "Radiation Scattered from a Plasma Produced by a Focused Ruby Laser Beam," Physical Review Letters, Vol. 13, No. 7, Aug. 17 1964, pp. 227-229.
20. Ramsden, S. A. and Savic, P., "A Radiative Detonation Model for the Development of a Laser-Induced Spark in Air," Nature, Vol. 203, No. 4951, 1964, pp. 1217-1219.
21. Daiber, J. W. and Thompson, H. M., "Laser-Driven Detonation Waves in Gases," The Physics of Fluids, Vol. 10, No. 6, June 1967, pp. 1162-1169.

22. Ahlborn, B. and Strachan, J. D., "Dynamics of Step Heat Waves in Gases and Plasmas," Canadian Journal of Physics, Vol. 51, 1973, pp. 1416-1427.
23. Ramshaw, J. D. and Dukowicz, J. K., "APACHE: A Generalized-Mesh Eulerian Computer Code for Multicomponent Chemically Reactive Fluid Flow," Report LA-7427, Los Alamos Scientific Laboratory, Los Alamos, NM, Jan. 1979.
24. Srivastava, B. N., Theophanis, G., Limpaecher, R., and Comly, J. C., "Flow and Discharge Characteristics of Electron-Beam-Controlled Pulsed Lasers," AIAA Journal, Vol. 19, No. 7, July 1981, pp. 885-892.
25. Quan, V., Persselin, S. F., and Yang, T. T., "Computation of Reacting Flowfield with Radiation Interaction in Chemical Lasers," Paper AIAA-82-0402, presented at AIAA 20th Aerospace Sciences Meeting, Orlando, Florida, Jan. 11-14, 1982.
26. Ragaller, K., Egli, W., and Brand K. P., "Dielectric Recovery of an Axially Blown SF<sub>6</sub>-Arc After Current Zero: Part II--Theoretical Investigations," IEEE Transactions on Plasma Science, Vol. PS-10, No. 3, Sept. 1982, pp. 154-162.
27. Brand, K. P., Egli, W., Niemeyer, L., Ragaller, K. and Schade, E., "Dielectric Recovery of an Axially Blown SF<sub>6</sub>-Arc After Current Zero: Part III--Comparison of Experiment and Theory," IEEE Transactions on Plasma Science, Vol. PS-10, No. 3, Sept. 1982, pp. 162-172.

AUTHORS	VOLTAGE	CURRENT	PULSE WIDTH	RISETIME	JITTER	REP RATE	VELOCITY	PRESSURE	GEOMETRY
1. Baranov, Malyuta, Mezhevov, & Napartovich (1976)	30 kV	.1A (.1 J/pulse)	20-40 $\mu$ s	---	---	4-5 Hz	M=2	---	2-D converging- diverging nozzle; electrodes downstream of throat
2. Rebe (1976)	20 kV	---	---	---	---	500 Hz	M=1.5	54 psia	annular converging- diverging nozzle
3. Faltens, Reginato, Hester, Chesterman, Cook, Yokota, & Dexter (1978)	220 kV	42 kA	50 ns	12 ns	2 ns	1 kHz	50 m/s	150 psig	coaxial nozzle with third, coaxial trigger electrode
4. Malyuta & Mezhevov (1980)	40 kV	10 kA	>100 ns	---	.5 $\mu$ s	4 kHz (up to 9 kHz)	---	<120 psi	2 coaxial, conical electrodes separated by diaphragm with small hole to allow flow
5. Ramrus & Shannon (1980)	100 kV	10 kA	---	100 $\mu$ s	---	up to 250 Hz	~3 m/s	40 psig	2 coaxial electrodes, one with annular flow passage, using downstream UV trigger electrode
6. Naff, Sojka, & Zeehandelaar (1980)	52 kV	20 kA	100 ns	---	5 ns	1850 Hz	~100 m/s	< 90 psig	coaxial electrodes, with tangential swirl gas injection, and midplane trigger electrode
7. Watson (1980)	~30 kV (.47J/pulse)	100 ns	20 ns	~4 ns	1 kHz	~35 m/s	100 psia	flow between 3 spherical electrodes in a line; middle electrode fitted with UV trigger	
8. Molen, Kirby, & Kuhlman (1982)	20 kV	1 kA	---	10 $\mu$ s	---	~5 kHz*	M=1.5	< 20 psiq	2-D converging- diverging nozzle; electrodes at throat

\*recovery times measured to be 0.2 ms

Table 1 Performance of Typical Previous Gas Blown Spark Gaps

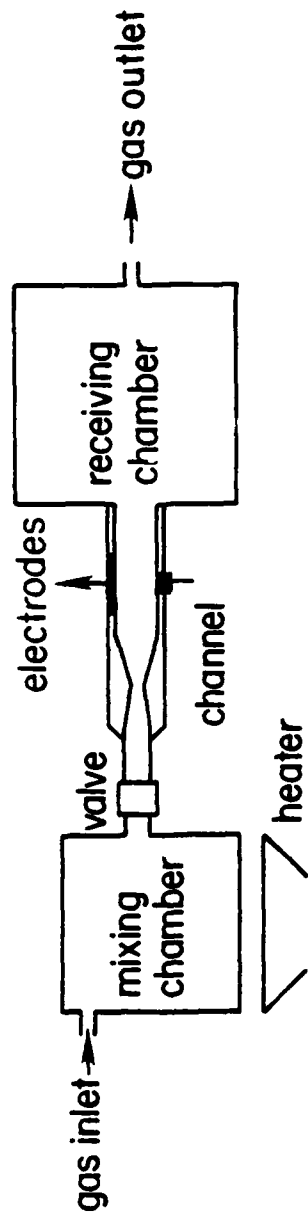


Fig. 1. Schematic of apparatus of Baranov et al. (1976)

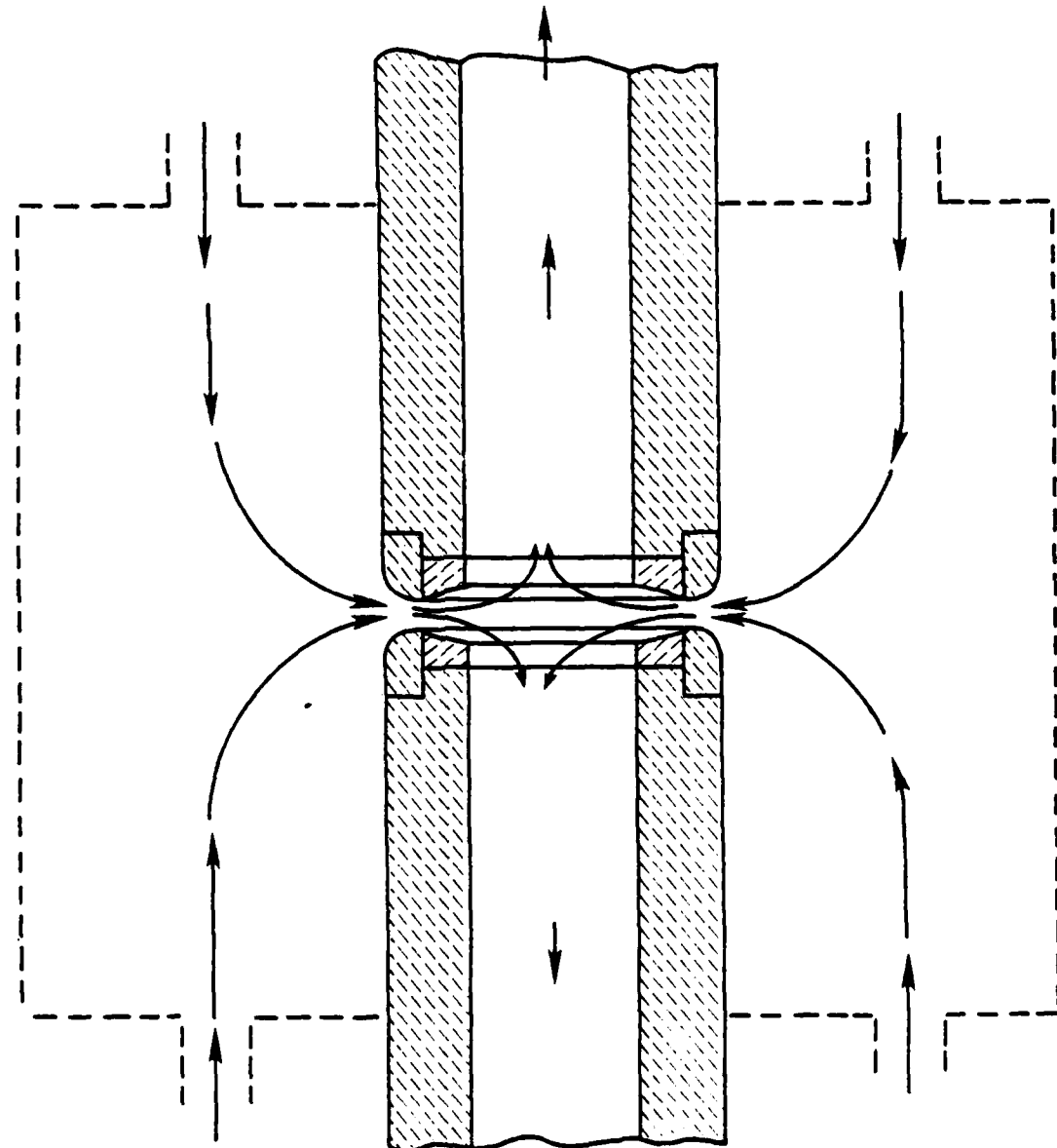


Fig. 2. Schematic of supersonic axial spark gap by Rebe (1976)

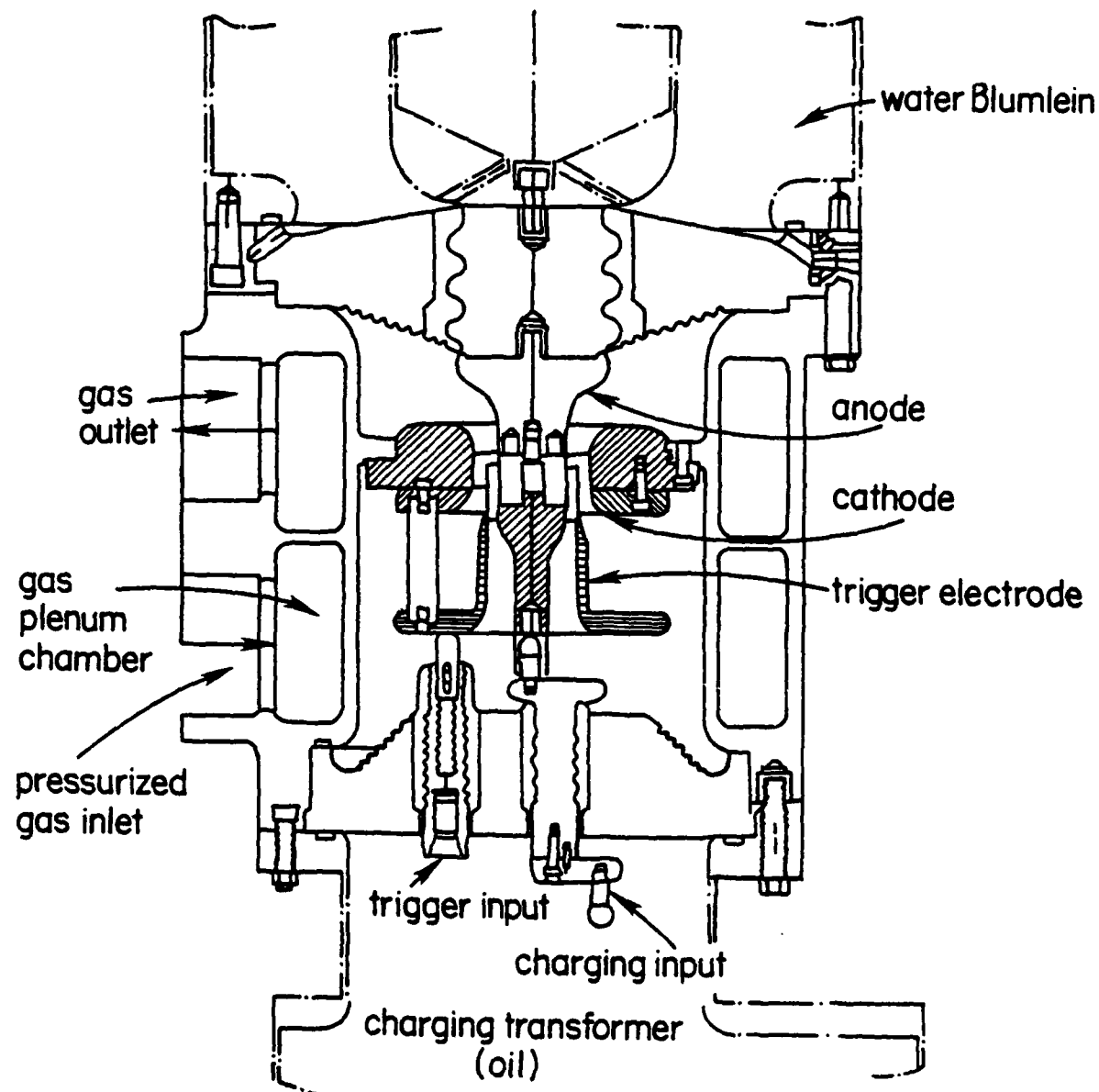


Fig. 3. Cross section of spark gap by Faltens,et al., (1978)

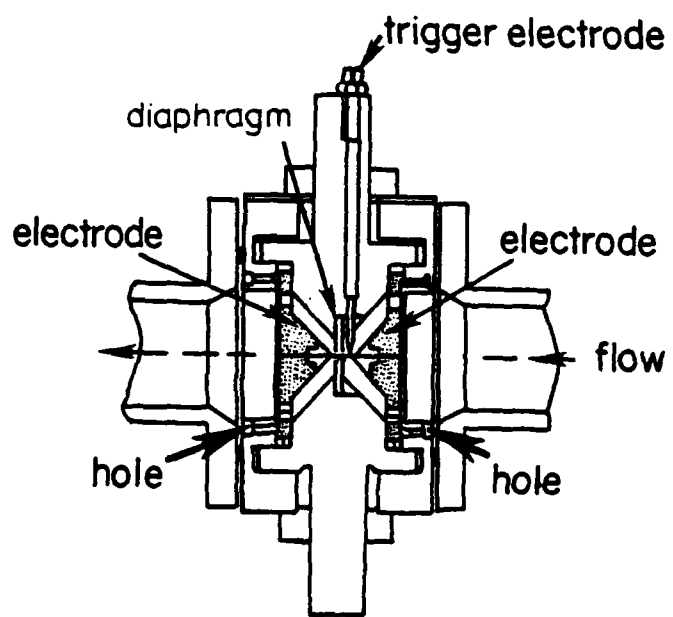


Fig. 4. Spark gap by Malyuta and Mezhevov (1979)

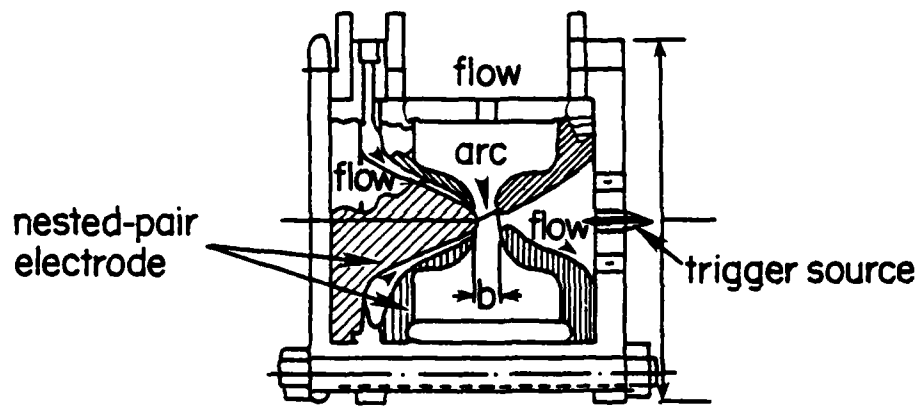


Fig. 5. Cross-section of spark gap by Ramrus and Shannon (1980)

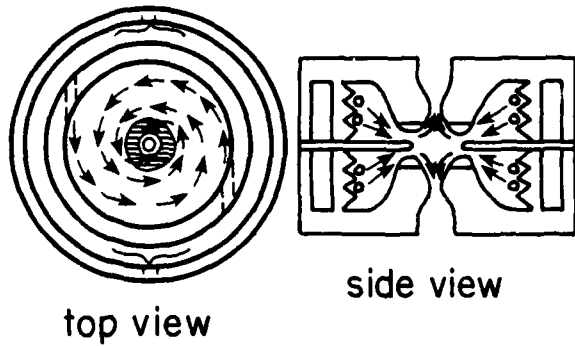


Fig. 6. Schematic of vortex-flow spark gap switch by Naff et al (1980)

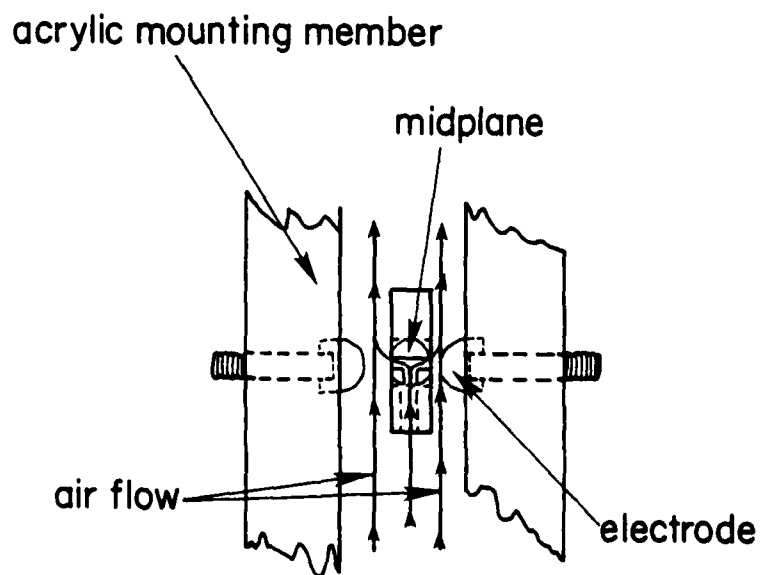


Fig. 7. Spark gap by Watson (1980)

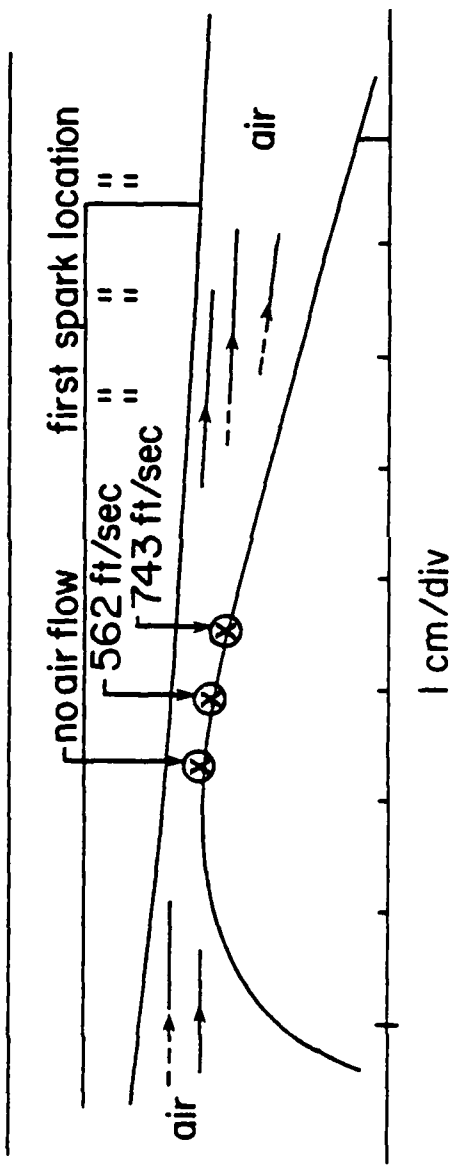


Fig. 8. Profile of flowing spark gap and the location of the first spark channel (Molen, Kirby and Kuhlman, 1982)

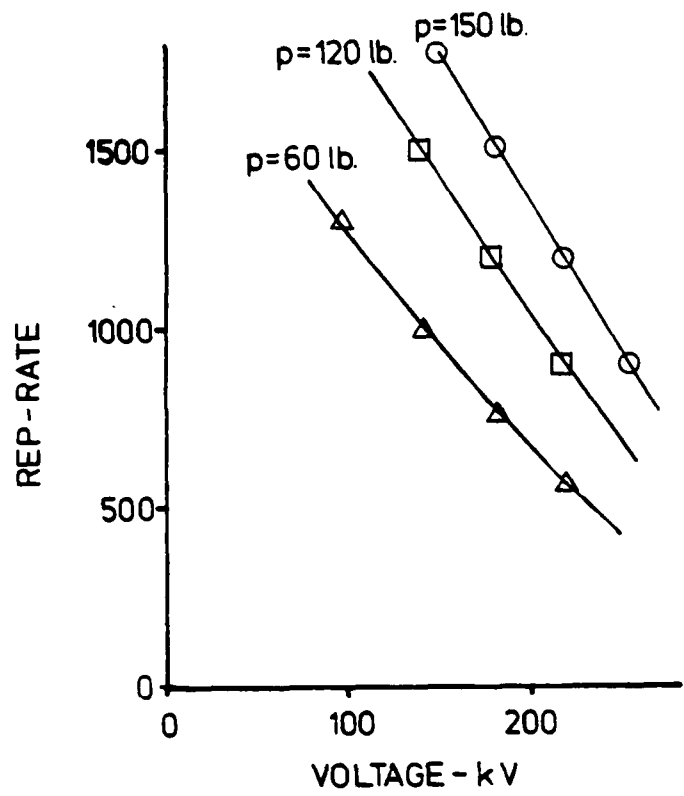


Fig. 9 Rep.-rate vs. voltage and pressure, from Faltens et al.  
(1978)

BLOCK DIAGRAM OF THE LOW VOLTAGE EXPERIMENT

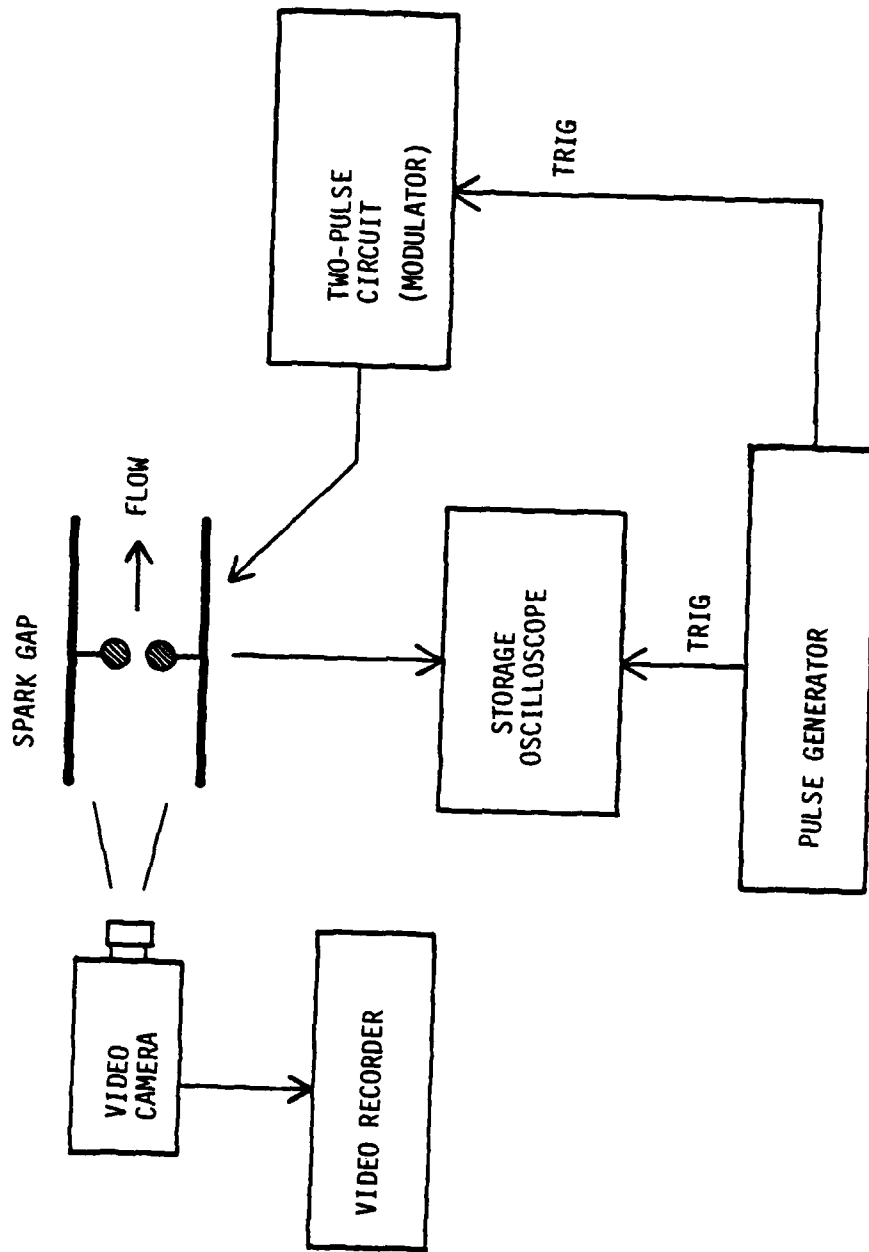


Fig. 10 Block Diagram of the Low Voltage Experiment by Mollen et al (1982)

NON-DIMENSIONAL PRESSURE DISTRIBUTIONS  
IN LOW ENERGY GAP EXPERIMENT

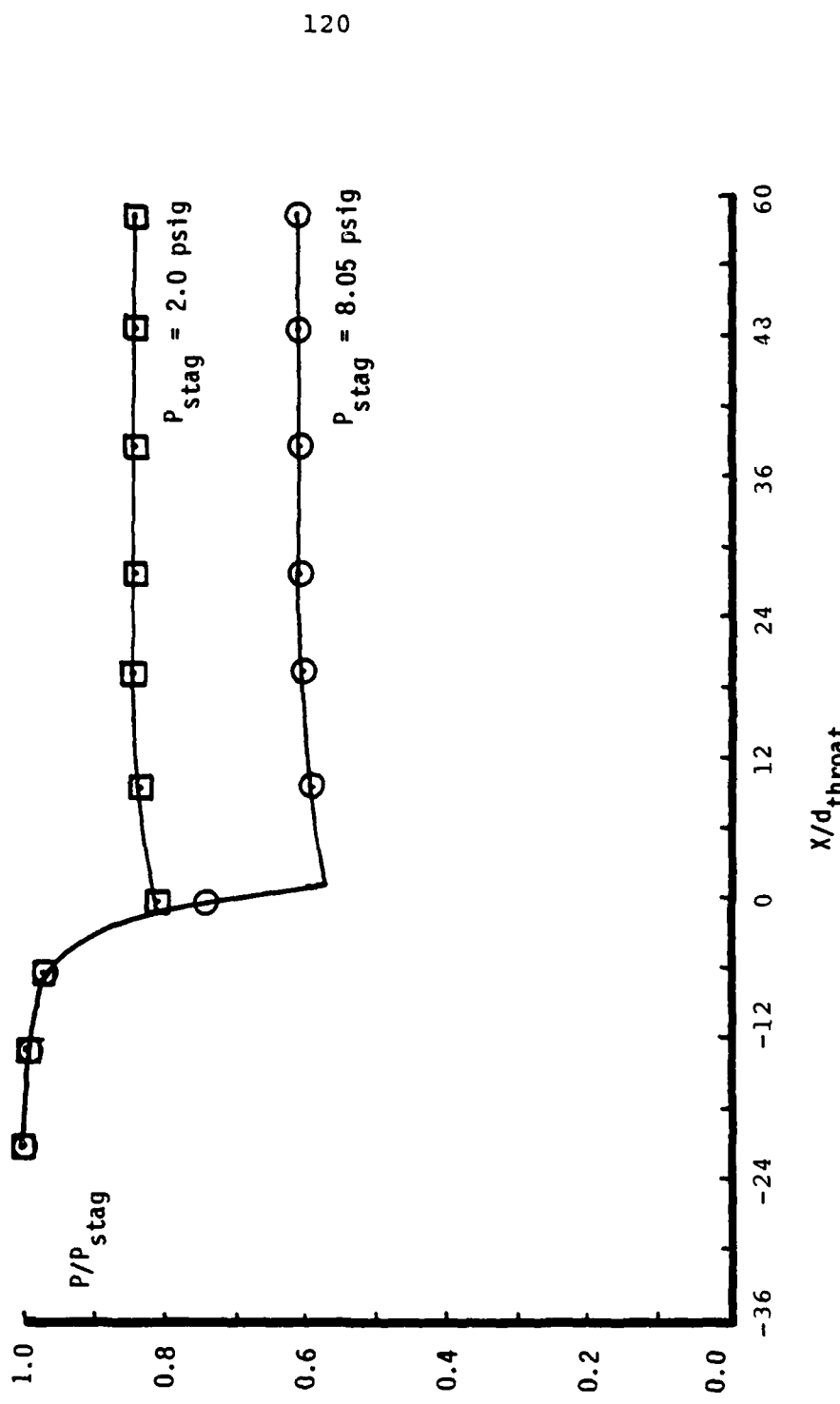


Fig. 11 Non-dimensional Pressure Distributions in Low Energy Gap Experiment

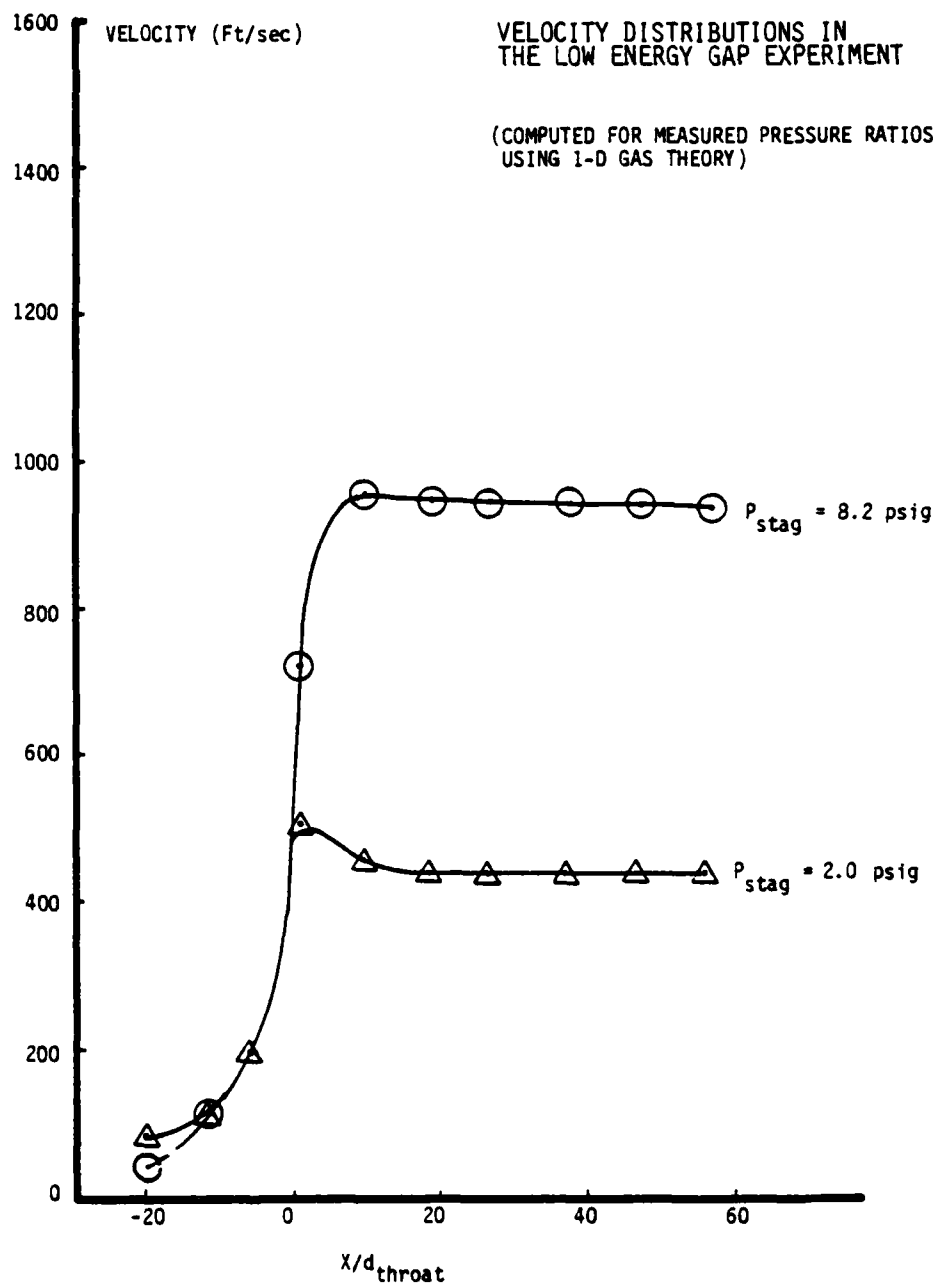


Fig. 12 Velocity Distributions in the Low Energy Gap Experiment

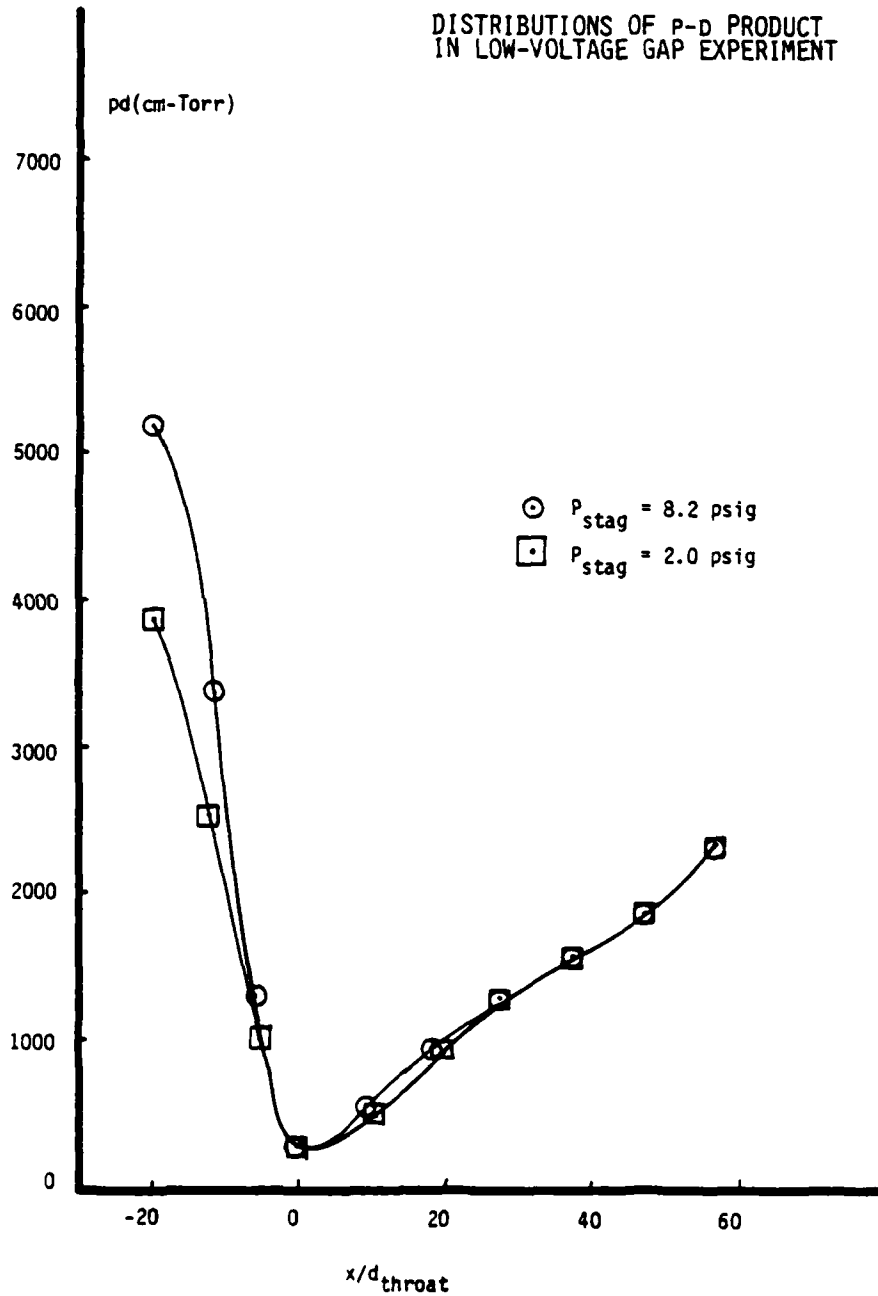


Fig. 13 Distributions of P-D Product in Low-Voltage Gap Experiment

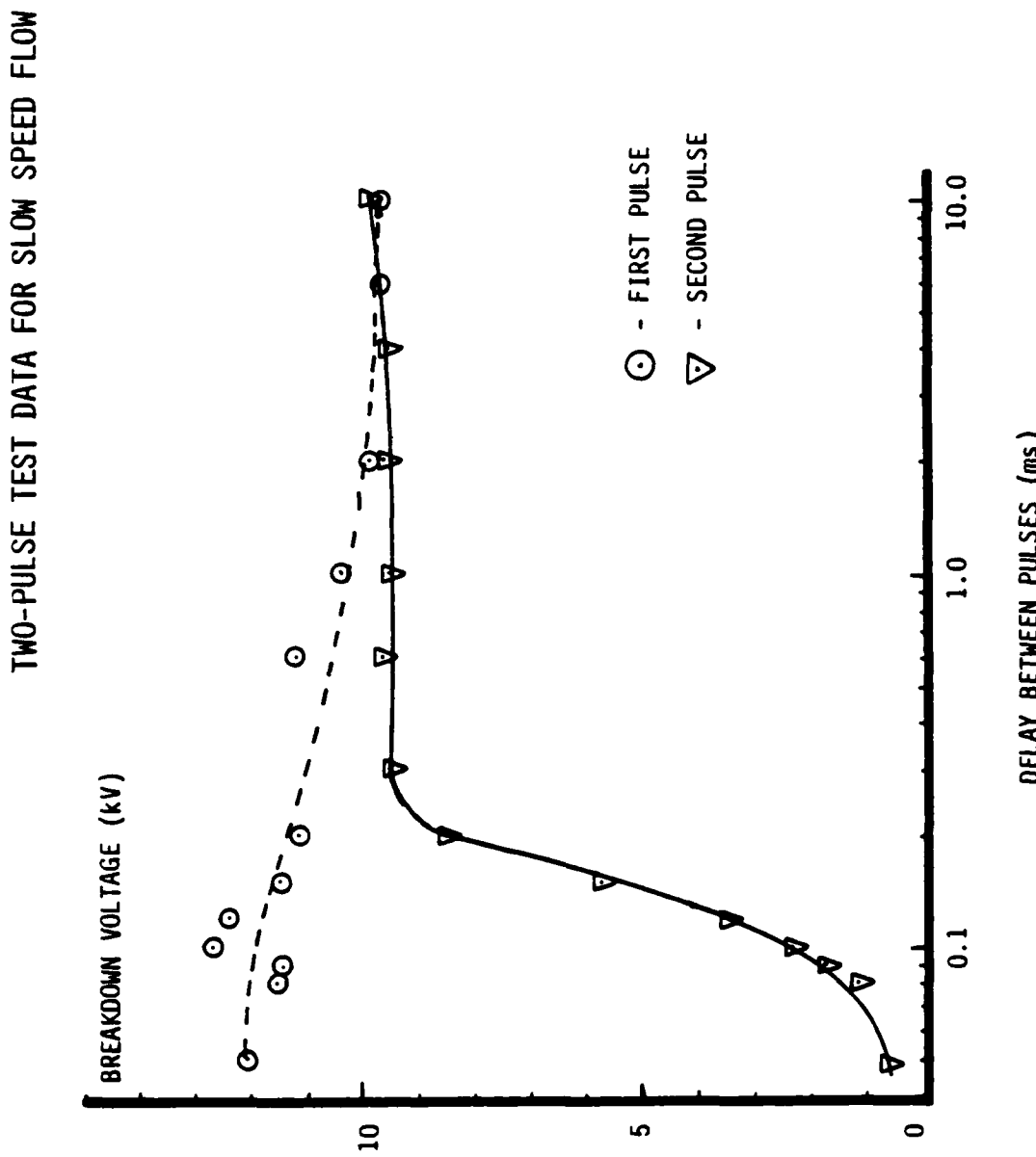


Fig. 14 Two-Pulse Test Data for Slow Speed Flow

## TWO-PULSE TEST DATA FOR MEDIUM SPEED FLOW

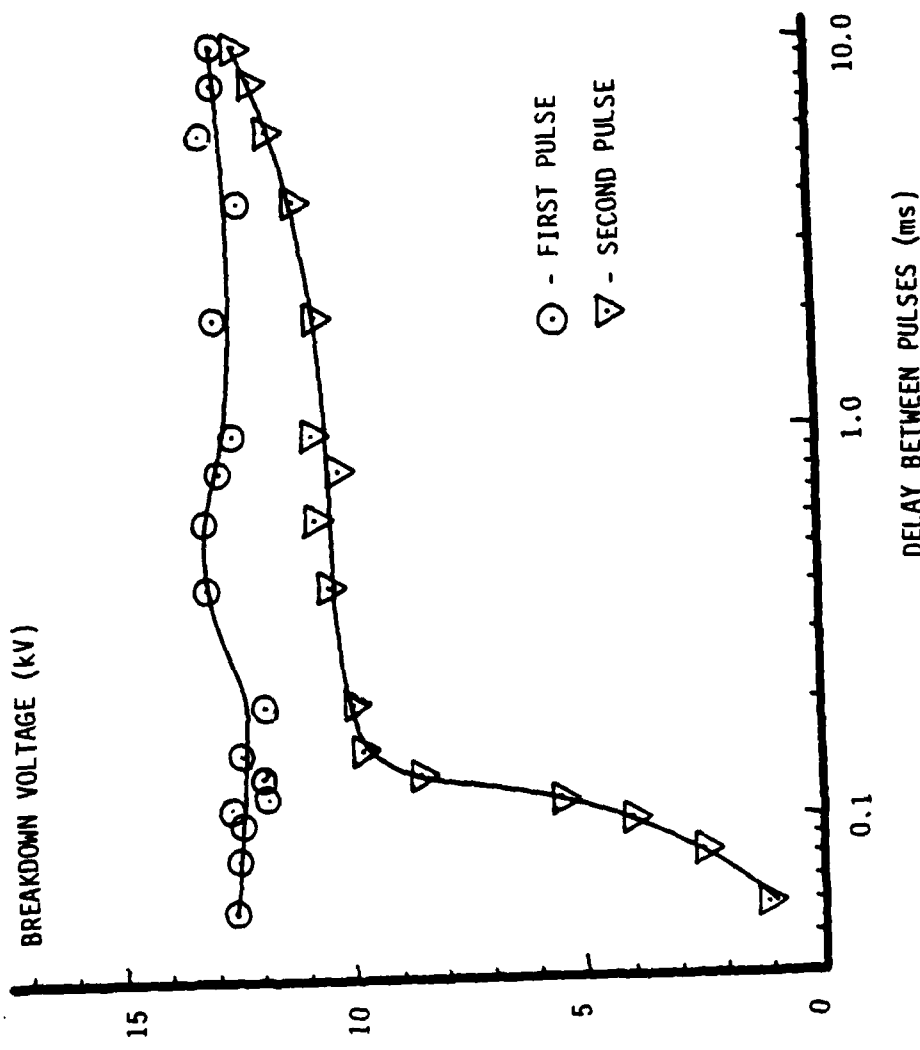


Fig. 15 Two-Pulse Test Data for Medium Speed Flow

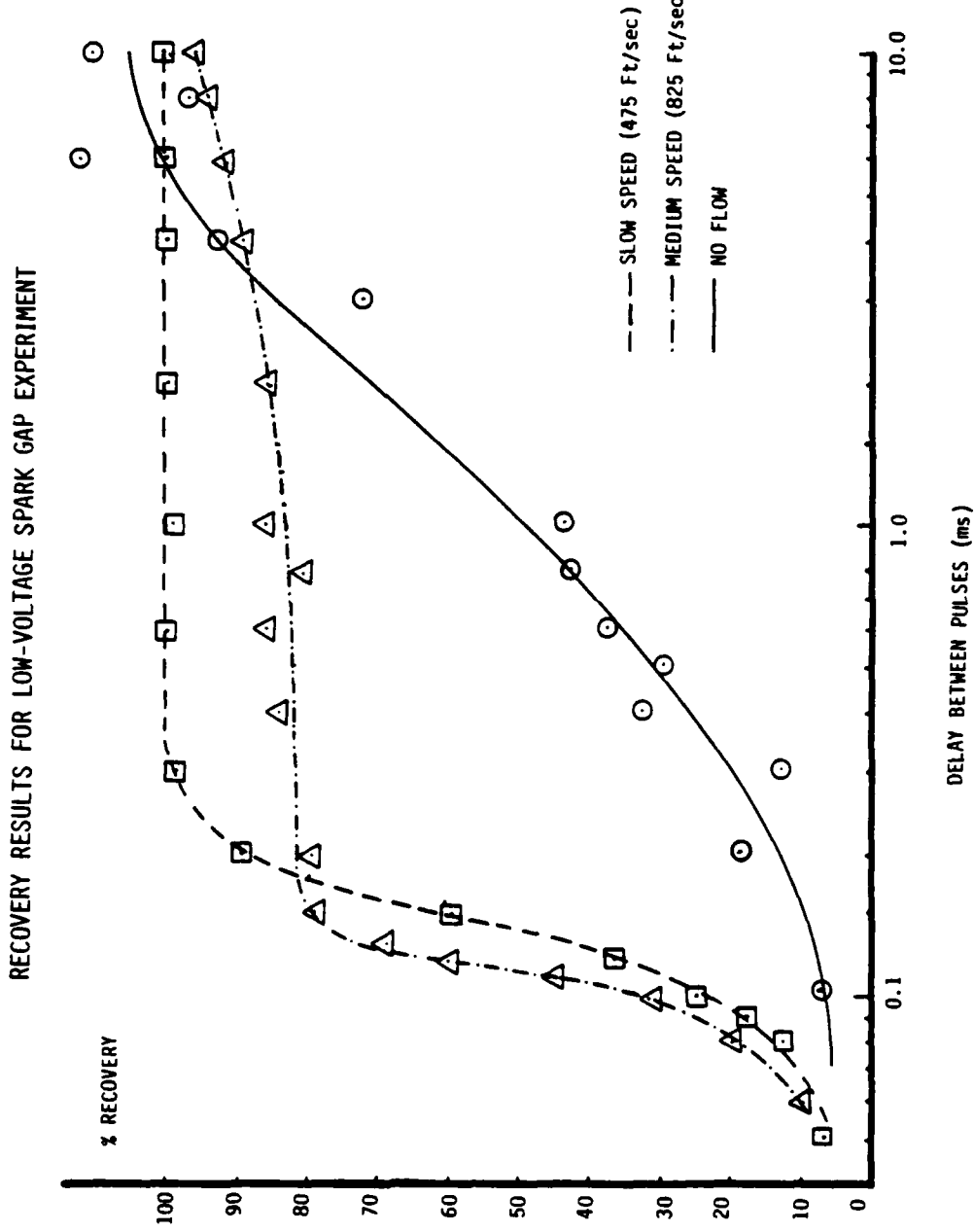


Fig. 16 Recovery Results for Low-Voltage Spark Gap Experiment

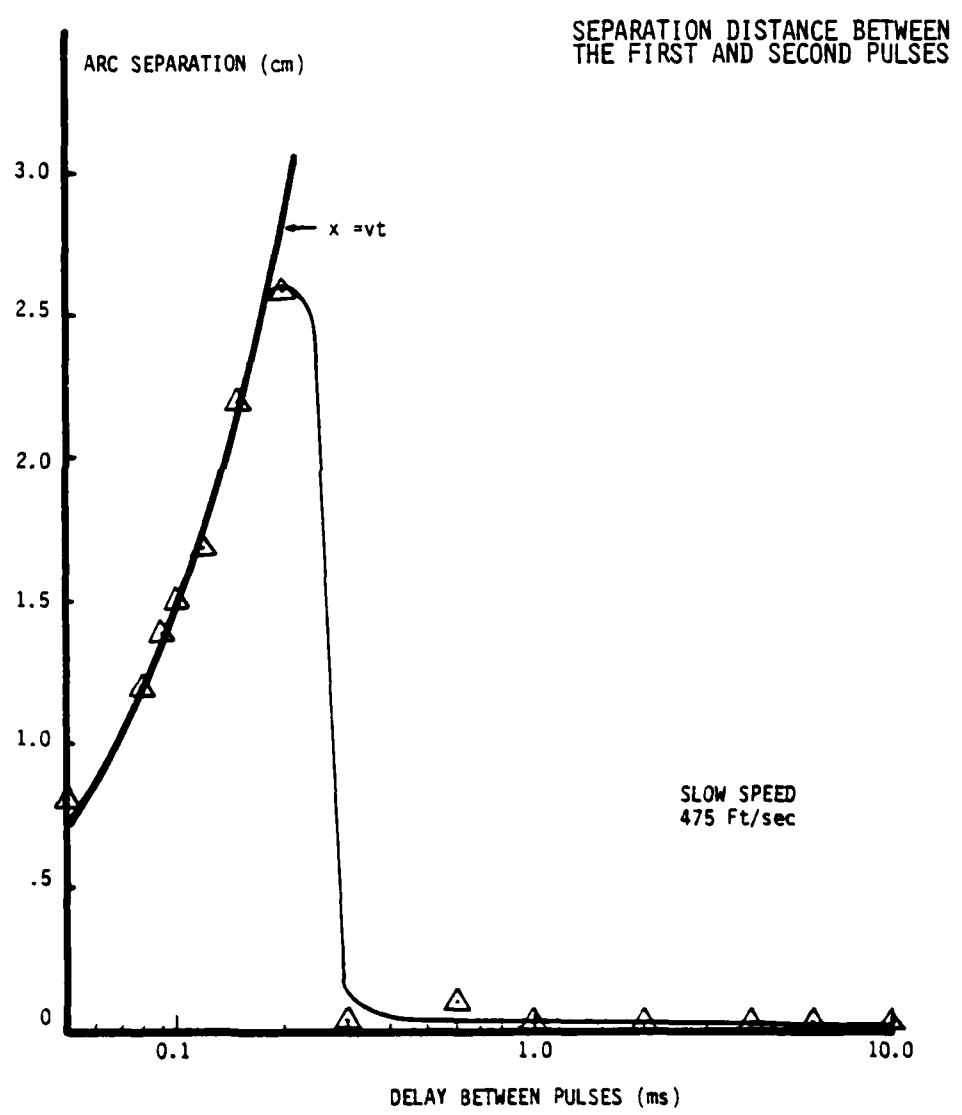


Fig. 17 Separation Distance Between the First and Second Pulses

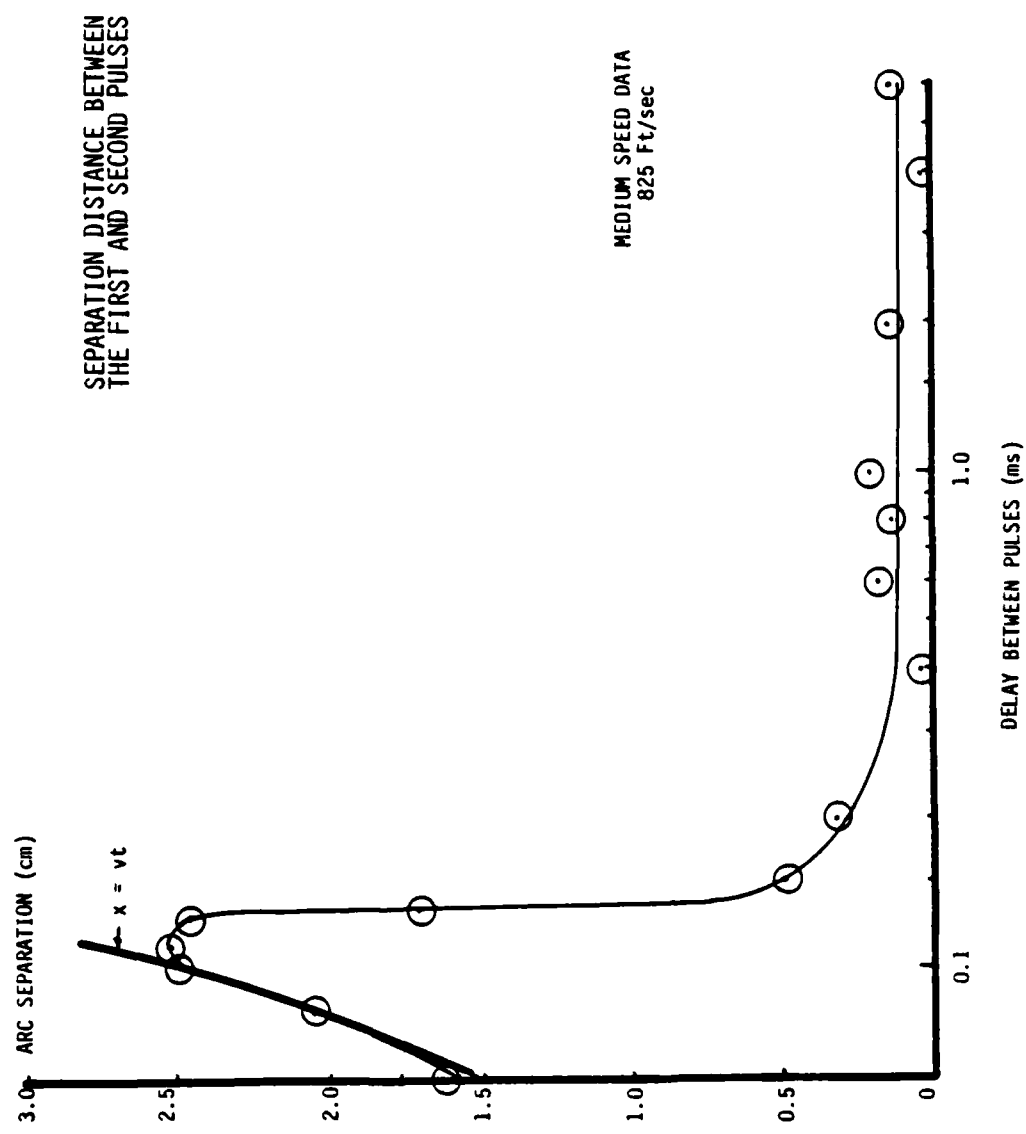


Fig. 18 Separation Distance Between the First and Second Pulses

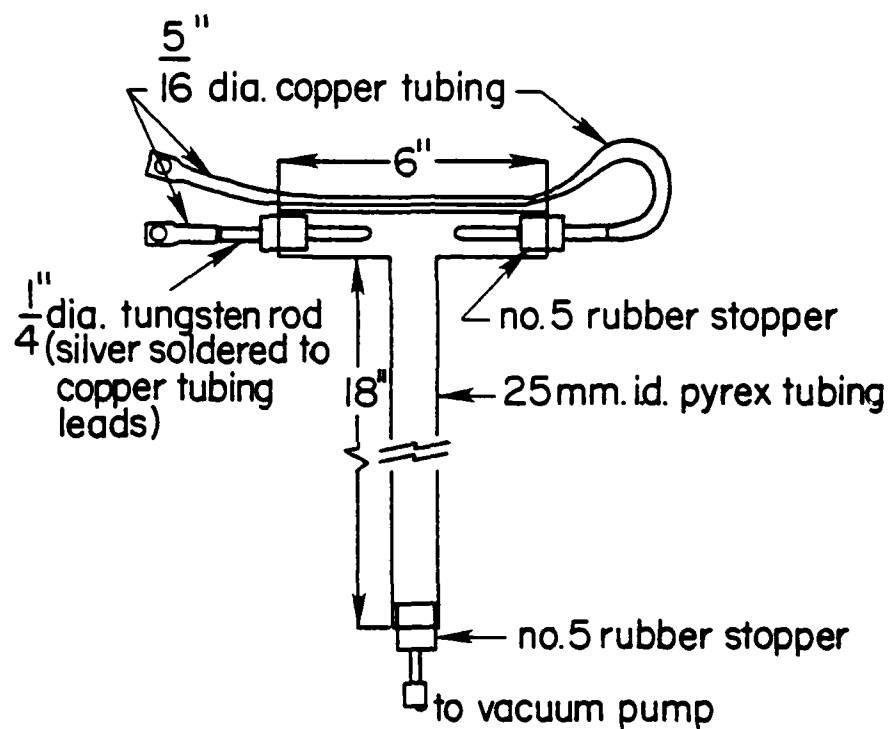


Fig. 19. Detail of T shock tube used by Scholz and Anderson (1970)

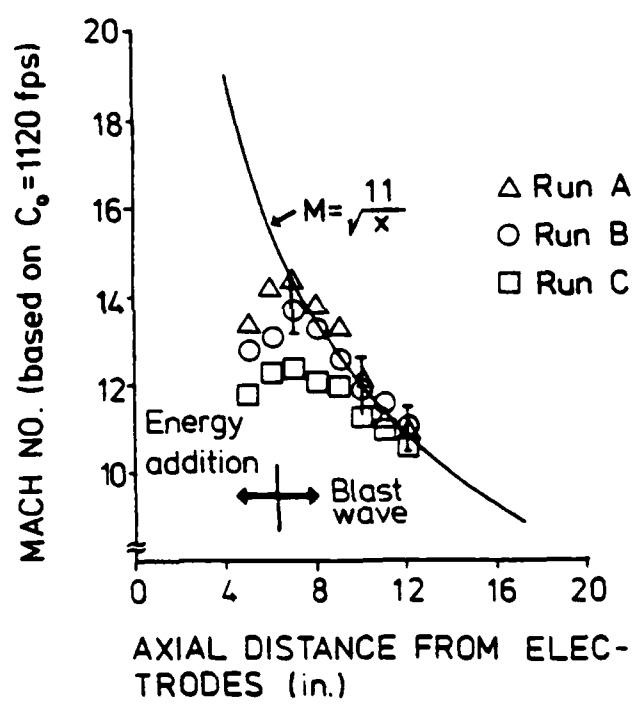


Fig. 20 Luminous front velocity versus distance, from Scholz and Anderson (1970)

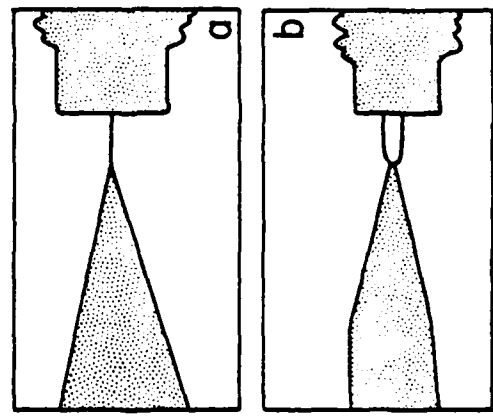


Fig. 21. Schematic of spark discharge images reconstructed from holograms.  
a)  $\text{delay} \leq 50\text{nsec}$ ; b)  $\text{delay} = 1\mu\text{sec}$ , from Stabnikov and Tombak (1972)

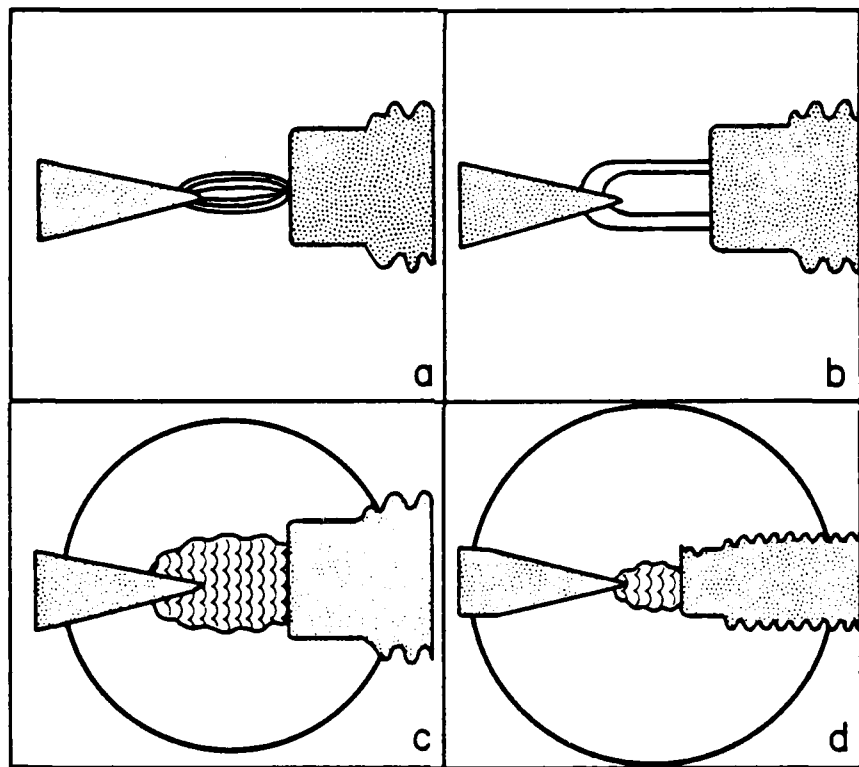


Fig. 22. Schematic of laser shadowgrams of a spark discharge. (a) 1; (b) 3; (c) 10; (d) 30  $\mu$ sec, from Stabnikov and Tombak (1972)

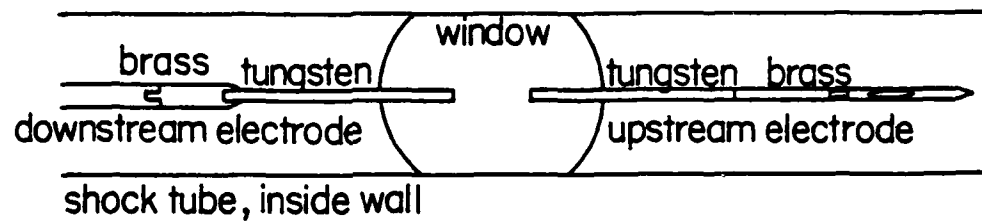


Fig. 23. Schematic of shock tube used by Howatson and Rowe (1972)

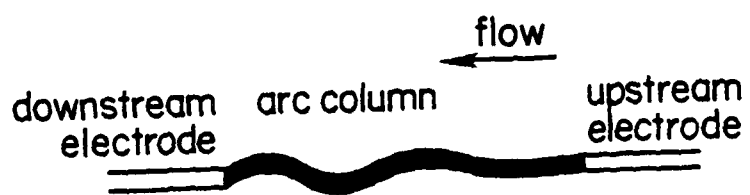


Fig. 24. A schematic diagram of a direct photograph of the arc, from Howatson and Rowe (1972)

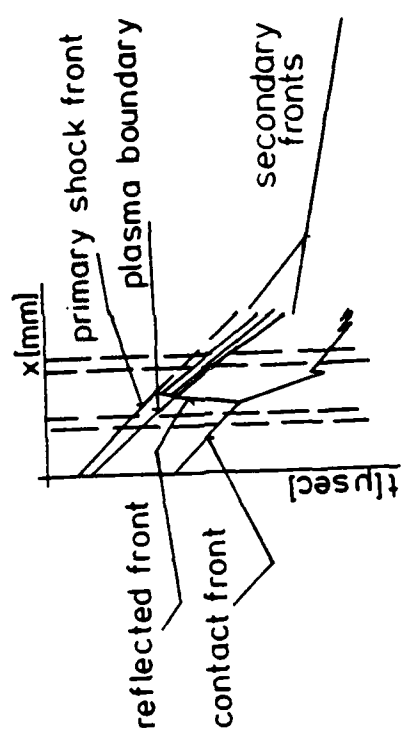


Fig. 25 Schematic of streak photographs for various initial pressures  $B_0 = 6.8 \text{ kG}$  from Klingenberg (1968)

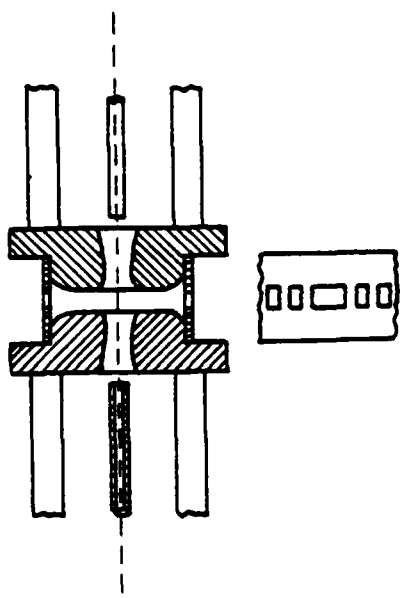


Fig. 26. Double-nozzle flow configuration with turbulence grid for the production of a disturbed inflow, from Schade and Ragaller (1982)

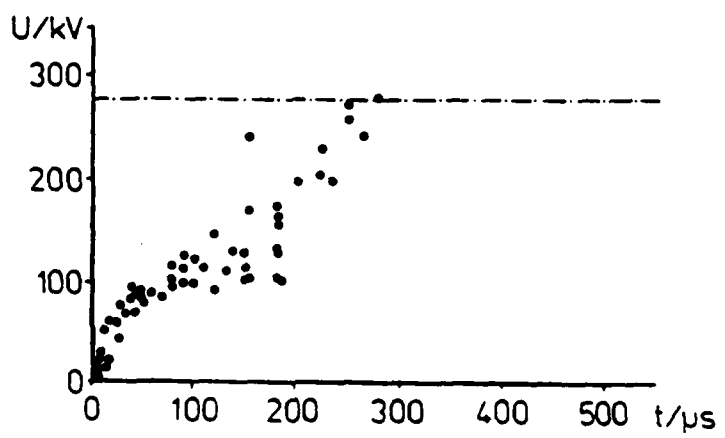


Fig. 27 Recovery characteristic for double flow nozzle geometry of Schade and Ragaller (1982); no turbulence grid

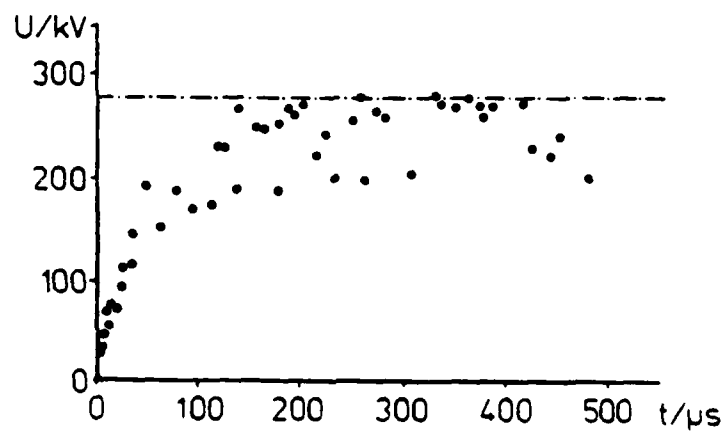


Fig. 28 Recovery characteristic for double flow nozzle geometry of Schade and Ragaller (1982); with turbulence grid

## Appendix A

Summary of Flow Visualization Work of Pederson and Carper

Since the main text of the paper was written, the author has become aware of additional work on flow visualization in an air blown spark gap conducted by Pederson and Carper \* at low velocity. This work clearly documents, that for sufficiently short interpulse time delays, the second arc can occur downstream of the location of the original arc, in agreement with results by Molen et. al. (ref. 8 in main text) discussed in the main body of the present paper. A brief summary of this work will be given in this Appendix, since this independent investigation has yielded results similar to those obtained by Molen et. al. (ref. 8), as well as providing additional insight into the flow physics.

The apparatus used by Pederson and Carper consisted of two, one inch diameter, hemispherical-tipped brass electrodes spaced 0.15 inches apart. Air at atmospheric pressure was blown between at speeds ranging from 5 to 22 ft ft/sec. First pulse breakdown occurred at 10-12.4 kV, depending upon the air velocity; peak currents were between 200 and 450 A. The pulselwidth was 10-20  $\mu$ s. An interferometer was used, along with high speed cameras operated at framing rates of 4800 or 9600 frames per second, to observe density variations in the flowfield in the interelectrode region caused by the arcs.

---

\* Pederson, R.J. and Carper, H.J., "Flow Visualization in a Gas Blown Spark Gap," Proceedings of the Ieee 15 Pulsed Power Modulator Symposium (IEEE publication 82 CH 1785-5), pp. 107-109, Baltimore, MD, June 114-16, 1982.

At the low velocities attained in this study, the first pulse breakdown was observed to occur at the location of minimum electrode separation, corresponding to the location of the minimum value of the product of pressure times electrode spacing.

However, for sufficiently small interpulse separations (smaller than the transit time for the products of the first arc to leave the interelectrode region), the second arc was observed to occur downstream of the location of the first arc. This restrike occurred at a larger electrode separation than the first and propagated through the heated region due to the first pulse.

Also, expansion of this heated region was visible as it convected in the flow direction. The upstream side of the heated gas region was observed initially to propagate upstream, and then to move downstream at a velocity which was smaller than the undisturbed air velocity. Finally, the wall boundary layers on the electrodes could be visualized, in that the heated gas due to the arc near the surfaces of the electrodes was found to move downstream much more slowly than the heated arc products near the center of the flow channel. Some separation of the air flow from the downstream side of each electrode could be seen.

Thus, this work provides additional insight into the flow phenomena which occur in the interelectrode region of a gas blown spark gap.

Appendix B  
Introduction to Flow Effects

The following appendix was prepared as a brief introductory summary of the types of physical flow and heat transfer phenomena which influence gas flow spark gap performance. This appendix consists of a series of briefly worded figures which list main ideas; these figures were used at the Repetitive Spark Gap Operation workshop to introduce non-mechanical engineers to basic flow and heat transfer phenomena. Much more detailed discussions on gas dynamics may be found in the book, The Dynamics and Thermodynamics of Compressible Fluid Flow, by A. Shapiro, volume 1, Ronald Press, 1953, while boundary layers and turbulence are discussed in Boundary Layer Theory, by H. Schlichting, 6th edition, McGraw-Hill, 1968.

### Introduction to Flow Effects

Gas flow switch performance influenced by flow parameters such as:

- velocity
- pressure
- shocks or detonation waves
- laminar or turbulent flow

Above all are influenced by geometry.

How do  $p_{\text{stag}}$ ,  $p_{\text{exit}}$ , or area changes influence flow in converging-diverging nozzle?

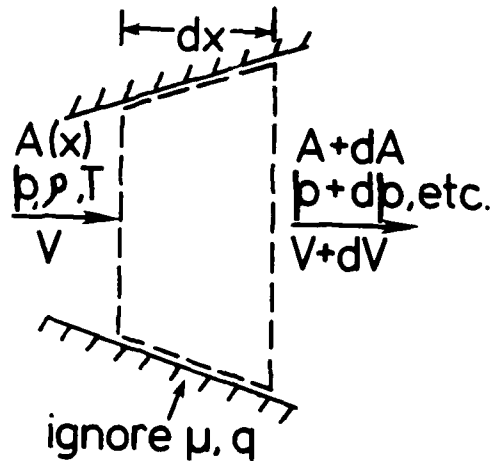
- see Shapiro

- for 1-D flow, one obtains the following:

$$\text{mass cons.} \quad d(\rho AV) = 0$$

$$\text{momentum} \quad dp + \rho V dV = 0$$

$$\text{energy} \quad dh + V dV = 0$$



Combine to yield:

$$\frac{dA}{A} = \frac{dp}{\rho V^2} (1 - M^2)$$

$$M = \text{Mach number} = \frac{V}{c}$$

$c$  = sound speed

- if  $M < 1$        $dA > 0$    yields    $dp > 0$
- if  $M > 1$        $dA > 0$    yields    $dp < 0$
- if  $M = 1$        $dA, dp$  rel'n indeterminant

Quantitatively relate (p, T, ρ, V) to A:

- for ideal gas ( $p = \rho RT$ ,  $h = C_p T$ )

energy becomes

$$h_o = h + \frac{V^2}{2} , \text{ or}$$

$$T_o = T + \frac{V^2}{2C_p} , \text{ or}$$

$$\frac{T_o}{T} = 1 + \frac{\gamma-1}{2} M^2 , \quad \gamma = \frac{C_p}{C_v}$$

- since flow isentropic,  $\frac{p}{p_o} = (\frac{T}{T_o})^{\frac{1}{\gamma-1}}$

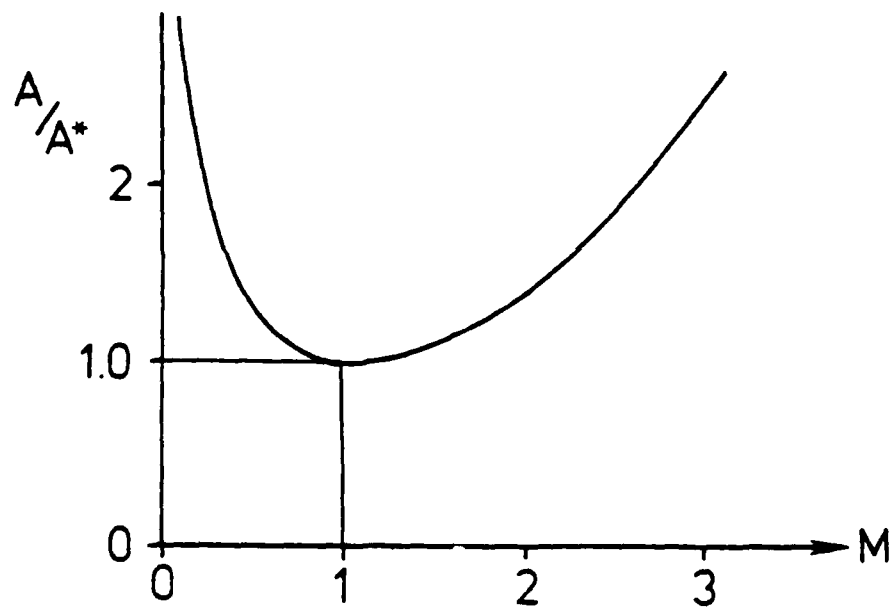
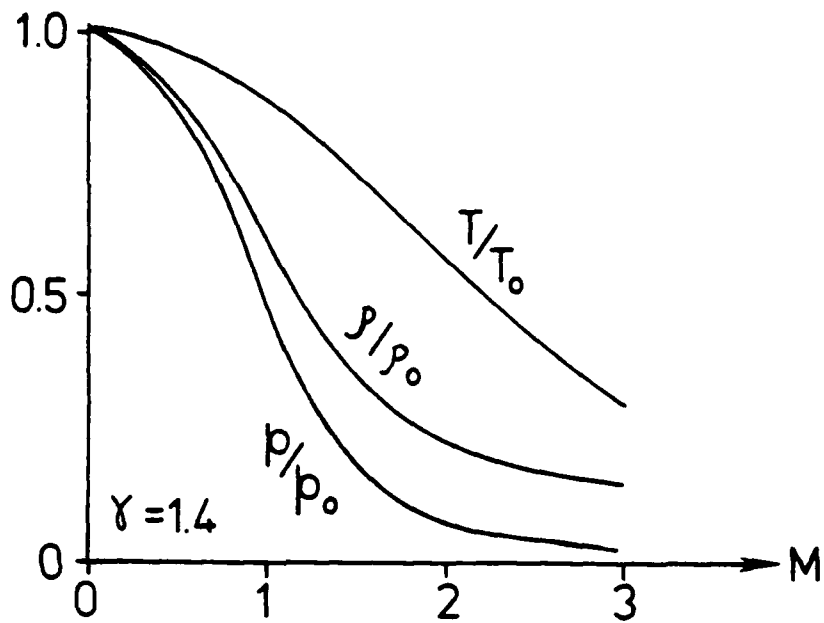
$$\frac{\rho}{\rho_o} = (\frac{T}{T_o})^{\frac{1}{\gamma-1}}$$

- mass flux constant =  $\rho AV$ , so

$$\frac{A}{A^*} = \frac{1}{M} [(\frac{2}{\gamma+1})(1 + \frac{\gamma-1}{2} M^2)]^{\frac{\gamma+1}{2(\gamma-1)}}$$

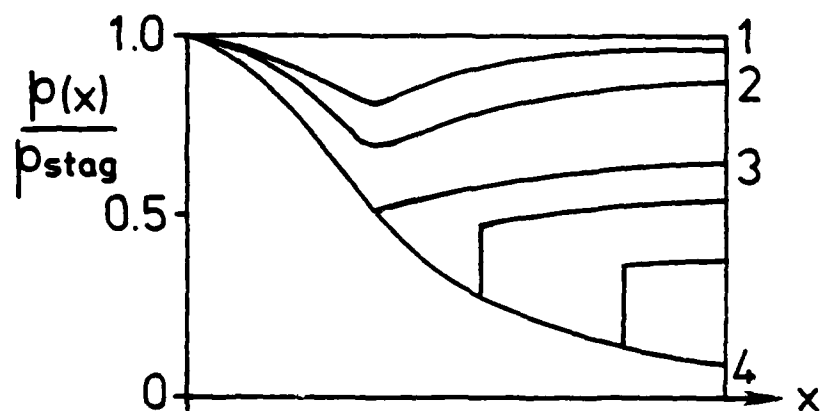
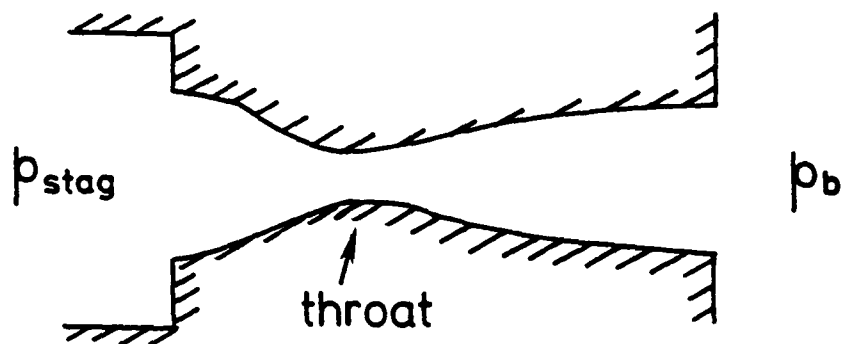
-tabulated for various γ

Qualitative behavior of isentropic relations:



Nozzle performance determined by:

- geometry
- back pressure
- stagnation pressure



## Normal shocks (stationary)

$$\text{Mass} \quad \rho A V = \text{const.}$$

$$\text{Momentum} \quad p + \rho V^2 = \text{const.}$$

$$\text{Energy} \quad h + \frac{V^2}{2} = \text{const.}$$

- for ideal gas, downstream conditions determined by  
gas  $\gamma$ , and upstream  $M_1$

$$M_2^2 = \frac{M_1^2 + \frac{2}{\gamma-1}}{\frac{2\gamma M_1^2}{\gamma-1} - 1}$$

$$\frac{p_2}{p_1} = \frac{2\gamma}{\gamma+1} M_1^2 - \frac{\gamma-1}{\gamma+1}, \text{ etc.}$$

- again, tabulated for various  $\gamma$
- $p$ ,  $T$ ,  $\rho$  increase, while  $V$ ,  $M$ ,  $p_{\text{stag}}$  decrease
- moving 1-D shocks similar - fix ref frame to wave
- oblique shocks similar - velocity component normal to wave

Real nozzle performance qualitatively as above,  
but complicated by:

- multidimensional flow  
 $V = V(x, y)$ , etc.
- boundary layers at walls
- shock-boundary layer interaction  
(shocks not normal)
- turbulence
- separation
- heat transfer

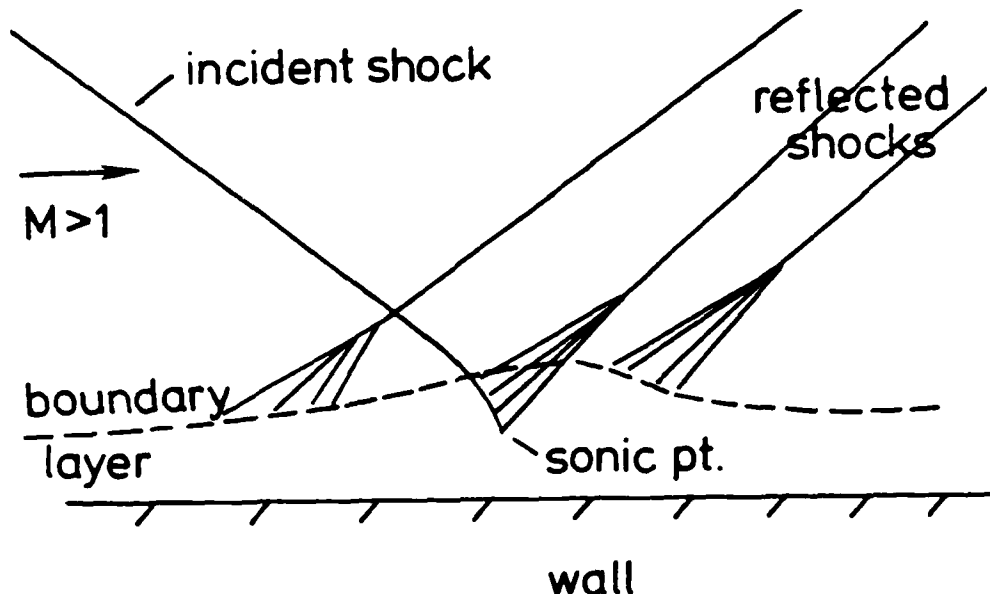
#### Reynolds Number

$$Re = \frac{\rho VL}{\mu} = \frac{\rho V^2}{\mu \frac{V}{L}} = \frac{\text{inertial effects}}{\text{viscous effects}}$$

- as  $Re$  increases, viscous effects decrease wrt inertial effects
- as  $Re$  increases, viscous effects (shear) become confined in thin regions near walls, called boundary layers
- $Re$  a key parameter in determining transition of b.l. from laminar to turbulent
- $Re$  a key parameter in determining boundary layer thickness,  $\delta$ , and skin friction

## Shock-boundary layer interaction

- refer to Shapiro, Vol. 1, pp. 581-83



- can lead to separation or transition
  - boundary layer separation point defined as
- $$\tau_w(x_{sep}) = 0$$
- shock - b. l. interaction smaller for turbulent b. l. than for laminar b. l.

## Turbulent Flow

- arises due to instability of laminar flow at large  $Re$  (refer to Ch.16-17 of Schlichting)
- not deterministically understood
- common flow state for most engineering applications
- assume all fluid properties broken into mean and fluctuation; i.e.,

$$\mathbf{V} = \bar{\mathbf{V}} + \mathbf{v}' \quad \text{where}$$

$\mathbf{v}'$  = turbulent fluctuation

sub into momentum and time-avg:

$$\rho \frac{\vec{dv}}{dt} = -\nabla \bar{p} + \rho \vec{g} + \mu \nabla^2 \bar{\mathbf{V}} - \frac{\partial (\rho v_i' v_j')}{\partial x_j}$$

Reynolds  
Stresses

Characterize turbulence by:

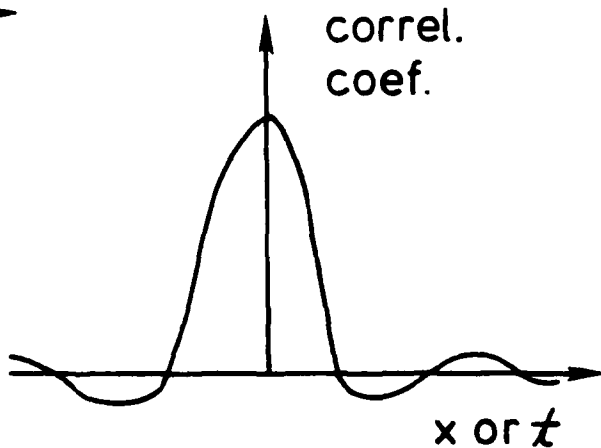
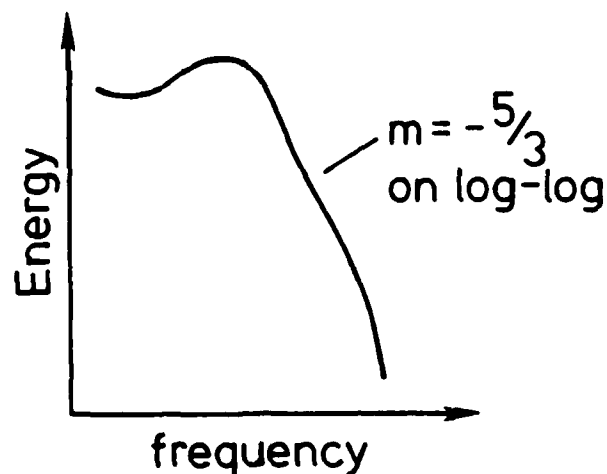
- is 3-D, unsteady, irregular, vorticular, occurs over a wide range of length scales ("eddy sizes") from a max (geometry) to a min (viscosity)
- turbulence intensity

$$I = \sqrt{\overline{(u')^2}} / \bar{u}$$

or

$$I = \sqrt{1/3(\overline{u'^2} + \overline{v'^2} + \overline{w'^2})} / \bar{u}$$

- spectra, correlations, etc.



Turbulence leads to:

- more mixing
- more shear, skin friction
- more heat transfer
- more energy dissipation
- increased pressure drop
- less chance of boundary layer separation

Control or generation of turbulence:

- to decrease turbulence:
  - streamlining; contouring
  - favorable pressure gradient - relaminarize
  - smooth walls
  - suction through walls
  - long-chain molecules or fibers
  - near wall passive devices (riblets, LEBUs)
  - wall cooling for gases
- to generate turbulence or transition, do the opposite, or use screens or grids or wall trips

## Heat transfer by gas flow (convection)

- refer to Ch. 12 and Ch. 23 of Schlichting
- there exists an analogy between heat transfer and skin friction, valid for

2-D flow  
 no radiation  
 no viscous dissipation  
 no compressibility

$$N = 1/2 C_F Re f\left(\frac{X}{L}, \text{Pr}\right)$$

where

$$N = \text{Nusselt No} = \frac{hL}{k} = \frac{qL}{k\Delta T}$$

Re = Reynolds No

$$C_F = \text{skin friction coeff} = \frac{\tau_w}{\frac{1}{2} \rho U^2}$$

$$\text{Pr} = \text{Prandtl No} = \frac{\mu Cp}{k}$$

$h$  = Connective heat transfer coefficient

- for flat plate, simplifies to

$$N = 1/2 C_F Re$$

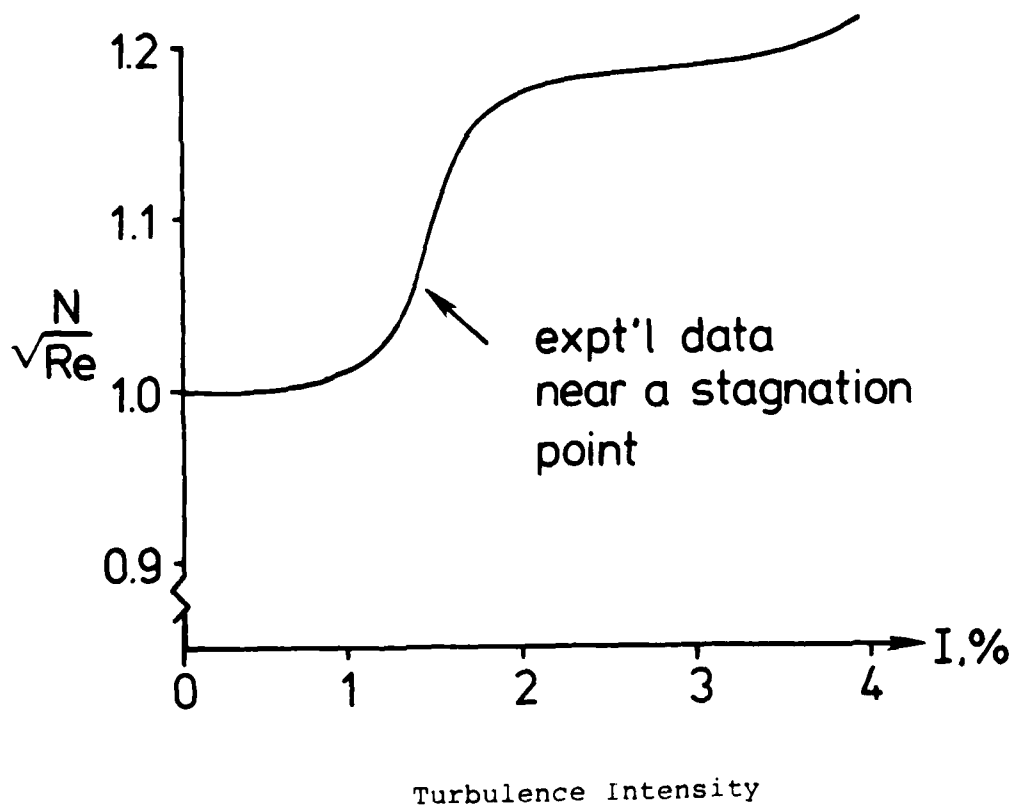
assuming  $\text{Pr} = 1$

- also valid for turbulent flow
- heat transfer ~ skin friction

## Convective heat transfer (con't)

to increase heat transfer:

- increase surface area
- wall cooling (increase  $\Delta T$ )
- wall roughness (but  $\tau_w$  increases more)
- free stream turbulence (again,  $\tau_w$  increases more than  $q$ )



SURFACE PHENOMENA IN SPARK GAPS

L. E. Murr

Department of Materials Science and Engineering  
Oregon Graduate Center  
Beaverton, Oregon 97006

A Presentation at  
A DoD Sponsored Workshop  
on  
"REPETITIVE SPARK GAP OPERATION"

Tamarron, Colorado  
January 17-19, 1983

CONTENTS

	<u>Page</u>
INTRODUCTION . . . . .	1
CHEMICAL AND PHYSICAL PROCESSES IN SPARK GAPS. . . . .	2
CHARACTERIZATION OF SURFACE PHENOMENA IN SPARK GAPS. . .	3
SOME EXAMPLES OF SURFACE PHENOMENA AND CHARACTERIZATION OF SPARK GAP MATERIALS. . . . .	38
GENERAL SUMMARY. . . . .	53
REFERENCES . . . . .	54
APPENDIX . . . . .	56

This presentation contains copyrighted material which should not be reproduced without permission from the publisher (Marcel Dekker, Inc., New York). This material is acknowledged where appropriate. The author is also grateful to Dr. C. Stein (AFWL) whose early efforts to encourage some understanding of spark gap degradation have contributed to this presentation.

INTRODUCTION

High power, repetitive spark gaps represent a somewhat unique technological example of complicated, interrelated physical, chemical, and electrical processes which are ultimately manifested in a host of real and potential materials degradation and alteration phenomena. While there have been a number of investigations concerned with an evaluation of electrode and insulator (dielectric) materials as candidates for high performance spark gap operation (1-6), there have been only a few studies aimed at characterizing materials degradation in spark gaps (7-9). These latter studies must certainly be regarded as preliminary since they have not been concerned with the systematic elucidation of the mechanisms involved in the alterations in the materials which occur, especially in the context of surface phenomena involving changes in structure, composition and topography. Our current understanding of surface phenomena associated with repetitive spark gap operation is sketchy at best. Spark gap candidate materials have thus far been utilized largely on the basis of performance testing and evaluation which did not involve detailed materials characterization studies.

At the present time, there are few systematic correlations between surface structure or related surface phenomena for either electrode or insulator materials and spark gap performance criteria. In fact in recent studies of Rohwein (10), brass electrodes with three drastically different surface finishes exhibited no perceptible difference in partial discharge inception voltage either before or after the electrodes were pitted by discharges in bulk transformer oil. However, Suzuki, et al (5) have claimed that the arc erosion resistance improves with the reduction of tungsten grain size, and with tungsten content, in tungsten alloy composite electrodes. There is no similar data for more homogeneous alloys such as brass.

Because of the erosion and surface alteration which occurs in a repetitive spark gap application, it is doubtful that surface phenomena can be treated separate from bulk microstructure. In addition, it is possible that because of temperature gradients, diffusion, and other related processes, recrystallization and grain growth are sure to occur in electrodes. Shock wave effects could also influence the occurrence and concentration of crystal defects, a phenomenon well characterized for explosive and laser shock events in many metals and alloys, (11,12).

#### CHEMICAL AND PHYSICAL PROCESSES IN SPARK GAPS

The chemical and physical processes occurring in repetitive, high-energy spark gap switches are only beginning to be elucidated. The spark gap regime itself consists of three principal components:

- THE ELECTRODES
- THE INSULATOR
- THE FILLER GAS

In the presence of a high-energy spark, the filler gas can be altered and the electrodes heated. Radiation in the arc can bombard the insulator and the associated shock pulse can impinge upon both the electrodes and the insulator. Spark erosion of the electrode surfaces can occur along with chemical reactions with the filler gas or impurities in the gas. The spark induced electrode surface erosion can produce metal ejection and deposition within the gap regime, coating the insulator surface, and ejected or desorbed matter from the electrode can react with the filler gas. Electrode heating can lead to diffusional phenomena and microstructural alterations including

selective desorption such as dezincification in brass electrodes and electromigration in high current conduction pulses.

These complex, synergistic phenomena might be depicted schematically as illustrated in Fig. 1 and Fig. 2. The macroscopic changes characterizing spark gap materials degradation are illustrated in Fig. 3 which shows electrode alteration (erosion, composition changes, structural changes) and insulator modification (metal deposition and other reaction product formation).

There are several examples of process characterization which support some of the reaction features depicted in Fig. 1. In the work of Murr, et al (8) which examined brass electrodes arcing in air, copper oxides were identified on the electrode surface and dezincification of the electrode center was readily apparent. In the more recent work of Gordon, et al (9), copper and tungsten fluorides were identified on copper-containing tungsten electrodes arcing in SF<sub>6</sub>. Metal deposition on insulators as a result of electrode vaporization has been observed as well (8,9). The emission of gases from both the electrodes and the insulator can add to the reaction processes. Water vapor can contribute to the formation of complex hydroxides, and oxygen can also react to form CO<sub>2</sub>. Gas emission from the electrodes can contribute to blister formation and associated surface alteration.

#### CHARACTERIZATION OF SURFACE PHENOMENA IN SPARK GAPS

It is unlikely that surface structure at the atomic or molecular level will play a significant role in spark gap operation because at this level the structure is continuously changing.\* As a consequence, surface phenomena might be regarded as transitional, and rather than a simple Gibbs dividing surface (13) the "surface" might be regarded as an interfacial phase whose

\*Some exceptions may be observed such as reactions at dislocations and grain boundaries intersecting the surface.

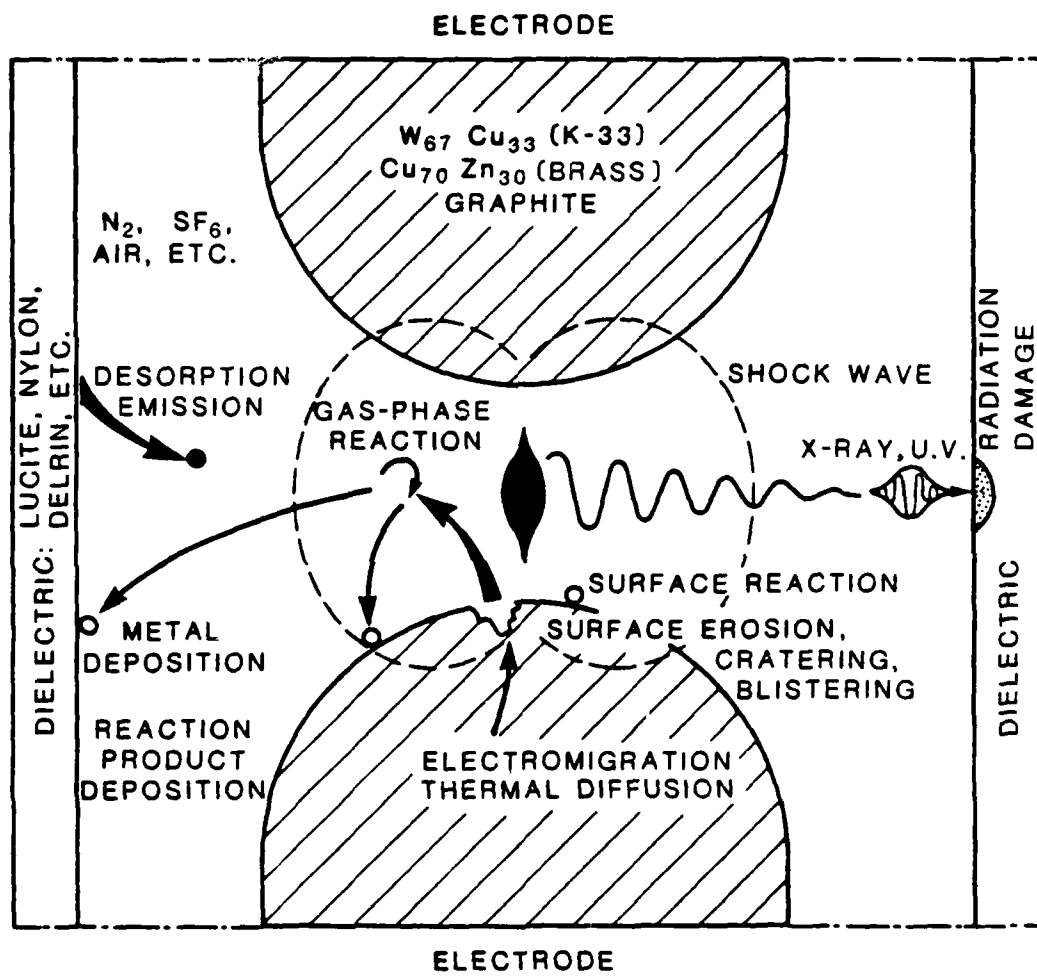


FIG. 1

Schematic representation of the more apparent chemical and physical processes associated with repetitive spark gap degradation.

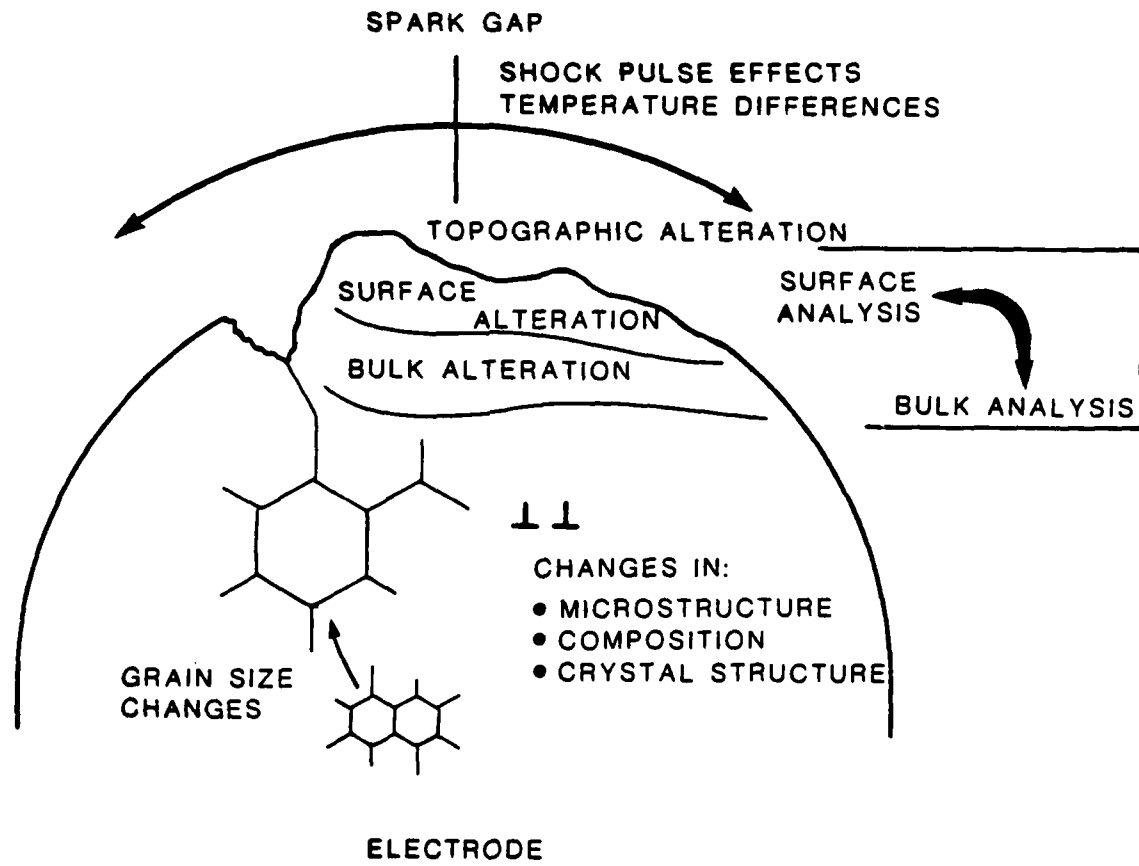


FIG. 2

Simple concept for structural alteration and degradation of spark-gap electrode.

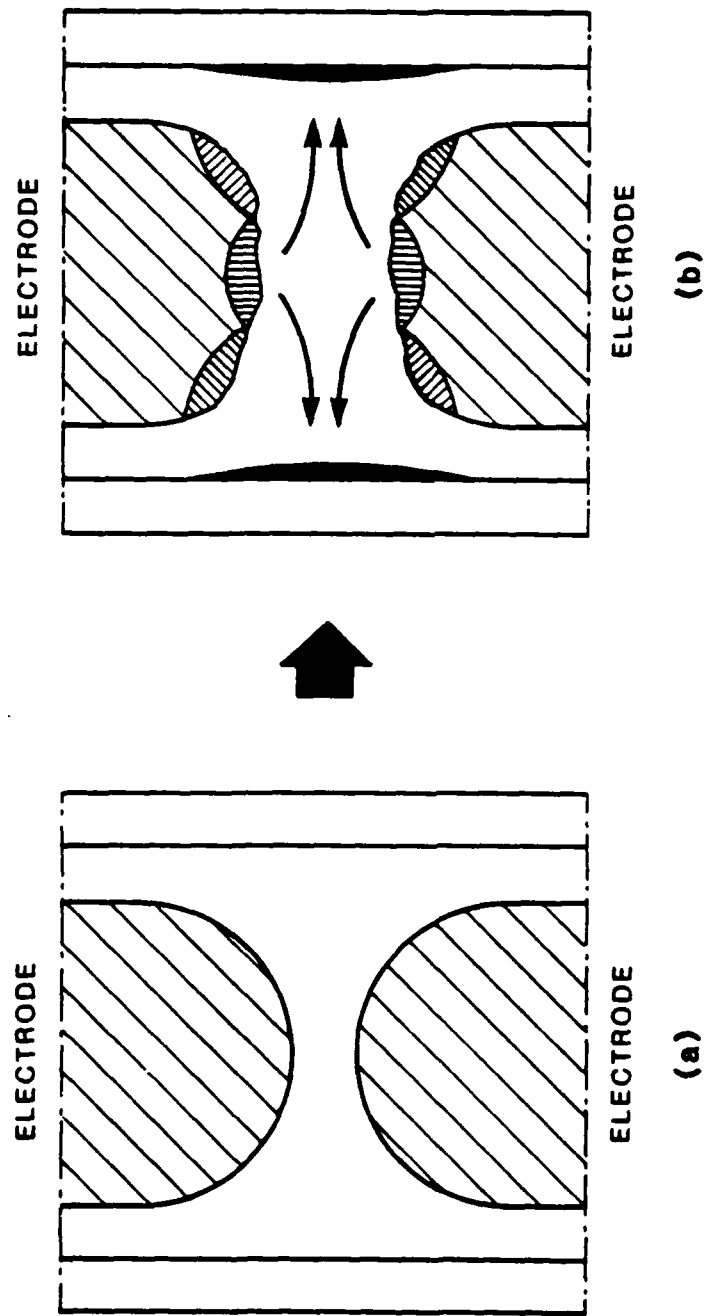


FIG. 5

Macroscopic features of spark gap degradation

dimensions could conceivably vary from less than 10 Å to more than 0.1 µm. At the latter dimension, we must regard this regime as a new bulk phase or reaction product which has added new structure and additional interfaces, including possibly grain or phase boundaries within the new regime. In addition to reaction products, surface erosion, desorption of material, electromigration, vaporization, and related phenomena can contribute to alteration as shown in Fig. 3. This alteration is associated with changes in the gap dimensions, electrode geometry, etc. In order to effectively characterize these actual and anticipated processes (as depicted schematically in Fig. 1-3), it is necessary to observe structural and microstructural changes of the surface and to be able to simultaneously analyze the composition of the surface and near surface regime. It is also important to connect the surface regime with the bulk, and surface alteration with alterations occurring in the bulk, especially for the electrodes. Consequently, we need to relate surface structure and composition with bulk structure and composition as illustrated in Fig. 2. Because of the electrode geometry and electrode degradation creating irregular topographies, etc. and the characterization necessary to understand these phenomena in detail, we must utilize a range of analytical techniques capable of providing structural, microstructural and microchemical information about both the "surface phase" and the bulk phase components of insulating materials and electrodes in the spark gap environment.

Although both static and dynamic (in-situ) analysis can be useful, the more amenable or tractable approach will involve direct observations and microanalysis following specific periods utilizing a given set of operating parameters.

There are a range of powerful and generally accessible microanalytical techniques which can contribute to the detailed characterization of spark gap materials and materials alteration and degradation. These include a variety of spectrometers utilizing electron, ion and "optical" sources and detectors, and microscopes utilizing electron and ion optics for high resolution ( $<0.1 \mu\text{m}$ ) and even light microscopy or optical metallography for lower resolution.

The ability to connect bulk structure and composition with surface structure and composition will likely require a range of analytical techniques and resolutions in order to put microstructure in perspective with macrostructure.

Optical spectroscopy is in many instances a convenient analytical technique because of the ability to detect signal perturbations as a result of composition or microstructural changes *in-situ*. Thus the ability to direct a signal into the spark gap environment and study its properties upon exiting the environment provide a dynamic analysis. The various optical spectroscopies allow signal absorption profiles or related signal features to be monitored as a measure of structural characteristics through comparison of input/output signal features.

Table 1 summarizes many of the more contemporary electron and ion spectroscopies. While many of these can provide useful insight into the properties and behavior of spark-gap materials, and are capable of surface resolution at or near the atomic level, they are cumbersome and not readily available. We shall therefore limit our discussion here to a few of those which can provide a wealth of information regarding surface phenomena. Some examples of the basic mechanisms involved in some of the more common electron spectroscopic methods are shown in Fig. 4 in the context of fundamental mechanisms involved in Energy Dispersive X-ray Spectroscopy (EDS/EDX), Auger Electron Spectroscopy

TABLE 1 (From L. E. Murr, Electron and Ion Microscopy and Microanalysis: Principles and Applications, Marcel Dekker, Inc., New York, 1982.)

TABLE 4.3 Summary of the principal features of different electron and ion microprobe techniques

26

Acronym	Technique	Incident (exciting) radiation	Particle emitted	Sample Penetration	Lateral resolution	Detection Limit	Detectable element range	Materials application obtained
AES	Auger electron spectroscopy	electron at 0.1-5 keV	Auger electron	0-10 Å	0.1-0.3 μm	0.1%	>Li	any solid matter, adsorbate analysis, elemental analysis of surface
EDS/EDX or EDXA	Energy dispersive x-ray spectroscopy	(10-30 keV)	Characteristic x-ray photon	>μm	>μm	0.1%	>Na	any solid matter, elemental analysis of bulk or near surface regime
EID	Electron-induced desorption	electrons at 20-1300 eV	neutral particle or ion absorbed	none	—	<0.1%	—	solid surfaces
ELS/EXLS	Electron energy loss spectroscopy	electron* at 750 keV	inelastically scattered electron	0.01-0.1 μm	<0.04 μm	<0.1%	>Li	any solid thin film; elemental analysis
EPMA/WDS	Electron probe microanalysis/wavelength dispersive (x-ray) spectrometry	electron at 0.5-40 keV	characteristic x-ray photon	0.02-2 μm	>μm	<0.1%	>Li	any solid matter, elemental analysis (near-surface composition)

\*Field-emission source. Note that in most cases listed the conventional electron or ion emission source is implicit. Use of field-ionization or field-emission sources will improve the performance.

ELECTRON AND ION PROBE MICROANALYSIS

ESCA	Electron spectroscopy for chemical analysis	U.V. photons	photo-electron	~5-20 Å	0.2-1 μm	0.1%	>Na	any solid, gases, frozen liquids; elemental composition, chemical binding, electronic states
FDS	Field-desorption spectroscopy (see imaging atom-probe mass spectroscopy next)	—	—	—	—	—	—	—
IAPMS/APFM	Imaging atom-probe mass spectroscopy/atom-probe field-ion microscopy	—	ion or ions desorbed from surface	individual layers can be pulse desorbed	single atom	single atom	all elements and isotopes	many metal and semiconductor whiskers, adsorption phenomena, depth profile, crystallographic data, etc.
HEIS	High-energy ion scattering	(see RBS)	—	—	—	—	—	—
ISS	Ion scattering spectroscopy	ion at 25-10 <sup>3</sup> eV	same as incident	first exposed layer at any time	1-100 μm	0.1% to 100 ppm (bulk)	>Li	all solid matter, elemental composition, location of adsorbed species, semiquantitative depth profile
LEIS	Low-energy ion scattering	ion 20-2000 eV	same ion as incident	5-10 Å	<100 μm	0.1%	>Li	any solid material, elemental composition, depth composition profile, adsorbed species.

SUMMARY AND COMPARISON OF MICROANALYSIS TECHNIQUES

(Continued on next page)

TABLE 1 (Continued)

TABLE 4.3 (continued)<sup>†</sup>

Acronym	Technique	Incident (exciting) radiation or particle	Particle emission	Sample penetra- tion	Lateral resolu- tion	Detect- tion	Detectable element range	Materials applica- tions and informa- tion obtained
PIXE	Proton- induced x-ray emission	ion(pro- ton) 2- 200 keV	charac- teristic x-ray photon	<1μm	<500μm	0.1-10	>Na	any solid material, bulk elemental com- position; depth com- position profile
RBS (HEIS)	Ruther- ford back- scattering	ion $10^5$ - $10^7$ e <sup>+</sup>	same ion as inci- dent	<10μm	1-3μm	0.1%	>C	Thick solids, quan- titative elemental composition, crystal orientation, surface stoichiometry
SAM	Scanning Auger mi- croscopy/ microana- lysis							
SCANNIR	Surface com- positional analysis by neutral and ion impact radiation	ion <4 keV	sputtered excited neutral particle or ion	exposed layer	<100μm	>0.1%	>Li	solid materials, ap- proximate elemental composition of sur- face layers
SIMS	Secondary ion mass spectro- scopy	ion $10^3$ - $10^6$ eV	secondary (surface) ion	exposed layer, (<10 Å)	0.1-1μm	0.1 ppm	>H	solid materials: ele- mental composition of the surface; depth composition profile (sample destruction)

<sup>†</sup>You should note that the sensitivities, etc. given refer ideally to a dedicated technique on analytical system. There is sometimes a loss of sensitivity, etc. when the technique is part of an integrated-modular system. (See Ref. 69 for additional details and applications of SIMS, ISS, AES, XPS, etc.).

UPS/XPS	ultra- violet photoelec- tron spec- troscopy/ x-ray photo- electron spectro- scopy	U.V. or x-ray photon	photo- electron	10-30 Å	<10 <sup>1</sup> μm	1%	>Na	solid materials; work function ana- lysis, adsorbed molecules, electro- nic states of sur- face, approximate chemical composi- tion
---------	--	----------------------------	--------------------	---------	---------------------	----	-----	--

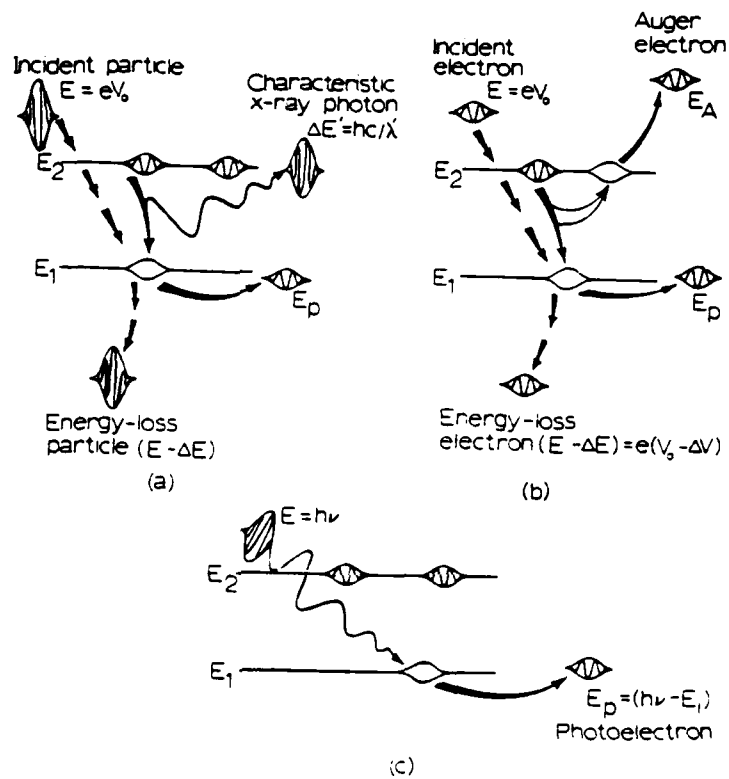


FIG. 4

Atomic and molecular ionization processes involving single and multiparticle transitions associated with inelastic scattering. (a) Primary particle of energy  $E$  producing photoelectron of Energy  $E_p$  and characteristic x-ray of energy  $E'$ , and energy-loss (exit) particle, (b) Primary electron of energy  $E$  producing photoelectron of energy  $E_p$ , Auger electron of energy  $E_A$ , and energy-loss (exit) electron, (c) Incident x-ray photon of energy  $E$  produces only photo electron of energy  $E_p$ . (Fig. 4.17 in Ref. 14)

(AES), and ESCA or X-ray Photo-electron Spectroscopy (XPS). In EDX and AES electrons interacting with a sample target produce characteristic X-rays or electrons, respectively, which are detected and displayed in electron optical systems as illustrated schematically in Fig. 5 for characteristic X-rays, and in Figs. 6 and 7 for characteristic or Auger electrons. Auger electron signal display can be in the form of a spectrum or a gated CRT display producing a characteristic element map of an area. When this feature is coupled with a secondary electron detector in an electron optical arrangement typical for a scanning electron microscope (SEM) as illustrated for example in Fig. 8, a scanning Auger microscope results which can provide the kind of versatility in surface structure and composition as illustrated in the examples shown in Figs. 9 and 10. This characteristic mapping of elements can also be very conveniently performed for EDX analysis as illustrated in Fig. 11.

From the examples shown in Figs. 9-11 it should be apparent that (with reference to Table 1) small reaction products, inclusions, or surface phases can be readily identified with an elemental sensitivity in the case of Auger spectroscopy for lithium, while for EDX analysis it is above oxygen. Neither of these techniques can distinguish the specific features of compound formation including oxidation states, etc. This determination requires the selectivity of ESCA and other spectroscopies.

When a solid sample is irradiated with a beam of electrons, a number of events occur producing modifications in the primary beam and secondary emissions, including characteristic X-rays, optical photons, etc., as illustrated schematically in Fig. 12. The ability to detect and operate on these various emission profiles can provide not only for surface characterization, but characterization of deeper-level phenomena, including bulk effects in thin films,

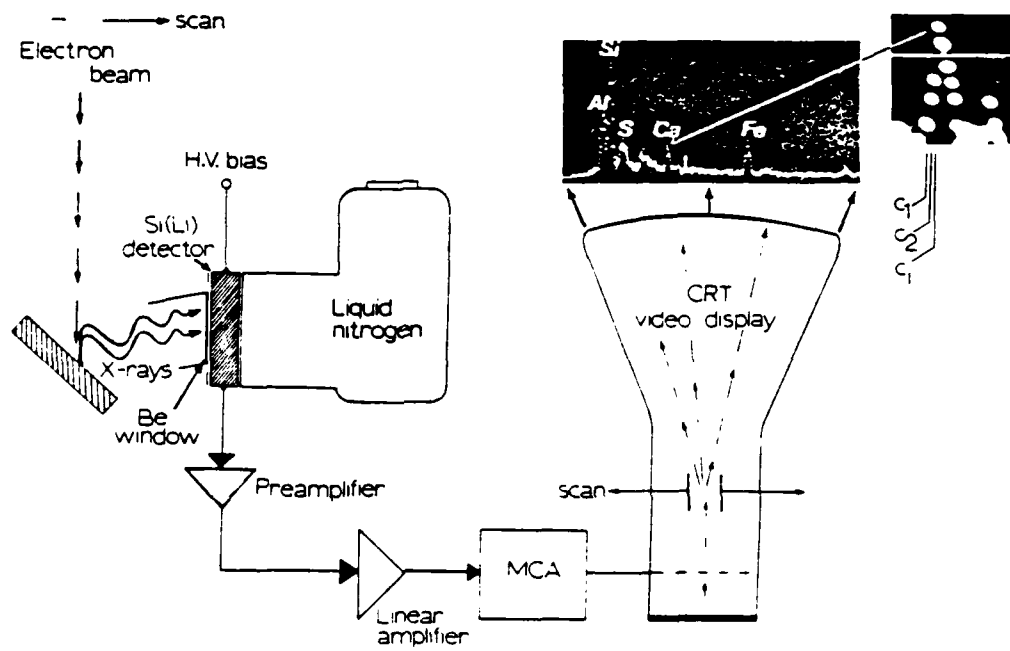


FIG. 5

Schematic diagram of solid-state EDX detection system with CRT spectrum display. The enlargement of the signal portion shows the individual channel voltage level corresponding to the total counts stored in that channel, corresponding to a particular energy fraction for the characteristic x-ray photons. (From Fig. 4.10 in Ref. 14)

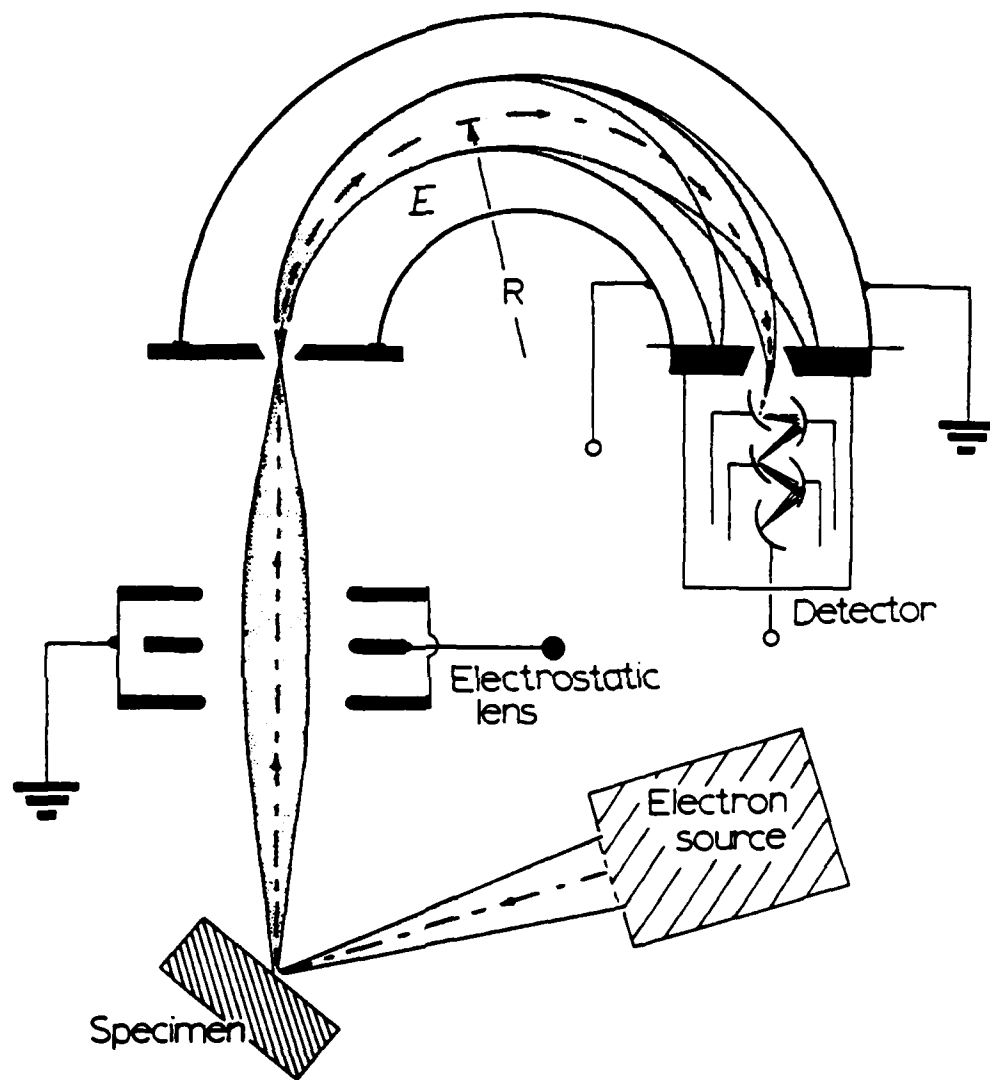


FIG. 6

Simple electrostatic analyzing system for Auger electron spectroscopy based upon characteristic velocity (energy) separation. (From Fig. 4.18 in Ref. 14)

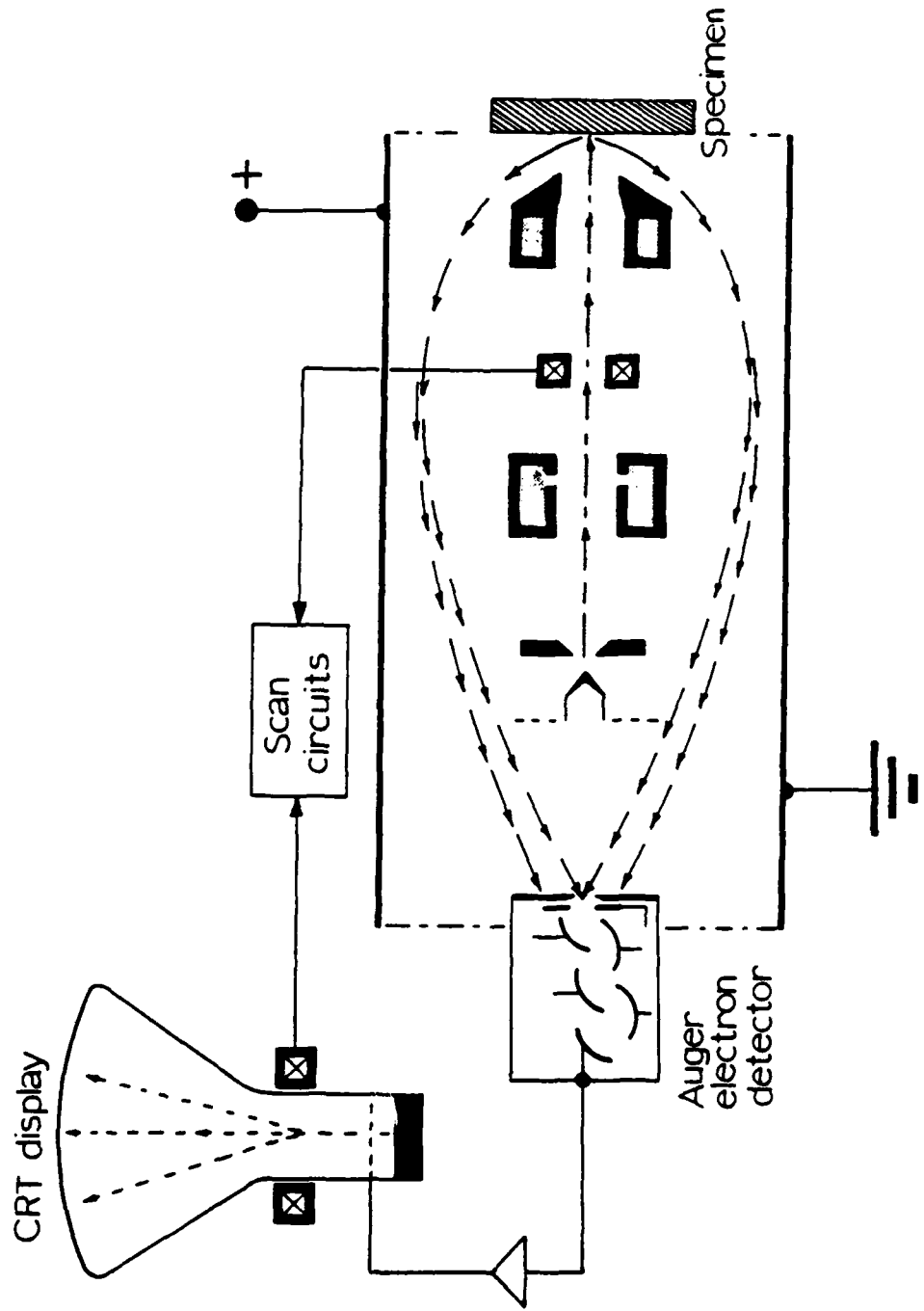


FIG. 7

Scanning Auger microprobe utilizing electrostatic, cylindrical-mirror electron analyzer with an internal electron source. (Fig. 4.29 in Ref. 14)

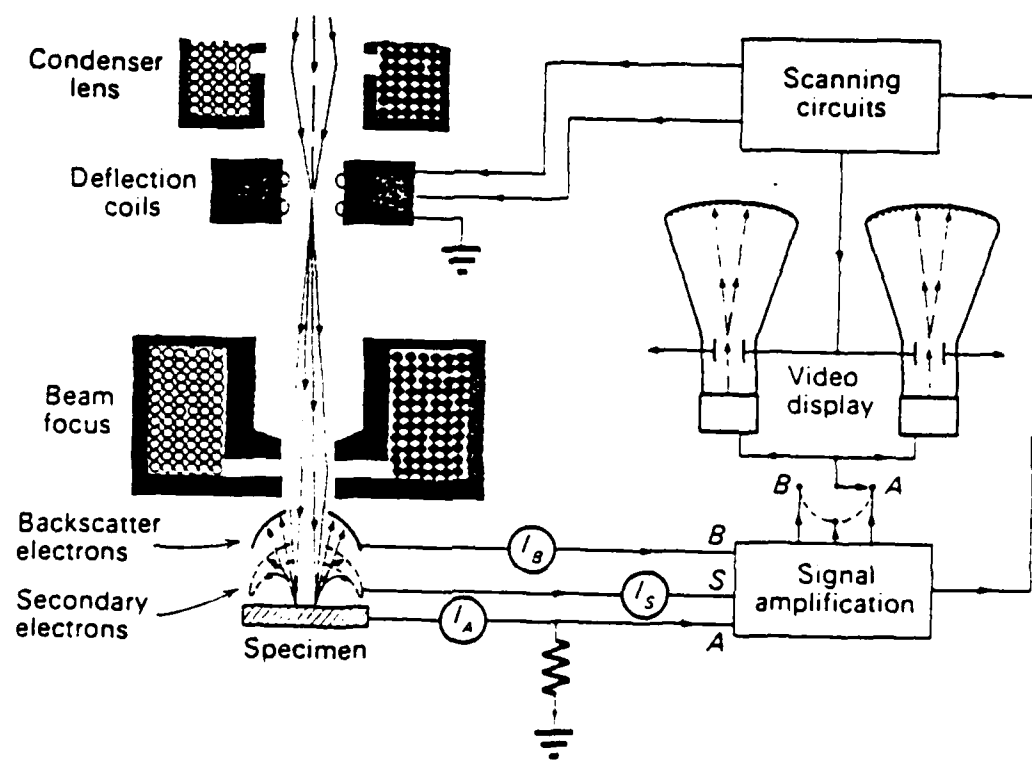


FIG. 8

Scanning electron probe system (SEM) schematic showing detection/display for secondary, backscattered, and absorbed electron signal data. (From Fig. 4.16 in Ref. 14)

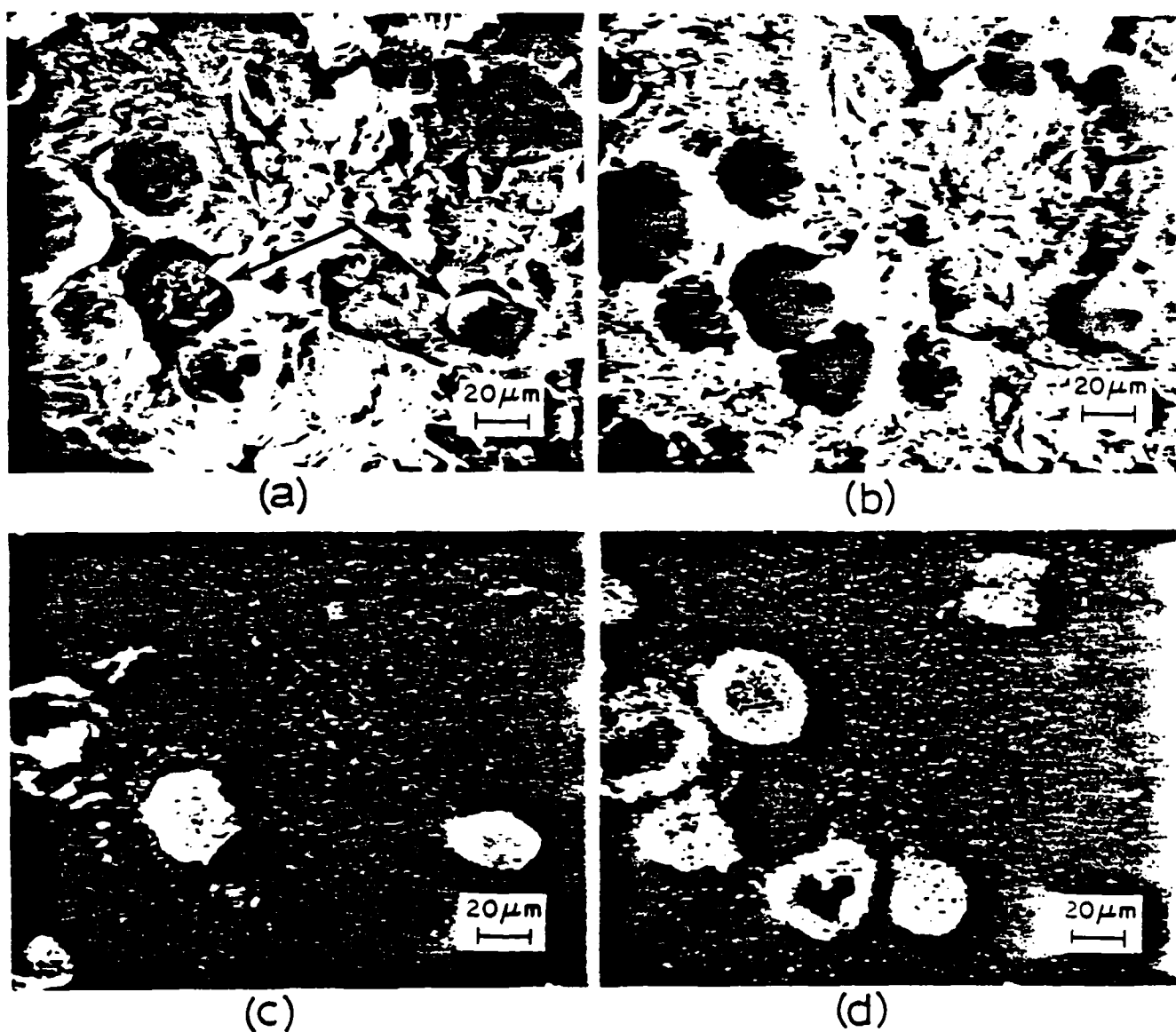


FIG. 9

Identification of carbide precipitates and zones of selective segregation of elements on the fracture surface of a modular cast iron in the SEM.  
 (A) Secondary electron image of the fracture surface, (B) Characteristic Fe-Auger image (46 eV Auger electron map), (c) Characteristic C-Auger image showing the precipitates in (a) (arrows) to be carbides (27 eV Auger electron map), (d) Characteristic Sb-Auger image (460 eV Auger electron map).  
 (Courtesy of Dr. A. Joshi from Fig. 5.45 in Ref. 14)

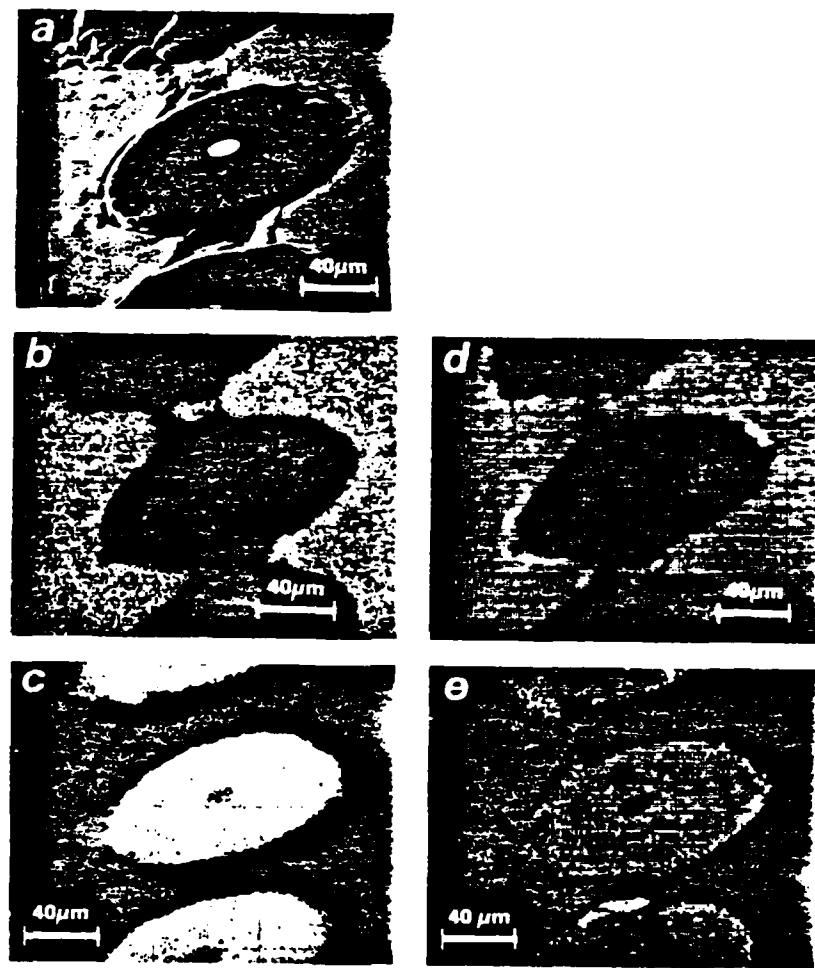


FIG. 10

Comparison of Auger and EDX elemental maps for boron fiber-reinforced titanium. (a) SEM image, (b) and (c) show Auger electron images of Ti and B respectively, (d) and (e) show corresponding EDX images (maps). (Courtesy of Dr. A. Joshi, Perkin-Elmer, Physical Electron Division, from Fig. 4.30 in Ref. 14)

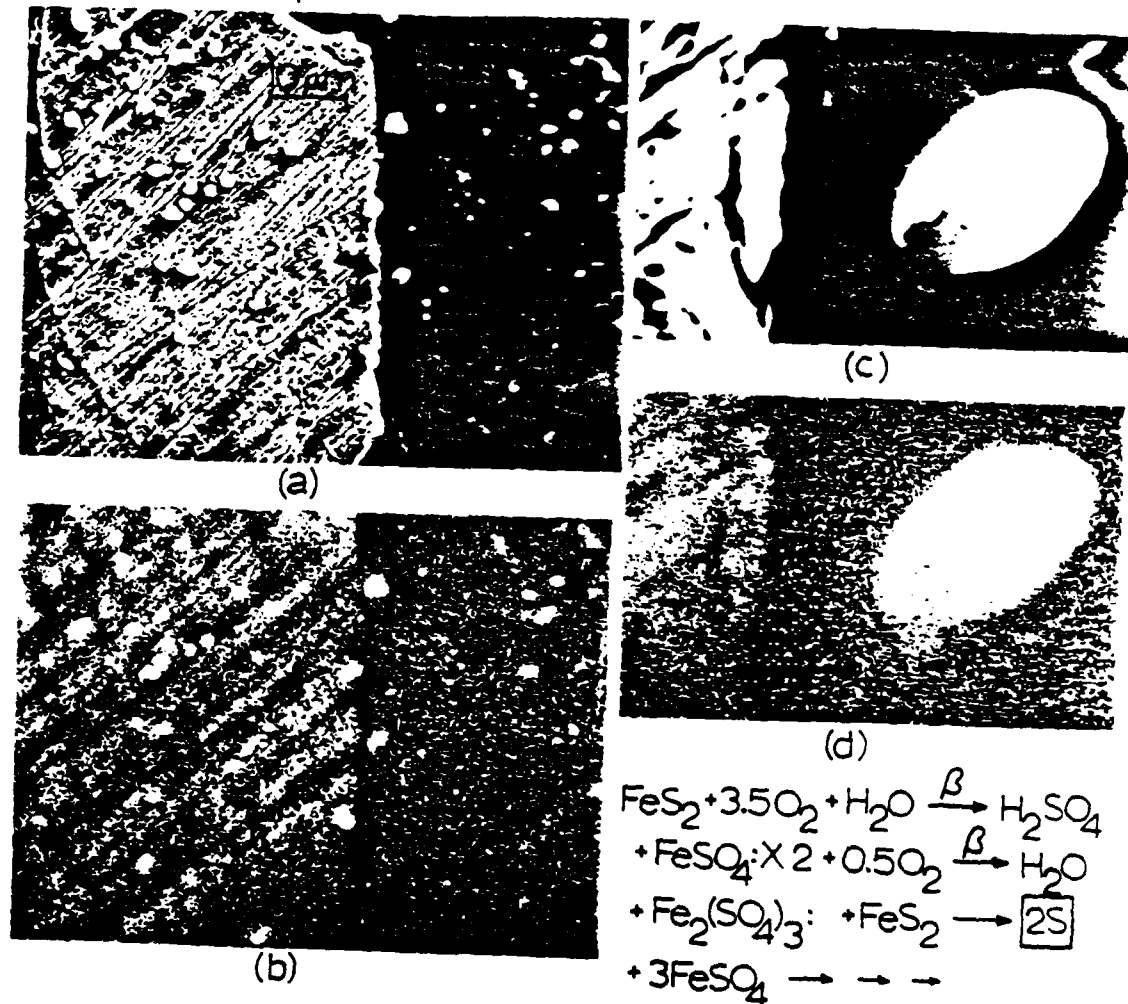


FIG. 11

Sulfur crystals formed on the surface of a leached quartz-mineral containing a reacted pyrite inclusion. (a) Secondary electron (SEM) image of leached pyrite inclusion in quartz matrix showing sulfur crystal precipitates formed on the surface as a reaction product according to the reactions shown, (b) sulfur characteristic energy-dispersive x-ray map of the area in (a). Note the sulfur image features in the pyrite region as well along etch pits and preferential etching along polishing lines, (c) Magnified view of individual sulfur particle on the quartz surface to the right of the pyrite inclusion [(arrow) in (a)]. (d) Sulfur characteristic x-ray map of (c). (From Fig. 5.44 in Ref. 14)

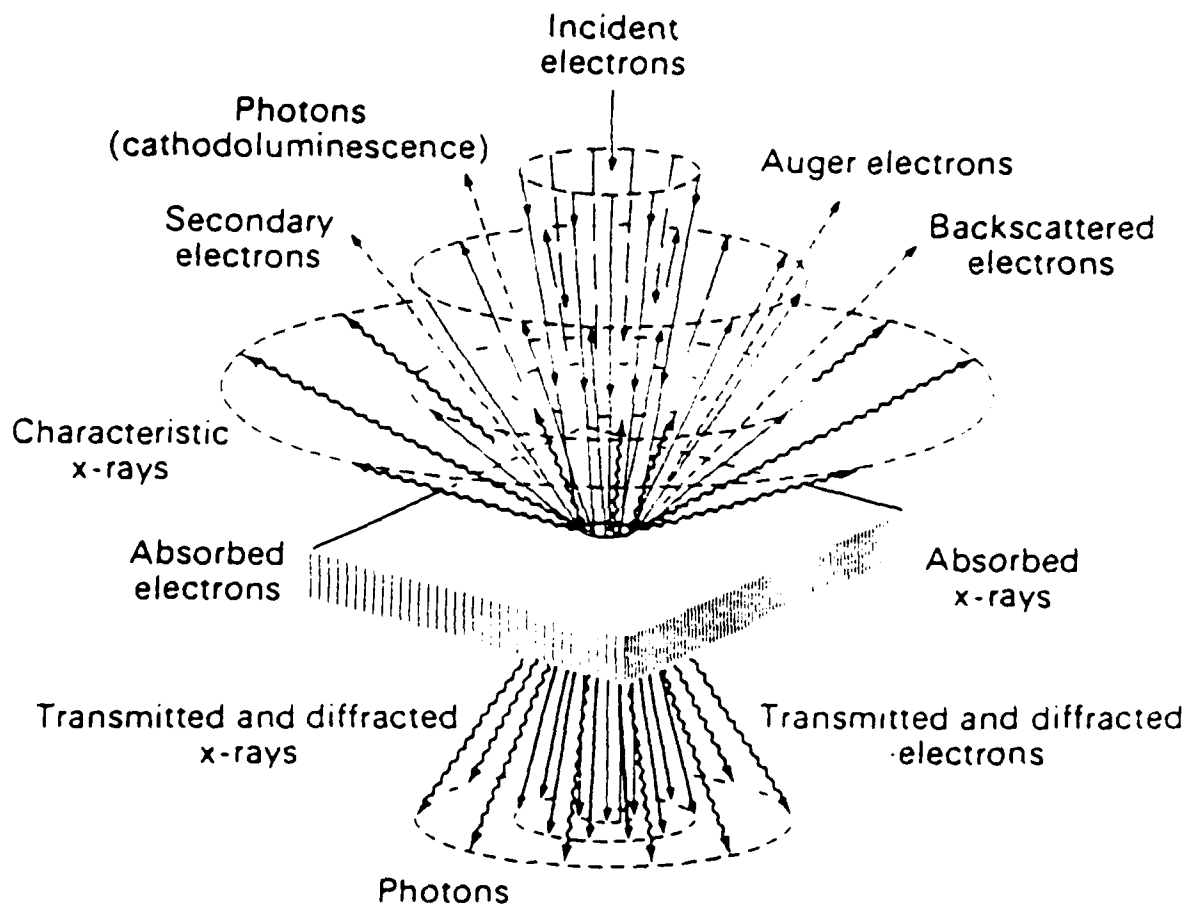


FIG. 12

Reaction and interaction of electron beam encountering  
a solid. (From Fig. 4.1 in Ref. 14)

etc. The implications for observing surface structure in the scanning electron microscope (SEM) internal microstructure in the transmission electro microscope (TEM), the analysis of electron diffraction phenomena, etc. should all be apparent in the schematic of Fig. 12.

There are similarities to Fig. 12 when an ion beam interacts with a sample. There are also some unique differences. These features are illustrated for comparison in Fig. 13. Ion spectroscopies can provide some alternatives and compliments to electron spectroscopy. In addition, it is possible to image surface features utilizing the ion emission. Some of these possibilities are illustrated in the schematic diagrams of Figs. 14 and 15. Transmission ion microscopy is also possible for thin film samples but the resolutions achieved have not been very encouraging by comparison with transmission electron microscopy. Elemental mapping of surface features utilizing ion spectroscopy appears similar to Figs. 9-11 but the spatial resolution is sometimes not as good. The concept illustrated in Fig. 14 involves a scanning ion beam. Secondary ion mass spectrometry (SIMS) is a convenient analytical format in this system along with scanning ion microscopy (SIM). Ion beams will of course produce localized sputtering and this feature can be used to promote depth profiles. In other words the surface of a spark gap electrode could be observed by secondary electron emission (SEM) and analyzed using either characteristic X-rays or electrons. An ion source could also be used to examine the surface and the surface could be systematically eroded away, systematically analyzing the underlying material. This can provide for the connection between the surface and bulk regimes as alluded to above.

Such processes could be incorporated into a microanalysis scheme shown conceptually in Fig. 16. One might refer to such a system as an integrated modular

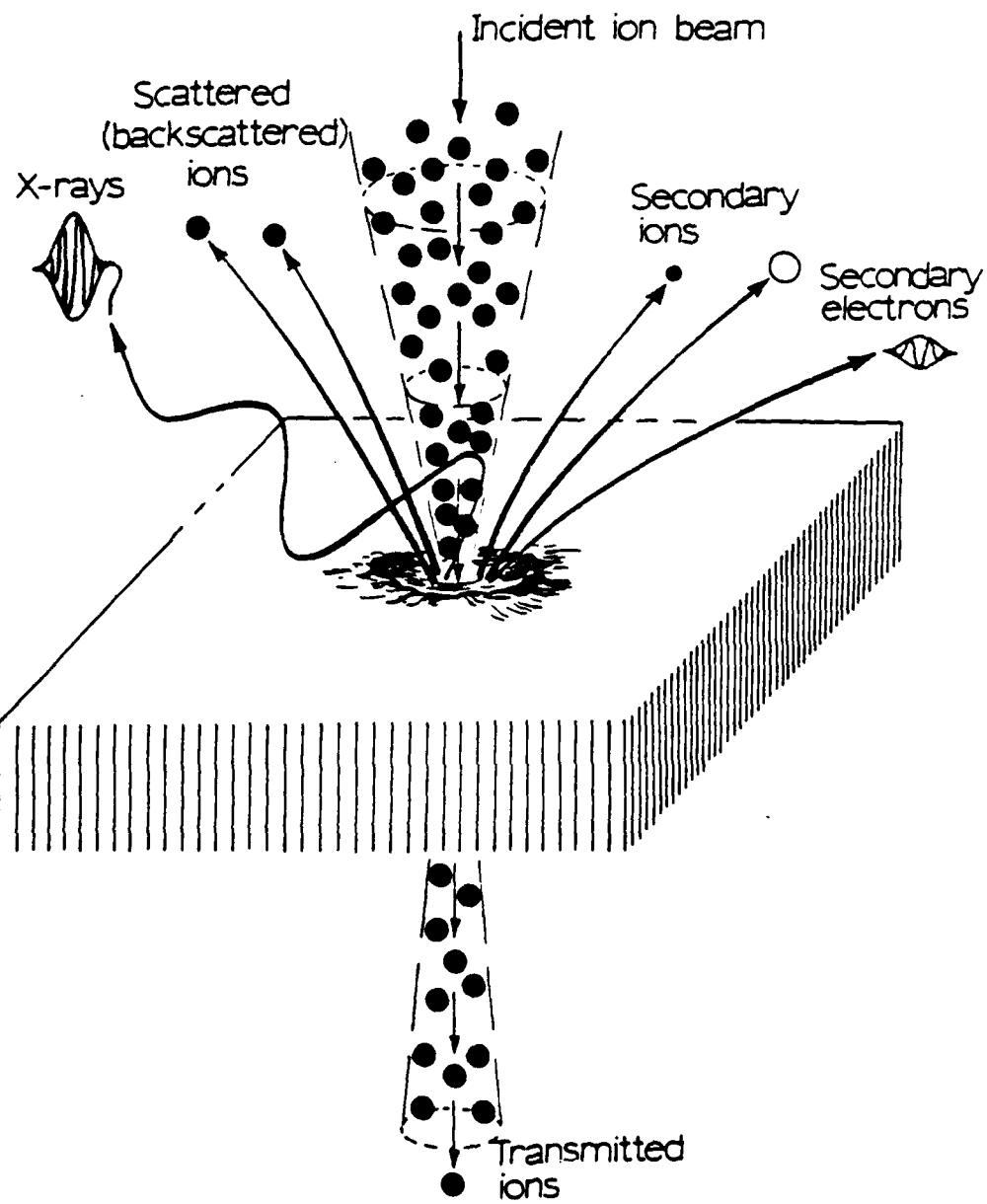


FIG. 13

Principal reaction and interaction features of ion beam encountering a solid. (From Fig. 4.39 in Ref. 14)

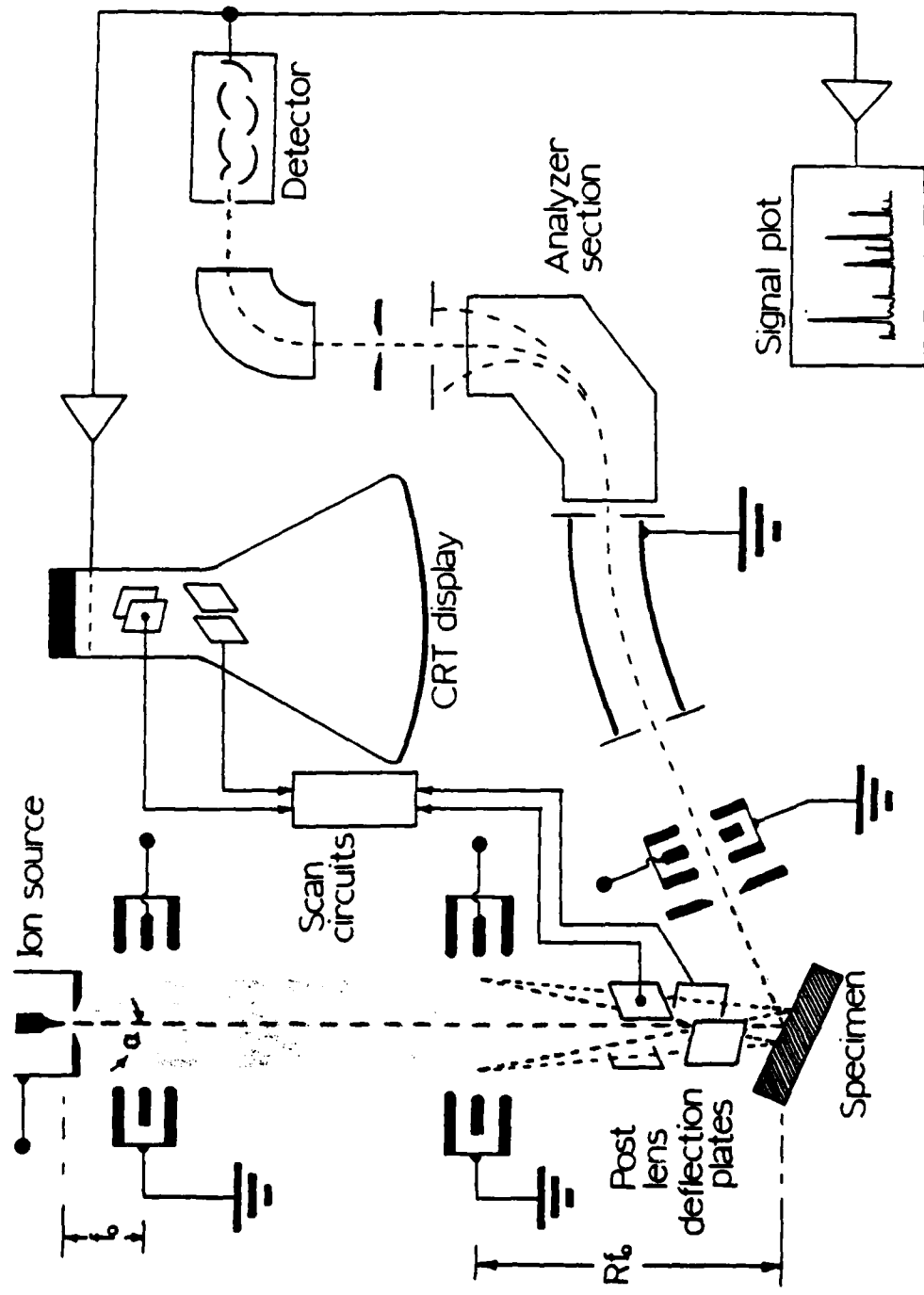


FIG. 14

Schematic representation of a scanning ion microscope (or microprobe) design utilizing a field ionization (high-brightness) source. (From Fig. 4.40 in Ref. 14)

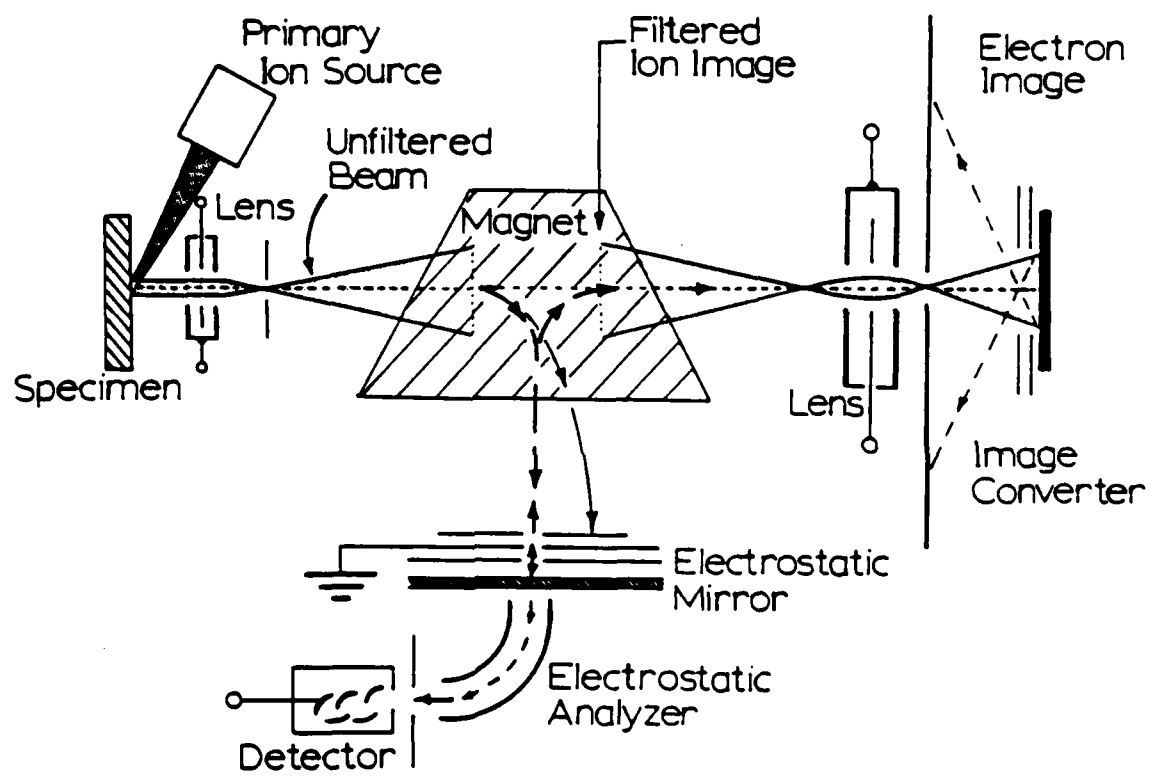


FIG. 15

Schematic diagram of an ion microscope. (From Fig. 5.49 in Ref. 14)

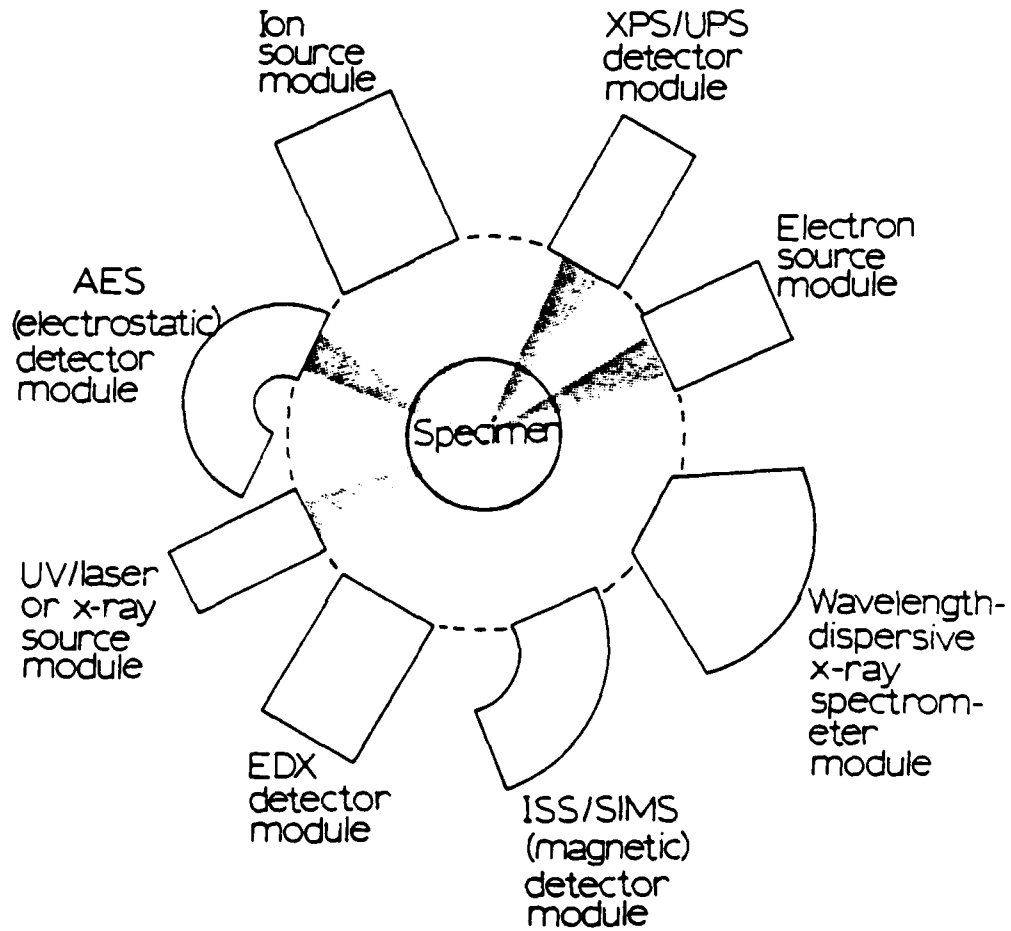


FIG. 16

Schematic representation of an integrated, modular, microanalysis system utilizing a spherically symmetric module array. (From Fig. 4.50 in Ref. 14)

microanalysis system. Such systems are in fact in use, and can appear as shown in Fig. 17. This concept can also be applied to the investigation of thin film samples which afford an even more extensive characterization capability when one considers the full implications of Fig. 12. The analytical electron microscope (AEM) is a realization of these implications, allowing TEM or scanning transmission electron microscopy (STEM), diffraction and microdiffraction, scanning electron microscopy, EDX, and other signal operations, including electron energy loss spectroscopy (EELS), depicted schematically in Figs. 18 and 19, and illustrated in Fig. 20. The analytical features to be realized from such a system are illustrated in Figs. 21 to 25.

It must be recognized that only a few of the more promising and available microanalytical techniques have been emphasized and illustrated in this brief presentation. For a more complete treatment of electron and ion microscopy and microanalysis the reader is directed to Ref. 14. (See Appendix)

There are some features of sample preparation which need to be discussed briefly. Indeed there are numerous techniques which can and must be utilized to effectively characterize not only surface phenomena, but also bulk structure and composition in connection with the surface phenomena (14). Actual surface features can be preserved in sample preparation by placing a lacquer on the surface and electropolishing or chemically polishing the bulk sample segment from the opposite side. Electron microscopy on such thin films with a preserved surface can correlate surface features with defect structures in the "surface phase", and into the bulk. The preservation of surface features in order to make a connection to bulk phenomena is also important in characterizing other microstructures and more macrostructures. For example, connecting microstructural views of surface degradation or alteration with the intrinsic bulk microstructure or grain structure may be important. This can be

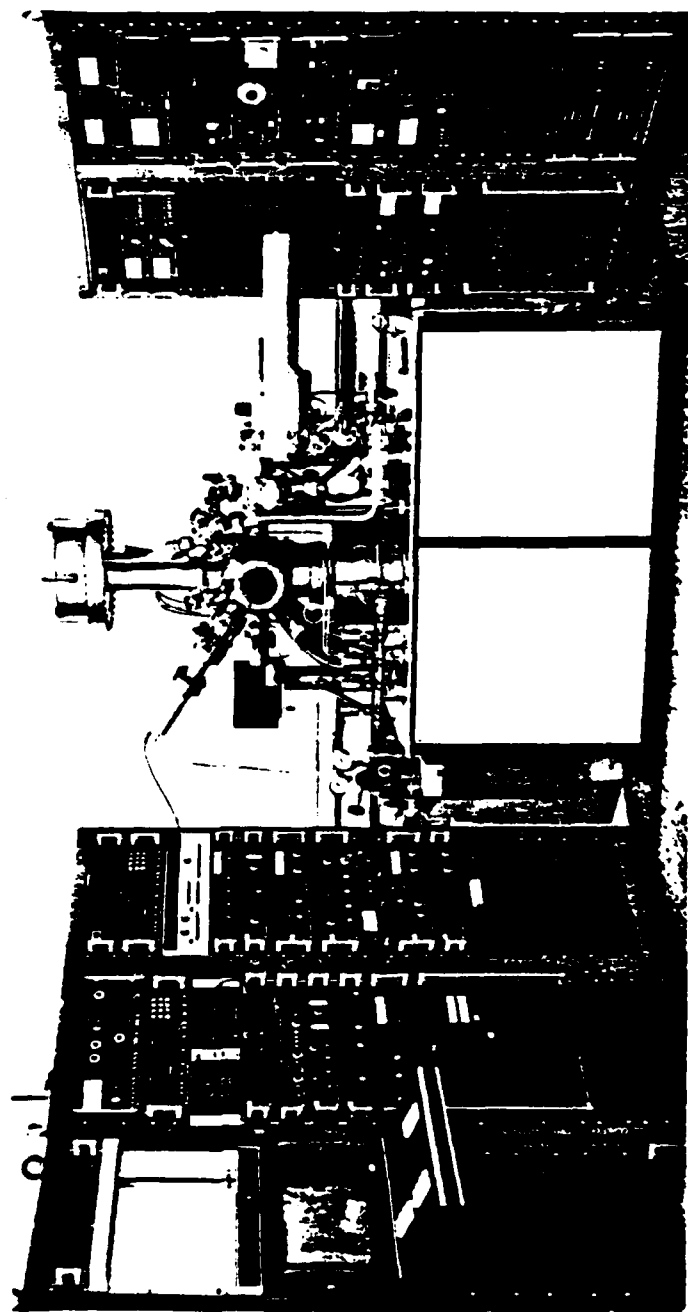


FIG. 17

Commercial surface analysis system for XPS, UPS, AES, SIMS, ISS, SAM (See Table 1).  
(Courtesy INFICON Leybold-Heraeus, Inc., from Fig. 4.51 in Ref. 14)

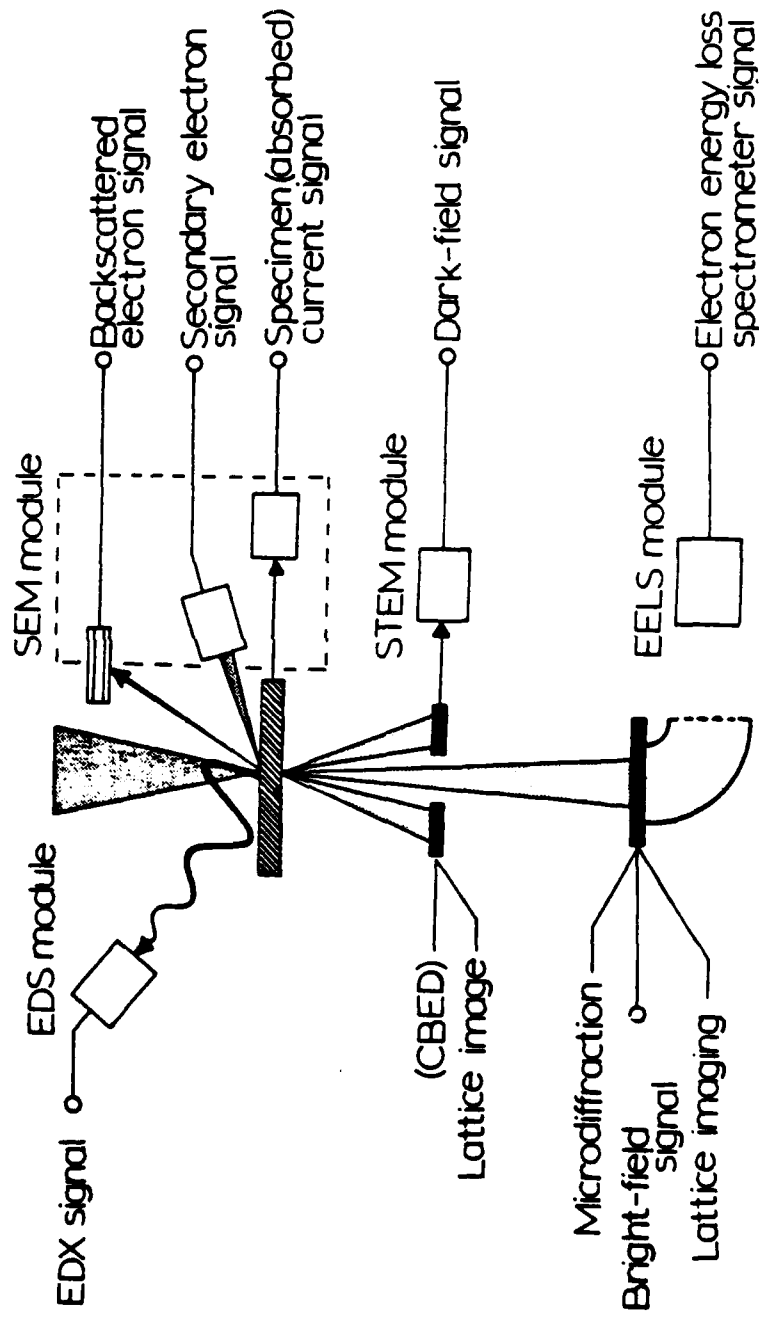


FIG. 18

Schematic diagram depicting the AEM concept. Signal and image information commonly available is noted. Other source or detector modules could conceivably provide additional signal information. Note that operation in the SEM, STEM, or other beam rocking modes, etc. requires a system of deflection/scan coils above the specimen which is not shown. (From Fig. 7.68 in Ref. 14)

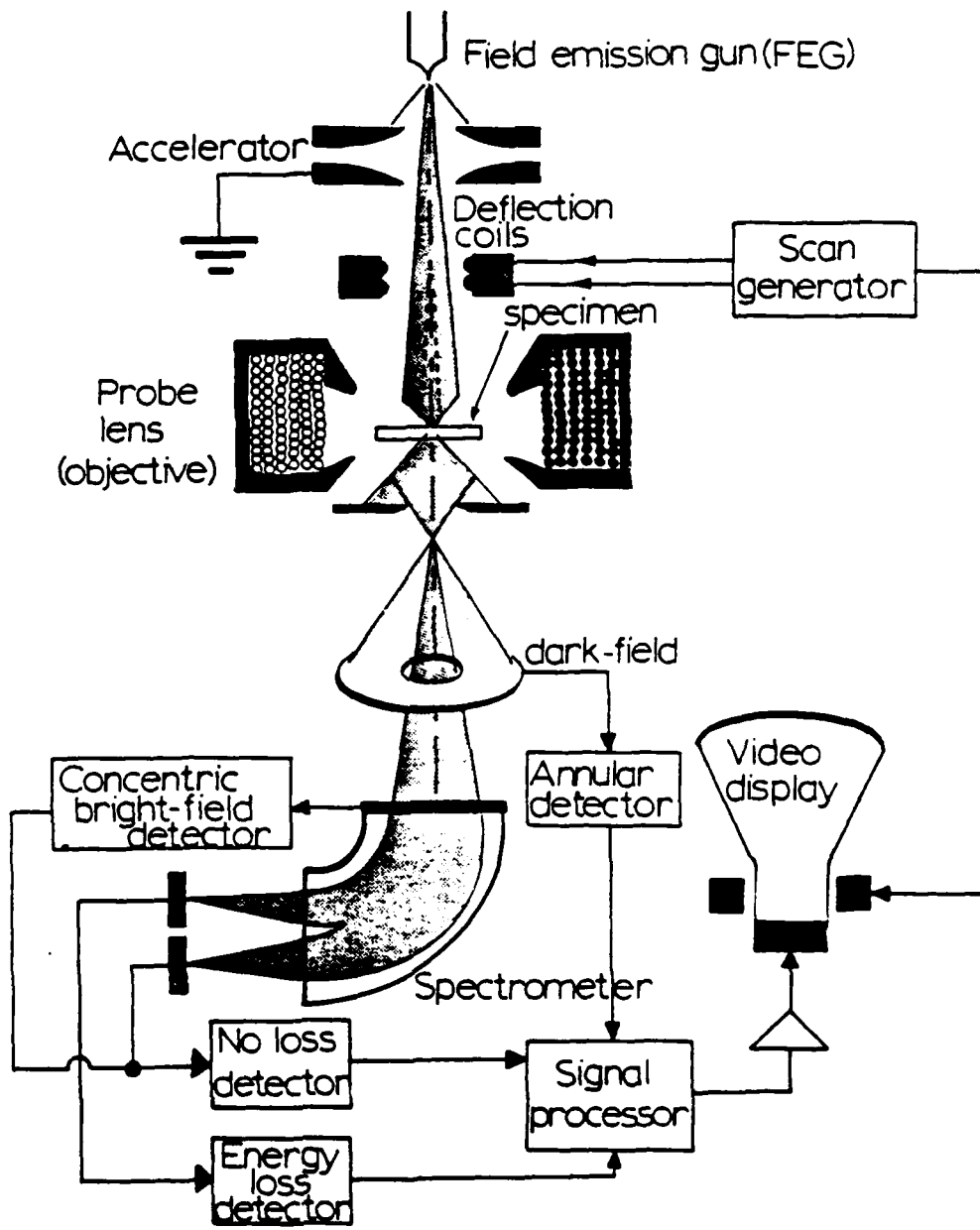


FIG. 19

Schematic diagram of a scanning transmission electron microscope (STEM). Only the objective or probe lens is shown. In practice several additional lenses may be included in the beam forming processes before and after the specimen, respectively. (From Fig. 7.66 in Ref. 14)

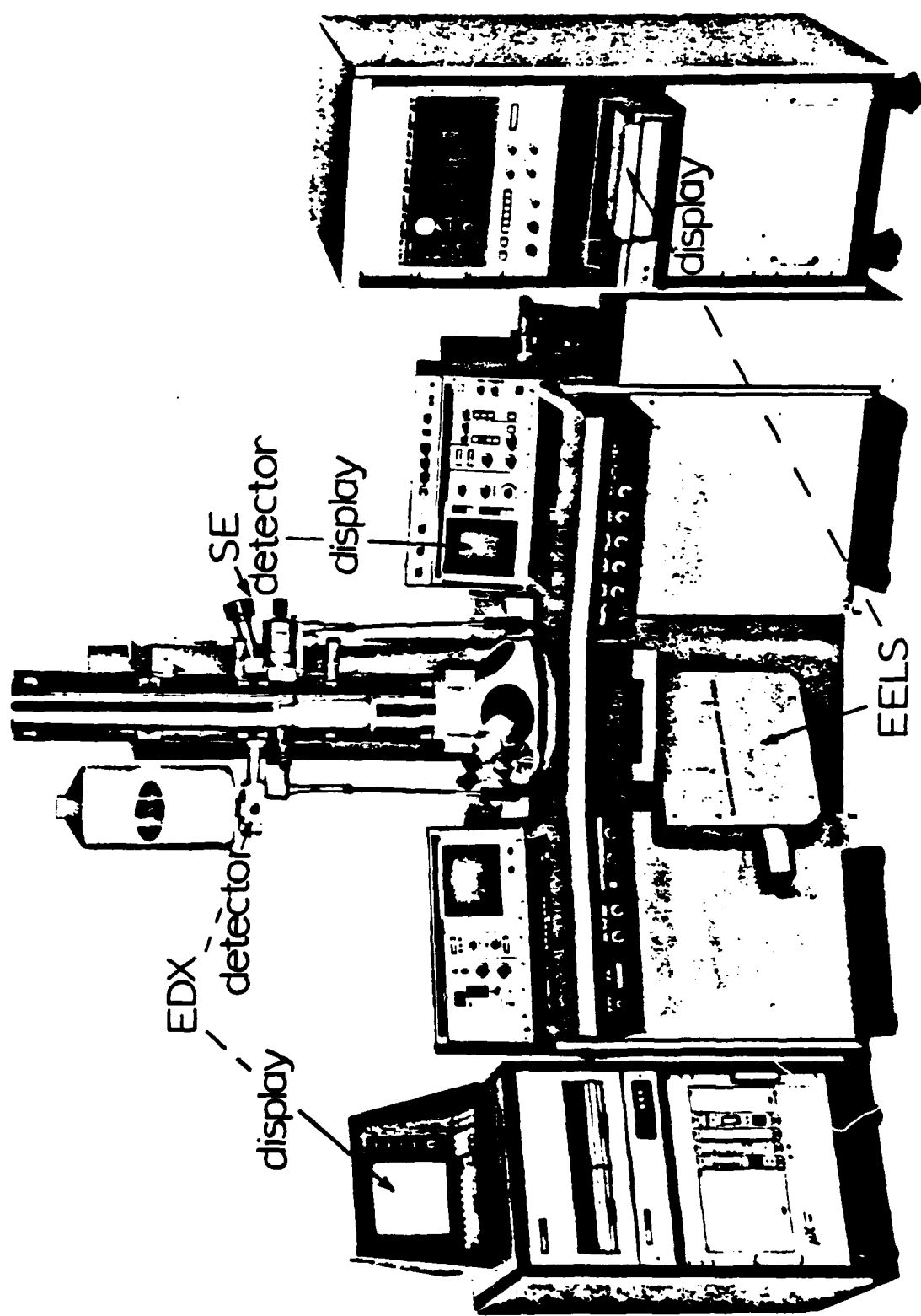


FIG. 20

Commercial AEM, Hitachi H-600 analytical electron microscope fitted with STEM, SEM, CTEM, EDX and EELS system modules. The secondary electron detector (SE) and EDX displays are noted. (Courtesy of Hitachi, Ltd., Tokyo, Japan, from Fig. 7.69 in Ref. 14)

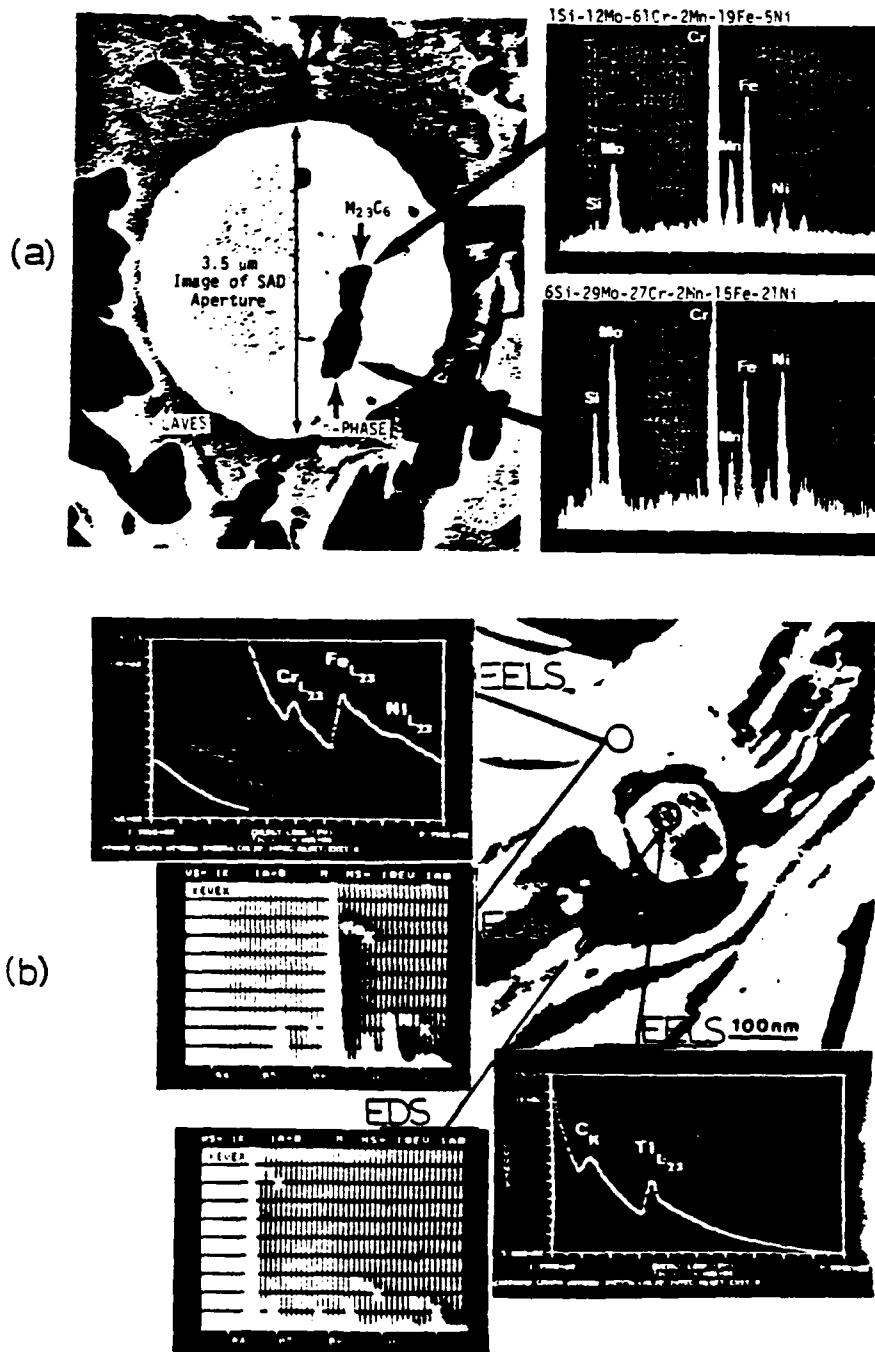


FIG. 21

EDS and EELS analysis in the AEM. (a) Carbon extraction replica of 30% cold-worked 316 stainless steel aged 10,000 h at 600°C (showing two morphologically similar but chemically distinct precipitates using EDS (Courtesy Dr. P. J. Maziasz); (b) EELS and EDS spectra from TiC in a 316 stainless steel matrix. The carbon is only observed in the EELS spectrum. The image is a CTEM bright-field image of the precipitate following aging of the stainless steel for 24 h at 900°C. (Courtesy of N. J. Saluzec and P. J. Maziasz). (From Fig. 7.70 in Ref. 14)

AD-A132 688

WORKSHOP ON REPETITIVE SPARK GAP OPERATION HELD AT  
TAMARRON COLORADO ON JANUARY 17-19 1983(U) BATTELLE  
COLUMBUS LABS DURHAM NC M O HAGLER ET AL. 20 MAY 83

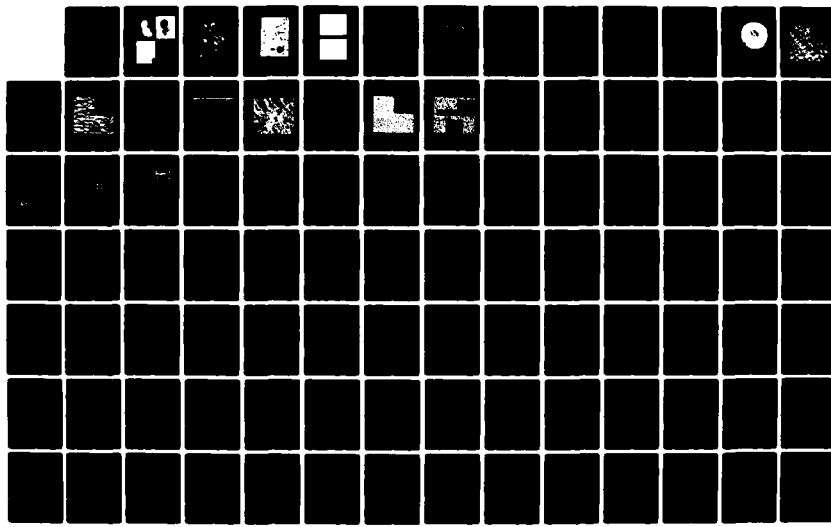
UNCLASSIFIED

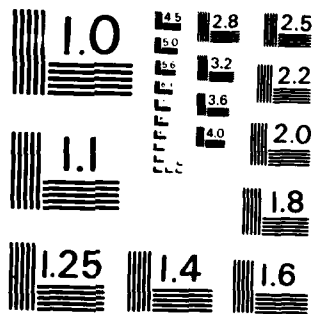
DAAG29-81-D-0100

F/G 9/1

3/4

NL





MICROCOPY RESOLUTION TEST CHART  
NATIONAL BUREAU OF STANDARDS - 1963 - A

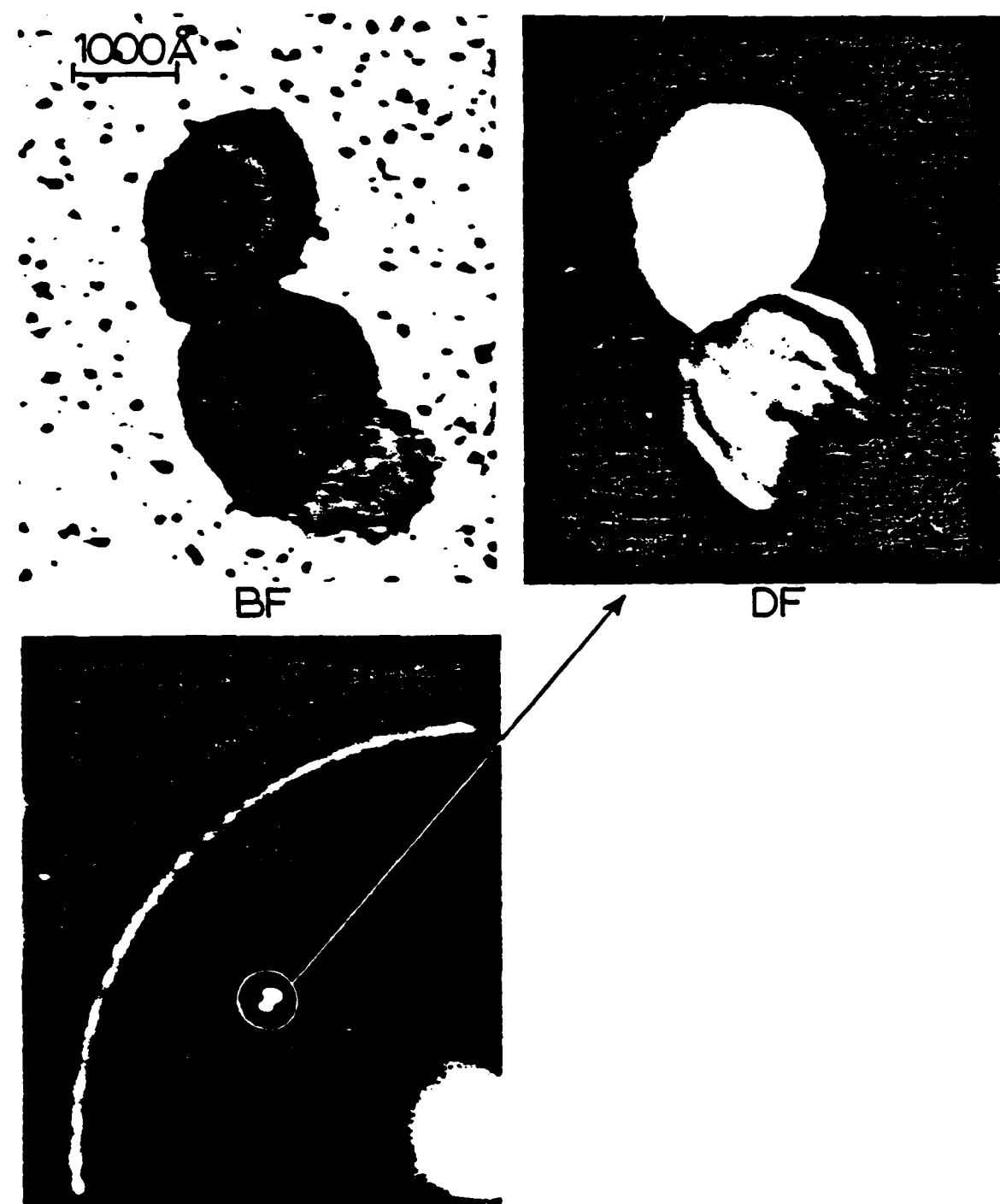


FIG. 22

Bright-field (BF) and dark-field (DF) electron micrographs of  $\text{Cr}_2\text{O}_3$  bicrystal electroplated on surface of thin nickel foil and observed in TEM. The selected-area electron diffraction pattern shows Ni rings which can be used to calibrate. (From Fig. P7.28 in Ref. 14)



FIG. 23

Semi-coherent interface structure for NiAl precipitates in Fe-12Cr-5Ni-4Al alloy. Dislocations are locked between particles are also apparent. Numerous precipitates are selectively etched from the matrix leaving a hole in the thin foil. This is simply an illustration of the ability to distinguish dislocations and precipitate or small-phase regimes in the TEM.

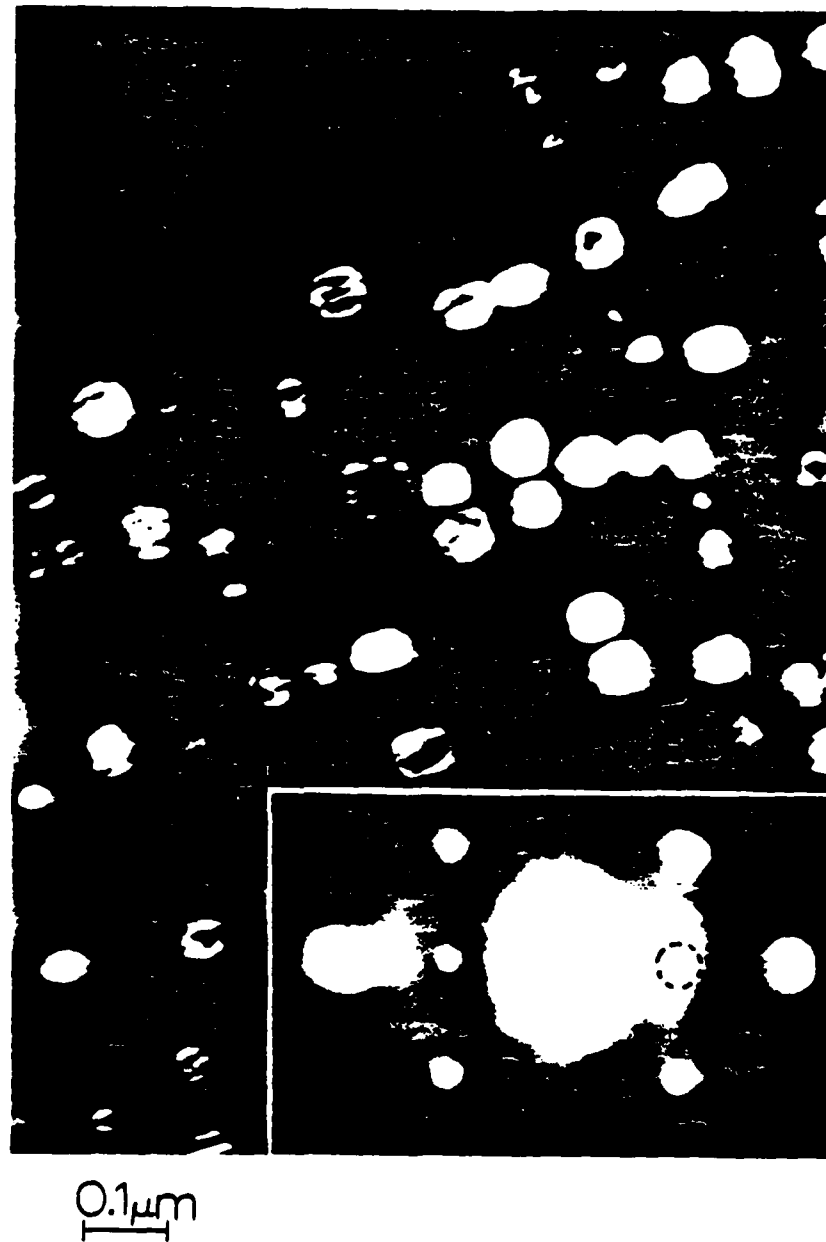


FIG. 24

(100) selected-area electron diffraction pattern (insert) showing superlattice reflections and (100) superlattice spot (circled) dark-field electron micrograph. The precipitates are from a region adjacent to that shown in Fig. 23.

190

NIAL PRECIP.  
PHA22 ADD .020KEY/CH 300. SECS<sup>1</sup>

800 10.220  
300.

Al Cr Fe Ni

NIAL PRECIP.  
PHA22 ADD .020KEY/CH 300. SECS<sup>1</sup>

800 10.220  
109.

FIG. 25

EDX spectra obtained in the TEM for NiAl precipitate at the edge of a foil similar to Figs. 23 and 24 with a stationary beam dwelling on the area including the precipitate (upper spectra). The lower spectra represents an area between precipitates. Note the difference in the nickel and aluminum peaks. It is not possible to produce accurate quantitative data because of the background scattered from adjacent regions. However there is certainly the expected qualitative differences. (Thanks to Fred Greulich at Sandia Livermore for making his Phillips 300 TEM available.)

accomplished by using a lacquer mask on a portion of the surface, and selectively, chemically, or electrochemically removing a surrounding region thereby revealing microstructures connected with the surface features. These features are illustrated conceptually in Fig. 26.

Flakes of reaction products can also be scrapped from regions of an electrode or insulator surface for analysis, and sufficiently thin flakes on the surface could be examined directly within the transmission electron microscope or AEM.

In the section which follows (and included in the Appendix) some examples of surface phenomena and surface characterization of spark gap materials are presented. These examples are certainly neither exhaustive nor completely representative examples of spark gap surface phenomena. In fact they serve to illustrate the general lack of attention to what must ultimately be faced up to as a crucial materials problem in pulsed power systems.

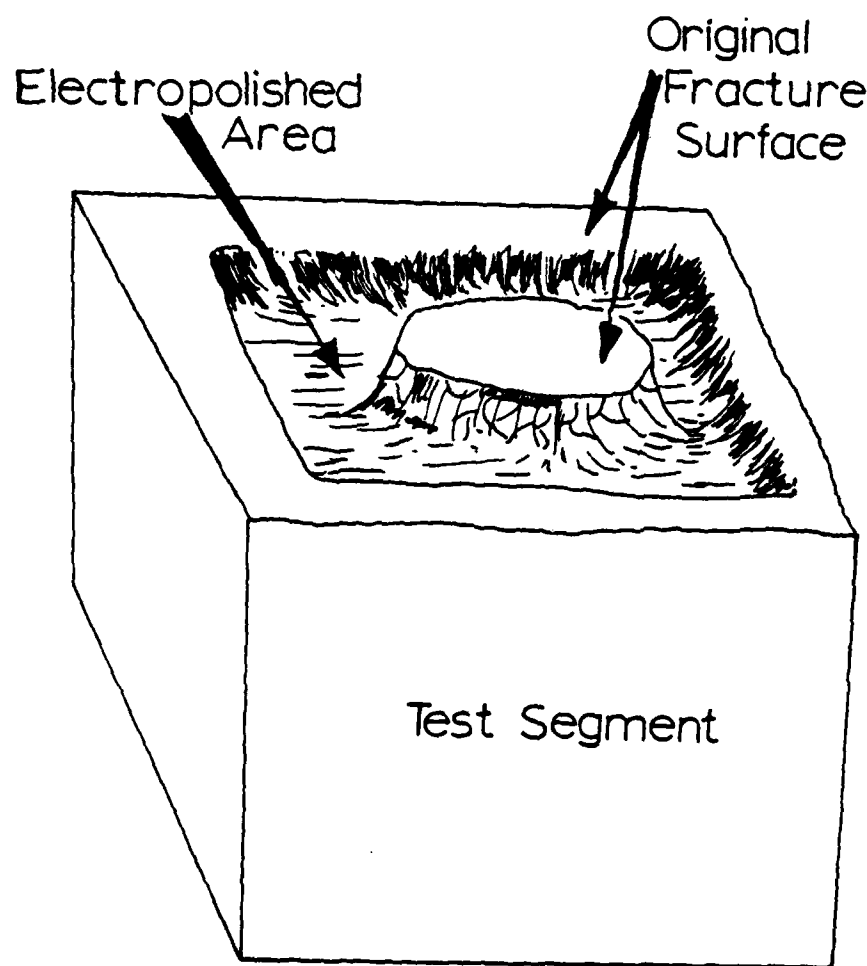


FIG. 26

Schematic representation of a technique for preserving the fracture surface or other surface regime and comparing it with the corresponding bulk microstructure. Surface segments to be preserved are coated with a stop-off lacquer while the unlacquered areas are electropolished to reveal underlying microstructure. (From Fig. 5.42 in Ref. 14)

SOME EXAMPLES OF SURFACE PHENOMENA  
AND CHARACTERIZATION OF SPARK GAP MATERIALS\*

\*Based upon an exhibit composed by Dr. C. Stein  
for the New Mexico Showcase for Technology,  
October, 1981 from an original study included in  
the Appendix: "A Preliminary Study of the  
Degradation of High Energy Switch Materials" (8).

# A PRELIMINARY STUDY OF THE DEGRADATION OF HIGH ENERGY SWITCH MATERIALS.

L.E. MURR: Oregon Graduate Center

F.L. WILLIAMS: University of New Mexico

D.M. SMITH: University of Denver

P. PREDECKI: University of Denver

S.H. WANG: New Mexico Institute of Technology

(Materials Kindly Provided by Texas Tech University)

## ABSTRACT

A preliminary study of the nature of the damage to an electrode and some insulator materials comprising high energy spark-gap switch system is presented.

## ANALYTICAL TECHNIQUES USED IN THIS STUDY WERE:

1. Scanning Electron Microscopy
2. Transmission Electron Microscopy
3. Optical Metallography
4. Energy Dispersive X-Ray Microanalysis
5. Electron Microprobe Analyses
6. Auger Electron Analysis
7. Electron Spectroscopy for Chemical Analyses
8. Fourier Transform Infra Red Analyses.

## OBJECTIVE

To demonstrate that the degradation mechanisms effecting the performance of high energy spark-gap switches can be elucidated by a synergism of sophisticated microanalytical techniques.

## BACKGROUND

Spark-gap switches for pulse-power applications are required to transfer enormous quantities of electrical power in extremely short pulses for extended periods of time. This places severe burdens on the life times of switch materials.

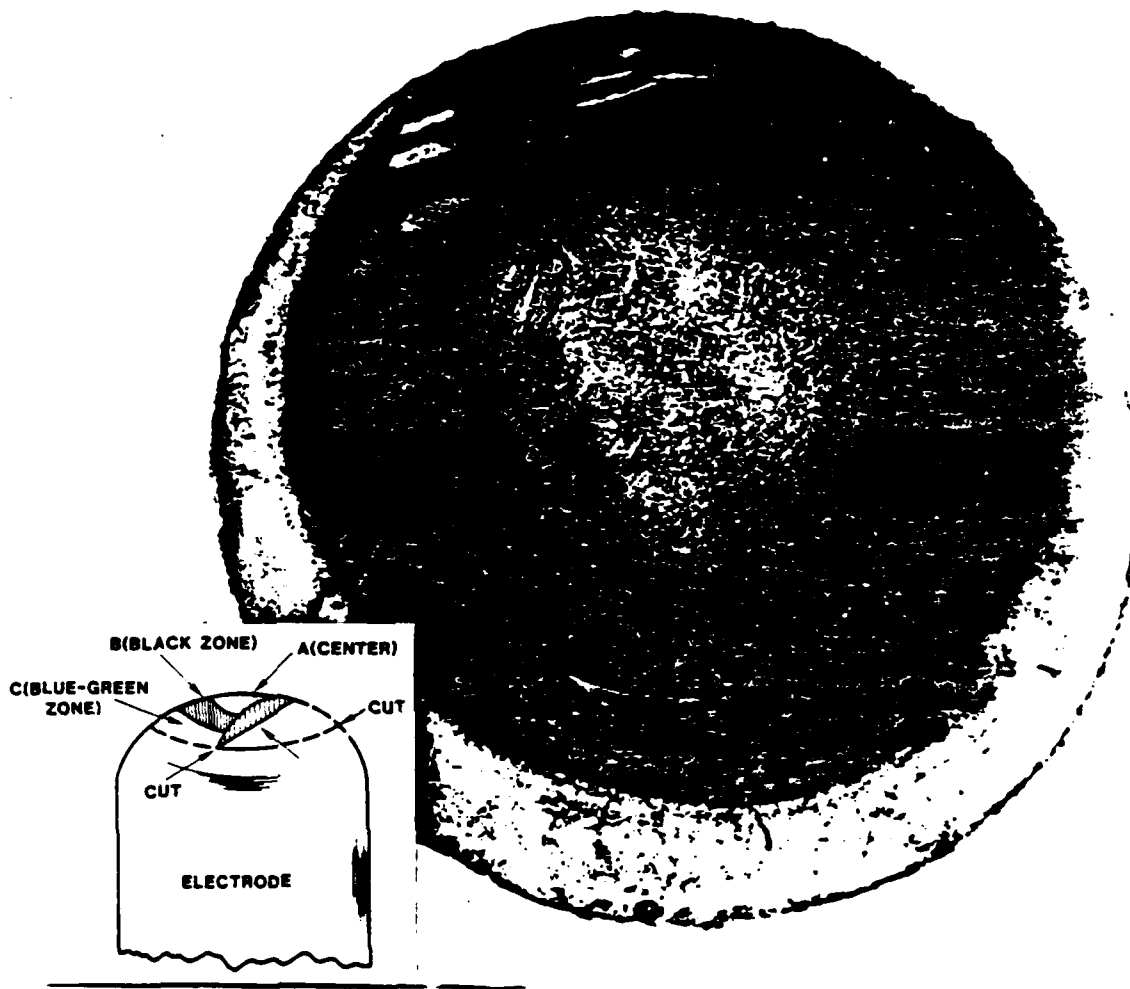
## HOW DO THESE MATERIALS DEGRADE?

WHAT ARE THE EFFECTS OF THE FOLLOWING OPERATING VARIABLES ON THE LIFE TIMES OF THESE MATERIALS?

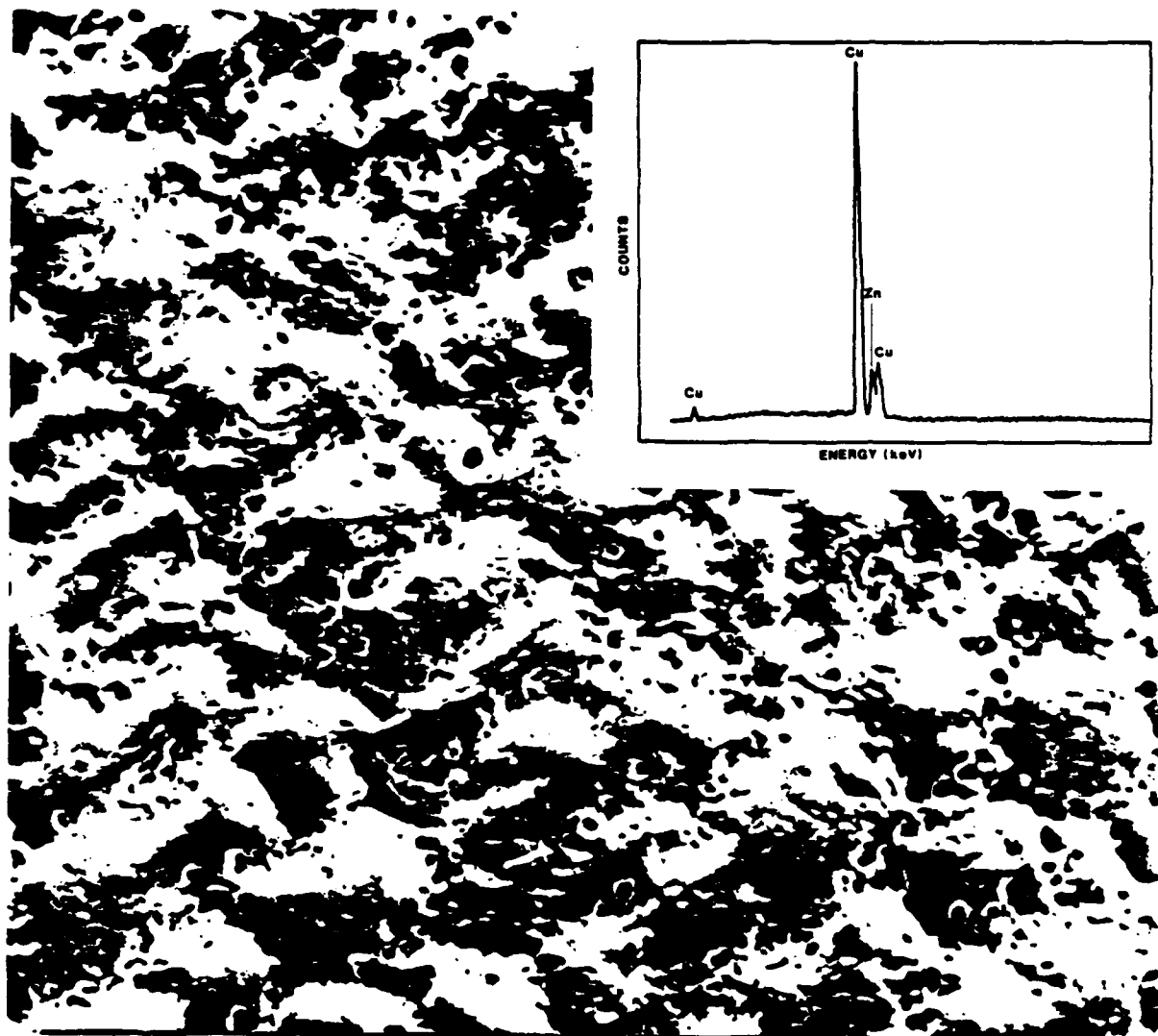
Peak Current  
Peak Voltage  
Current Density  
Pulse Time  
Rep. Rate  
Quenching Gas Composition  
Quenching Gas Pressure  
Polarity of the Electrodes

## SPARK-GAP SWITCH ELECTRODE STUDY

MATERIAL:	Brass: 70% Copper — 30% Zinc
TOTAL NUMBER OF SWITCHING SHOTS:	406,000
VOLTAGE:	Varied from 40,000 — 66,000 volts
OPERATING GASES:	The switch was used in 9 experiments involving nitrogen, air and carbon dioxide.
GAS PRESSURE:	1 to 2 atmospheres
ELECTRODE PREPARATION:	Lathe machined; smoothed with emery cloth; polished with alumina powder; cleaned in acetone and methanol.
ELECTRICAL SYSTEM:	Capacitance — $0.82\mu f$ Load Resistance — 1 ohm

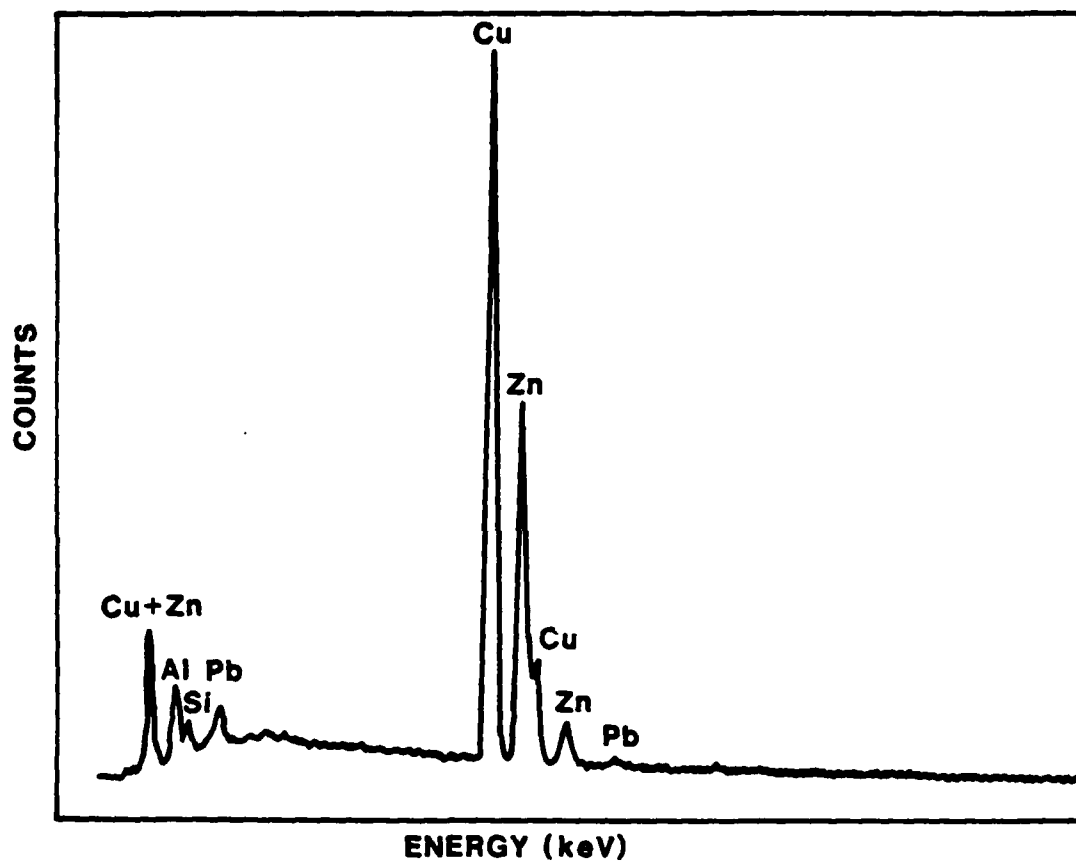


Schematic diagram of brass electrode showing various places of microscopic investigations.

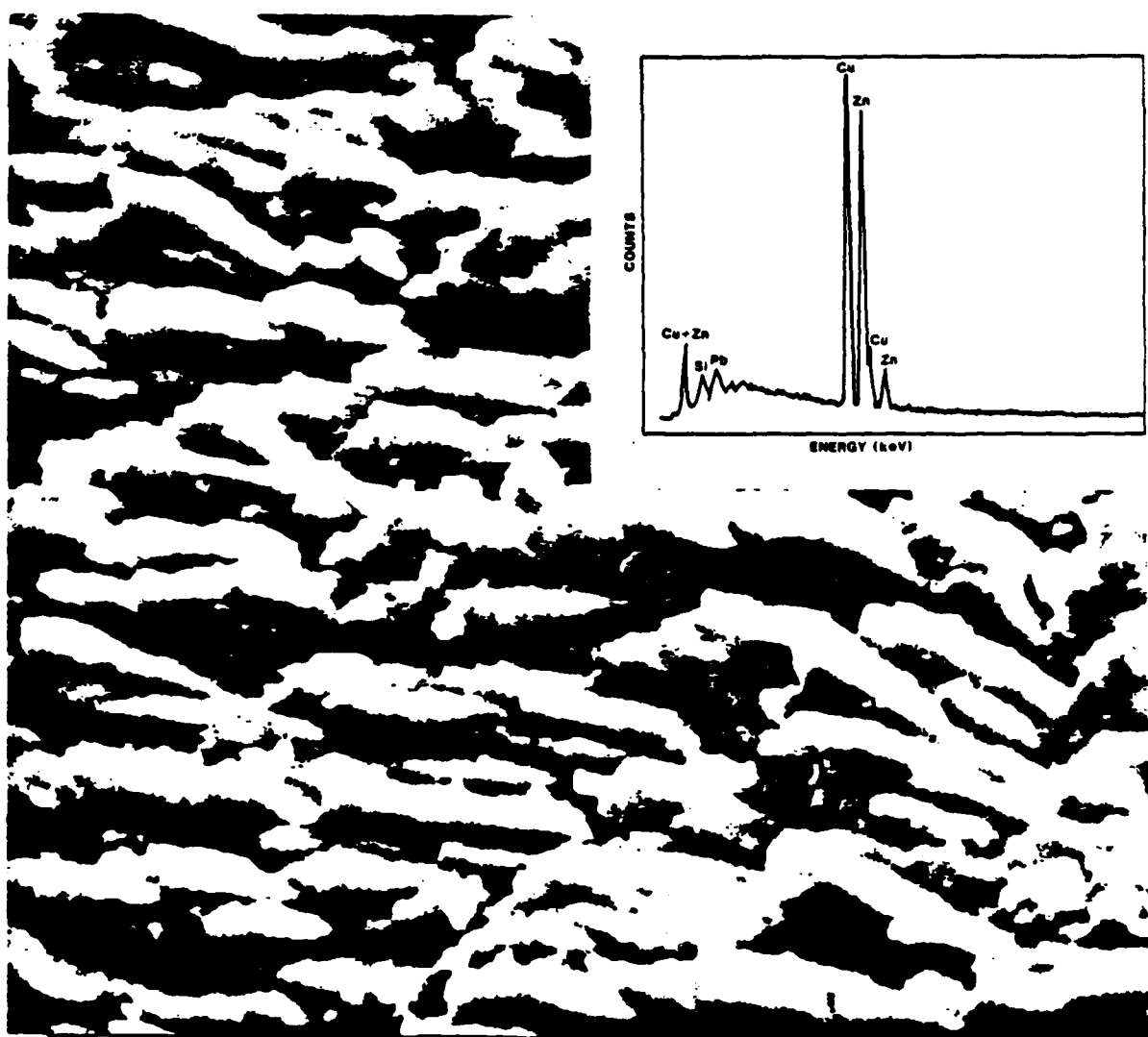


Scanning electron microscope picture of the central region of the electrode surface after 406,000 shots. Note the gas pockets due to zinc vaporization.

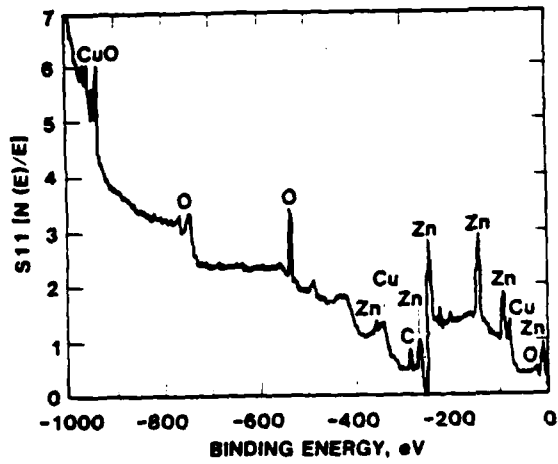
INSERT: Energy dispersive x-ray analyses shows depleted zinc content. Compare with zinc content of undamaged material.



**Elemental energy dispersive x-ray analyses of undamaged section of brass electrode. Note higher zinc content.**

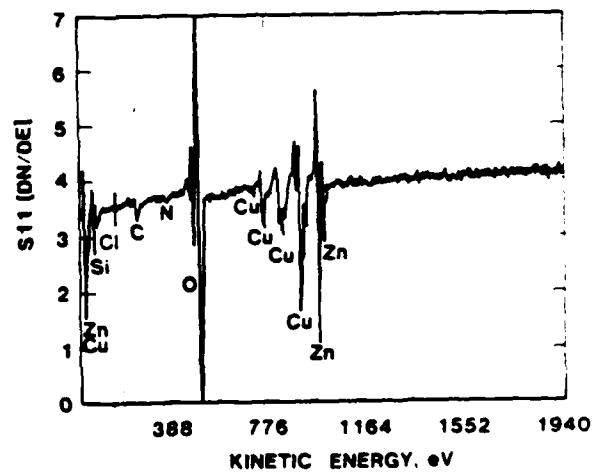


**Scanning electron microscopy of black zone surrounding central region of the brass electrode. Black color is probably zinc oxide.  
INSERT: Energy dispersive x-ray analyses. Note that the zinc content exceeds that of the undamaged brass indicating that zinc was deposited here from the central region.**



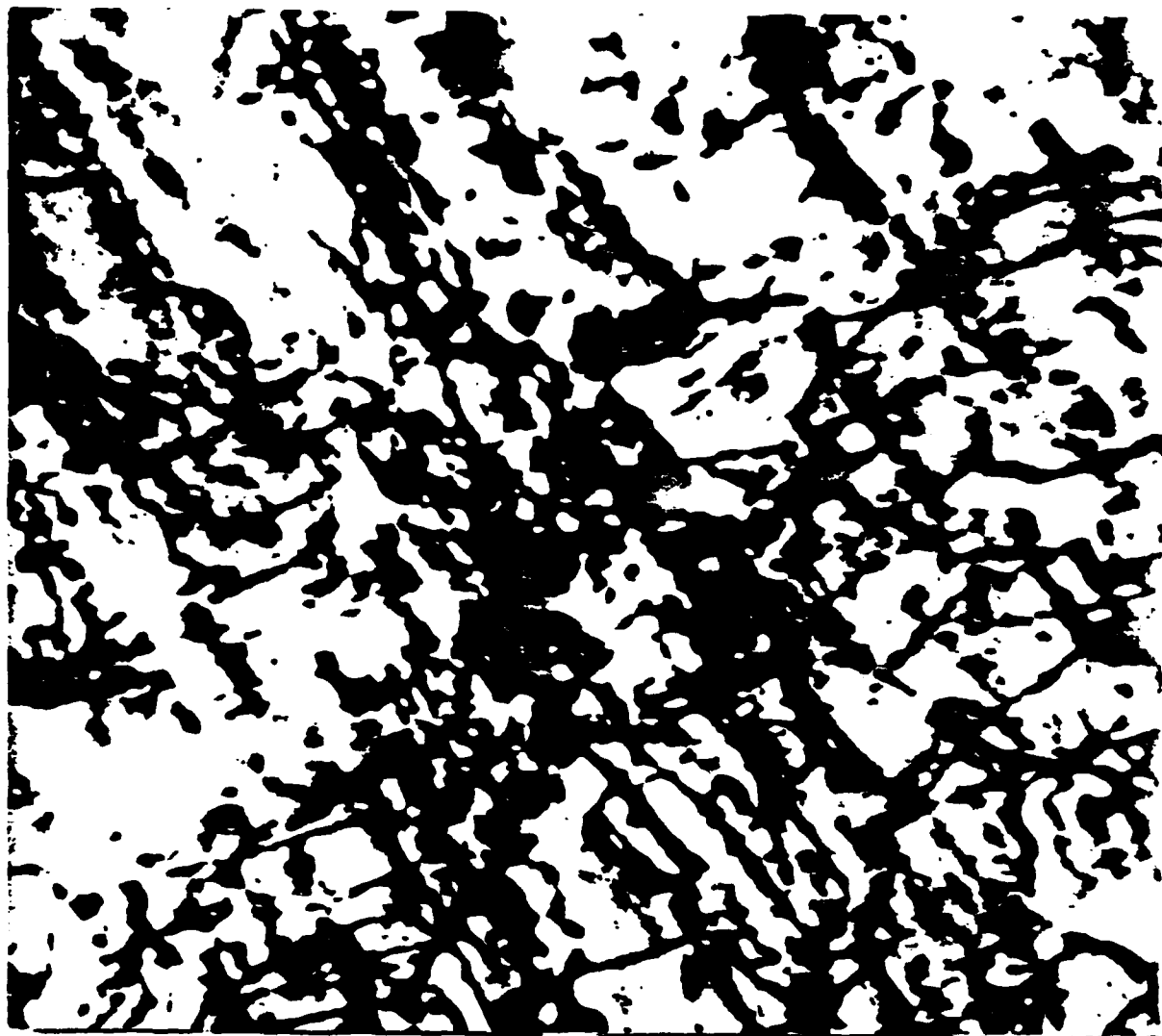
**Auger Electron Spectroscopy of black zone surrounding central region of brass electrode.**

**Electron Spectroscopy for chemical analyses of black zone surrounding central region of brass electrode. The presence of zinc oxide and copper oxide is indicated. Note high zinc to copper ratio due to deposition of vaporized zinc.**





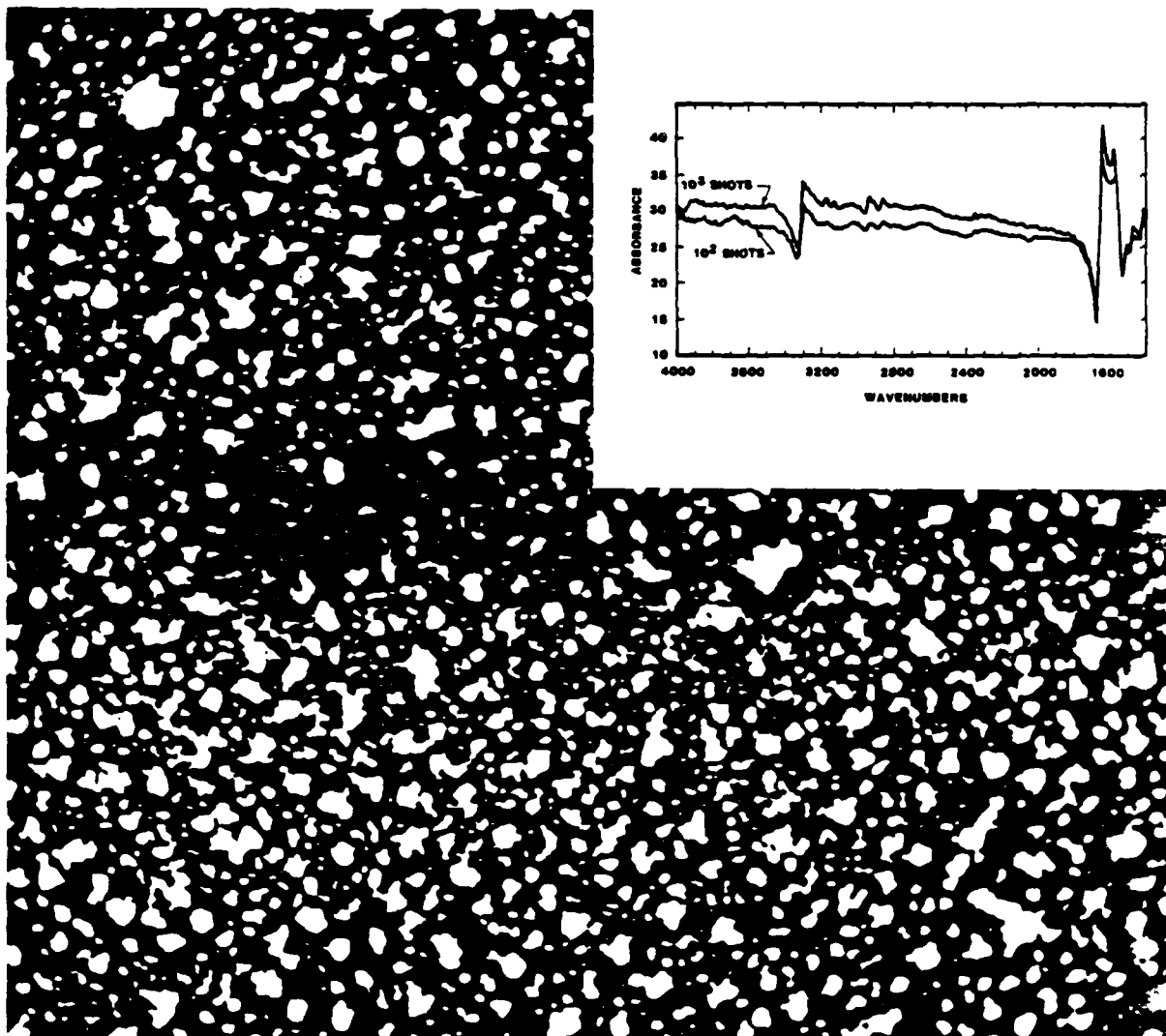
Optical Microscopy of polished cross section of Brass Switch  
Electrode.



**Bright Field Transmission Electron Micrograph taken of circled region (A) in the Optical Micrograph of Figure . Shows dislocations and dislocation loops indicative of a highly cold worked metal.**

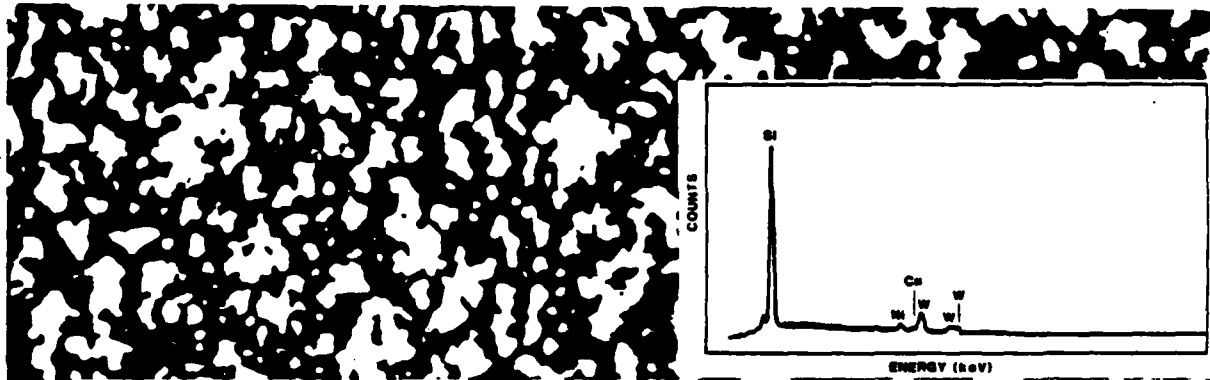
**SWITCH INSULATION MATERIALS STUDY**

<b>Insulation Material:</b>	<b>Nylon</b>
<b>Spark-Gap Electrodes Used to Damage Insulator:</b>	<b>Tungsten Alloy Composite with Copper and Nickel</b>
<b>Distance Between Electrode and Insulator:</b>	<b>2.54 cm</b>
<b>Gas Used in Switch:</b>	<b>Air</b>
<b>Voltage:</b>	<b>33,000 Volts</b>
<b>Total Number of Switching Shots:</b>	<b>1,000</b>
<b>Pulse Time:</b>	<b>1 microsecond</b>
<b>Electrical System:</b>	<b>Capacitance 2<math>\mu</math>F Load Resistance 0.25 ohms</b>



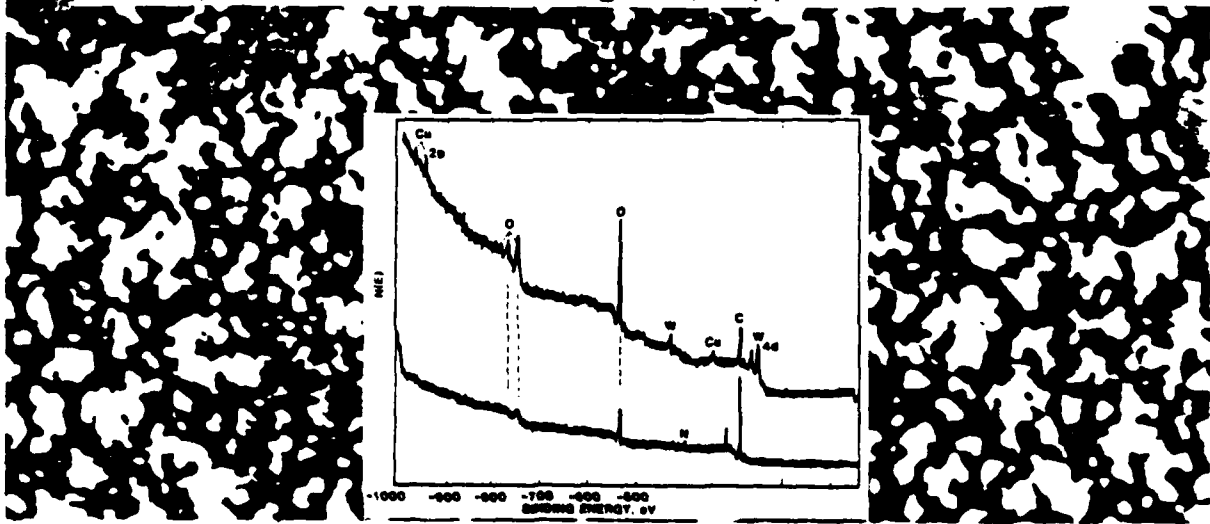
**Scanning electron micrograph of nylon insulator surface after 100 shots.**

**INSERT: Fourier Transform Infra Red Spectroscopy of the surface of Nylon after 100 and 1000 shots showing increased absorption due to deposition of sputtered metal particles.**



**Scanning electron micrograph of nylon insulator surface after 1000 shots.**

**INSERT: Energy dispersive x-ray analyses of nylon insulator surface after 1000 shots. Shows that the deposite of sputtered metal particles consists of tungsten, copper and nickel.**



**Electron Spectroscopy for Chemical Analyses of Nylon Insulator surface after 1000 shots (upper curve). Corroborates the presence of tungsten, copper and nickel deposited from spark-gap electrode.**

## CONCLUSIONS

1. Even in simple switching systems where the complications of quenching gas reactions are absent, considerable alterations and damage to the surfaces of electrodes and insulators takes place during operation.
2. The brass electrode material was observed to have vaporized its constituents and to deposit them back onto the electrode at a distance away from the central plasma jet area.
3. The nylon insulator material was damaged in only 100 shots by the almost continuous layer of deposited material sputtered from the tungsten alloy electrode.
4. Microstructural and microchemical changes in switch materials were observed and confirmed by a synergistic use of sophisticated diagnostic instruments.
5. Damage mechanisms in materials used for high power pulse switches can be effectively determined by an interdisciplinary approach.

GENERAL SUMMARY

No self-respecting presentation would be complete without a summary. But in reality there is not much to summarize in the context of either observing surface phenomena or understanding surface phenomena in spark gap materials. This presentation has provided a brief overview of techniques for characterizing surface phenomena in spark gaps and a few examples were presented. The treatment has been far from being exhaustive. It is hoped that the prospects for understanding surface phenomena in spark gaps presented here will provide some incentive to begin some really meaningful, systematic studies of spark gap degradation and the associated mechanisms. This should also lead to a meaningful evaluation and design of satisfactory (efficient) materials for repetitive, high-energy spark gap operation.

REFERENCES

1. S. Levy, "Spark-gap Erosion Studies," USAECRDL Report No. 2454, April, 1964.
2. J. E. Gruber and R. Suess, "Investigations of the Erosion Phenomenon in High Current, High Pressure Gas Discharges," Max Planck Inst. für Plasma-physik, Garchin, Bei Muchen IPP 4/72, Dec., 1969.
3. F. Heitzinger, "The Properties of Tungsten-Copper Composite Materials on Arc Erosion Resistance," Seminar Composite Materials in Electrotechnics, Oberursel, Germany, Oct., 1977.
4. G. Marchesi and A. Maschio, "Influence of Electrode Materials on Arc Voltage Waveforms in Pressurized Field Distortion Spark Gaps," in 5th Int. Conf. Gas Discharges, U.K., Sept. 1978.
5. Y. Suzuki, Y. Kawakita, M. Kume, and M. Kawai, "A 150 kV, 100 kA Spark Gap Switch for Marx Generators," in 3rd Int. Pulsed Power Conf., Albuquerque, N. Mex., June, 1981, pp. 444-447.
6. L. B. Gordon, M. O. Hagler, M. Kristiansen, and H. C. Kirbie, "Investigations of a 60 kV, 5 cm Spark Gap for Several Electrode, Insulator, and Gas Types," ibid, pp. 376-378.
7. G. L. Jackson, K-C. Yuan, L. L. Hatfield, and M. Kristiansen, "Surface Damage of Dielectrics in a Spark Gap," ibid, pp. 289-292.
8. L. E. Murr, F. L. Williams, D. M. Smith, P. Predecki, and S-H. Wang, "A Preliminary Survey of High-Energy Switch Materials Degradation: Spectroscopic and Microscopic Characterization," ibid, pp. 77-80.
9. L. B. Gordon, M. Kristiansen, M. O. Hagler, H. C. Kirbie, R. M. Ness, L. L. Hatfield, and J. N. Marx, "Material Studies in a High Energy Spark Gap," Proc. IEEE, to appear in *Transaction Plasma Science*, Dec., 1982.
10. G. J. Rohwein, "Partial Discharge Testing of Bulk Transformer Oil," in 3rd Int. Pulsed Power Conf., Albuquerque, N.Mex., June, 1981, pp. 420-423.
11. O. T. Inal and L. E. Murr, "Laser Shock-Induced Microstructural Changes and a Comparison with Explosive Shock-Induced Phenomena in Metals: Field-ion and Electron Microscopic Studies," J. Appl. Phys., 49 (4), 1978, pp. 2427-2434.

12. M. A. Meyers and L. E. Murr (eds.), Shock Wave and High-Strain-Rate Phenomena in Metals: Concepts and Applications, Plemum Press, New York, 1981.
13. L. E. Murr, Interfacial Phenomena in Metals and Alloys, Addison-Wesley Publishing Co., Reading, Mass., 1975.
14. L. E. Murr, Electron and Ion Microscopy and Microanalysis: Principles and Applications, Marcel Dekker, Inc., New York, 1982.

211

APPENDIX

From: Proc. 3rd IEEE International Pulsed Power Conference,  
Albuquerque, N. Mex., 1981.

A PRELIMINARY SURVEY OF HIGH-ENERGY SWITCH MATERIALS DEGRADATION: SPECTROSCOPIC AND MICROSCOPIC CHARACTERIZATION

L.E. Murr<sup>\*</sup>, F.L. Williams<sup>\*\*</sup>, D.M. Smith<sup>\*\*</sup>, P. Predecki<sup>\*\*</sup> and S.-H. Wang<sup>\*</sup>

<sup>\*</sup>New Mexico Institute of Mining and Technology, Socorro, New Mexico 87801

<sup>\*\*</sup>Now at: Oregon Graduate Center, Beaverton, Oregon 97006

<sup>\*\*</sup>University of New Mexico, Albuquerque, New Mexico 87131

<sup>\*\*</sup>University of Denver, Denver Research Institute, Denver, Colorado 80208

A preliminary study of the nature of damage to some electrode and insulator materials comprising high-energy spark-gap switch systems is presented utilizing a synergistic, interdisciplinary microanalytical approach. This approach involves the analysis of electrode surfaces and bulk sections utilizing techniques of scanning and transmission electron microscopy, optical metallography, energy-dispersive X-ray microanalysis, electron probe microanalysis, Auger electron spectroscopy and electron spectroscopy for chemical analysis; and insulator analysis involving Fourier transform IR analysis, scanning electron microscopy, energy-dispersive X-ray microanalysis, Auger electron spectroscopy, and electron spectroscopy for chemical analysis.

Introduction

Switches to be utilized in pulsed-power applications will be required to transfer enormous quantities of electrical energy in extremely short time pulses for extended periods of time. This will place severe burdens on the lifetime of the particular switch materials. Compounding the materials aspects will be the complexity of the switch environment and the synergism of the damage mechanisms which will include erosion and corrosion at elevated temperature, electrical and mechanical stress, the interaction of the quenching gases with the switch electrodes and insulating materials, vaporization, and sputtering, and deposition of electrode material or plasma-generated reaction products within the switch environment, melt-zone displacements, spallation, microstructural and/or molecular alterations in the switch or insulator materials due to plasma-induced radiation damage and other, related degradation phenomena.

The elucidation and diagnosis of these degradation problems will be a necessary and initial step in the direction of actually designing and fabricating special materials capable of surviving the abuse of the pulsed-power switching environment. This will require a synergism of modern microscopic and microanalytical tools which will tax the state of the art in modern materials characterization, and provide a certain incentive for expanding the frontiers of materials science.

The characterization of switch materials degradation will ultimately require electrode damage effects to be correlated with a range of operating variables which will include peak current and voltage, current density, pulse time, rep rate, quenching gas composition and pressure, switch (electrode) polarity.

It is the purpose of this paper to provide a very preliminary view of some of the degradation phenomena alluded to above for a few specific switch components subjected to conditions simulating actual operating variables. It is also the purpose in providing this view to demonstrate the diagnostic synergism available through modern microanalytical instrumentation in the materials sciences.

Experimental Details and Analytical Procedures

In our preliminary experiments we chose to examine a brass (Cu30Zn) electrode subjected to a total of

406,000 pulses at voltages ranging from 40 to 66 kV in 9 separate experiments involving nitrogen, air, and carbon dioxide gases at pressures of either 1 or 2 atmospheres. This system involved a capacitor equivalent of 0.82  $\mu$ F and a load resistance of 1 ohm. This electrode (5 cm diameter) was formed on a lathe, smoothed with emery cloth, polished with alumina powder, and cleaned in acetone and methanol. During the course of pulsed power operation (between test series) the electrode was cleaned with ethanol and wiped with tissue paper.

In addition to the brass electrode, we examined several polymer insulating materials including Delrin, Nylon, and Lucite. These materials were all part of the same test series involving a tungsten alloy composite electrode (containing copper and nickel). These insulators stood circumferentially about the electrode a distance of 2.54 cm. The system was operated in air at a pulsing potential of 33 kV. The ringing discharges were dumped through 2  $\mu$ F at a 0.25 ohm load, in 1  $\mu$ s to produce a total rise time (+ and -) of 2  $\mu$ s. Samples of each insulator were examined which were exposed to 10<sup>2</sup> and 10<sup>3</sup> "shots" or pulses respectively.

A cap was cut from the brass electrode to remove the hemispherical end. This cap was examined uncoated in a scanning electron microscope (SEM) (Hitachi HSS-2R) fitted with an energy-dispersive X-ray spectrometer. Following this initial SEM analysis, the cap was examined in an Auger electron spectrometer (AES) and analysis was also performed by electron spectroscopy for chemical analysis (ESCA) [or X-ray photoelectron spectroscopy (XPS)]. Following these examinations, the cap was sliced in half to allow for polishing across the section area for optical metallographic analysis and 0.02 cm slices were cut. From these 0.02 cm slices, 2 mm diameter discs were punched and these were electropolished in a Fischionne twinjet polisher to form small electron-transparent regions near the disc center. The electropolished discs were then examined in a Hitachi 200F transmission electron microscope (TEM) at an accelerating potential of 200 kV. One half of this section was also examined in an electron microscope fitted with a secondary electron (SEM) detector. The details of the electrode sample sectioning are illustrated in Fig. 1.

Small sections were cut from larger insulator (Delrin, Lucite and Nylon) sections which were contaminated initially by Si as a result of the cutting tool or cutting medium. Some of these smaller sections were examined in the AES/ESCA units while others were examined by single-reflection Fourier transform-infrared spectroscopy (FT-IR). Representative samples were also examined in the SEM.

Results and Discussion

Electrode Examination

Figure 2 shows a sequence of secondary electron images at different magnifications of the surface region in the center of the electrode corresponding to the zone directly impinged upon by the plasma discharge stream (See Fig. 1). This region corresponds to the maximum temperature rise over the electrode surface, and Fig. 2

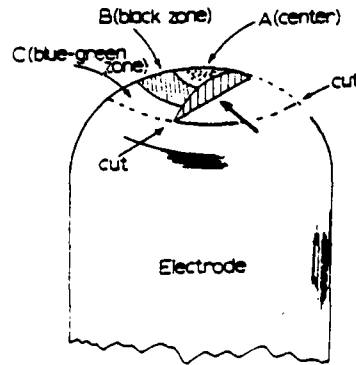


Fig. 1. Schematic view of brass electrode showing specific zones resulting from switch operation as discussed in the text. The cuts indicated describe the removal of the electrode end and the sectioning of this cap in half.

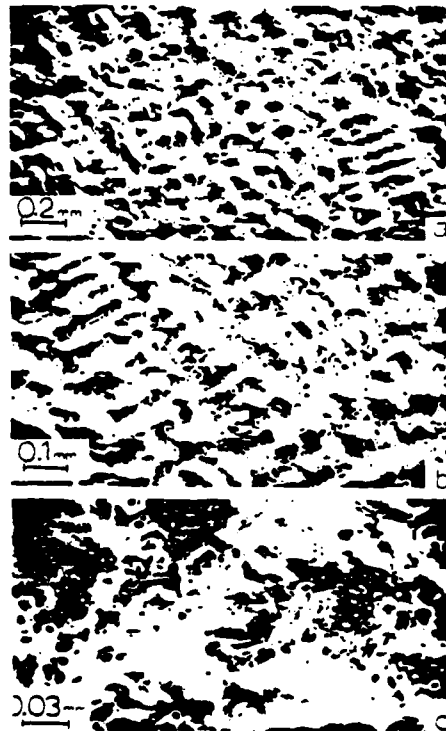


Fig. 2. Secondary electron (SEM) images of the central electrode surface zone indicated in Fig. 1(A). (a) Low magnification view, (b) Higher magnification view, (c) Higher magnification view showing gas pockets due to vapor emission and dezincification (zinc vaporization).

shows clear evidence of melting; vaporization of the interior zinc. The dezincification of the central zone is confirmed in the comparison of the central zone X-ray analysis with the analysis for the undamaged electrode material below the point from which the hemispherical end section (Fig. 1) was cut. This is shown in Fig. 3.

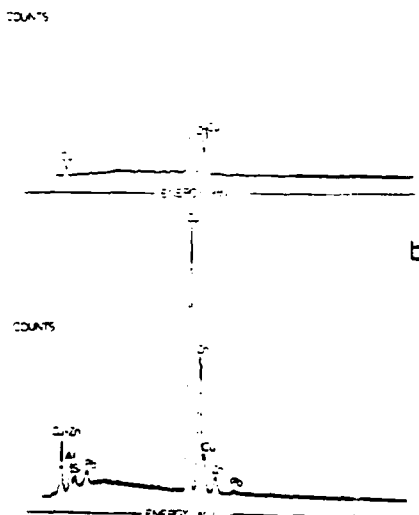


Fig. 3. Comparison of characteristic (elemental) energy-dispersive X-ray analysis in central electrode zone corresponding to Fig. 2(c). (a) with the undamaged electrode material (b). These differences were also confirmed by electron microprobe analysis which showed the depletion of both zinc and lead in the central zone (A).

The area adjacent to the central region (A in Fig. 1) was characterized by a black zone surrounding it (B in Fig. 1). Fig. 4(a) shows the transition region between zones A and B in Fig. 1 while Fig. 4(b) shows the mid-region in the black zone. This zone was observed to be rich in zinc, as shown in Fig. 4(c), and because of the color it is assumed to be rich in black zinc oxide ( $ZnO$ ). Copper oxide (tenorite) could also be intermixed in this zone. The presence of these metal oxides was confirmed by non-scanning electron probe AES and ESCA analysis as shown in Fig. 5. Figure 5(b) in fact illustrates directly the presence of  $CuO$ . Comparison of the AES spectrum in Fig. 5(a) with that for the central zone also showed a dramatic difference in the  $Cu/Zn$  ratio consistent with the electron microprobe analysis and the energy-dispersive X-ray analysis shown in Figs. 3(b) and 4(c).

Examination of the blue-green zone (zone C in Fig. 1) indicated a mixed reaction zone dominated by  $Cu_2O$ . The  $Cu/Zn$  ratio was essentially the same as that for the unaltered electrode bulk with the exception of apparent lead depletion.

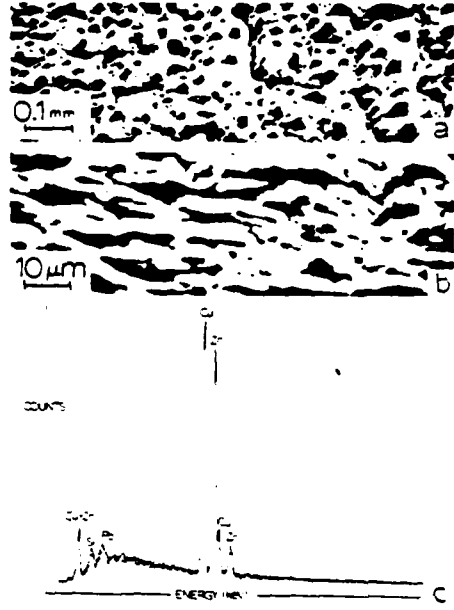


Fig. 4. SEM images and elemental X-ray (energy-dispersive) analysis of the region adjacent to the central zone (zone B in Fig. 1). (a) Transition region between A and B (Fig. 1); (b) Mid-section of zone B (Fig. 1); (c) X-ray analysis of region shown in (b).

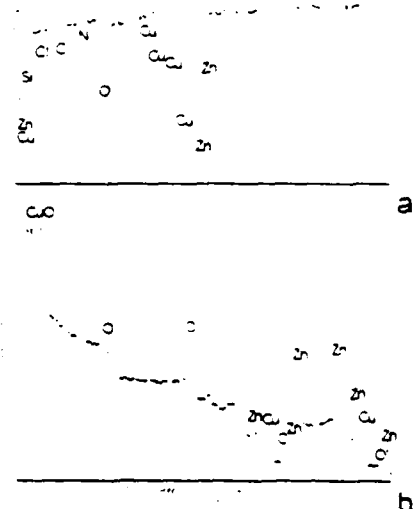


Fig. 5. AES(a) and ESCA(b) analysis of black region (B) in Fig. 1 (corresponding to the surface regime illustrated in Fig. 4(b) and (c)).

The alterations within the surface region and the correlation of this zone with the electrode interior is illustrated in Fig. 6(a) while Fig. 6 (b) and (c) show the details of an electrode section interior as observed in the TEM. The TEM images reveal dislocation substructure which exists roughly 2 mm below the central region surface [shown circled in (a)].

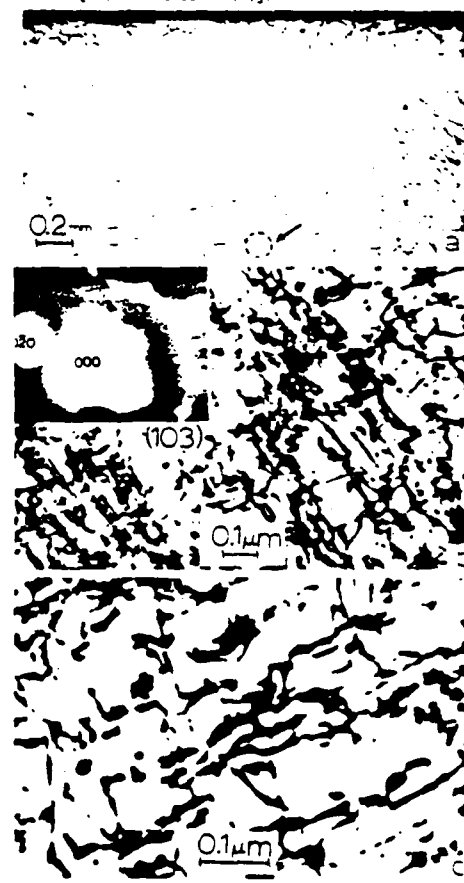


Fig. 6. Examination of electrode surface section along the direction of the arrow in Fig. 1. (a) Optical metallography view at low magnification. (b) TEM bright-field image in a grain area about 2 mm from the central surface region [near the region circled in (a)]. Selected-area electron diffraction pattern insert is indicative of surface orientation shown. (c) magnified view of area in (b) showing dislocations and dislocation loops.

#### Insulator Examination

FT-IR absorbance subtraction spectra for each of the polymer materials (Delrin, Nylon and Lucite) showed higher absorbance for the larger number of shots ( $10^5$  as compared to  $10^3$ ) as shown for example in Fig. 7.

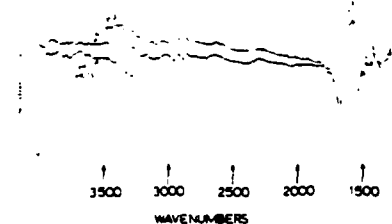


Fig. 7. FT-IR analysis of Nylon insulator showing characteristic absorbance after  $10^2$  and  $10^3$  shots.

While Nylon and Delrin showed no new functional groups formed in the surface, the difference spectrum of Lucite showed some new functionality which appeared to be unsaturation. All samples showed a roughening substantially greater than the undamaged materials, and this feature as well as the increased absorbance was attributed to metal deposition on the surfaces. This feature was confirmed by examination of the samples in the SEM as well as by ESCA. Figure 8 shows that considerable deposition from the tungsten alloy electrode occurred, and the deposition increased with increasing number of pulses ( $10^2$  as compared to  $10^3$ ). The presence of Cu, Ni, and W in the deposit is indicated in the X-ray analysis shown in Fig. 8(c) while Fig. 8(d) is indicative of the probable oxidation of these metals. The particulate nature of the deposit as shown in Fig. 8(a) and (b) is probably due to oxide formation.

#### Summary and Conclusions

We have demonstrated in this preliminary study that even in simple switching systems where complex quenching gas reactions are absent, considerable distortion and alteration occurs in the electrode surface as well as the insulator surface. The electrode material in a brass and a tungsten alloy was observed to be vaporized by the discharge cycles and deposited as oxides and possibly some free metal onto the insulator surfaces. The microstructural and microchemical features of these alterations were observed and confirmed by an interdisciplinary and synergistic use of microanalytical diagnostic instruments mainly involving electron probe or electron beam techniques. However the implications of using other systematic ion beam analysis techniques should be apparent in the expansion of this synergistic approach to materials analysis applied to pulsed power, high-energy switching systems.

#### Acknowledgments

It is a pleasure to thank Dr. Lyn Hatfield of the Physics Department at Texas Tech who supplied the materials examined in this paper and provided their case histories. We are grateful to Ms. Karen Couch of New Mexico Tech for her help in the SEM work and G. Conrad, K. Keil, and C.C. Allen of the Metatech Institute at JNM for electron microprobe analyses. Finally the encouragement and discussions with Dr. C. Stein are also gratefully acknowledged.

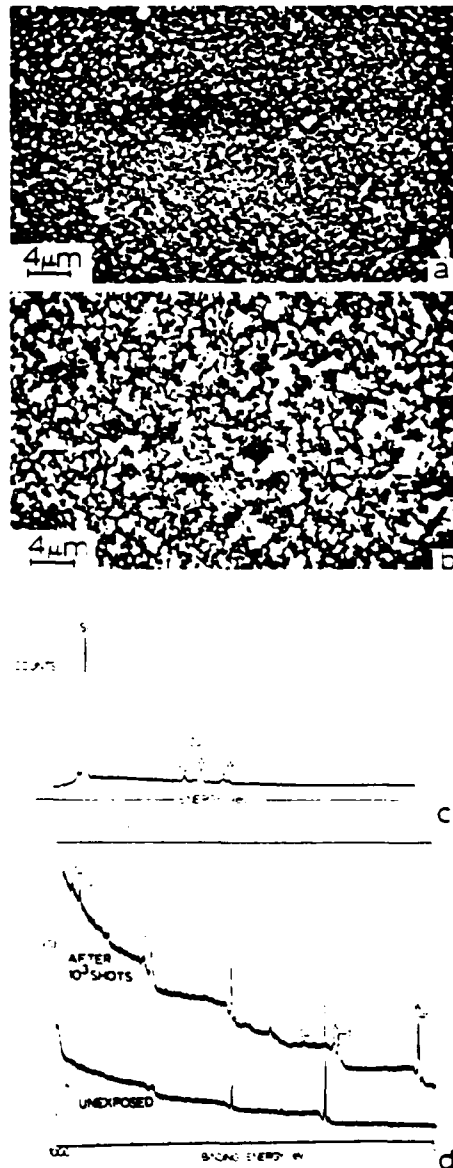


Fig. 8. Nylon insulator alteration. (a) surface deposit appearance after  $10^2$  shots (SEM). (b) Surface deposit appearance after  $10^3$  shots (SEM). (c) Energy-dispersive X-ray analysis of area in (b). (d) ESCA analysis of area similar to (b) corresponding to  $10^3$  shots and comparison with the original, unexposed material.

216

GROUP REPORTS

## THERMAL AND GAS DYNAMIC EFFECTS

G. Marshall Molen  
(Chairman)

Herbert Carper  
(Co-Chairman)

This working group has addressed two of the principal concerns in the design of a high-pressure spark gap that is intended for repetitive operation. In this section the opinions and conclusions of the group as they relate to thermal and gas dynamic effects in spark gaps are summarized. All members of the group have made valuable contributions to this effort both in terms of their comments at the workshop as well as their written contributions to this report. Each member's understanding of spark gaps was enhanced in the open and diligent discussions. As many of the issues presented here represent the collective wisdom of the group, it is difficult to give individual credit; however, the names of the contributors are included when possible.

## A. INTRODUCTION

A principal consideration in the design of a spark gap intended for continuous, repetitive operation is the recovery of the gap and the corresponding reproducibility over an extended period of time. The latter is also related to the useful life of the switch which must often exceed  $10^7$  operations. For high-power spark gap switches which are intended to operate at repetition rates exceeding several hundred pulses per second, the gas must generally flow through the switch so as to affect recovery by removing the arc products.

At higher repetition rates (e.g., 1 kHz-10 kHz) the gas dynamics become particularly important and the corresponding flow fields must be carefully controlled.

The reproducible performance of the switch is also strongly dependent upon thermal considerations. A repetitively-operated spark gap must necessarily reach an equilibrium condition such that the dielectric properties of the switch remain fairly uniform and the other materials (e.g., electrodes) are not subjected to excessive temperature that may result in premature failures. The erosion of electrode materials and the damage to surrounding insulators are specific concerns.

Gas flow and thermal effects in the spark gap are clearly interrelated. The flowing media can be used to not only "sweep-out" debris from the region but as a method of cooling the electrodes. Turbulence in the flow field can also provide an effective mixing of the heated gas so as to remove strong temperature and density gradients. In addition, the gas flow can be effective in minimizing the arc debris that is deposited on the surrounding insulators.

#### 1. Group Objectives

The primary objective of the group was the evaluation of the thermal and gas dynamic effects on the operation of a spark gap operated in a repetitive mode. These effects were found to be particularly relevant to spark gaps as described below:

##### Thermal Effects

- a. The removal of heat from the switch body so as to reach an acceptable equilibrium temperature (considered

a straight-forward engineering consideration).

- b. The removal of heat from the arc channel so as to affect recovery of the gap.

#### Gas Flow Effects

- a. The removal of arc by-products from the gap region.
- b. Assist in the removal of heat from the arc channel.
- c. The adverse consequences of gas flow such as
  - (1) electric field distortion (motion of charged particles)
  - (2) enhanced electrode erosion
  - (3) shock perturbations
  - (4) excessive power requirements.

#### 2. Approach

The approach that was pursued in the discussions so as to address these effects can be briefly described as follows:

- a. Presentations by group members to discuss relevant experience.
- b. Identify the principal considerations relating to thermal and gas flow effects.
- c. Establish what is known about these considerations (state-of-the-art).
- d. Evaluate the relative significance and trade-offs.
- e. Identify any fundamental limitations.
- f. Recommend topics for further study.

#### 3. Limits of Deliberations

So as to effectively deal with the pertinent issues the following limits were placed on the group deliberations:

- a. Emphasize fundamental problems rather than engineering details.
- b. The discharge is considered as a single, constricted arc with a corresponding cylindrical shock wave.
- c. Fundamental arc breakdown processes are not considered.
- d. Did not consider triggering mechanism except for perturbations it may introduce in the flow field (this is not to suggest that triggering is not important).
- e. Primarily considered discharges with pulse-widths less than 1  $\mu$ s.
- f. Primarily considered high peak power gaps (e.g.,  $I > 1$  kA,  $V > 150$  kV).

#### B. FUNDAMENTAL CONSIDERATIONS

The fundamental considerations relevant to the group's discussion of repetitive spark gaps are divided into two distinct areas. The first area addresses thermodynamic considerations while the second concerns the gas flow. The topics in each area are described in Tables I and II, respectively. As the thermal processes and gas dynamics are interrelated, several of the topics could equally well appear in either table. Presented in this section is a discussion of the individual topics and the implications which they have to the design of a repetitive spark gap.

TABLE I

## THERMAL CONSIDERATIONS

- a. Energy Dissipated During Formative Stage of the Arc
- b. Conduction Losses of Arc Column
  - Heat loss into gas
  - Heat loss into electrodes
- c. Shock Waves and Dissipation of Energy
- d. Cooling Mechanisms
- e. Phase Change of Electrode Material
- f. Reduced Dielectric Strength of Heated Gas
- g. Insulator Materials for High Temperatures

## TABLE II

## GAS FLOW CONSIDERATIONS

- a. Purpose of Gas Flow
- b. Limitations on Flow Speed
- c. Effects of Turbulent Mixing
  - "Clean-out" boundary layers
  - Turbulent dispersion of arc products
- d. Pump Losses and Energy Requirement
- e. Effects of Gas Flow on Erosion
- f. Clearing Factor
- g. Electrode Boundary Layer Control
- h. Geometry Considerations
- i. Electric Field Distortion by Arc Products
- j. Gas Species
- k. Gas-Handling Configurations

1. Thermal Considerationsa. Energy Dissipated During the Formative Stage of the Arc  
(S. Byron) -

The minimal energy that must be deposited in the gas to form a conducting channel is that required to heat the gas to a temperature that is sufficient to achieve a high electrical conductivity. For fast discharges (e.g.,  $\leq 100$  ns), the gas atoms remove minimal energy, and the gas density remains constant. In general, the gas in the arc column reaches local thermodynamic equilibrium (LTE) for the high electron densities and current densities of interest. As a representative example, the electrical conductivity for argon is shown in Fig. 1 as a function of temperature where the gas is at 1 atm and in LTE. Above one percent ionization the degree of ionization has minimal effect on the conductivity. As shown in the figure, the conductivity continues to increase as  $T^{3/2}$  as described by Spitzer<sup>1</sup>. Similar behavior is found for other gases. One may conclude that the temperature in the arc channel must exceed  $10^4$  °K to achieve a high electrical conductivity and that temperatures exceeding this value do not significantly increase the conductivity.

The minimal energy required to form the arc is easily calculated by summing the thermal energy of the atoms, the dissociation energy, and the ionization energy. As an example, a temperature of  $2 \times 10^4$  °K and fractional ionization of 10% is assumed. At this temperature the gas is fully dissociated in the arc channel. The results of such calculations are shown in Fig. 2 for several gases, and it should be noted that the gases with

# ELECTRICAL CONDUCTIVITY AND SWITCH LOSS DURING CONDUCTION PERIOD

224

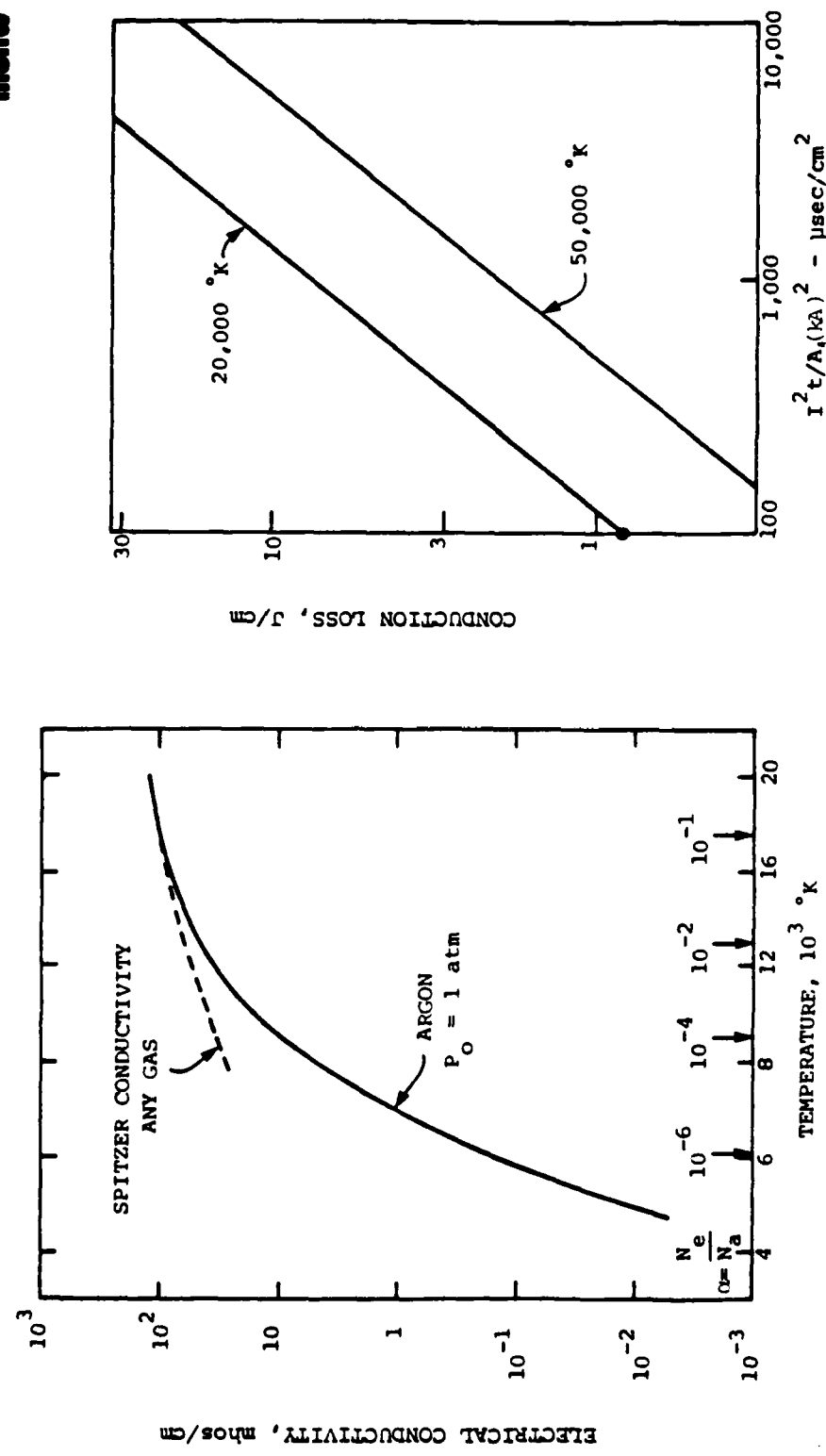


Figure 1

Figure 3

CALCULATED FORMATIVE ENERGY DENSITY  
VERSUS MEASURED HOLDOFF FIELD STRENGTH FOR  
VARIOUS SWITCH GASES

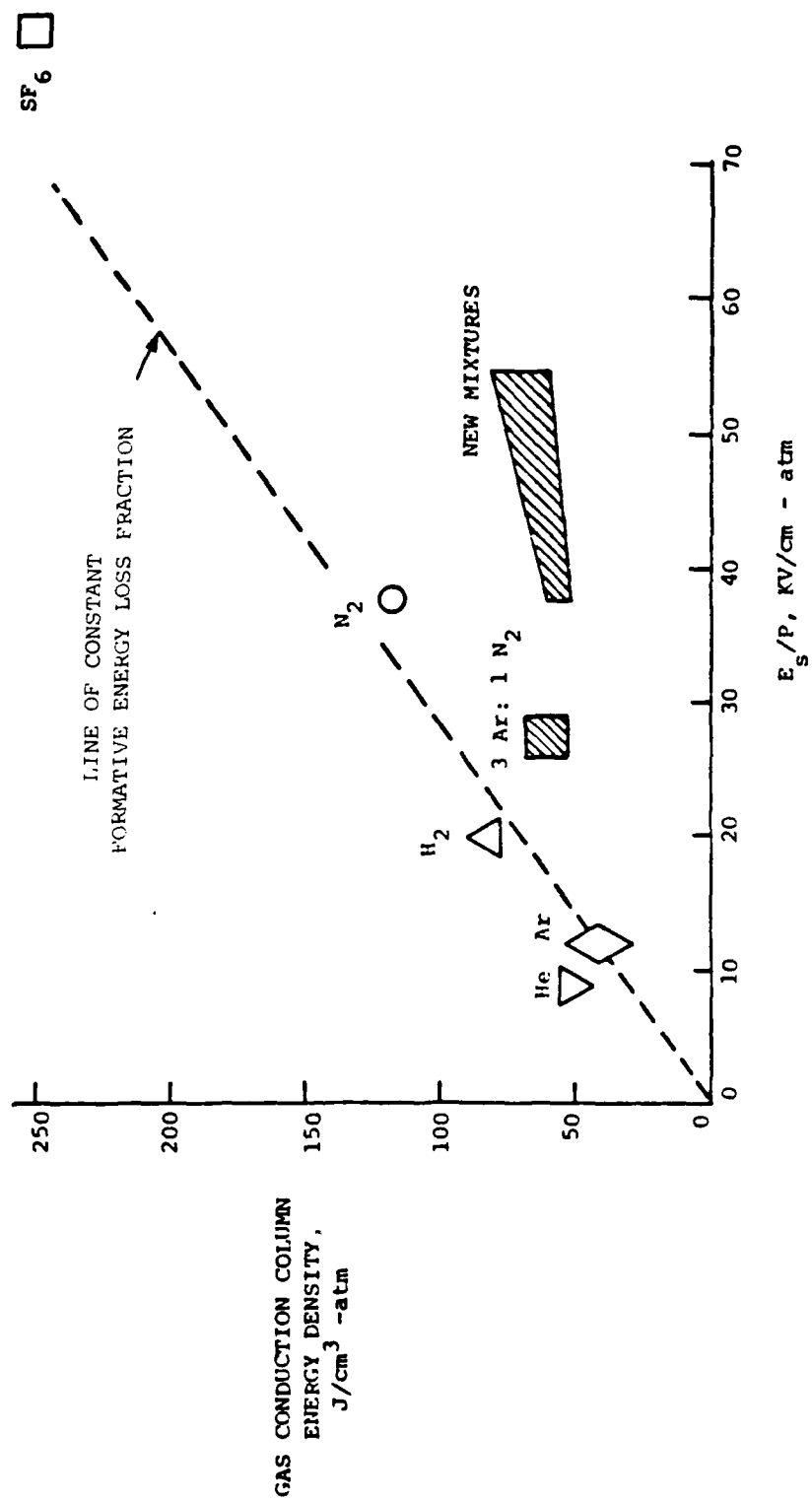


Figure 2

higher dielectric constants require a correspondingly higher energy investment. Certain mixtures may provide lower commutation energy at reasonably high dielectric strengths.

So as to complete the calculation of minimal commutation energy, the arc column diameter must also be determined. Various models and empirical formulas are available in the literature<sup>2</sup>. Typically the channel diameter is nearly independent of the initial gas density and varies as  $t^{1/2} I^{1/3}$  where  $I$  is the total current and  $t$  is the pulse duration. For  $I = 20$  kA and  $t = 100$  ns, the diameter in air is approximately 2.5 mm and the minimal formative energy approximately 5 J·cm<sup>-1</sup>·atm<sup>-1</sup>. For slower discharges, the radial gas motion reduces the gas density within the arc column and correspondingly reduces the commutation energy.

b. Conduction Losses of Arc Column (S. Byron) -

A simple estimate of the conduction loss can be calculated using

$$W_{\text{cond}} = I^2 R t = \frac{I^2 \ell t}{\sigma A}$$

where  $\ell$  is the gap length,  $A$  is the cross-sectional area, and  $t$  is the pulse duration. This expression is shown graphically in Fig. 3 using the Spitzer conductivity for  $\sigma$ . As an example, a length of  $\ell = 3$  cm,  $\sigma = 200$  mho/cm, an arc diameter of 2.5 mm, and a current of 20 kA is assumed. The resistance  $R$  is found to be 0.3  $\Omega$  and the corresponding voltage drop is 6 kV with an energy loss of 12 J for a 100 ns pulse. From this example, we see that the conduction loss is approximately the same as the formative loss in air at 2.5 atm as previously calculated.

Available scaling information suggests that larger currents in a single channel will have larger conduction loss than commutation loss for the 100 ns pulse considered. This is thus an incentive to consider multiple spark channels to carry large currents.

The conduction energy loss is primarily used to increase the degree of gas ionization and has little effect on either the temperature or the conductivity. For the above example, radiation loss is relatively small. The blackbody emission at  $2 \times 10^4$  °K is  $10^6 \text{ W/cm}^2$  providing 0.25 J loss for the 100 ns pulse. Radiation loss for slower discharges can play a more significant role.

Another energy loss during the conduction phase is the heat input to the electrodes themselves. There are four sources of heat input which include:

- 1) ohmic heating in the electrode material,
- 2) local heating by gas at the arc attachment spot,
- 3) convective heat transfer from the gas to the electrode during the interpulse period, and
- 4) radiation from the spark column to the electrode.

Ohmic heating in the electrode is generally considered small. However, for high current spark channels near the arc attachment spot, the current density may reach  $10^6 \text{ A/cm}^2$  or more over a surface diameter of about 2 mm. For an electrode material with an electrical resistivity of  $10^{-5}$  ohm·cm, the skin depth is about 0.1 mm for a 100 ns duration current pulse. Thus, the surface current

density is approximately  $5 \times 10^6 \text{ A/cm}^2$ , the resistive component of the electric field strength along the surface is 50 V/cm, and the corresponding voltage drop along the surface is about 5 V along a 1 mm radial distance. Thus the ohmic input to each of the electrodes can be comparable to the work function of the electrode material.

A significant fraction of the local gas heating at the arc attachment point is also transferred to the electrodes during and after the arc. The power input to the gas in the sheath region is the electrode fall voltage (roughly equal to the ionization potential of the gas, i.e. 10 V to 20 V) times the total current. This energy can be lost by radiation from the discharge in the direction away from the electrode region and the remainder transferred to the electrodes by radiation and thermal conduction. Approximately one half of the radiated energy is in the direction away from the electrode.

The major energy loss in the switch results from the energy deposited in the arc channel. However, this source is removed from the electrodes and the energy reaches the electrode surface primarily by radiation which is distributed over the electrode surface rather than localized at the arc attachment spot. The energy deposited in the arc column of the gas is divided into radiation re-emission, blast wave energy, and residual thermal energy in the gas. Each of these contributions is approximately equal. Thus each electrode may receive 5 to 10 percent of the energy deposited in the arc column by radiation. The total energy deposited in the arc

column can itself be of the order of 10 percent of the switched energy. Radiation from the arc column provides the major heat load to the electrodes for high power, high PRF spark gap switches. The electrode heat load is sufficient to require active cooling for repetition rates exceeding about 100 Hz. Gas flow cooling is simplest but is adequate only at moderate values of average power transfer through the switch.

c. Shock Waves and Dissipation of Energy (W. Moeny) -

One of the longer-term effects of the arc formation is the production of a cylindrical shock wave. As much as 1/4 to 1/2 of the arc formation energy is removed as the arc expands. These waves may reflect from the solid walls into the arc region or even upstream in the gas flow so as to produce local density gradients. For high repetition rate spark gaps, the gradients may affect the gap recovery. As the shock waves are assumed to be cylindrical in shape, the waves will lose their energy as  $1/r^2$  and will dissipate rapidly unless reflected or focused by the walls. If required, the waves could be damped using acoustic absorbers in the side walls.

d. Cooling Mechanisms (B. Wright) -

For a repetitive spark gap operated in a burst mode, the thermal energy can either be removed during the time between pulses (real-time cooling) or over the longer time interval between bursts. For the latter case, the energy is stored in the thermal mass of the electrode.

The design calculations for the thermal storage mode are rather straightforward as one need only consider the differential between the ambient temperature and the maximum allowable temperature. This maximum temperature is a function of the reduction in hold-off voltage because of the heating of the gas in the boundary layer adjacent to the electrode. As an example, the  $E/N$  ratio in this layer is doubled when operated at a temperature of  $300^{\circ} \text{ C}$ . This may then result in avalanching, corona, and a modification of the profile of the virtual electrode, all of which degrade the switch performance. If one restricts the change in  $E/N$  to 25%, only a maximum electrode temperature of  $100^{\circ} \text{ C}$  or  $\Delta T = 75^{\circ} \text{ C}$  is permissible. For this example, with a 2 kg electrode, 30 kJ per burst could be tolerated. A switch operating at 90% efficiency could then switch a total energy of 300 kJ. It is assumed for this calculation that all losses in the gap are distributed uniformly throughout the electrodes and cooling by the gas flow is neglected.

For real-time cooling, liquid flow through the electrodes themselves is considered as the best choice. The power that must be removed,  $P_L$ , is the energy loss per pulse times the repetition rate. If deionized water is used as the coolant, the flow rate in gpm is given by  $P_L/(265 \Delta T)$ . This calculation likewise neglects cooling by the flowing gas.

e. Phase Change of Electrode Material (H. Carper) -

The characteristics of high-current arcs are such that electrode material is vaporized at the arc roots either by melting and evaporation or by sublimation. Although this is a rather complicated process that is not well understood, the phenomenon should be considered when calculating an energy balance for the electrical to thermal energy conversion. It is not clear how much energy is involved in this process; however, the condensation and re-solidification do result in a thermal input to the gas and electrodes. Perhaps a more serious concern is the erosion of the electrode material as a result of this phase change.

f. Reduced Dielectric Strength of Heated Gas (B. Wright) -

The boundary layer of gas that is in contact with the heated metallic electrodes may have a significantly lower dielectric strength. Specific examples of the reduction in  $E/N$  have been presented in an earlier section. It is not unreasonable to expect that the dielectric strength of the gas in this boundary layer may be reduced to only 1/5 of the colder gas. This could have the effect of slightly changing the electrode boundary profile and the corresponding gap length. This has the net effect of reducing the self breakdown voltage of the gap as well as perturbing the potential distribution within the gap. The heated boundary layer can often be cooled by the use of turbulent mixing.

g. Insulator Materials for High Temperatures (G. M. Molen) -

The identification of insulating materials for use in a switch that may be subjected to high temperature is a topic that has been addressed by the Materials and Chemistry Group. It is appropriate to note, however, that the wall materials are subjected to a particularly harsh environment. The insulators will receive a radiative heat flux from the arc column and thermal conduction from the adjoining electrodes. In addition, uv-radiation from the arc will substantially degrade many materials, and debris deposited on the insulator walls reduces the dielectric strength of the material. The best choice of insulating materials for this application is probably a ceramic with a high thermal shock resistance.

2. Gas Flow Considerations

a. Purpose of Gas Flow (B. Wright) -

Gas flow in a repetitively-operated spark gap can be successfully employed for four separate functions:

- 1) improving the switch recovery,
- 2) cooling the electrodes and insulators,
- 3) breaking-up bubbles of ionized gas in the boundary layers adjacent to the electrodes,
- 4) keeping the arc debris from the insulator surfaces.

For a given set of operating parameters, each of these functions may require a different flow rate. The principal objective of gas flow is usually the first function whereby

the gas flow is used to move the arc products a considerable distance from the initial channel before the voltage is reapplied. The relevant parameter is usually called the "clearing factor." This application of gas flow is closely related to the third function when the gas flow also "cleans out" the boundary layer.

Electrode cooling need not necessarily be accomplished by gas flow, as other mechanisms such as liquid cooling can be effectively utilized. Likewise the switch geometry can be used to keep the arc debris from the insulator.

b. Limitations on Flow Speed (W. Moeny) -

A fundamental limit on the recovery of a high-repetition rate spark gap is the ability to move the arc products a sufficient distance from the gap before the voltage is again reapplied. The gas velocity thus becomes a limiting factor on the maximum repetition rate of the gap unless other means are employed to quench the arc. The critical scaling factor is the stagnation speed of sound; that is, the speed of sound of the gas when at rest. As the gas is accelerated to supersonic velocities, the Mach number increases; however, the speed of sound in the medium drops resulting in only a slow increase in the velocity above Mach 1. The limiting velocity is given by<sup>3</sup>

$$v_{mx} = a \sqrt{\frac{2}{\gamma-1}}$$

where  $a$  is the stagnation sound speed and  $\gamma$  is  $c_p/c_v$ .

In practice, this limit on the gas velocity is achieved at Mach 4 to Mach 6 where the pumping losses are high. For molecular gases,  $\gamma \approx 1.4$  such that  $V_{mx}/a \approx 2.2$ . Thus a factor of two, at most, can be gained by using supersonic flow. A more practical limit may be speeds just below or just above Mach 1 so as to avoid thermal choking as the gas is heated while at the same time avoiding excessive compressor losses.

Thus a critical factor in the design of a repetitive spark gap is the selection of the gas itself. Gases with low molecular or atomic weight, such as helium or hydrogen, have a high acoustic speed ( $a = \sqrt{\gamma RT}$ ) but poor dielectric strength. On the other hand, a good insulating gas, such as SF<sub>6</sub>, has a low acoustic speed. An alternative would be a gas mixture which has a high acoustic speed and yet good dielectric properties. A possible example would be a mixture of SF<sub>6</sub> in helium or argon. Perhaps a better, but more difficult mixture would be flourine in helium.

c. Effects of Turbulent Mixing (W. Moeny and J. Kuhlman) -

Turbulent mixing has two principal effects on the gap recovery:

- 1) dispersion of the arc products by free-stream turbulence and
- 2) "clean-out" of the arc products from the boundary layers.

Substantial free-stream turbulence can effectively disperse the arc products by eddy mixing. The large coherent structures can entrain arc products and effectively mix them with neutral gas so as to cool the arc products. The arc products may be sufficiently dispersed so that their conductivity is negligible. Theoretical techniques are also available to analyze the turbulent intensity and entrainment rate so as to evaluate the effectiveness of the process.

For a boundary layer that is laminar, arc products can be retained along the walls for many flow transit times. For this case, metal vapor from the electrode can cause a substantial increase in the recovery time. A turbulent boundary layer will instead provide enhanced mixing so that the arc products are dispersed and the corresponding dwell-time in the wall layer is reduced. This can serve to improve the recovery time by reducing the required clearing factor.

Enhanced turbulent mixing by vortex generators is one passive approach that works well for rather small gaps (lower voltages). A very effective but power intensive approach is the use of boundary layer suction to remove the boundary layer so as to prevent downstream prefires. The power requirements are usually quite high and represent a substantial penalty on the system.

The advantage of the turbulence to assist in the gap recovery (or corresponding decrease in the clearing factor)

may be counterbalanced by two adverse effects. First, it is expected that turbulent boundary layers will lead to enhanced electrode erosion due to the larger wall shear stresses as compared to a laminar boundary layer. Measurements by Martin<sup>4</sup> indicated a ten-fold increase in erosion for a turbulent flow relative to the erosion measured for a more laminar flow. Another possible adverse effect is the increased dissipation of the flow kinetic energy. For the relatively high velocities considered (near sonic speeds), the energy dissipated by the turbulent flow may lead to substantial increases in the power required to produce the gas flow.

d. Pump Losses and Energy Requirements (J. Kuhlman) -

The compressor energy requirements for a closed-loop, continuously operating gas flow system may be computed as

$$P = K(1/2 \rho v^2)Q$$

where  $\rho$  and  $v$  are the gas density and velocity between the electrodes, respectively; and  $Q$  is the gas volume flow rate. The factor  $K$  varies widely and depends upon the efficiency of the gas flow system. A lower bound on the magnitude of  $K$  is approximately one, but a poorly designed system could easily be as much as ten times greater. One should note that the power requirements then scale with the gas density (or pressure for room temperature operation) and the gas velocity to the third power. Needless to say, this energy is dissipated in

the flow circuit, and the heat must be removed along with the energy dissipated in the arc. A heat exchanger is usually required to achieve steady-state, continuous operation.

The stagnation pressure increase across the compressor or fan, so as to produce a given flow speed, is given by Shapiro<sup>3</sup> as

$$\frac{(1 + \frac{\gamma-1}{2} M^2) (\frac{\rho_02}{\rho_01})^{\frac{\gamma-1}{\gamma}} - 1}{\frac{\gamma-1}{2} M^2} \approx 0.75 .$$

This equation has been found to be in good agreement with performance data for high-speed wind tunnels that operate from low subsonic Mach numbers up to  $M \approx 5$ .

e. Effects of Gas Flow on Erosion (M. Molen, H. Carper, and T. Burkes) -

In an earlier discussion it was suggested that turbulence at the boundary layers may lead to enhanced erosion of the electrodes. This was supported by Martin<sup>4</sup> who noted a ten-fold increase. The enhanced erosion will add metallic debris to the gas stream which may negate any advantage of the use of turbulent boundary layers to improve the switch recovery.

Vaporization of the electrode material is known to occur at the arc roots in a high-current discharge. This process occurs either by sublimation (e.g. graphite) or by melting and evaporation (e.g. copper or brass). If a substantial

amount of the vaporized material re-solidifies on the electrode, the erosion rate will be low. For a gas blown gap, however, the vaporized material may be confined in the relatively thin hydrodynamic boundary layer near the electrodes. For this case the amount of material that re-solidifies on the electrodes will be strongly affected by the gas velocity in the boundary layer and by the characteristics of the flow field, i.e., whether laminar or turbulent. For high velocities the vaporized metal may be swept downstream before it re-solidifies on the electrode thus causing the erosion to be high. There is evidence, however, to suggest that electrode cooling can result in reduced erosion<sup>5</sup>.

Another primary concern is how the accelerated erosion of the electrodes will affect the useful life of the switch. For applications that required the gap to operate for  $10^6$  operations or more, this process must be carefully controlled. Laminar flow at the boundaries would have a decided advantage over turbulent flow for these applications.

f. Clearing Factor (G. Rohwein)-

The clearing factor for a switch that employs flowing gas may be defined as the gas volume changed in the electrode region between pulses divided by the switch electrode volume. The amount of gas required to effectively restore the dielectric strength to a spark gap between pulses is influenced by a number of factors which include:

- (1) Time before the voltage is reapplied to the gap  
(accounts for combined effects of PRF, DC dwell time,

residual heater or ionization effects from previous pulses, degree of recovery, etc.).

- (2) Gas flow field
- (3) Electrode and switch housing geometry
- (4) Duty cycle (i.e. burst mode or continuous repetition)
- (5) Other cooling mechanisms (e.g. heat sinks, liquid coolant, etc.)

For low to moderate pulse repetition rates (e.g.  $\leq$  100 pps) in low to high energy systems, one wishes to maximize the effectiveness of the gas flow in terms of restoring the dielectric strength. Effective utilization of the gas minimizes the mass flow rate, or more specifically, the external power required to furnish the compressed gas. Therefore, techniques such as turbulence may be employed to enhance the cooling and mixing of the arc products for this class of spark gaps.

In experiments conducted at Sandia Laboratories, for example, it has been found that the clearing factor can be reduced to zero for burst mode operation of low and high voltage gaps if the PRF does not exceed about 50 pps and the total number of pulses is less than 10 or 15. For continuous operation, however, the clearing factor required may be as high as 0.5 to 1.0.

Another comparison can be made relative to the flow pattern. If the entire gas volume that flows between the electrodes does not contribute to the dielectric recovery, a larger total gas volume will be required. For example, a low voltage (e.g.  $< 100$  kV) gap with closely spaced electrodes is more effectively

cleaned with a high-velocity vortex flow than with a strictly radial flow or low-velocity vortex flow. The high-velocity vortex flow mixes the ionization products uniformly in the total volume and maintains a consistent quality of gas in the switch region. The increase in the required gas volume to prevent pre-fires has been measured in a gap at Sandia Laboratories. A factor of three increase in gas volume was measured when operated with a low-speed vortex flow as compared with a high-velocity vortex flow. This example is only to illustrate that significant differences in gap recovery can be observed when different flow methods are employed. Similar arguments can be made for the high-voltage range (e.g.  $\geq 1$  MV).

#### g. Electrode Boundary Layer Control

In earlier discussions the significance of the boundary layer has been addressed. Several techniques for controlling this layer have been suggested. This topic is, however, complex because of the interrelation between the flow characteristics (e.g. laminar or turbulent), the electrode erosion, and the gas-handling power requirements.

#### h. Geometry Considerations (S. Byron, G. Rohwein and M. Molen) -

The geometric features of a spark gap are influenced by a number of related considerations. Among these are:

- (1) Operating voltage range
- (2) Peak current capability
- (3) Energy and charge transfer
- (4) Pulse repetition rate and duty cycle

- (5) Switch lifetime
- (6) System constraints (e.g. inductance, airborne requirements, space limitations, etc.)
- (7) Preferences of the designer.

As an example, radical differences are apparent in spark gaps designed for operation at voltages less than 100 kV as compared with multi-megavolt spark gaps which are almost always cylindrical in configuration. The lower voltage gaps would typically be used for currents less than 100 kA, at repetition rates less than 100 pps, and may be designed for low inductance. These gaps would have closer spaced electrodes that could effectively utilize high-speed vortex flow to clean and cool the switch region. Although vortex flow can be used in the larger volume electrode geometries required for high-voltage gaps, the vortex flow has not been found to be as effective as axial flow techniques for this class of switches.

The electrode size is influenced by the energy per pulse, the maximum current, the peak power, and the lifetime requirements to name a few. As an example, the electrode area available affects the useful life of the switch. In addition, the gas flow geometry may be strongly affected by inductance constraints. For example, a 1 nH to 5 nH rail gap would have a radically different geometry and flow field configuration as compared with a 50 nH cylindrical gap.

It is thus apparent that the pulse-repetition-rate operating regime has a major impact on the flow geometry. Low to moderate repetition rates (50 to 300 Hz) permit the use of vortex and recirculating flow to clear and mix the gas heated by the arc

with the ambient cool gas so as to achieve switch recovery. However, high repetition rates (1 to 20 kHz) require strong, forced convection to clear the heated gas from the electrode region prior to the next applied voltage. A fundamental upper limit on the repetition rate is given by

$$\text{PRF}_{\max} = \frac{a}{kdF}$$

where  $a$  is the sonic speed,  $d$  is the gap separation,  $k$  is an aspect ratio correction (ranging typically from 0.5 to 2), and  $F$  is the required clearing factor to assure adequate gas clearing. As an example using a high-speed switch gas such that  $a \approx 4$  to  $8 \times 10^4$  cm/sec, and assuming a 4 cm gap,  $k = 1$ , and  $F = 1$ , the maximum repetition rate is 10 to 20 kHz. Clearly the gap dimension cannot be increased without a corresponding decrease in repetition rate.

Another key consideration in the design of a gas-blown switch is to insure that there are no flow separation zones or wakes on the electrodes in regions where the spark may strike. If this occurs, flow separation will permit the electrode vapor and arc-heated gas to remain near the high electrical stress region much longer than the flow clearing time. This has been observed to reduce the hold-off voltage significantly.<sup>6</sup>

The flow geometry must also be designed to restore the flow pattern quickly following the blast wave from the arc column. The blast wave can affect both the free stream and the boundary layer. This issue is especially important for high PRF switches and is one motivation for using a flow Mach number that is near or slightly greater than 1. It is possible for the upstream

moving blast wave produced by the arc column to reverse the incoming free stream flow and establish a new flow pattern that tends to go around the region of spark heated gas. This effect can be overcome by various flow geometries. One approach is to use a high free-stream dynamic pressure (which prevents flow reversal). Another approach is to use a choked-orifice plate just upstream of the spark region to provide significant free-stream overpressure which reflects the blast wave and rapidly restarts the free stream flow. The orifice plate approach was demonstrated 10 years ago in pulsed laser development work.<sup>7</sup> A third approach is to use sidewalls to confine the free-stream flow thus reducing the time to reestablish the unperturbed flow pattern.

In addition to restoring the free-stream flow pattern, it is also important that the boundary layer flow be restored. Because of the low speed of the boundary layer fluid, it is most susceptible to reversal and flow separation by the high overpressure of the blast wave from the spark channel. The boundary layer must clear the electrode vapor from the high electrical stress region prior to the next pulse. To accomplish this at high PRF, special attention must be given to the upstream flow contour to assure a favorable pressure gradient along the channel walls which encourages boundary layer stability and attachment. For subsonic flows the downstream flow contour normally must not diverge too rapidly ( $<7^{\circ}$  half angle) or the diffuser pressure rise will lead to turbulent boundary layer separation.

Because of the slow downstream channel divergence that is required to retain stable attached boundary layers, there is a

fundamental difficulty in clearing the spark column gas downstream and providing rapid recovery of the switch hold-off voltage. Several flow geometries are illustrated in Fig. 4 to aid in this process. The advantages and difficulties for each of these concepts are listed in Table III. The use of downstream droplet (mist) injection to cool the hot gas in a pulsed laser device has been demonstrated previously.<sup>8</sup> In addition, the use of downstream insulator wedges to define the downstream edge of an externally sustained, moderate-voltage diffuse electric discharge has also been demonstrated.<sup>9</sup>

To increase the mixing of the hot gas in the arc channel with the surrounding cool gas as it moves downstream, the use of nonuniform free-stream flow has been suggested. The non-uniformity can result from either small-scale turbulence induced by upstream grids or screens, or it can be gross variations in free-stream velocity and corresponding shear layers in the spark column gas produced by a segmented upstream nozzle design. For very high PRF switches operating at near sonic flow speeds, large-scale eddy mixing is probably required because of the short interpulse time available.

Another issue that affects high PRF switch geometries is the location of the trigger in a manner that is consistent with high speed flow. One approach is triggering by a midplane electrode that is used in conjunction with two adjacent flow systems. However, for high-voltage switching, laser triggering may be required to reduce the formative time lag and jitter. The problem of geometrical integration of the laser trigger with high PRF

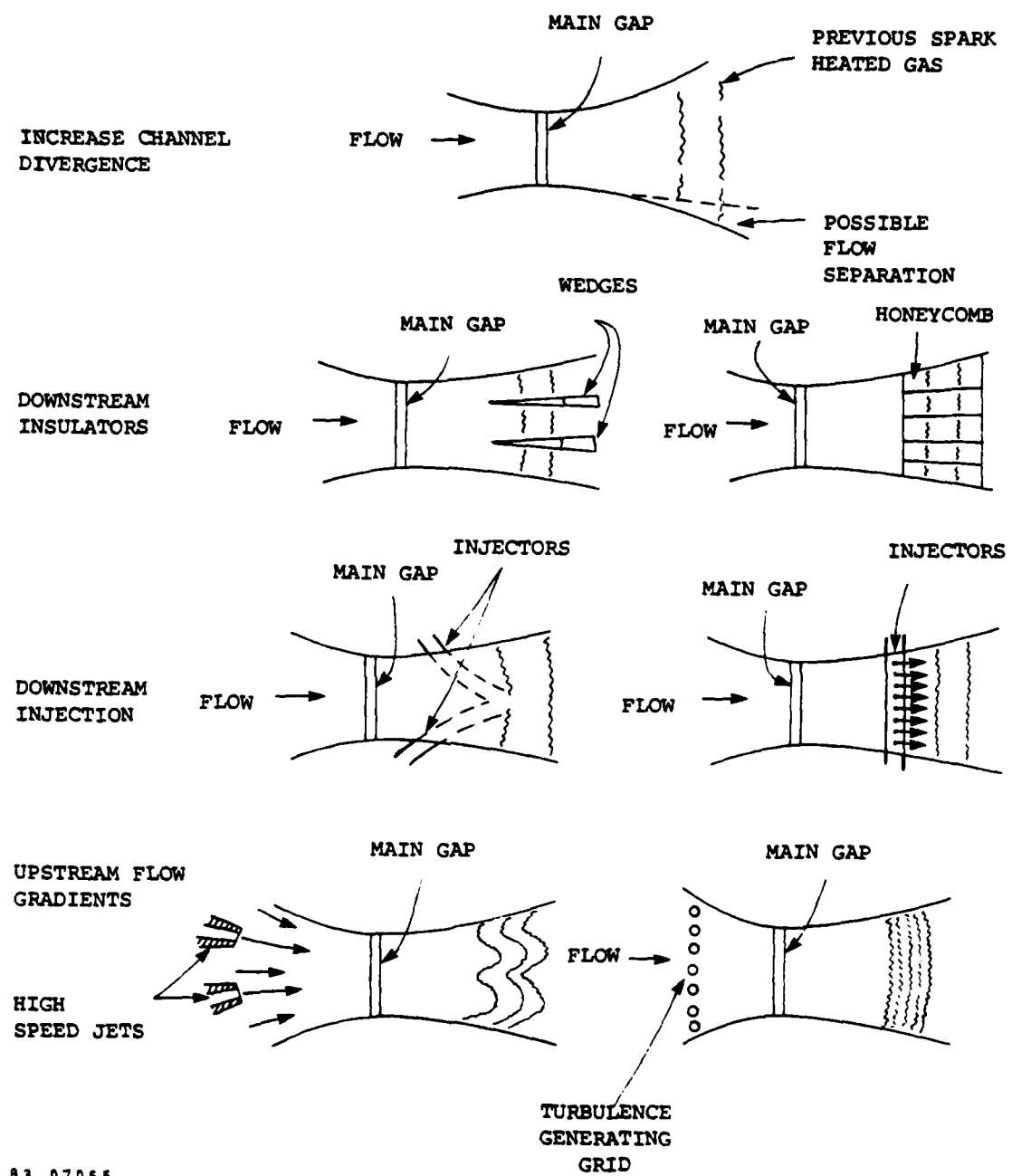


Figure 4. Various Configurations to Reduce the Recovery Time of High PRF Spark Gap Switches.

TABLE III  
FLOW CONFIGURATIONS TO REDUCE TIME FOR DOWNSTREAM GAS  
TO RECOVER TO FULL SPARK GAP HOLD OFF VOLTAGE

<u>APPROACH</u>	<u>PURPOSE</u>	<u>MAJOR DIFFICULTIES</u>
<u>Rapid downstream channel divergence</u>	<ul style="list-style-type: none"> <li>• Reduce electric stress on spark heated gas swept downstream</li> </ul>	<ul style="list-style-type: none"> <li>• Flow separation</li> <li>• Unknown holdoff of thermally striated gas</li> </ul>
<u>Downstream Insulators</u>		
<ul style="list-style-type: none"> <li>• Electrode termination</li> <li>• Freestream wedges or honeycomb</li> </ul>	<ul style="list-style-type: none"> <li>• Separate electrode from spark heated gas swept downstream</li> <li>• Break spark heated gas into segments</li> </ul>	<ul style="list-style-type: none"> <li>• Insulator flashover</li> <li>• Flow separation at electrode-insulator joint</li> <li>• Insulator flashover</li> <li>• Insulator heating</li> </ul>
<u>Downstream Injection</u>		
<ul style="list-style-type: none"> <li>• Wall jet of attaching or cooling additives</li> <li>• Free stream jets of liquid droplets for cooling or attachment</li> </ul>	<ul style="list-style-type: none"> <li>• Quench plasma conductivity by attachment</li> <li>• Raise plasma density by cooling</li> </ul>	<ul style="list-style-type: none"> <li>• Remote injectant mixes slowly with free stream gas</li> <li>• Insulator flashover</li> </ul>
<u>Upstream Flow Gradients</u>		
<ul style="list-style-type: none"> <li>• Nonuniform jet velocities</li> <li>• Free stream turbulence</li> </ul>	<ul style="list-style-type: none"> <li>• Displace spark heated gas into separate segments</li> <li>• Increase mixing of spark heated gas with ambient cold gas</li> </ul>	<ul style="list-style-type: none"> <li>• Insulator flashover</li> <li>• Insulator flashover</li> <li>• Small scale turbulence causes slow mixing</li> </ul>

switches was not addressed in this workshop and needs further study.

The use of multichannel sparks to reduce the switch inductance in high PRF switches was considered only briefly in this workshop. Recent developments in multichannel rail-gaps for single pulse and moderate PRF operation (to 100 Hz) at low voltages (to 50 kV) are encouraging.<sup>10</sup> The possibility of extending multichannel operation to high voltage and high PRF with high reliability requires further study. The philosophy adopted by the workshop group is that the solutions found to deal with the high PRF problems of a single spark channel can be applied directly to multichannel operation. This will obviously increase the gas volume flow required to clear all of the spark channels.

i. Electric Field Distortion by Arc Products (W. Moeny) -

The electric field distribution in the gap is related to the conductivity distribution by Laplace's equation

$$\nabla \cdot \sigma \vec{E} = 0$$

where it is assumed that the gas is macroscopically neutral (no space charge) and where  $\sigma$  is the conductivity. The electric field in the gap will be distorted when the hot, conductive column is blown downstream. For high PRF, the field distortion will occur during the recovery phase and can result in pre-fires and reduced recovery rates. Proper management of the fields will partially compensate for the field distortion. Computer models are also available to evaluate the effect of the arc products.

j. Gas Species -

For gas-blown switches, the most important considerations in selecting a gas are the dielectric strength, sonic speed, and the extent to which the gas will react with the switch materials. In a previous section, the relative significance of the sonic speed and dielectric strength were considered.

k. Gas-Handling Configurations (M. Molen) -

The two gas-handling configurations considered are the blow-down tunnel and a continuously-operating closed tunnel driven by a fan. The selection of an appropriate configuration is primarily an engineering decision. Sonic speeds are most easily obtained for short durations using the blow-down tunnel; however, some time delay may be required before the maximum velocity is established. This configuration is primarily applicable to burst modes in which the individual bursts are separated sufficiently in time so that the reservoir can again be recharged.

A closed, recirculating tunnel will perhaps permit the greatest flexibility; however, the system is usually more complex. This configuration removes the restriction on the burst rate; however, a heat exchanger will probably be required to remove heat resulting from frictional losses and the electrical discharge.

### C. RECOMMENDATIONS

After an extensive review of the relevant thermal and gas flow considerations, the group recommended that several topics should be thoroughly studied. These research topics have been grouped into four areas as described below:

#### 1. Electrode Erosion

- a. Conduct further experiments to determine how erosion is affected by flow speed and flow state (e.g. laminar vs. turbulent).
- b. An improved model for electrode erosion and how products are entrained in the gas needs to be developed.

#### 2. Dielectric Properties

- a. Recovery experiments with gas mixtures which have a high breakdown strength and high acoustic speed.
- b. Calculations of the distortion of the electric field in a switch by arc products.

#### 3. Thermal Problems

Evaluate relative significance of various electrode cooling schemes including gas and liquid cooling.

#### 4. Gas Flow

- a. Shock waves - study acoustic waves at high repetition rate and how they may affect gas channel (e.g. wave strength, damping mechanisms and reflections).
- b. Experiments to measure clearing factor for different geometries where flow characteristics are carefully quantified.
- c. Boundary layer considerations
  1. Study effect of turbulence in boundary layer

- to clean-out arc products.
2. Study methods to control boundary layer thickness, mixing, cleanout.
  - d. Upstream methods to break up spark channel
    1. Use of free-stream velocity distributions (non-uniform).
    2. Introduction of free-stream turbulence to disperse arc products.
  - e. Downstream methods to improve recovery
    1. Effects of non-uniform density and temperature levels.
    2. Divergence of gap spacing.
    3. Injection of additives
      - a. Mist spray to cool gas
      - b. Attachers to lower conductivity
    4. Insulator structures placed in gas flow (e.g. wedges) to separate arc column into segments or to cool and quench column.

## D. REFERENCES

1. L. Spitzer, Jr., Physics of Fully Ionized Gases, Interscience Publishers, Inc.: New York, 1956.
2. J. M. Meek and J. D. Craggs, Electrical Breakdown of Gases, John Wiley & Sons: New York, 1978.
3. A. H. Shapiro, The Dynamics and Thermodynamics of Compressible Fluid Flow, Vol. 1, Ronald Press, 1953.
4. J. C. Martin, "Million Volt Repetitive Spark Gaps," Proceedings of the Workshop on Switching Requirements and R & D for Fusion Reactors, EPRI Rept. ER-376-SR, 1976.
5. J. T. Naff, R. J. Sojka, and E. P. Zeehandelaar, "Design and Performance of a High Repetition Rate Spark Gap Switch at 50-kW Power Levels," 14th Pulse Power Modulator Symposium, 1980.
6. W. Kimura and S. Byron, "Flow Technology for High PRF Railgap Switches," MSNW Report 1205, March, 1982.
7. S. Byron, et.al., "Acoustic Wave Attenuation in Pulsed Electric Discharge Lasers," MSNW Report No. 7279-1 (1972).
8. W. J. Thayer III, V. R. Buonadonna, and W. D. Sherman, "Pressure Wave Suppression for a Pulsed Chemical Laser," AIAA Journal 18, 657 (1980).
9. E. L. Klosterman and S. R. Byron, "Electrical and Laser Diagnostics of an 80 kW Supersonic cw CO Electric Laser," J. Appl. Phy. 50, 5168 (1979).
10. D. B. Cohn, W. H. Long, Jr., E. H. Stappaerts, M. J. Plummer, and J. B. West, "Multichannel Switch Triggered by Low-Voltage Auxiliary Discharges," Rev. Sci. Instrum. 53, 253 (1982).

## APPENDIX A

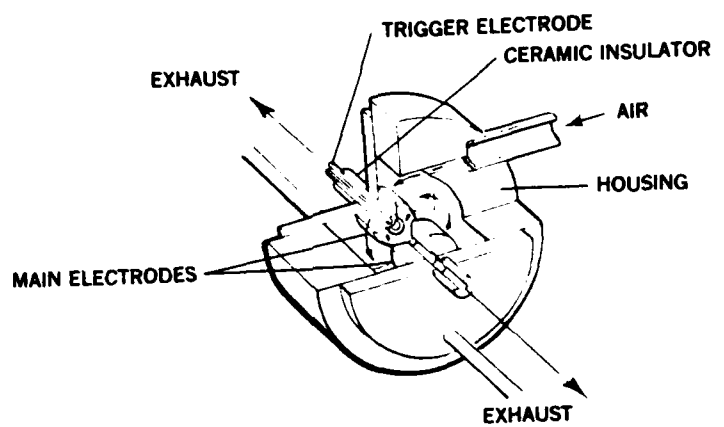
GAS-BLOWN SPARK GAPS FOR  
REPETITIVE PULSE POWER SYSTEMS

G. Rohwein

A growing variety of spark gap switches are being used in repetitive pulse power systems. Their specific design features are primarily influenced by a combination of operational and system requirements. The principal technical factors that must be considered in the design of a spark gap include operating voltage, maximum current, coulomb capacity, maximum pulse repetition rate, duty cycle, lifetime, inductance limitations, configuration constraints, operational stability, and jitter. Any one, or a combination of these factors, can have dominant influence on the design of a given switch. Duty cycle, for example, may in the case of a continuous-operating switch require large-area electrodes and provisions for high-volume gas flow. If the same system were operated in an intermittent burst mode at the same maximum pulse repetition rate, small-area electrodes and little or no gas flow would be required. This is only one example of the many differences that occur in the design of a switch.

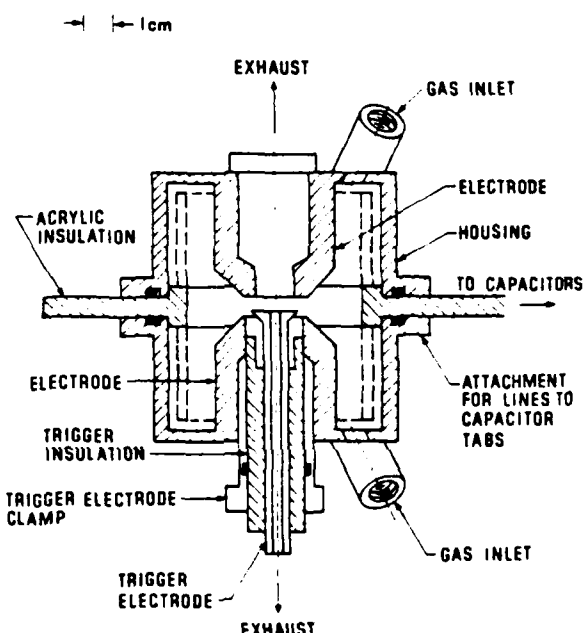
In this appendix a variety of low to high voltage switch designs are illustrated. Salient features are listed but no attempt is made to evaluate the relative merits of the switches.

COMPACT IN-LINE ELECTRODE TRIGATRON GAP<sup>1</sup>  
WITH SLOW VORTEX GAS FLOW



Operating Voltage	50 kV
Peak Current	< 10 kA
PRF	100 pps
Life	$\sim 10^6$ shots
Duty Cycle	continuous

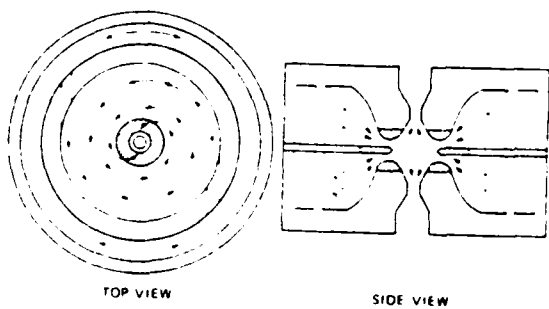
IN-LINE ELECTRODE, TRIGATRON GAP<sup>2</sup>  
 WITH SLOW VORTEX GAS FLOW PATTERN



Schematic cross-section of a Marx switch.

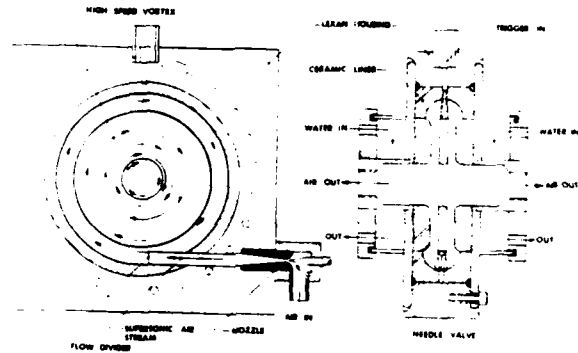
Operating Voltage	100 kV (under oil)
Peak Current	60 kA
PRF	50 pps
Life	< 10 <sup>6</sup> shots
Duty Cycle	intermittent burst

IN-LINE THREE ELECTRODE GAP<sup>3</sup>  
WITH FAST VORTEX GAS FLOW PATTERN



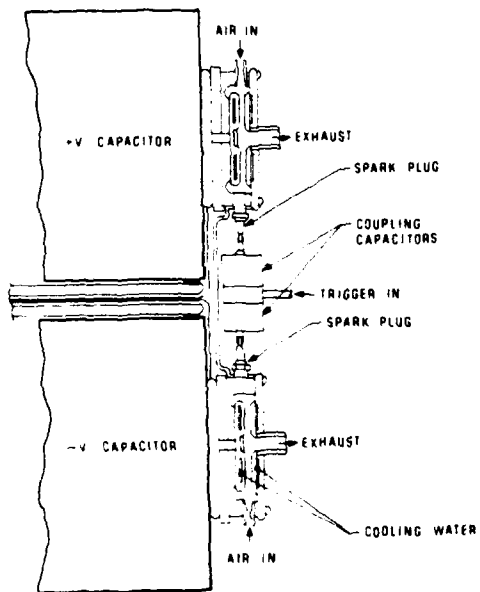
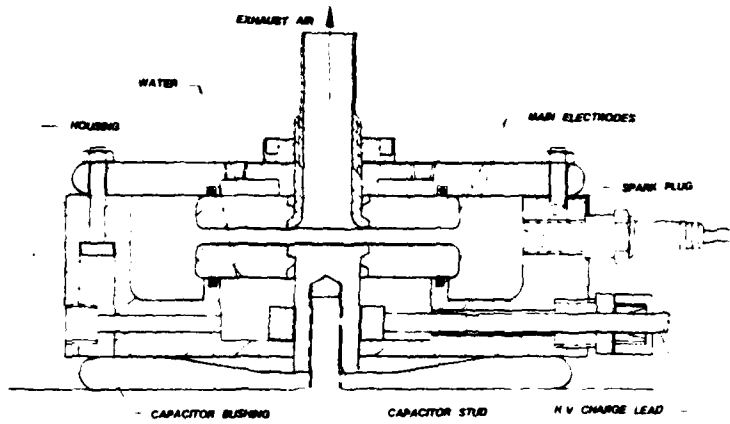
Operating Voltage	50 kV
Peak Current	20 kA
PRF	1000 pps
Life	$10^7$ shots
Duty Cycle	continuous

THREE-ELECTRODE FLAT BUTTON GAP<sup>4</sup>  
WITH FAST VORTEX GAS FLOW PATTERN



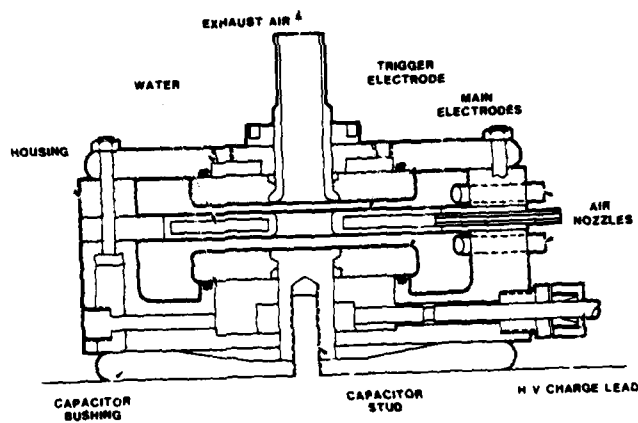
Operating Voltage	60 kV
Peak Current	60 kA
PRF	100 pps
Life	$\sim 10^7$ shots
Duty Cycle	continuous

TWO-ELECTRODE FLAT BUTTON HALF-SWITCH<sup>5</sup>  
 WITH FAST VORTEX GAS FLOW PATTERN



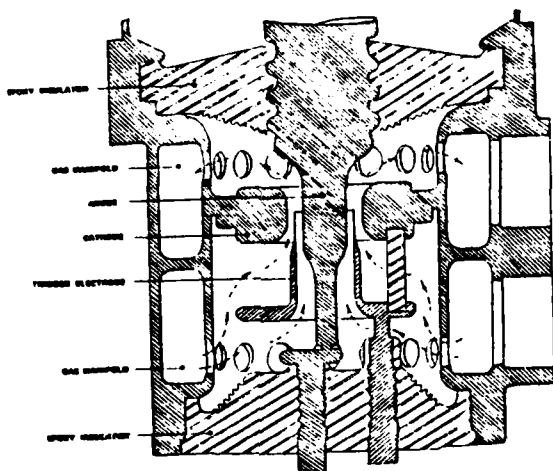
Operating Voltage	40 kV/section
Peak Current	100 kA
PRF	100 pps
Life	$\sim 10^7$ shots
Duty Cycle	continuous

THREE-ELECTRODE FLAT BUTTON GAP<sup>6</sup>  
WITH FAST VORTEX GAS FLOW PATTERN



Operating Voltage	60 kV
Peak Current	100 kA
PRF	100 pps
Life	$\sim 10^7$ shots
Duty Cycle	continuous

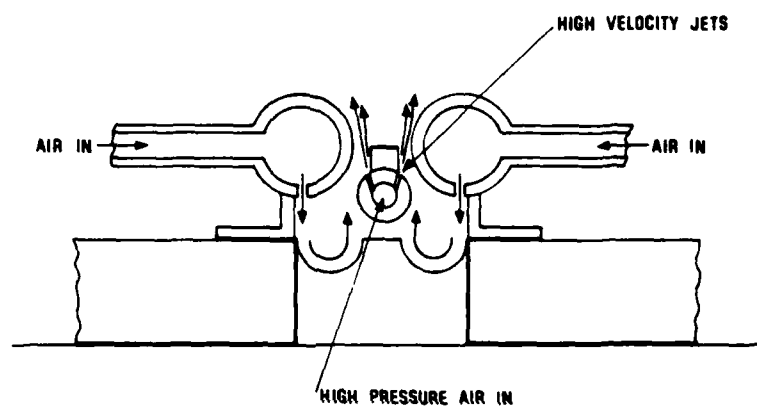
COAXIAL THREE-ELECTRODE GAP<sup>7</sup>  
WITH COAXIAL GAS FLOW PATTERN



Cross section view of coaxial midplane  
spark-gap switch. The dashed line shows  
pattern of gas flow used to cool gap.

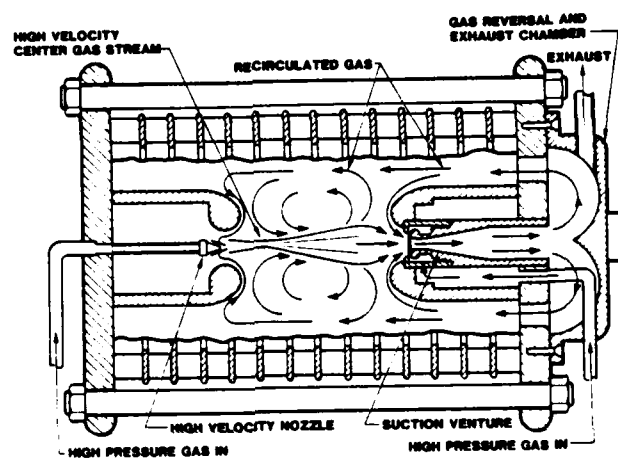
Operating Voltage	250 kV
Peak Current	20 kA
PRF	1000 pps
Life	$\sim 10^7$ shots
Duty Cycle	burst mode

THREE-ELECTRODE RAIL GAP<sup>3</sup>  
WITH LINEAR GAS FLOW PATTERN



Operating Voltage	25 kV
Peak Current	80 kA
PRF	200 pps
Life	$5 \times 10^6$ shots
Duty Cycle	continuous

TWO-ELECTRODE HIGH VOLTAGE GAP<sup>9</sup>  
WITH AXIAL RECIRCULATED GAS FLOW



Operating Voltage	2 MV
Peak Current	100 kA
PRF	100 pps
Life	$\approx 10^7$ shots
Duty Cycle	continuous

## REFERENCES

1. M. T. Buttram and G. J. Rohwein, "Operation of a 300 kV, 100 Hz, 30 kW Average Power Pulser," Proc. IEEE Thirteenth Pulse Power Modulator Symposium, Buffalo, NY, June 20-22, 1978, pp. 303-308.
2. M. T. Buttram, "Development of a 50 Hz, 250 kV, 500 ns, 500 kW Average Power Pulser," Proc. IEEE Fourteenth Pulse Power Modulator Symposium, Orlando, FL, June 3-5, 1980, pp. 195-200.
3. J. T. Naff, R. Sojka, E. P. Zeehandeloor, "Design and Performance of A High Repetition Rate Spark Gap Switch at 50 kW Power Levels," Proc. IEEE Fourteenth Pulse Power Modulation Symposium, Orlando, FL, June 3-5, 1980, pp. 21-24.
4. W. J. Sarjeant and G. J. Rohwein, "Critical Pulse Power Components," Proc. Sixteenth IECEC Conference, Atlanta, GA, August 9-14, 1981, pp. 161-175, Vol I.
5. G. J. Rohwein, "A Low Jitter Spark Gap Switch for Repetitively Pulsed Parallel Capacitor Banks," Proc. IEEE Fourteenth Pulse Power Modulator Symposium, Orlando, FL, June 3-5, 1980, p. 1-4.
6. G. J. Rohwein, K. R. Prestwich, SAND83-0106, "Conceptual Design of a Compact Microwave Modulator," (Albuquerque: Sandia National Laboratories, February, 1980).
7. H. B. McFarlane and R. Kihara, "The F x R One-Nanosecond-Jitter Switch," Proc. IEEE Fourteenth Pulse Power Modulator Symposium, Orlando, FL, June 3-5, 1980, pp. 9-11.
8. M. T. Buttram and G. J. Rohwein, "Operation of a 300 kV, 100 Hz, 30 kW Average Power Pulser," Proc. IEEE Thirteenth Pulse Power Modulator Symposium, Buffalo, NY, June 20-22, 1978, pp. 303-308.
9. G. J. Rohwein, "High Voltage Spark Gap," (unpublished) Albuquerque: Sandia National Laboratories, 1980.

## ENGINEERING IMPLICATIONS

M. Buttram - Chairman

## A. INTRODUCTION

Spark gaps have achieved a prominent position as laboratory switches where high powers and energies are involved. They are rugged, relatively reliable, inexpensive, and easy to fabricate. Paradoxically, they have not been a great success outside the laboratory, largely because they are not quite rugged enough (they wear out), they are generally not quite reliable enough, and techniques to make them reliable can be rather costly. The key philosophical point of the Repetitive Spark Gap Workshop is that repetitive spark gaps can and should be "productized" for non-laboratory applications. The goal of the workshop is to identify ways to improve the performance of spark gaps so that they can move out of the laboratory. The obvious contributions to be made by the Engineering Implications Group are:

- (1) To identify ways to improve the performance of spark gaps, realizing that the range of projected uses can not be decoupled from reliability and versatility that can be engineered into the spark gaps themselves.
- (2) To assess the state-of-the-art in spark gap development and project where the development of spark gap switches may go.

(3) To identify research needed to make meaningful improvements in spark gaps. Items 1 and 3 of these issues will be discussed in the material to follow. Item 2 will be discussed elsewhere in the workshop's proceedings.

#### B. WHERE ARE HIGH PRESSURE GAS SPARK GAPS REQUIRED

The role of spark gaps in repetitive pulsed power systems will ultimately be determined by what is required (funded) and by the competitiveness of spark gaps when compared to alternative switching schemes. A variety of switches are needed in virtually every pulsed power system, starting with control of the power source. In the past the power source has almost always been a DC power supply operating at less than 100 kV. This will probably change as rapidly discharging rotating machinery becomes available. Probably the typical power source voltage will not increase beyond 100 kV, however. The power level is raised by some number of pulse-time compression stages, each with appropriate switching, then the power is delivered in a specified form to the load. Voltage amplification may have occurred, somewhere in the microsecond regime, typically. Historically spark gaps have on occasion been used at each stage of this pulse compression cycle but clearly there are better options in some cases. A comparison of the options available for each stage of the pulse compression is one way to estimate where spark gaps are really needed.

First, the initial energy store must be charged. It is best if this is done, on command, if and only if it is desired to initiate a pulse compression sequence. DC charging or a charge and hold cycle followed by a long swell time unnecessarily

stresses the first energy storage component, which is undesirable. This initial power conditioning probably is best done with semiconductors. A kilovolt, kiloamp SCR conducting for one millisecond can transfer nearly a kilojoule, allowing rather high average power to be achieved with a few long lived, relatively reliable components. Junction semiconductors do not maintain this competitive advantage at later stages in the compression cycle. The same kilovolt, kiloamp SCR if it could be triggered in a microsecond could only pass one joule. As a result, the number of components escalates to a level that is probably prohibitive. Although SCR's used in series-parallel combinations could conceivably be useful for microsecond type pulses, particularly at modest energy levels and high repetition rates, few pulsed power systems have attempted to use their characteristics due to lack of engineering data on their  $dI/dt$  and peak current performance. Also, in some applications (10-50 kV) in this pulse regime thyratrons can reliably achieve the same performance as a bank of SCR's and a pulse transformer.

Skipping over the microsecond regime, briefly, leads to the nanosecond time scale where peak power has escalated into the range from gigawatts to perhaps many terrawatts. Voltages may be in the megavolt regime and  $dI/dt$  (and inductance) dominate the design problem. Thyratrons are useful at low voltages (<100 kV) but become progressively suspect at higher voltages. Rates to tens of kilohertz are achievable with them. At higher voltages spark gaps are useful for low rates (< 1 kHz), and saturable

inductors have been demonstrated to 500 kV and probably will work to higher voltage. Light activated bulk semiconductors and glow discharges are candidates being evaluated. Both are conceptually compatible with high voltage and high repetition rate. Neither is burdened with the overhead of experimentally determined limitations that characterize their better understood competitors. Magnetic switches are perceived to have a competitive advantage in this time regime because they are essentially rate insensitive and robust. They do lack triggerability and operating voltage range, and they are limited to time compressions of near a factor of three per stage. In addition, they are bulky, heavy, and expensive. Any of these limitations might disqualify magnetics for certain applications. Typically, the next alternative is a spark gap.

Finally there is the intermediate, "microsecond" regime, three orders of magnitude (or more) of time compression between the initial charging and the high-power nanosecond regime. As previously pointed out, semiconductors are probably not interesting here. Magnetic compression over three orders of magnitude at factors of 3 to 5 per stage is undesirable. Glow discharge switches have an arc down problem: they turn into spark gaps. Light activated bulk semiconductor might work but there are issues of overheating and thermal runaway. The leading candidates are the discharge devices, thyratrons, ignitrons, vacuum, and high-pressure spark gaps. All are competitive at low voltage, repetition rate, and average power. Generally, the

high-pressure spark gap is the simplest, sturdiest, least expensive option when it can be used. The low-pressure devices tend to be attractive at high repetition rates. The high-pressure spark gap dominates at high voltage and high power. For high voltage and high repetition rate service, low-pressure switches may be necessary.

This is summarized in Table 1. To recapitulate regarding high-pressure spark gaps; they have a dominant position in the microsecond regime, which could be greatly enhanced by improving their repetition rate limits. Spark gaps are also useful in the nanosecond regime, their primary deficiencies there being repetition rate limitations and reliability. Spark gaps are still the most versatile pulsed power switch.

Table 1    Switches Applicable to Various Time Regimes

<u>msec</u>	<u>μsec</u>	<u>nsec</u>
junction semiconductors	high-pressure spark gaps	saturable inductors
thyatrons	thyatrons	spark gaps
ignitrons	vacuum switches	glow discharge switches
spark gaps		light activated bulk semiconductors

## C. WHAT IS THE POTENTIAL FOR SPARK GAPS?

Table 2 is a listing of some parameters affecting spark gap operation. It is probably not complete and the parameters are clearly not independent. The table serves to give a feeling for the dimensionality of the space within which the spark gap designer must work. Such a large number of parameters can give the spark gap designer a bit of latitude in developing a design but it can also hide the constraints of a gap operation due to the multitude of parameter interactions. The parameters have been grouped into dependent and independent ones by somewhat arbitrarily assigning those parameters that are particularly associated with repetitive operation to the dependent class. A typical design sequence begins with the specification parameters being given, which somewhat constrains the range of design parameters available. What freedom is left is used to achieve the repetition rate, lifetime and reliability levels required. Subsequent sections will consider these three dependent parameters.

Table 2 Spark Gap Parameters

<u>Dependent Parameters</u>	<u>Independent Parameters</u>	
		<u>Specification Parameters      Design Parameters</u>
Rep Rate	Voltage	Trigger
Lifetime	Jitter (Time and Voltage)	Gas
Reliability	dI/dt (initial)	Electrode Material
Average Power	I(t)	Flow Pattern
Duty Cycle	Energy Per Pulse	Flow Volume
	Pulse Length	Sonic/Subsonic Flow
		Pressure
		Gap Spacing
		Geometry
		Electrode Cooling
		Insulator Material

Repetition Rate

In the high power spark regime for a two-pulse experiment<sup>1,2,3</sup>, spark gaps recover within about 20 ms, rather independent of current, voltage, electrode material, or gas. The only limitation is that the pulse length be in the few microsecond range. Longer (ms) pulses presumably heat the electrodes sufficiently that they keep the gas hot and diffuse after the pulse is over<sup>3</sup>. This recovery becomes even better at low current (<<1 kA) but the higher currents, being the subject of this workshop, are of greater interest. This suggests, but does not prove, that for continuous pulsing the cooling (gas flow) required to reach a given repetition rate is controlled more by voltage than peak current. The argument goes as follows. The effect of current on the post-discharge recovery rate of the spark gap is the same whether the gap is continuously pulsed or only pulsed twice. Thus current is not a factor. The voltage, however, controls the Pd (pressure x gap spacing) for the gap. Pd, together with the repetition rate determines the gas flow requirements. To illustrate the model, Fig. 1 can be used to derive the relationship. The voltage V is assumed, giving a specific Pd. The active electrode area is assumed to be a circle of radius d to minimize field enhancements on the electrode tips. The volume of stressed gas is  $\sim d^3$ . Assuming that for proper recovery this volume needs to be flushed N times between pulses gives a flow rate (in SCFM) of

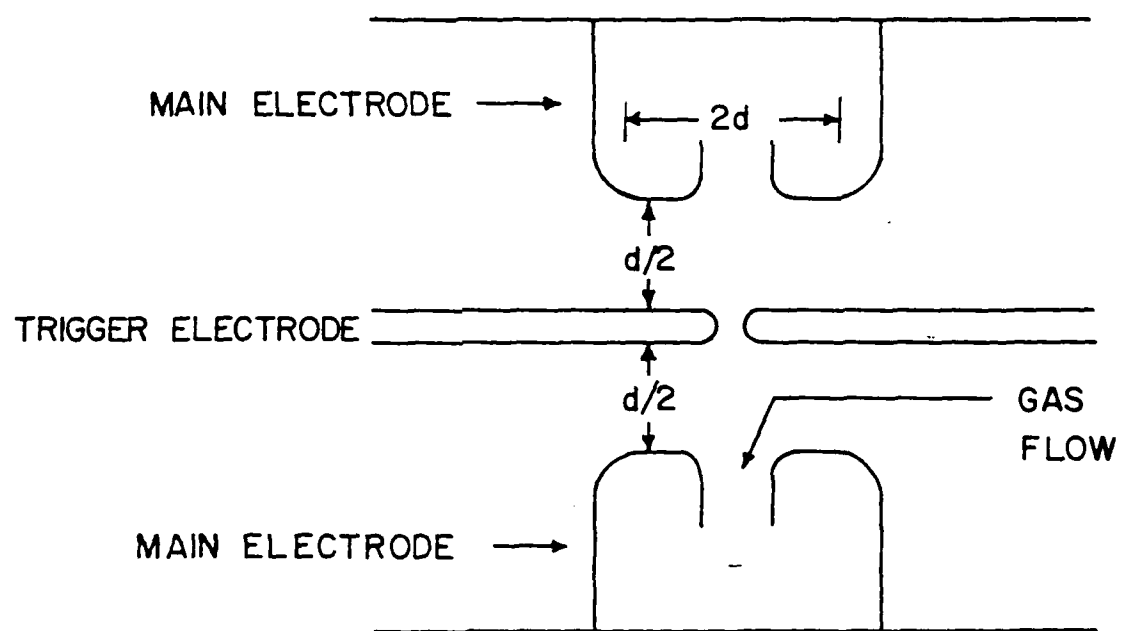


Fig. 1 Geometry of a simple spark gap used to model the recovery process

$$\text{Flow} = \frac{\text{Volume} \times N \times P}{\text{time between pulses}}$$

$$= (d^3) \times N \times P \times \text{Rep-rate}$$

$$\propto (d^2 \times \text{voltage} \times \text{Rep-rate})$$

High pressure and small spacing seem to be in order up to the point that they start to create reliability problems (High pressure and small d apparently aggravate the tendency of spark gaps to prefire independent of repetition rate<sup>4</sup>). Attempts to reduce the flow by reducing d could well be stifled by the inability to force the required gas volume through the small gap. Current data would indicate a proportionality constant

$$\frac{\text{SCFM}}{\text{cm}^2 \text{kV-Hz}} \text{ in the } 10^{-3} \text{ to } 10^{-4} \text{ range.}$$

This is perhaps the simplest conceivable model of recovery. It's validity is untested and surely can be improved upon. But it allows predictions of the performance of an arbitrary switch scaled from one data point. Even a crude model is valuable, for with it improvements in flow pattern, flow speed, electrode cooling, geometry, etc., can be more easily compared to previous results. Measurements of the proportionality constant and indeed of the real dependence of repetition rate upon the design and specification parameters is needed.

Three important issues need to be considered at this point. First there is a lot of point data, i.e., geometries, flow rates, etc., that permit operation at a specific voltage, average power, and repetition rate, but the actual parametric behavior of spark gaps is almost universally a mystery. For example, if a 250 kV certified spark gap needs to be upgraded to 350 kV, what incremental gas flow rate is required at a given repetition rate? Flow rate requirements ought to scale with voltage, but to what power? The Engineering Implications Group strongly supports experiments to determine such parametric behavior, together with theoretical modeling to tie the data together and facilitate extrapolation. Furthermore, it was felt that a frequently updated compilation of spark gap data ought to be developed.

Second, the discussion to this point tends to imply that gas purging is the only solution to spark gap recovery. Historically, purging has received all the attention, but as it becomes impractical at higher repetition rates other schemes may finally be cultivated. Other options have been offered. Breakdown dominated by formation time effects has been shown<sup>6</sup> to recover at a kilohertz in two-pulse experiments, without the need for purging. Heat removal by phase change from aerosols in the gas could be useful. If spark gaps could be engineered to operate at high temperatures where the arc channel heating represents a smaller deviation from the ambient conditions, perhaps recovery could be enhanced. These alternatives should be investigated.

Third, it is necessary to address the questions of how the dependence of "maximum allowable repetition rate" upon some parameter might be defined. Typically a gap is built together with a suitable trigger system and gas flow or other design parameters are varied until some degree of stability, say 1% prefires, is achieved. This is not really sufficient data. If a geometrically equivalent gap needs to be operated at 50% higher voltage and 0.01% prefires, there is no way to extrapolate to the required design parameters.

A suggested solution would be to measure the self-breakdown distribution of the test spark gap at very low rate and to repeat the measurement at high rate as a function of gas flow. The difference between the two distributions would be a measure of the lack of proper recovery. The mean breakdown, standard deviation, asymmetry moment (third moment or skew) and perhaps the absolute lowest self-firing voltage might be used to compare these distributions. Data exist at low rates (< 10 Hz) which are of the general form of Fig. 2. These data might be appropriate for two hemispherical electrodes (brass or graphite), 1 cm apart in air or SF<sub>6</sub>, with 100 kA, 100 kV discharges. If the low repetition rates distribution can be reestablished at high repetition rates by purging, one might legitimately regard the gap as having been operated successfully at that rate. When, at a given rate, it is no longer possible to restore the voltage

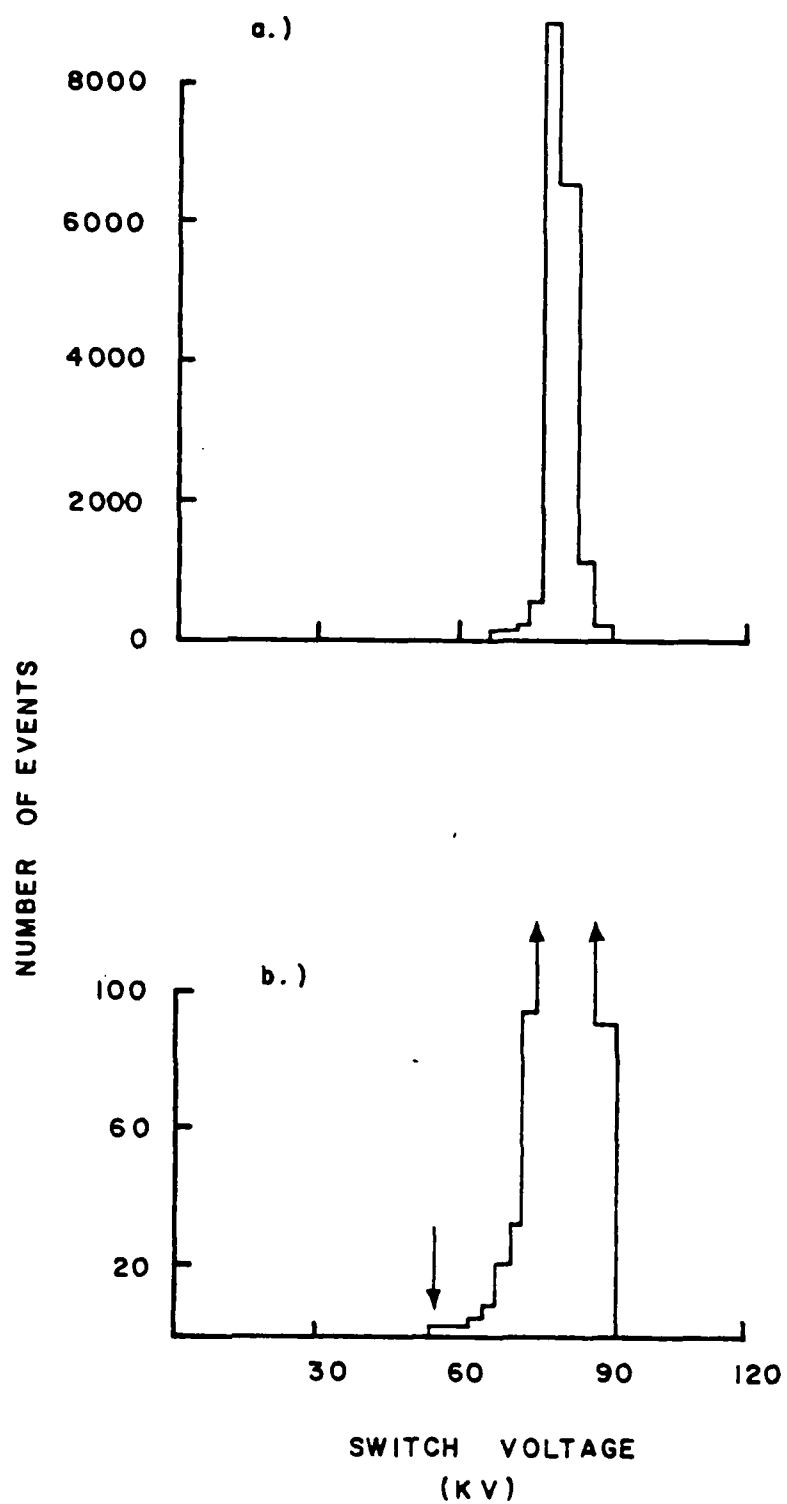


Fig. 2 Spectrum of self-breakdowns of two-electrode spark gap illustrating the low voltage "tail"

distribution by an achievable gas flow the gap is at least questionable for use at that rate. If there is still a well-defined lowest breakdown voltage and if the gap can be triggered at even lower voltage, operation at, or above, that rate might well be possible.

The foregoing is a reasonable test for self-breaking gaps and those without field distortion triggers. If a given gap, when triggered, breaks down over a smaller electrode area than would be sparked to in a self-break test, that reduced area might lead to thermal problems before the larger area self-break tests show difficulties. In that case a different type of experiment would be required. It is suggested that two parallel generators be used to drive the gap. One would charge the gap at the desired rate. Once charged, the spark gap would be triggered. Every Nth shot would be untriggered. A second generator would then charge the gap to a voltage sufficient for self-firing. The distribution of those self-firings would be compared to the equivalent distribution for firings at low rate. Equivalence, within specified limits, would be the signature of proper spark gap recovery at the rate under test.

These particular experiments seem reasonable although they are probably not unique and there may be better options. The primary goal at point is to emphasize the need for some standardized experiments to explore the parameters affecting

spark gap recovery. The experiments need to be done at high power because that is the frontier of the field. It is desirable that the experiments be limited by the spark gap parameters and not by power supply availability, load capacity, trigger capacity, or gas capacity else the intrinsic switch parameters will never be determined. Unfortunately, the facilities for this type of testing tend to exist only in the larger, very highly program (device) oriented DoE and DoD laboratories, whereas the interest in performing exhaustive tests lies largely with the university community. A proper matching of capital resources and manpower ought to be a priority of the funding agencies.

#### Lifetime

The lifetime of spark gaps is dominated by damage done to the electrodes by the spark discharge. This is not said to exclude the possibility of failures of the insulator due to hot gas, UV, or heating from the electrodes. The point to be made is that the electrodes must be damaged in order to strike a spark, whereas a variety of techniques exist to protect the insulator. Specifically, the insulator may be protected by gas flow, geometrical isolation, and electrode cooling, among other options. Also, more robust materials than the plastics currently in common use are available, e.g., ceramics.

Electrode damage can be catastrophic or gradual. Catastrophic damage would include fracturing or any other macroscopic damage. An example would be the production of large surface projections. The limits at which catastrophic failure occur are not well known for single shot applications, let alone in repetitive service.

Erosion, the gradual wearing away of electrode material, is far more likely to trouble the designer of long-lived spark gaps than is catastrophic failure. Erosion limits the utility of field enhanced trigger electrodes, as the characteristic sharp edges are generally eroded away early in the life of the switch. A long-lived switch should be designed so that its electrodes erode away uniformly over a maximum of area.

Erosion is extremely difficult to quantify. Fortunately, it is often possible to design conservatively, thereby eliminating the need for accurate erosion data. For microsecond spark gaps, erosion is generally within a factor of 2 of 50 micrograms per Coulomb of charge. For nanosecond pulses the erosion rate is generally an order of magnitude greater. High gas flow rate and/or repetition rate seem to aggravate erosion. In the microsecond pulse regime where inductance is less of a problem, it is possible to design spark gap electrodes with larger cross-sectional areas to extend the life of these devices.

Reliability

Reliability is hard to quantify. It can be limited by triggering problems. For one application the fact that a switch fires each time it is triggered may be sufficient. In another application a switch may be deemed unreliable if its jitter is greater than 10 ns. Reliability also may be compromised by prefiring. Prefiring can result from electrode damage due to previous sparking, foreign matter in the gap (particles), gas contamination, heating (incomplete purging, etc.). Typical multiple, DC charged spark gap systems are operated below 60% of selfbreak to minimize prefires. A further reduction with respect to self-break might be required for incompletely recovered repetitive gaps. Unfortunately, spark gaps operated far from self-break are hard to trigger. This problem can be partially overcome at low voltage (less than a few hundred kilovolts) by use of a fast rising trigger voltage pulse with an amplitude well in excess of the switched voltage. Unfortunately, this technique becomes unattractive for megavolt switches. Something like laser triggering may be required.

For any given switch the problem of prefiring can be reduced by pulse-charging it as quickly as possible. This may only transfer the problem to earlier switches in the pulse compression chain, however. To reduce simultaneously the effect of not-too-early prefires and of jitter ("synchronized" switches) the

output of the switches can sometimes be linked by a common saturating core. All switches which have fired prior to saturation of the core will then produce synchronized outputs. Engineering systems to tolerate the properties of spark gaps rather than attempting to engineer all the problems out of the spark gaps themselves represents a reasonable design alternative.

#### D. CONCLUSIONS AND RECOMMENDATIONS

The Engineering Implications Group attempted to assess the need for spark gaps in repetitive pulsed power and to review the major design problems. Need is determined by the requirements of systems to be developed and by competition among the various types of switches available. A clear need was identified for microsecond switching. In nanosecond times there may be better options if cost, volume, and weight are not prime considerations. On the whole, spark gaps are still the most versatile of pulsed power switches and the engineering of repetitive spark gaps to commercially competitive levels of reliability and life time is crucial to the future of repetitive pulsed power.

There are many successful repetitive spark gaps but very little design data by which the design of spark gaps to meet new requirements can be extrapolated from current designs. "Standardized" experiments are needed to supply parametric variation data. Models ought to be developed to correlate the results. The experiments should be conducted on facilities where the results will not be limited by the available power supply, gas supply, trigger, etc. Alternatives to gas purging for spark gap quenching ought to be seriously investigated. The need for a broadly based central compilation of data relevant to spark gap design was emphasized.

The Engineering Implications Group was composed largely of people concerned with the design and use of repetitive spark gaps in a laboratory environment within the framework of DoD and DOE programs. This inevitably affected the conclusions drawn. The question of why repetitive spark gaps have never been commercially accepted was addressed but not really answered. Probably this was not the proper group of people to answer that question. Yet the answer is vital because the real future of repetitive spark gaps probably will be determined by the perception of the prospects for their commercialization or "weaponization".

References

1. G. McCann and J. Clark, AIEE Transactions, Vol. 62, p. 45, 1943.
2. R. Churchill, A. Parker, and V. Craggs, Journal of Electronics and Control, Vol. 11, p. 17, 1961.
3. H. Edels, D. Whittaker, K. Evans, and A. Shaw, Proc. IEEE, Vol. 112, p 2343, 1965.
4. T. Nitta, N. Yamada, Y. Fujiwana, IEEE PES Summer Meeting and EHV/UHV Conference, Vancouver, B.C., Canada, 1973.
5. V. Avrutskii, G. Goucharenko, E. Prokhorov, Sov. Phys. Tech. Phys., Vol. 18, p. 386, 1973.
6. M. Buttram, to appear in Proc. 4th IEEE Pulsed Power Conference, Albuquerque, NM, June 1983.

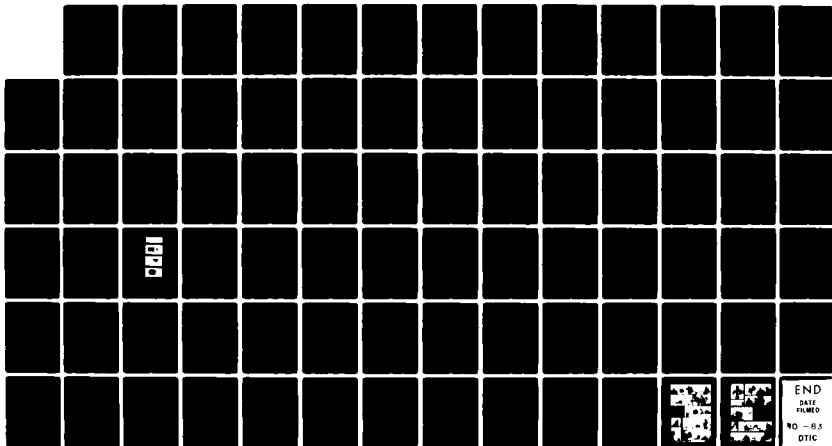
AD-A132 688 WORKSHOP ON REPETITIVE SPARK GAP OPERATION HELD AT  
TAMARRON COLORADO ON JANUARY 17-19 1983(U) BATTELLE  
COLUMBUS LABS DURHAM NC M O HAGLER ET AL. 20 MAY 83

UNCLASSIFIED DAAG29-81-D-0100

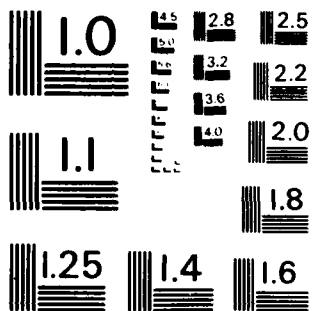
4/4

F/G 9/1

NL



END  
PRINTED  
FIMED  
NO - 85  
DTIC



MICROCOPY RESOLUTION TEST CHART  
NATIONAL BUREAU OF STANDARDS - 1963 - A

## MATERIALS AND CHEMISTRY

L. Hatfield - Chairman  
L. Gordon- Co-Chairman

M. Biondi	J. Marx
L. Christophorou	J. Mote
J. Ewing	L. Murr
J. Gustafson	E. Pfender
E. Kunhardt	P. Predecki

## A. Introduction

The group objectives were first of all to determine whether or not the entire parameter range for rep-rated spark gaps could be accommodated with known materials for electrodes and insulators. Second, are there certain properties of materials that might lead either to some fundamental limitation or to an improvement in rep-rated spark gap operation? The third objective was to attempt to understand synergistic system limitations, the system being the filler gas, the electrode material, and the insulator material.

## B. Organization

The discussion of materials divides naturally into two groups, gases and solid materials for electrodes and insulators. Chemistry problems arise when the three materials interact after passage of current through the gap. Therefore, after independent discussions of the two groups of materials the compatibility of the filler gas, the electrode material, and the insulator must be considered. This was the approach adopted by the group; two subgroups holding separate meetings on the two kinds of materials, later meeting together to discuss the synergistics.

**A. Gases**

Some of the required properties of the filling gas depend on the mode of operation of the repetitive switch. If the discharge in the gas is diffuse (either high or low pressure) then the recommendations of the Workshop on Diffuse Discharge Opening Switches apply and it is not appropriate to reconsider these here [1].

If the switch is to operate in the spark or arc mode, the recommendations are different. In the diffuse discharge mode, recombination and attachment play important roles in the rate of recovery of the dielectric strength of the gas. In the arc mode, the consensus is that the low density channel left after the arc is extinguished will determine the dielectric strength. Even if all charge carriers are removed through recombination and attachment, the low density channel must be dissipated or transported out of the high electric field region before the dielectric strength can recover. Therefore, in the discussion of the desired properties of the filling gas, it is assumed that the gas will be flowing rather than static.

The following list of desired properties of the filling gas is not prioritized. There are so many trade-off between properties that prioritization depends heavily on the particular application.

- Dielectric strength

High dielectric strength reduces the overall size of the spark gap, the amount of gas required, and the gas pressure required to stand off a particular voltage. These factors are related to characteristics such as inductance, cost of operation, and required strength of the pressure vessel, respectively. The dielectric strength should be measured during repetitive operation. Discounting the first few shots which occur in cold gas, the dielectric strength should be

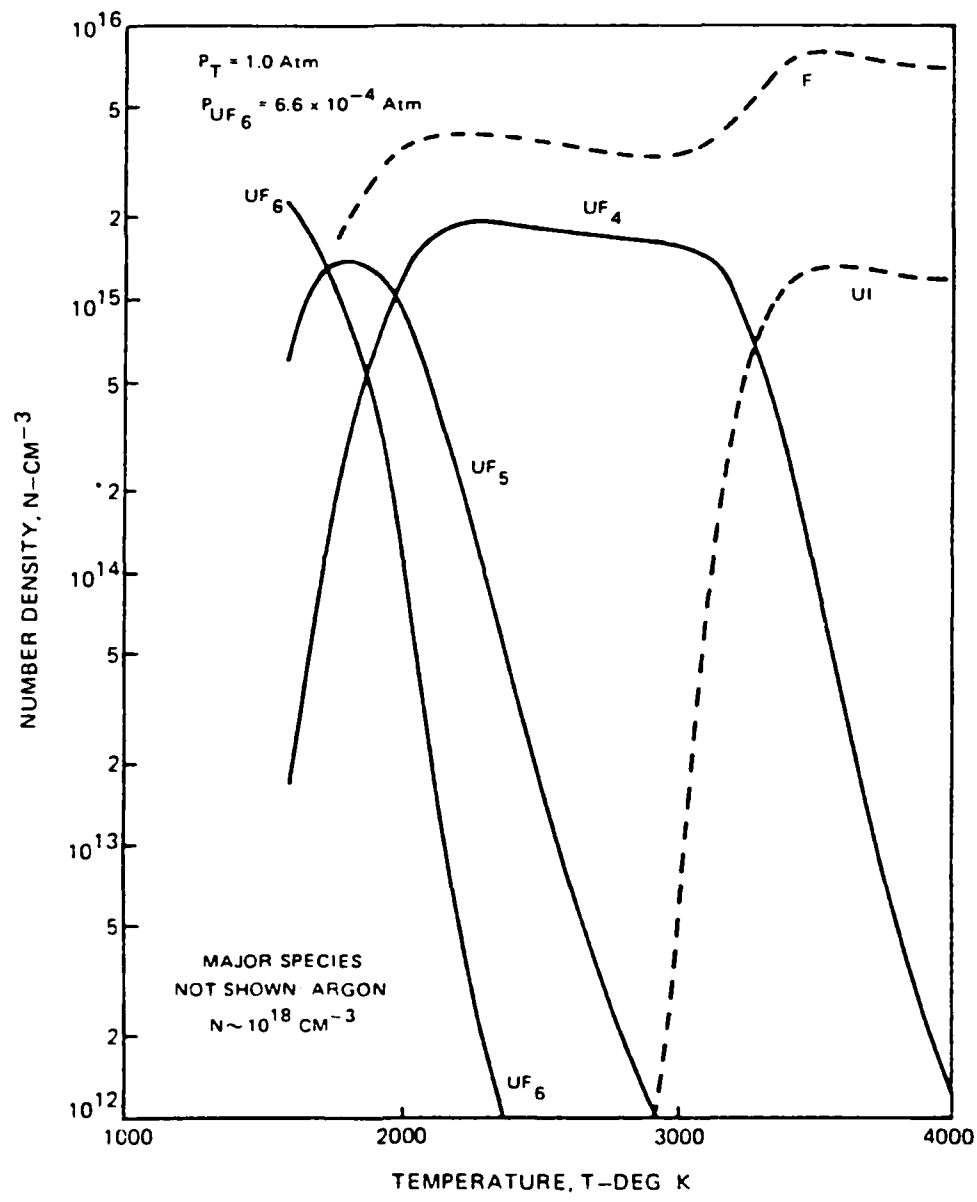


Fig. 1 COMPOSITION OF  $UF_6$ /ARGON MIXTURE AS A FUNCTION OF TEMPERATURE

measured in terms of the number of shots per unit volume required to reduce the strength by some factor. It should also be measured at the operating temperature of the gap since gas mixtures containing large molecules may exhibit significant decomposition. Figure 1 shows how  $\text{UF}_6$  decomposes as a function of temperature [2].

- Conductivity

High conductivity of the arc or plasma reduces electrical losses in the switch, which in turn lowers the gas temperature. The conductivity can be a function of the gas mixture, for example, attaching gases lower the conductivity in some cases.

- Recovery Rate

Thermal and hydrodynamic properties were not discussed by this group. The amount of energy radiated by the gas could be important in cooling. In someflowing systems attachment could be important. An example is a system in which an attaching gas is titrated into the dissipating arc channel remnant.

- Dissociation products

A gas mixture containing an attaching gas and/or a high conductivity gas, such as  $\text{C}_3\text{F}_8$  will dissociate in the arc [3]. The dissociation products could lower the dielectric strength of the mixture or be chemically reactive with other materials in the switch. These problems are exacerbated by the possibility of high gas temperatures.

- Deleterious effects on electrodes and insulators

The filling gas and the discharge products of the filling gas should not lead to chemical attack on the electrodes or insulators which would degrade the electrical characteristics of the gap. Some chemical reactions can be desirable. An example is the use of air with graphite electrodes. The oxygen combines with the carbon vapor and prevents carbon deposits on the insulator [4].

- Fast breakdown to arc mode

The formative time of the arc and the jitter in a triggered sparkgap depend on the glow to arc transition in the gas. A desirable filling gas would have a short formative time, leading to low jitter. The properties of the gas which affect this are not well understood.

- Cost

The cost per shot of the filling gas should be as low as possible. "Cost" should include the transportation and handling of the gas as well as the dollar value of the gas itself. A gas that is recirculated might be less costly than one which must be discarded even though the latter has a lower dollar value per unit volume. Also, an expensive gas should not be ruled out if it represents only a small fraction of the gas mixture.

#### B. Electrodes

The selection of materials for electrodes and insulators depends on the mode of operation of the switch, diffuse or arc mode, and the range of switch parameters to be covered. In particular, the maximum current density at the electrode surface and the mechanical shock generated may dictate the maximum erosion rate and minimum strength of material required, respectively. In the case of insulators used as pressure vessels, the gas pressure, which depends on the hold-off voltage required, may determine the minimum strength of materials. In addition, the gas circulation pattern in the switch could determine thermal properties of the insulator such as the melting point.

The following is a list of parameters suitable for determining the relative merits of a material to be used as an electrode. No priority is intended since that depends on the set of switch parameters to be satisfied.

- High thermal and electrical conductivity

Obviously, high electrical conductivity reduces losses in the switch. High thermal conductivity may be required for water cooling of electrodes.

- Low erosion rate

In a repetitive switch the erosion rate must be low enough to allow a reasonable number of shots before the electrical characteristics of the switch are degraded. However, automatic advance of the cathode or gas pressure adjustment could keep the breakdown voltage constant. Unfortunately, erosion has other implications, such as the amount of electrode material injected into the gap and changes in the electrode geometry and surface topography. There does not seem to be a good model for electrode erosion, which makes it difficult to decide which materials properties are important in erosion [5].

- Mechanical properties

Properties such as hardness, ductility, and fracture toughness are important considerations for machinability, ability to make electrical connections, and resistance to mechanical shock in the spark gap. Although these properties are known for most materials at ordinary temperatures, most are not known for the very high temperatures existing at the electrode surface during an arc. Progress in understanding of erosion processes may ultimately depend on data for these materials properties at high temperatures.

- Ejecta

Electrode material is injected into the gap as the electrode erodes. Ideally, these ejecta should not degrade the electrical properties of the filler gas and insulator. Benign ejecta would be those which have little effect on the gas and insulator, or improve their properties, or are removed (by gas flow, for example) before doing any harm.

- Metallurgy

The metallurgy of the electrode material determines changes in the surface topography and the chemistry occurring in the switch. Dendrites growing on the surface are clearly undesirable. Brass is an example of a material with the wrong metallurgy because the components of the alloy segregate at high temperatures. This leads to dendrite growth and widely different behavior under different conditions [4][6]. The chemistry occurring at the electrode surface may be important in the erosion rate.

- Compatibility with insulators and gases

This parameter includes chemistry in the arc, microparticle production rate and size (which may damage insulation), and such things as the nature of deposits formed on the insulator surface.

### C. Insulators

The following list of properties of materials to be used as insulators is not prioritized. The weight to be assigned to each property depends on the particular application. In a switch requiring high gas pressure, for example, the mechanical strength of the insulating material might be more important than surface resistivity.

- High standoff voltage

This is an obvious requirement. High standoff voltage (resistance to surface flashover) reduces the length of the switch and perhaps the diameter also, thereby reducing the inductance.

- Degradation rate

The rate at which the surface and bulk properties of the insulator degrade determines the lifetime or number of shots before replacement. Degradation of the electrical or mechanical properties can be caused by chemical reactions at the surface, UV radiation from the arc, and mechanical shock. In polymers, UV radiation combined with mechanical shock has been shown to be detrimental [7].

- Mechanical

The compressional strength, resistance to mechanical shock, and tendency for plastic flow are important for insulators which must also provide high pressure gas containment. Another mechanical property of importance is whether or not molten drops of ejected electrode material stick to the surface, and the nature of surface films of electrode material deposited from vapor. On some materials surface films are discontinuous and the surface resistivity is higher than it would be for a continuous film.

- Thermal

The melting or softening point of the material must be high enough for the operating temperature of the switch. Thermal expansion and resistance to thermal shock and thermal cycling are important in the lifetime of the material.

- Surface properties

Surface resistivity and resistance to the formation of surface tracks are important. A material with low surface resistivity may heat up when high voltage is applied to the switch. Surface resistivity plays some role in the surface flashover potential of a material and it is not clear that the highest surface resistivity gives the best results [8]. There is clearly a connection between the tracking on a surface and the gas in which the tracking discharge occurs. The thrust of investigations of tracking should be to find out enough about the processes to avoid tracking altogether.

- Compatibility with electrodes and gases

Materials that have components which react with electrode vapor or dissociation products of the gas should be avoided. An example of a compatible system would be a fluorinated polymer used with a gas containing fluorine as a dissociation product.

#### D. Synergistics of the system

The materials problem in a spark gap is complicated by the large number of chemical reactions and mechanical phenomena possible. The arc discharge produces high current densities on the electrode surface, high temperatures in the plasma, large mechanical and thermal shocks, and a broad spectrum of radiation. If the switch is operated in the diffuse discharge mode (high or low pressure), the plasma temperature is lower, current densities are lower, and mechanical and thermal shocks may be lower in amplitude. However, the plasma may be closer to the insulator, the radiation flux at the insulator may be higher (depending on the absorption length), and a larger percentage of the filler gas may participate in the chemistry. It is not clear that the materials problem is less difficult in a diffuse discharge switch. It is likely, however, that the various processes carry different weights for an arc or diffuse discharge switch.

To investigate this complicated synergism the group adopted the following procedure. Select a candidate gas subject to the requirements listed in the above discussion of filler gas properties. Then choose candidate electrode and insulator materials according to the criteria outlined in the above discussion of solid materials. These choices depend also on the range of switch parameters to be satisfied. A group exercise to illustrate the value of this procedure is presented as Tables I, II, and III. One of the results of this exercise is that some question marks appear in the tables indicating that data on some properties are not available. Note also that the tables consist of relative judgements on each proposed property separately, i.e., no weight is assigned to the properties. This means that figure of merit expressions need to be developed. These tables represent a starting point from which one can propose experiments to obtain a data base to be used for selection of new materials and development of figure of merit expressions.

#### D. Selection Criteria

The lists of desirable properties presented in part C above, can be used to determine the relative merits of candidate gases and gas mixtures, insulator materials, and electrode materials. An example is worked out below in the Tables I through III to illustrate qualitatively the nature of the problem and the many trade-offs involved. Tables IV and V are self explanatory.

Table I  
Selection Procedure for Gases

	initial shots	repetitive operation	Dielectric Strength	High Conductivity	Recovery Characteristics	Dissociation Products	Deleterious Effects	Fast Breakdown to Arc	Cost
85% / 15% Ar/Freon	++	+	+	+	+	+	-	?	+
SF <sub>6</sub>	++	++	o	+	-	-	-	?	-

++ = very good

+ = good

o = satisfactory

- = unsat. factor

Table II  
Selection Procedure for Electrode Material  
(85/15 Ar/Freon atmosphere assumed)

	<i>High Thermal and Electrical Conductivity</i>	<i>Erosion</i>	<i>Mechanical Properties</i>	<i>Ejecta</i>	<i>Metallurgy</i>	<i>Compatibility</i>
		<i>Rate</i>	<i>Uniformity</i>			
Graphite	o	o	+	-	+	++
Stainless Steel (304)	+	+	?	++	-	o

++ = very good

+ = good

o = satisfactory

- = unsatisfactory

Table III  
Selection Procedure for Insulators  
(85/15 Ar/Freon atmosphere assumed)

		F <sub>2</sub>	UV	Standoff Voltage	Degradation Rate	Mechanical Properties	Thermal Properties	Surface Resistivity	Tracking Characteristics	Compatibility
Lexan		++	-	o	+	--	+	-	-	-
A <sub>2</sub> O <sub>3</sub>		+	++	++	-	++	-	?	++	
Fused Quartz		+	-	-	--	++	-	?	-	

++ = very good

+ = good

o = satisfactory

- = unsatisfactory

-- = very bad

Table IV

Materials Parameters Pertinent  
to the  
Discussion of Electrode Materials

heat of vaporization  
melting point  
surface tension  
temperature coefficient of surface tension  
specific surface free energy  
vapor pressure  
fracture toughness  
thermal shock strength  
thermal conductivity  
electrical conductivity  
brittleness  
sputtering rates  
heat capacity

Table V  
Materials Commonly Used in Spark Gaps

<u>Electrodes</u>	<u>Insulators</u>	<u>Gases</u>
Tungsten	Lucite	Air
Molybdenum	Lexan	N <sub>2</sub>
W-Cu (K-33, Elkonite)	Blue Nylon	Ar
Stainless Steel	Delrin	SF <sub>6</sub>
Graphite	Al <sub>2</sub> O <sub>3</sub>	+ various mixtures of these

Materials which should be tried

Tantalum	Boron Nitride	Freon Mixtures
Ag-Graphite	Si <sub>3</sub> N <sub>4</sub>	WF <sub>6</sub> ?
W-Ag	Macor	Perfluorocarbons

#### E. Conclusions

The following list summarizes the conclusions reached as a result of the group discussion.

1. A better definition of a successful gas, electrode, insulator "system" is needed. One approach would be to study existing successful systems to determine why they work, and what limits there are on the range of parameters of operation.
2. Experiments should be done under "realistic" condition to establish a data base from which extrapolations of successful systems to other parameter ranges can be made.
3. Figure of merit expressions for all three classes of materials are needed. With enough data it might be possible to determine a figure of merit expression for a "system".
4. Data from other applications (for example, circuit breakers) should be used as a guide in choosing material combinations and new materials. Caution is necessary here because the physical conditions can be vastly different.
5. The best procedure for selecting a combination of materials is to choose a filler gas which fits the required switch parameters. Then choose electrode and insulator materials to be compatible with the gas and the switch parameters.
6. Standard experiments should include monitoring all switch parameters (voltage, current, jitter, etc.), plus conditions such as arc temperature, current density, shock wave amplitudes, etc., and pre and post surface analysis of electrodes and insulators.

7. In particular, erosion rates should be correlated with the current density in the arc and the specific heat flux at the electrode surface. The influence of a "memory" leading to preferred arc attachment points is important for repetitive sparks. Surface distortions due to erosion by one spark may lead to a preferred arc root for the following spark, thereby increasing the erosion rate.

#### F. Recommended Research

##### I. Gases

1. Figure 2 shows schematically an experiment suggested by A.H. Guenther to determine the effectiveness of attaching gases in a flowing gas repetitive switch. This experiment could be done in the geometry described by J.H. Kuhlman (Survey of Gas Flow -- etc., Fig. 8 which appears elsewhere in this report). The point is to disrupt the arc channel remnant and simultaneously inject an attaching gas. If the attaching gas can be mixed with the arc remnant quickly enough, the dielectric strength of the down-stream gas can be raised and restrike prevented. This could decrease the gas flow rate considerably. One of the freons is a good candidate for the attaching gas.
2. If the gas is recycled the composition may change due to repeated discharges. Measurements of the changes in composition due to cyclic operation at high temperature are needed for both short time (after one arc) and long time (many cycles) operation to study the decomposition and chemical recombination.

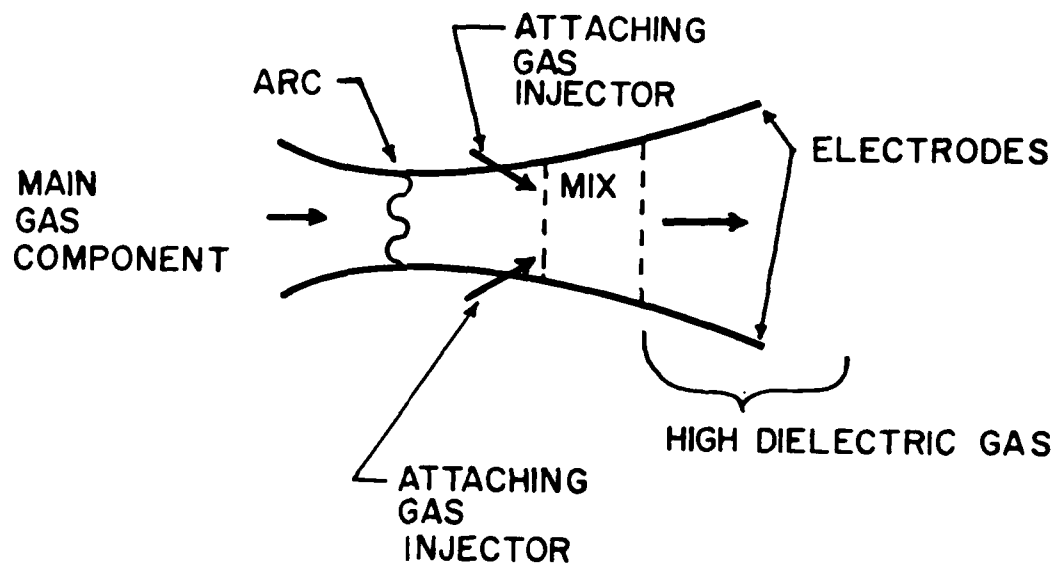


Fig. 2 PROPOSED SYSTEM TO USE GAS MIXTURE TO BEST  
ADVANTAGE

3. Other experiments are outlined in the report of the Tamarron Workshop on Diffuse Discharge Opening Switches (1982) [1] but to apply to repetitive arcs they must be done at high temperatures.

## II. Electrodes

1. The erosion rate and the mechanisms producing erosion appear to be poorly understood. Experiments under varied conditions are needed to correlate material properties with erosion rates and switch parameters. The erosion rate should be measured as a function of the usual switch parameters such as  $V$ ,  $I(t)$ , charge transferred, etc. plus gas flow rate and arc current density. In addition, quantities that pertain specifically to the electrodes should be measured or characterized. These include heat flux on the electrode surface, surface roughness, surface and bulk contaminants, and the mechanical properties of the electrode material at the operating temperature.
2. A characterization of the ejecta from the electrode is needed in order to study erosion mechanisms and insulator damage.
3. New materials (for example, Cermets) should be surveyed.

## III. Insulators

The properties of polymers, ceramics, and other insulators have not been adequately studied under the conditions existing in a repetitive spark gap. Lack of understanding of the synergistic effects presents the greatest problem. One approach is to monitor standoff voltage and spark gap performance versus number of shots for various insulators and then analyze the insulators for surface and bulk changes. Quantities of interest include the outgassing rate and optical transmission of the insulator, as a function of the radiation loading on the insulator.

## References

1. ARO Workshop on Diffuse Discharge Opening Switches, Tamarron, Colorado, January 13-15, 1982. (K. Schoenbach and M. Kristiansen, Texas Tech University, Editors).
2. "UF<sub>6</sub> Plasma Chemistry Reconstitution Experiments Using High Temperature Fluorine", W.C. Roman, presented at the 88th National Meeting of the AIChE, session 35, Philadelphia, PA, June 8-12, 1980.
3. "Gases for Possible Use in Diffuse-Discharge Switches", L.G. Christophorou, S.R. Hunter, J.G. Carter, and R.A. Mathis, *Appl. Lett.* 41, 147 (1982).
4. "Electrode Erosion in High Power Spark Gaps", A.L. Donaldson, R. Ness, M.O. Hagler, and M. Kristiansen, Proceeding of the Fifteenth Power Modulator Symposium, Baltimore, MD, p. 81, June 1982.
5. These three papers give erosion models:

V.E. II'in and S.V. Lebedev, "Destruction of Electrodes by Electric Discharges of High Current Density," *Sov. Phys. Tech. Phys.*, 7, 717 (1963).

E.W. Gray and J.R. Pharney, "Electrode Erosion by Particle Ejection in Low-Current Arcs," *J. of Appl. Phys.*, 45, 667 (1974).

G.S. Belkin and V. Ya. Kiselev, "Effect of the Medium on the Electrical Erosion Electrodes at High Currents," *Sov. Phys. Tech. Phys.* 23, 24 (1978).
6. Two papers giving results on brass are:

J.E. Gruber and R. Suess, "Investigations of the Erosion Phenomenon in High Current, High Pressure Gas Discharges," Max Planck Inst. fur Plasmaphysik, Garching bei Munchen, IPP 4/72, (Dec. 1969).

B. Carder, "Gas Spark Gap Electrode Heating and Erosion," Physics International Report, PIIR 12-74, (Dec. 1974).
7. "Increase in the Optical Damage Threshold of Polymethyl Methacrylate", M.V. Zakharova and N.P. Novikov, *Sov. Phys. Tech. Phys.*, 49, (1979).
8. "The Effect of Mn/Ti Surface Treatment on Voltage-Holdoff Performance of Alumina Insulators in Vacuum", H.C. Miller and E.J. Furno, *J.A.P.*, 49, 5416, (1978).

ELECTRICAL CHARACTERISTICS AND  
BREAKDOWN PROCESSES

J.M. Proud - GTE Laboratories  
R. Gripshover - Naval Surface Weapons Center  
(Co-Chairmen)

INTRODUCTION

This group very promptly interpreted its mission to be somewhat broader than its title implied. The strong consensus of the group was that diffuse discharge switches should be considered within the meaning of "spark gap," and, in fact, much of the attention of the group was drawn toward diffuse discharges. While considered with less emphasis, arc-type switches were evaluated with a focus on recovery solutions other than those involving gas flow for complete removal of arc residues.

The major objectives of the group were as follows:

- Identify fundamental limits and solution opportunities in fast recovery gaseous medium switches including arc and diffuse discharges.
- Note the capabilities and limits of competitive technology such as magnetic and low pressure switches.
- Define promising avenues for research and development with focus on rapid plasma switch recovery.

All of the participants in this group are to be congratulated for their diligent and highly interactive contributions. Most of this report is a com-

pilation of individual written contributions prepared at the conclusion of the Workshop. Authorship is noted as appropriate.

#### METHODOLOGY

##### Overview

The rationale for inclusion of diffuse discharges within the scope of this group's deliberations is based on the potential for minimal damage to the electrodes and gas medium in diffuse vs arc discharges. Thus, under conditions wherein the molecular nature of the switch medium can be preserved with minimal electrode contamination there may be opportunities for sophisticated and heretofore unstudied solution pathways to fast recovery, perhaps greatly exceeding the limits of recovery rate in gas blown arcs. At the same time, it is recognized that diffuse switch technology does not offer much competition, at present, to the low impedance, low loss properties of arc discharge spark gap.

Moreover, most of the available data base from which diffuse discharge switch studies may draw lies in diffuse laser discharge technology where requirements are often opposite to those of a repetitive switch. The risk is therefore substantial in pursuing a solution in diffuse discharges, but the potential payoff may offset this risk.

The approach in the following is to note the broad parameter range within which the needs for repetitive switching exist and to develop a general analysis of the switch function applicable to both arc and diffuse switch design. Subsequently, solution approaches involving both switch types are identified. Filamentation, electron transport and acoustic phenomena in diffuse discharges are then addressed. Finally, the major conclusions and recommendations are cited as developed by the group.

General Parameter Space - W. C. Nunnally

The parameter space for repetitive, high power spark gap applications is generally bounded as in Table A.

Table A

## Repetitive, High Power Spark Gap Parameter Ranges

<u>Parameter</u>	<u>Range</u>	<u>Unit</u>
Voltage	10's - 100's	kV
Current	10's - 100's	kA
Pulse Length	100's - 1000's	ns
Current Rise Time	10 - 100	ns
Rate of Current Rise	$10^{12} - 10^{13}$	A/s
Jitter	1 - 20	ns
Energy per Pulse	1 - 100	kJ
Pulse Repetition Rate	$10 - 10^4$	Hz
Recovery Time	$10^{-4} - 10^{-1}$	s
Inductance	5 - 500	nH
Average Power	0.1 - 10	MW
Peak Power	$10^9 - 10^{12}$	W

The very wide range combinations cover a very large, multidimensional volume of parameters space. The outstanding characteristics of Table A include the large peak powers and the large rate of current rise required when the switch is closed. The peak power is the highest at low repetition rates and lowest at the high repetition rates. The peak power requirements are plotted vs repetition rate in Figure 1.

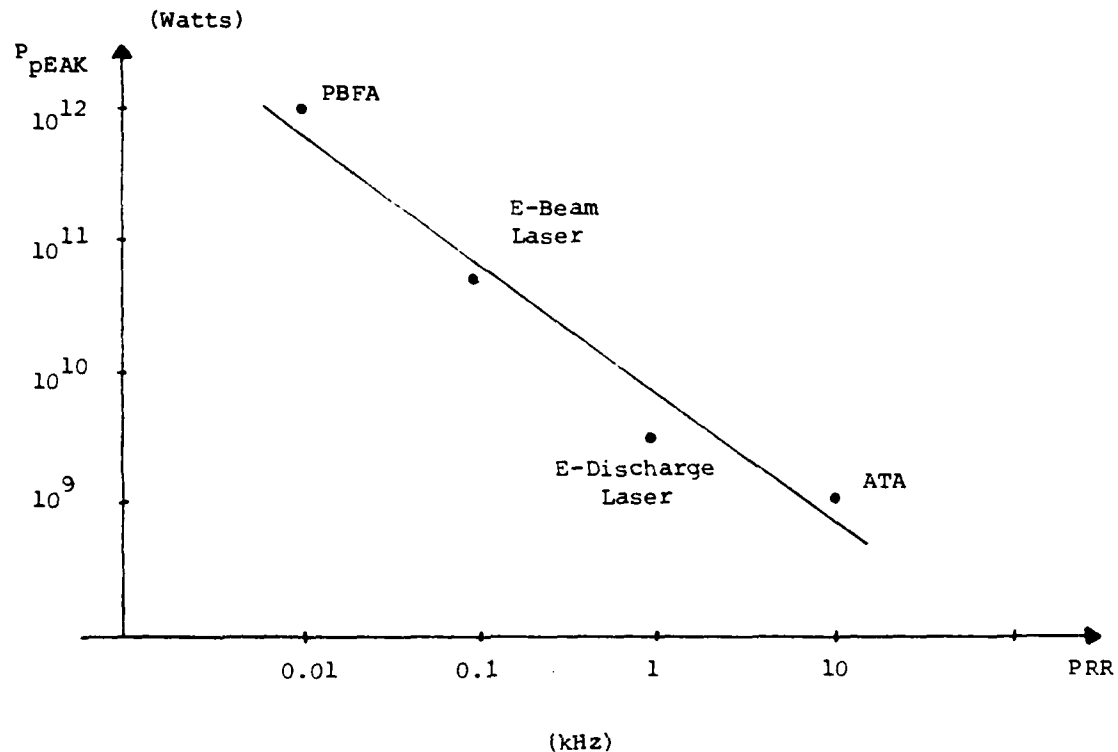


Fig. 1. Peak Power vs Pulse Repetition Rate

The approximate linear scaling and decrease of peak power with increased pulse repetition rate indicates the problem of repetitive pulse repetition rate operation of spark gap switches. Several applications have parameters in common. The highest peak power and the highest repetition rate system both have common electrical pulse lengths on the order of 100 ns. In addition, a rate of current rise of  $10^{12}$  A/sec is a general specification for nearly all applications.

## FUNDAMENTALS AND BACKGROUND

General Switch Analysis - D. Fenneman

Switches often appear at several locations along the power conditioning train of pulse power devices, but the most severe strain on switch technology usually falls on the final output switch which connects to the system load. A typical output switch arrangement is shown in Figure 2, placed between a charged pulse forming line (PFL) of impedance  $Z$  and its matched load of resistance  $R_L = Z$ . If, as the pulse power system engineer would wish it, the final output switch were ideal (i.e., of zero length and capable of changing from infinite resistance to zero resistance instantaneously), the load would experience a perfect square pulse of duration twice the electrical length of the PFL and of voltage one-half the charge voltage of the PFL. All the energy stored in the PFL would be delivered to the load. This does not occur in fact because of the finite size of the switch and because of the finite time it takes the switch to change from the very high resistance of the open state to the hopefully very low resistance (but still non-zero) conductive state.

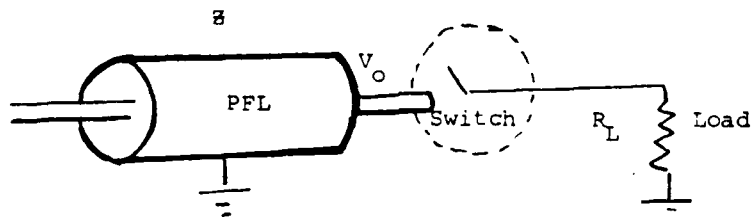


Fig. 2. Pulse Power System

Finite switch size leads to an inductive slowing of the load pulse rise time to times  $= L/R$ . For commonly required rise times of order 10 ns, it is apparent that switch inductance must be held to a few tens of nanohenries. The finite switch resistive fall time also limits the load pulse rise time. During this opening phase, or switch turn on time, the switch resistance is

greater than the load resistance and most of the power is going to the switch. Even when the switch is at its lowest resistance  $R_s \ll R_L$  the switch is consuming energy at a rate:

$$P_s = \frac{R_s}{R_L} P_L$$

Let us ignore inductive effects and compute the energy absorbed in the switch assuming it takes the switch  $t_o$  seconds to turn on completely and that it has resistance  $R_s (<< R_L)$  during the remaining time,  $t_p - t_o$ , of the pulse. We assume further that the voltage and current vary linearly with time during the turn-on period (Figure 3).

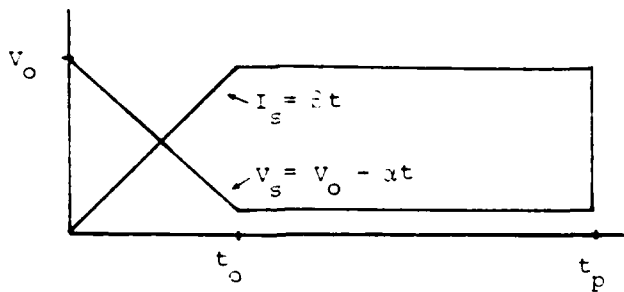


Fig. 3. Switch Turn-On

Note that the variation of switch resistance with time is not linear, but given by:

$$R_s(t) = \frac{V_o - \alpha t}{\beta t} \quad 0 \leq t \leq t_o \quad (1)$$

$$R_s(t) = \text{Constant} \quad t_o < t \leq t_p$$

The energy dumped in the switch during turn-on is:

$$\begin{aligned} \varepsilon_{so} &= \int_0^{t_o} I_s(t) V_s(t) dt \\ \varepsilon_{so} &= \left( \frac{V_o}{2} - \frac{\alpha t_o}{3} \right) \beta t_o^2 \sim \frac{IV_o}{6} t_o \end{aligned} \quad (2)$$

And the energy deposited in the switch during the remainder of the pulse time is:

$$\varepsilon_{ss} \approx \frac{IV_o}{2} \left( \frac{R_s}{R_L} \right) (t_p - t_o) \quad (3)$$

The ratio of these quantities is:

$$\frac{\varepsilon_{so}}{\varepsilon_{ss}} \approx \frac{1}{3} \left( \frac{R_L}{R_s} \right) \frac{t_o}{t_p - t_o} \quad (4)$$

so that more energy is often put into the switch during turn-on than during the steady state conducting phase. It is better perhaps to use an "effective" resistance of the switch:

$$\text{"R}_s\text{"} = \frac{\varepsilon_s}{\varepsilon_L} R_L > R_s \quad (5)$$

Of course, some of the deposited energy serves the useful purpose of producing conducting electrons within the switch.

Considering the switch as a simple volume partially bounded by parallel electrodes of cross-sectional area A, separated by distance d, the switch resistance (assuming uniform conductivity) is:

$$R_s = \frac{d}{\sigma A} \quad (6)$$

where  $\sigma$  is the conductivity of the switch plasma and can be written as:

$$\sigma = n_e e u \quad (7)$$

where  $n_e$  = electron number density ( $\text{cm}^{-3}$ )

$e = 1.6 \times 10^{-19} \text{ C}$  is the electronic charge

$\mu$  = the electron mobility which depends on the switch gas species and density.

and where we have neglected ionic mobility.

Further,  $n_e = N_e/Ad$ , where  $N_e$  is the total number of electrons in the switch volume. The mobility can be expressed as:

$$\mu = \frac{e}{m_e} \langle \tau \rangle_{90} \quad (8)$$

where  $m_e = 9.31 \times 10^{-31} \text{ kg}$  and  $\langle \tau \rangle_{90}$  is the "relaxation time for the current anisotropy." This is a measure of the time it takes collisions with the switch gas molecules to randomize any directed electron current after sudden removal of the directing field.  $\langle \tau \rangle_{90}$  depends on the switch gas density,  $n_o$ , and a gas kinetic quantity  $\langle av \rangle_{90}$  defined as:

$$\langle av \rangle_{90} = \int_0^{\infty} a(v) \cdot v \cdot f_e(v) d^3v \quad (9)$$

where  $a$  is the cross-sectional area for  $90^\circ$  collisions. Thus,  $\langle av \rangle_{90}$  depends not only on the switch gas species but also the distribution of the electrons in velocity space,  $f_e(v)$ . So:

$$\langle \tau \rangle_{90} = \frac{1}{n_o \langle av \rangle_{90}} \quad (10)$$

Expression (6) for a specified switch resistance shows that it is necessary to generate a total number of electrons,  $N_e$  given by:

$$N_e = \frac{d^2}{R_s e \mu} \quad (11)$$

or using (8) and (10)

$$N_e = \frac{m_e}{e^2} \cdot \frac{\langle av \rangle_{90}}{R_s} \cdot n_o d^2 \quad (12)$$

in order to achieve the desired resistance. Actually, it may be worse than this because of electron loss processes, it may be necessary to make a greater number  $N'_e$  given by:

$$N'_e = N_e \cdot \frac{t_p}{\langle \tau \rangle_l} \quad (13)$$

electrons to make sure we have the proper number of electrons during the entire pulse period.  $\langle \tau \rangle_l$  is the mean electron lifetime and is definable in analogy with  $\langle \tau \rangle_{90}$  as:

$$\langle \tau \rangle_l = \frac{1}{n_o \langle av \rangle_l} \quad (14)$$

If it takes  $\varepsilon_i$  joules to make one electron, it will be necessary to deposit at least:

$$\varepsilon = N_e \frac{t_p}{\langle T \rangle_l} \cdot \varepsilon_i \quad (15)$$

joules in the switch gas to manufacture the needed carriers or

$$\varepsilon = \frac{m}{e^2} \frac{\langle av \rangle_{90} \cdot \langle av \rangle_l}{R_s} n_o^2 d^2 \varepsilon_i t_p \quad (16)$$

joules.

There is one more external constraint to be considered: the switch must not suffer electrical breakdown in the open phase. Thus, it is required that the PFL charge voltage  $V_o$  and the switch self-break voltage  $V_B$  obey:

$$V_o \lesssim V_B = K n_o d \quad (17)$$

where  $K$  is a measure of the switch gas species breakdown strength and can have a safety factor included. Using this relation in the above expression for the energy which must be deposited in the switch gas, it is concluded that:

$$\varepsilon = \frac{m}{e^2} \left[ \frac{\varepsilon_i \langle av \rangle_{90} \cdot \langle av \rangle_l}{K} \right] \frac{V_o t_p n_o d}{R_s} \quad (18)$$

joules must be deposited in the gas at a minimum.

At the end of the pulse, the energy deposited in the gas to produce carriers will produce heating of the switch gas. Neglecting radiation losses or heat transfer to the walls, the temperature rise in the gas,  $\Delta T_g$  will be found from:

$$Ad n_o \frac{f}{2} k_b \Delta T_g = \varepsilon \quad (19)$$

where  $k_b = 1.38 \times 10^{-23}$  J/ $^{\circ}$ K, and  $f$  is the effective number of degrees of freedom of the switch gas species among which energy can be equipartitioned. Finally, noting that:

$$\frac{R_s}{R_L} \sim \frac{\varepsilon_s}{\varepsilon_L}$$

a design equation for the gas heating in a switch is obtained.

$$\Delta T_g = \left[ \frac{2 m_e}{k_b e^2} \right] \left[ \frac{\langle av \rangle_{90} \cdot \langle av \rangle_i \cdot \varepsilon_i}{Kf} \right] \frac{It_p}{A} \left( \frac{\varepsilon_L}{\varepsilon_s} \right) \quad (20)$$

This result has some interesting features.  $\Delta T_g$  depends on universal constants, kinetic properties of the switch gas, the pulse power system requirements, and the cross-sectional area of the switch, which is the only switch construct variable left to the switch designer. The density of the switch

gas does not appear in (20). This is because higher density corresponds to higher breakdown strength and also to more heat sink particles; these two considerations canceling the density effect on electron mobility and electron lifetime. Nor does gap length appear, being normalized out by the hold-off constraint:  $V_B = V_o = Kn_o d$ .

The pulse power system requirements make intuitive sense. The more current through the switch, the more the gas heating. The longer the pulse length, the more gas heating; and the higher the ratio of load energy to switch energy (sort of a switch efficiency factor) insisted upon by the pulse power system designer the more energy which must be used to make more conduction electrons, which ends up as more heat. This equation is not intended to be viewed as rigorous, but rather the end result of a systematic design iteration scheme, proceeding as outlined in this section. The gas temperature rise is an important clue to the recovery process in the switch and hence a way of predicting a repetition rate which might be achieved by the switch.

It is instructive to make a quick run through of a numerical example in order to obtain feeling for the magnitudes of the various quantities encountered. For the pulse power system of Figure 2, let  $V_o = 200$  kV,  $R_f = 2$  ohms, and the pulse time be 100 ns. With small switch losses assumed a priori, the load current is  $\approx 50$  kA, the power to the load is 5 GW. In the 100 ns pulse about 500 J are deposited in the load. If the switch turn on time is 10 ns, and the switch resistance during the rest of the pulse is required to be 0.04 ohm, then the ohmic energy which will be deposited in the switch is computed using equation (2) with  $\alpha \approx 2 \times 10^{13}$  Vs<sup>-1</sup> and  $\beta = 5 \times 10^{12}$  As<sup>-1</sup> and also equation (3):

$$\varepsilon_s = \underbrace{17}_{\text{Turn on}} + \underbrace{9}_{\text{Steady State}} = 26 \text{ J}$$

The number of electrons required to produce the desired 0.04 ohm resistance is:

$$N_e \approx 5 \times 10^{18} \text{ electrons}$$

where (6) is used with  $d = 4 \text{ cm}$  and  $\mu = 5 \times 10^2$  and it has been assumed that each electron will live for 100 ns. Before proceeding further, it is quite illuminating to compare the total number of electrons which must be made in the switch to the total number of electrons  $N_T$  transported across the switch to the load:

$$N_T = It_p / e = \frac{5 \times 10^4 \times 10^{-7}}{1.6 \times 10^{-19}} \approx 3 \times 10^{16} \text{ electrons}$$

Thus, we are transporting far fewer electrons than we produce in the switch. Also we are warned against thinking of the switch as a water faucet which is opened and then shut. In addition, the above consideration justifies the neglect of one or two eV per electron required to get the transported charges off the cathode.

To make  $5 \times 10^{18}$  electrons with  $\varepsilon_i \approx 15 \text{ eV}$  per electron will require:

$$\varepsilon_s = \frac{5 \times 10^{18} \times 15}{1.6 \times 10^{-19}} = 12 \text{ J.}$$

This says, even discounting the additional energy introduced into the gap by the switch trigger arrangement, there might be enough energy from ohmic deposition during the opening phase to produce the required carrier density. Indeed, it is well known experimentally that spark gaps will easily conduct high

currents in a self-sustained manner. The problem with high pressure constricted arcs appears in the equation for the temperature rise in the gas of an arc. Areas of  $0.01 \text{ cm}^2$  used in equation (20) will yield huge temperature increases to  $50,000^\circ\text{K}$  and above. True arc temperatures are probably closer to  $10,000^\circ\text{K}$ . This only means that equation (20) is not valid as the process is not constant volume; the radiation loss is considerable and so is damage energy to the electrode. The arc process, which is nature's way, makes a rarified channel in which electrons are more mobile. The point is that arc discharges, because of their small volume get very HOT. The inference is that spark gaps will not recover until the hot gas is physically removed from the switch volume.

Equation (20) does tell us that gas heating can be reduced by increasing the cross-sectional area as in a diffuse discharge switch. Increasing the cross-sectional area from  $0.01 \text{ cm}^2$  to  $1000 \text{ cm}^2$  reduces the temperature rise from tens of thousands degrees kelvin to a few degrees kelvin. Additionally, large electrode area reduces the emission current density requirements from hundreds of thousands of amps per square cm to only  $50 \text{ amps/cm}^2$  which is consistent with nondamaging cold cathode emission.

#### High Pressure Arc Switches - G. Schaefer and P. F. Williams

One of the principal problems encountered in designing rep-rated high pressure arc switches is the removal of the energy deposited in the switch during the on-time. There are two aspects to this problem: first, heat must be removed in order to limit the temperature rise of the switch, and second, the energy in the form of kinetic heat or in other forms will limit the breakdown voltage of the gap, thereby affecting recovery. We were primarily interested in problems relating to the second aspect. These problems may be reduced by 1) decreasing the energy deposited in the arc channel during the switch on-time; 2) speeding the removal of energetic products from the active region of the switch between closures, or 3) designing the switch so that it will be less sensitive to these effects. The second type of solution is com-

monly employed in rep-rated gaps by rapidly flowing fill gas through the active switch region. Above 100 pps, the required gas flow becomes large, and there seems to be a practical limit of about 1 kHz for present high-power switches. Although further work in this area will probably improve this figure, it seems appropriate to investigate other means of improving repetition rate.

In considering these alternative methods, it rapidly became clear that the mechanisms whereby the recovery is influenced by this remanent heat are not well understood. Undoubtedly, a major effect results from the increase in E/N caused by the heating of the arc channel, but other effects may also play an important role. The effect of electrode vapor on voltage recovery is not well understood. It has been shown that vapor from metallic electrodes expands into the gap on a 10-100  $\mu$ s time scale, and this vapor would be expected to reduce the hold-off voltage of the gap due to the low ionization energy of most metals or the possibility of Penning ionization. This effect has not been well documented. The metal atoms may be effectively removed by clustering or by reaction with the fill gas. The effect of metastable electronically or vibrationally excited species on hold-off is also very poorly known. In nitrogen, for example, both the A electronic state ( $^3\Sigma_u^+$ ) and the vibrational states have lifetimes at a pressure of one atmosphere in the order of 1 ms, making them effectively metastable for repetition rates about 1 kHz. Since different techniques will be needed to reduce the effects of each of these mechanisms, the first recommendation of the group is that further research be carried out to characterize better the role of such mechanisms in limiting the voltage recovery of high pressure arc switches.

Several ideas for improving the recovery of these switches were developed by the group. First, it was noted that the arc channel initially cools rapidly due to radiative heat transfer. Since this is a temperature-dependent mechanism, as the channel cools, radiative cooling rapidly becomes less efficient, and is overtaken at some time by convective cooling. It should be possible to design a spark gap to operate under the conditions prevailing at

about the temperature where the fast radiative cooling becomes inefficient. At start-up, the gap would have to be operating at well below self-breakdown voltage, and some means would have to be included to trigger the gap for the first shot(s). The delay and jitter as well as closing time of the first shot(s) would probably be substandard, but for many applications, even those requiring a burst mode, this should not be an important consideration.

It may be possible to partially compensate for the reduction in hold-off voltage at elevated temperatures by tailoring the fill gas composition so that the electron attachment rate is a strongly increasing function of temperature. Many molecular gases with a strongly temperature-dependent attachment cross-section are known. Some of them may not be suitable in this application since the arc will undoubtedly dissociate them, and, depending on other fill gas components, they may not regenerate in the original form, or may do so too slowly to be useful in improving repetition rate. Implementation of this suggestion will clearly not be simple.

For conditions where electrode vapor affects recovery, research on electrode materials and fill gas composition to reduce the effect should be carried out. A properly chosen electrode material could improve gap recovery by either reducing the amount of vapor ejected into the gap, or by reducing the effect on breakdown voltage of the vapor there. For example, the use of refractory materials may reduce the quantity of electrode material evaporated, or the use of a nonmetallic material such as graphite may reduce the effect of electrode vapor on breakdown voltage since it would have a higher ionization potential than most metals. The proper choice of fill gas composition could improve recovery by reacting rapidly with the electrode vapor to produce some relatively inert species. The group recommends that studies of this type be carried out, both at a basic research level, and later, at a development level.

As another possibility to improve the operation conditions of rep-rated spark gaps multichanneling has been discussed. Besides the lower inductance

of a multichannel gap which can be close to the inductance of a diffuse discharge switch, multichanneling has advantages with respect to all processes that are nonlinear with respect to the arc current for a given pulse length and voltage. Among these processes are, for example, electrode erosion and arc temperature. Multichanneling may reduce problems concerning the removal of electrode material and heat transfer. However, reproducible and controlled multichannel triggering still is a major problem in such a gap.

Multichannel triggering and the earlier mentioned requirement for triggering far below self-breakdown were the reasons to discuss triggering more in general. The following subjects and their interactions were considered to be the key issues:

1. trigger source (arc initiation, field distortion, laser);
2. basic trigger mechanism (in the case of laser triggering: evaporation of electrode material, photoionization, inverse bremsstrahlung, photodetachment, etc.);
3. breakdown mechanism;
4. arc formation and arc products depending on triggering;
5. influence of rep-rate on the trigger requirements;
6. triggering far below self-breakdown;
7. trigger access (engineering issue).

It was pointed out that many of the basic processes involved in triggering such as the basic trigger mechanisms and breakdown mechanisms are not yet well understood and need further investigations. For example in UV volume laser triggering in SF<sub>6</sub>, it is not clear whether photoionization or photode-

tachment plays a major part. The specific problems of triggering of rep-rated gaps such as the influence of gas heating and electrode material vapor on the different trigger mechanisms have not yet been investigated at all.

The possibility of triggering far below self-breakdown seems to be a major importance in the operation of triggered rep-rated gaps. Measurements of the hold-off voltage clearly show that the breakdown statistics become worse and the spatial region of self-breakdown is not necessarily the region of the triggered breakdown. As mentioned earlier, the first triggering of a gap designed for operation at higher temperature and the controlled multichannel triggering require that triggering methods capable of triggering breakdown of strongly under-volted gaps be investigated. For example, laser triggering easily closes switches biased at 80% SBV with subnanosecond jitter. Switches biased at less than 50% SBV can be triggered, but with degraded delay and jitter. The trade-offs involving gap voltage, laser power, and delay and jitter are not well known in the strongly under-volted regime and more work should be carried out. Electron beam triggering is also capable of triggering even strongly under-volted gaps with low delay and jitter, and should be investigated for use.

#### Generation of High Pressure Diffuse Discharge - A. E. Hill

High repetition operation imposes that we remove vast quantities of heat from the switch lest it self-destruct. The more diffuse the discharge or the larger the number of spark channels, the less is the power density and the easier it is to remove this heat. Furthermore, we can use geometry to good advantage to lower the inductance when the discharge is diffuse. How then might we achieve this worthy goal? Two classes of problems conspire against us: the first class involve avalanche breakdown processes, followed by ionization and attachment instabilities whose time constants fall within the single pulse period. We may look to the laser community for much of their solution. The second class has to do with the particular requirement for extremely high repetition rates coupled with the logistics problem that it is

impractical to exchange the working fluid on a per-pulse basis. Namely, those stability phenomena whose time constants are long compared to one pulse length can effect succeeding pulses--not just the next pulses but over time periods spanning perhaps ten pulses! But there is good news and bad news--some phenomena (i.e., metastable formation, metastable and ion diffusion, delayed atomic transition UV generation, and certain desirable chemistry) will help to diffuse later discharges while other processes (i.e., reflected acoustic waves) can devastate the distribution of successive plasmas. Still other processes, such as molecular vibrational storage of thermal energy can be either very beneficial or very harmful, depending on how their transition times compare to the inter-pulse time.

Let us begin by discussing the formative process. Here we must set the stage for uniform breakdown by supplying a bed of microscopically, homogeneously distributed free electrons from which to nucleate a large number of spatially distributed micro-avalanches. Furthermore, they must begin almost simultaneously, and develop significant electron number densities on a time scale which excludes the development of local variations in E/n, followed by communication to adjacent volumes at electromagnetic propagation velocities. This growth time depends strongly on the initial electron number density. We note that natural cosmic background ionization ( $n_e = 10^3 - 10^5$ ) will not provide sufficiently low jitter. Therefore, parallel avalanches and "current hogging" can be expected if we rely on only natural background initial ionization. This leads at once to ionization and attachment instabilities and later to thermal instabilities--and in general to the demise of our stable plasma before it ever formed.

Not all types of pre-ionization provide the required initial spatial uniformity, particularly those which invoke electrode boundary effects (as related to fast single pulse stability) or those which have particularly large ionization cross-sections (as related to slower, multiple pulse stability). In these cases a delay is necessary during which time diffusion processes can produce the necessary spatial homogeneity. For lasers, several hundred nano-

seconds delay may be used. However, for switches, the available time is much shorter--perhaps less than 10 ns if we wish to trigger the switch volume uniformly at nearly a single point in time prior to its self-breakdown.

Why not simply allow the discharge to self-form following ionization? Probably, it forms too slowly at an initial  $E/n$  which is limited to that characteristic or perhaps 90% of the open circuit hold-off voltage. If, on the other hand, we apply trigger pulses to some midplane geometry, it is possible to achieve  $E/n$  values exceeding two to four times the breakdown potential in a time interval faster than the avalanche can develop. Since the trigger pulse impedance can be high, we should be able to produce the necessary  $dV/dt$  while limiting energy to a small fraction of that being switched. Additionally, we can tailor the gas composition to have high attachment rates at high  $E/p$  and low attachment rates at low  $E/p$ . This, in combination with hitting the gas with extremely overvolted pulses buys both stability during plasma formation and switch efficiency after the plasma impedance collapses. That is, the plasma collapses to a lower final resistivity.

Finally, electrode shapes must be tailored to avoid localized regions where E-fields are higher than the mid-plane value, since arc breakdown would initiate from such regions before the necessary mid-plane E-field values could be reached.

Figure 4 shows a generalized schematic of a high pressure diffuse switch which provides application of the mechanisms discussed above. Here, an X-ray pre-ionization source is indicated, which represents a logical choice in higher pressure systems. The delay may or may not be necessary, depending on the intensity, spatial distribution, and pulse width of the X-ray pulse.

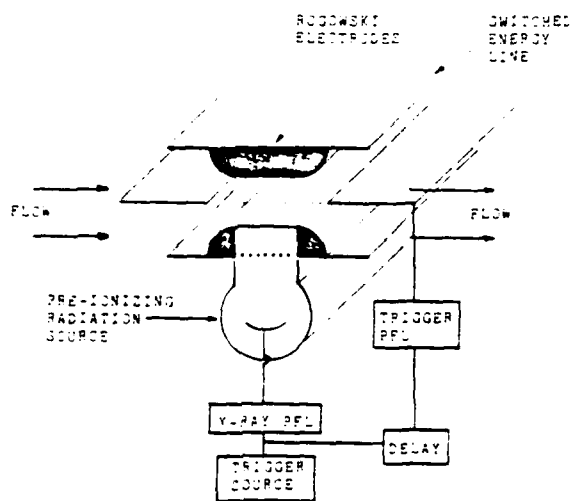


Fig. 4. Generalized high pressure diffuse switch (Courtesy of Plasmatronics, Inc.)

The combination of uniform volume pre-ionization followed by a delayed, very short voltage pulse whose magnitude exceeds the steady state breakdown potential by a factor of three to five has been experimentally shown to produce uniform volume discharges in high pressure electro-negative gases. If then followed by a much lower, but appropriately chosen gap potential, high density currents can be stably conducted for much longer time periods.<sup>1</sup> Figure 5 shows examples of high current short pulse (100 ns range), diffuse plasmas which have been pre-ionized with an electron beam. Atmospheric pressure plasmas have also been stabilized for much longer time periods ( $> 2\mu s$ ) at lower current densities with photo pre-ionization. These experiments were slanted toward loading large amounts of energy into the plasma for laser pump applications. Although we wish to minimize this energy deposition in switches, the physics of controlling the plasma remains the same for both cases. We simply change the gas properties to minimize the required sustaining voltage instead of maximizing it.

This discussion was directed primarily toward the goal of achieving large volume, high pressure diffuse switch operation. However, the same discussion also would apply to a distributed, multi-channel spark gap device. Only the electrode and trigger geometry would change. The latter choice would be favored only if means to lower the sustaining potential of a high pressure diffuse switch cannot be found or, if the needed pulse length exceeds the high pressure plasma stable period in its diffuse, low voltage sustaining state.

#### Filamentation in Diffuse Discharge Switches - E. E. Kunhardt

Presently, the pressurized (triggered or untriggered) spark gap is heavily used as the switch in fast, high power switching operations. When a high voltage is applied to a spark gap filled with a gas at a few mm pressure, the transition from insulating gas to a highly conducting arc may be divided into three phases as the voltage falls and the current rises. These phases

---

<sup>1</sup> A. E. Hill, Appl. Phys. Lett. 22, 670 (1973).

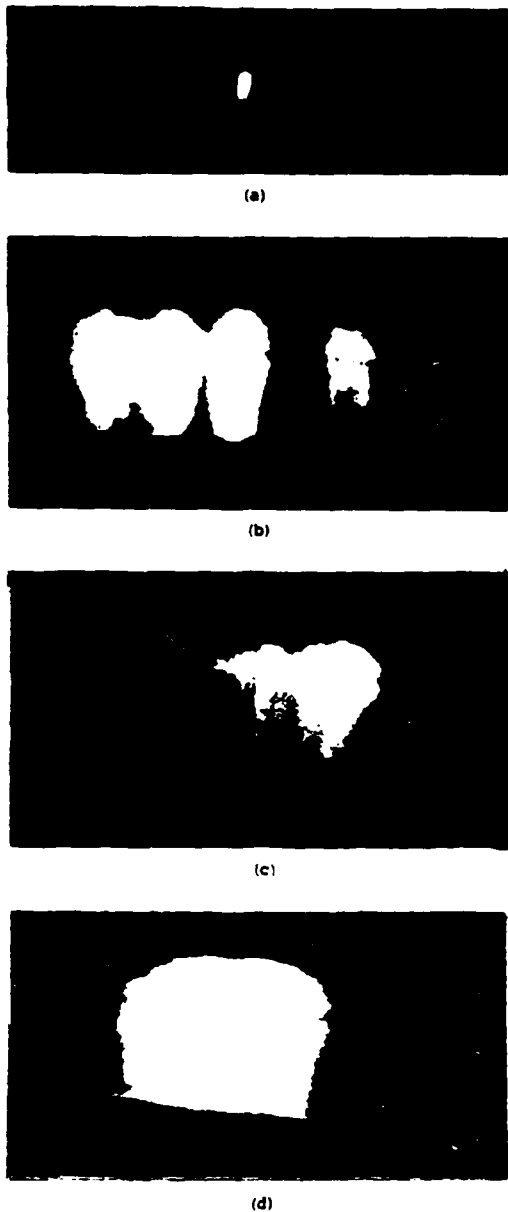


**Fig. 5.** Various stages of diffuse plasma formation at high pressures by means of electron beam pre-ionization in combination with over-volted avalanche techniques. Main current pulse duration is between 50 and 100 nanoseconds, all cases. (a) Single spark breakdown occurs when pre-ionization is deleted. Conditions: 25KV across 1cm gap; 15% SF<sub>6</sub> in Helium at 1 atmosphere total pressure. (b) Multiple channel breakdown occurs due to insufficient overvoltage initiation. Conditions: 20KV across 1cm gap; 15% SF<sub>6</sub> in Helium at 1 atmosphere total pressure;  $4 \times 10^{10}$  electrons/cm<sup>2</sup> pre-ionization. (c) Diffuse breakdown which is filamented by an attachment instability owing to insufficient pre-ionization. Conditions: 25KV across a 1cm gap; 15% SF<sub>6</sub> in Helium at 1 atmosphere total pressure; 5-Beams pre-ionized as in (b); discharge current density = 128 a/cm<sup>2</sup>. (d) Diffuse breakdown properly pre-ionized and over-volted, but pinched to 1/2 normal diameter owing to high current density of 3500 a/cm<sup>2</sup>. Conditions: 20KV across 1/2cm gap; 10% N<sub>2</sub> in Helium at 1 atmosphere total pressure.  $i_{beam} = 1$  a/cm<sup>2</sup> at 250 KV; 200 nsec ionizing 2-beam pulse produced an initial  $5 \times 10^{13}$  electrons/cm<sup>2</sup>. (Courtesy of Plasmateronics, Inc.)

correspond to the Townsend, the glow, and the arc discharges. As the pressure of the gas in the gap is increased, the glow phase becomes very short in duration. In particular, if the applied voltage is much higher than the static breakdown voltage, the glow state disappears and spark breakdown occurs via streamer formation directly to the arc stage.

For the gas pressures at which spark gaps are filled, the phase of operation is the arc. The glow phase is practically absent. The arc phase is characterized by a highly conducting high temperature, narrow channel (about 0.1 cm radius) with relatively high inductance, causing high electrical erosion. The rate of current rise in this phase is smaller than in the glow phase, while  $d^2i/dt^2$  is higher. Since the glow is a volumetric or diffuse discharge, it has a number of properties that make it desirable as a switching phase. Among them, it has large  $di/dt$ , causes low electrode erosion, and offers the possibility of using chemical kinetics to manipulate its properties and for higher rep-rate operations.

Thus, it would be desirable to extend the period of the glow phase at high filling gas pressures, and use it to do the switching. To do this, it is imperative that the causes for the transition, from a diffuse (glow) to a filamentary (arc) discharge, be understood. Note that operation as a hybrid switch (both glow and arc phases) may also be desirable. The problem of what causes this transition as the pressure is increased has been investigated extensively. A number of reviews have been written.<sup>2 3 4</sup> Most of these investigations have been directed to explaining the transition in non-self-sustaining

---

<sup>2</sup> Y.I. Bychkov, Y.D. Korolev, and G.A. Mesyats, Usp. Fiz. Nauk. 126, 451 (1978).

<sup>3</sup> R.A. Haas, Phys. Rev. A 8, 1017 (1973).

<sup>4</sup> E.P. Velikhov, V.D. Pis'mennyi, and A.T. Rakhimov, Usp. Fiz. Nauk. 122, 419 (1977).

discharges, in particular, volumetric discharges externally sustained by an electron beam. It was pointed out<sup>5</sup> that the analysis of this transition is usually carried out within the theory of the stability of spatially uniform plasmas; whereas, experimental studies of the dynamics of the transition,<sup>6 7 8</sup> have shown that, as a rule, the beginning of the filamentation appears near one or both electrodes and propagates across the gap. The regions near the electrodes, for a number of reasons, are associated with large electric fields, which seem to be necessary for the initiation of the filamentation. In general, arcing or filamentation may be considered as developing in two stages: the formation of a small volume with high electron density and the subsequent propagation of this region across the gap.<sup>10</sup>

For a given set of parameters, it is not known precisely which mechanisms initiate the nucleation center leading to filamentation. It is likely that those mechanisms that have been proposed as creating bulk plasma instabilities are responsible for initiating the filamentation near the

---

<sup>5</sup> A.M. Dykhne, and A.P. Napartovich, Sov. Phys. Dokl. 24, 632 (1979).

<sup>6</sup> Y.S. Akishev, I.I. Gorodnicheva, A.I. Zakharchenko, A.P. Napartovich, and V.V. Ponomarenko, Teplofiz. Vys. Temp. 18, 1121 (1980).

<sup>7</sup> Y.D. Korolev, and A.P. Kuzeev, Teplofiz. Vys. Temp. 13, 861 (1975).

<sup>8</sup> Y.S. Akishev, S.V. Pashkin, and N.A. Sokolov, Fiz. Plazmy 4, 858 (1978).

<sup>9</sup> Y. Sakai, J. Appl. Phys. 50, 6471 (1979).

<sup>10</sup> Y.I. Bychkov, Y.D. Korolev, and G.A. Mesyats, Usp. Fiz. Nauk. 126, 451 (1978).

electrodes. There are other mechanisms which are particular to the electrode regions.<sup>11 12</sup>

There have been proposed two general models of bulk instabilities leading to filamentation: the thermal and ionization instabilities.<sup>13 14 15</sup> The thermal instability is due to the fact that strong heating of the gas leads to an increase in E/N, causing further heating and further increases in E/N and a rise in conductivity leading to filamentation. The ionization instability occurs when the Joule heating of the electron gas exceeds the energy lost by electrons in collisions with the background. It should be noted that these two models are "generic" in the sense that there are many different processes that can cause the heating of the gas, and the subsequent increase in E/N, and the increase in ionization. The presence of any one process is dependent on the nature of the gas and the E/N value at which the discharge operates. Examples of processes in molecular gases causing the heating of the gas are: vibrational-vibrational relaxation,<sup>16</sup> rotational-translational energy

---

<sup>11</sup> A.M. Dykhne, and A.P. Napartovich, Sov. Phys. Dokl. 24, 632 (1979).

<sup>12</sup> Y.D. Korolev, G.A. Mesyats and A.P. Kuzeev, Sov. Phys. Dokl. 25, 573 (1980).

<sup>13</sup> Y.I. Bychkov, Y.D. Korolev, and G.A. Mesyats, Usp. Fiz. Nauk. 126, 451 (1978).

<sup>14</sup> R.A. Haas, Phys. Rev. A 8, 1017 (1973).

<sup>15</sup> E.P. Velikhov, V.D. Pis'mennyl, and A.T. Rakhimov, Usp. Fiz. Nauk. 122, 419 (1977).

<sup>16</sup> V.Y. Baranov, F.I. Vysikailo, et. al., Fiz. Plazmy 4, 50 (1978).

transfer,<sup>17</sup> and electronic-electronic collisional quenching and vibrational quenching by atomic species<sup>18</sup> and ionization growth due to multistep ionization,<sup>19</sup> and ionization from collisions of vibrationally excited molecules.<sup>20</sup> The time scales for heating associated with each process depend on the discharge parameters and filling pressure. The times range from hundreds of nanoseconds to milliseconds. A number of these processes may occur simultaneously and for given conditions it may be difficult to determine which process is dominant, if any.

Discharges in gas mixtures, where one of the components is an electron attaching gas such that the attachment coefficient increases in the field, exhibit an attachment instability.<sup>21</sup> This occurs because fluctuations giving an increase in electric field lead to an increase in attachment and a further increase in field, and so on. Oscillations in the megahertz region due to these instabilities have been observed in externally sustained e-beam discharges for low values of E/N ( $E/N < 1.2 \times 10^{-16}$ ) in  $N_2:CO_2$  mixtures. At higher values, these oscillations disappear and only filamentation is observed. The connection, if any, between the attachment stability and the initiation of filamentation is not yet known.

---

<sup>17</sup> W.L. Nighan, Phys. Rev. 2, 1989 (1970).

<sup>18</sup> J.P. Boeuf, and E.E. Kunhardt, 35th Gaseous Electronics Conference, Dallas, TX (1983).

<sup>19</sup> Y.I. Bychkov, Y.D. Korolev, and G.A. Mesyats, Usp. Fiz. Nauk. 126, 451 (1978).

<sup>20</sup> L.S. Rolak, I.A. Sergeev, and D.I. Slovetskii, D.I. Teplo. Vys. Temp. 15, 15 (1977).

<sup>21</sup> D.H. Douglas-Hamilton, and S.A. Mani, J. Appl. Phys. 45, 4406 (1974).

In e-beam sustained diffuse discharges, high field regions near the electrodes may be created due to nonuniform ionization by the beam. In these regions, it is possible that avalanche multiplication may lead to the formation of classical streamers and subsequent filamentation.<sup>22</sup>

Near the electrodes, the initiation of filamentation may be due to instabilities associated micro-protrusions from the electrodes. These may be due to heating of the gas in the intensified field of the micro-protrusion and/or due to plasma flares produced by the explosion of heated micro-protrusion.<sup>23 24 25 26</sup> Instabilities driven by temperature gradients in the cathode layer have also been proposed.<sup>27</sup>

In self-sustaining discharges, as proposed for the switching phase, regions of high fields near the electrodes are inherent and are likely centers for the initiation of filamentation. For these discharges, the time to filamentation is short, tens to hundreds of nanoseconds. The use of external UV radiation to create photoelectrons uniformly over the surface of the

---

<sup>22</sup> G.A. Mesyats, Sov. Tech Phys., Lett. 1, 292 (1975).

<sup>23</sup> Y.I. Eychkov, Y.D. Korolev, and G.A. Mesyats, Usp. Fiz. Nauk. 126, 451 (1978).

<sup>24</sup> Y.D. Korolev, G.A. Mesyats, and A.P. Kuzeev, Sov. Phys. Dokl. 25, 573 (1980).

<sup>25</sup> G.A. Mesyats, Sov. Tech. Phys. Lett. 1, 385 (1975).

<sup>26</sup> G. Ecker, W. Knoll, and O. Zoller, Phys. Fluids 7, 2001 (1964).

<sup>27</sup> R.J. Turner, Appl. Phys. 52, 681 (1981).

cathode<sup>28</sup> <sup>29</sup> and the use of slightly resistive electrodes<sup>30</sup> <sup>31</sup> has allowed the extension of the glow phase to around 0.5  $\mu$ s.

This duration is sufficient for a number of applications. However, a number of other issues need to be investigated to ascertain the feasibility for using glow phase switches. These issues concern the overall switch efficiency and the conjecture that with diffuse discharges it is possible to have lower erosion, higher rep-rate, and avoid the need for flushing the gas in the interelectrode region after each shot.

#### Electron Transport - J. N. Bardsley

In a repetitive diffuse discharge switch, one must provide a gas which can support two phases with respect to electrical conductivity. In the conducting phase, the electron drift velocity must be high, preferably above  $10^6 \text{ cm s}^{-1}$ , with a relatively low potential difference. On the other hand, when the switch is open, the gas must be able to withstand breakdown against a large applied voltage. Furthermore, these desired properties must be maintained through several cycles and should not be lost through gas heating or electrode fragmentation.

This behavior appears unnatural, since one would normally expect high conductivity for large potential difference and lower conductivity for low voltage. It is possible, however, to control the conductivity optically, by

---

<sup>28</sup> J. Koppitz, and Z. Naturforsch, 22a, 1089 (1967).

<sup>29</sup> V.Y. Aleksandrov, D.B. Gurivich, L.V. Kulagina, M.S. Lebedev, and I.V. Podmoshenskii, Sov. Phys. Tech. Phys. 20, 62 (1975).

<sup>30</sup> A.F. Gibson, T.A. Hall, and C.B. Hatch, IEEE, J.Q.E. QE-13, 801 (1977).

<sup>31</sup> P.D. Slade, and A. Serafetinides, IEEE, J.Q.E. QE-14, 321 (1978).

irradiating the discharge with laser light, or to choose a gas in which electron attachment is more efficient for faster electrons. In addition, recent experiments have revealed the existence of several gas mixtures in which the electron drift velocity peaks at a low value of E/N and decreases significantly as the field is increased. This can be achieved most easily with an argon buffer, because of the deep Ramsauer-Townsend minimum in the electron scattering cross-section.

Let us consider a switch with an electrode separation of 4 cm, filled with gas at 1000 torr. To withstand a potential of 200 kV during the open state, the critical value of E/N, at which breakdown occurs, must exceed 150 Td (or  $E/p > 50 \text{ V/torr cm}$ ). During the conducting state the potential difference must be much lower if significant losses are to be avoided. A potential of 2 kV, leading to an E/N of 1.5 Td, might be satisfactory.

A full discussion of the relative merits of different gas mixtures would be inappropriate here. Instead we will cite some typical values of properties of gases which seem to be attractive candidates. Efficient conduction at low field strengths can be achieved by using fluorocarbons such as  $\text{CF}_4$ ,  $\text{C}_2\text{F}_6$  or  $\text{C}_3\text{F}_8$ . A mixture of 5-20% of one of these gases in Ar leads to an electron drift velocity which peaks above  $1 \times 10^7 \text{ cm s}^{-1}$  at low values of E/N. In such mixtures, current densities of  $50 \text{ A/cm}^2$  can be achieved with electron densities of  $3 \times 10^{13} \text{ cm}^{-3}$ , which require ionization fractions of only  $10^{-6}$ . Such low ionization densities permit the switch to be driven at relatively low power levels, thus reducing the problems of gas heating in repetitive switches.

The fluorocarbons also have desirable attachment properties. For example, in  $\text{C}_3\text{F}_8$  the attachment rate is around  $10^{-12} \text{ cm}^3 \text{ s}^{-1}$  for energies below 0.4 eV but rises to  $10^{-19} \text{ cm}^3 \text{ s}^{-1}$ . The critical value of E/N, at which self-breakdown occurs is over 300 Td for pure  $\text{C}_3\text{F}_8$  and approximately 150 Td for a mixture of 30%  $\text{C}_3\text{F}_8$  in Ar.

It seems that by doubling the pressure or electrode spacing specified above, one might be able to design an acceptable switch using a mixture of 10-15%  $C_3F_8$  and 85-90% Ar. However, more basic data must be obtained before one can predict whether such a mixture could sustain many cycles without serious degradation. One must study the subsequent reactions of the negative ions that are formed during each open phase. The effects of gas heating and electrode fragmentation upon the electron transport properties must be clarified. The pressure dependence of the transport coefficients must be explored further. Carbon deposition upon the electrodes should be minimized, perhaps through the addition of carbon inhibitors such as  $SF_6$ . The presence of significant amounts of  $SF_6$  would increase the hold-off voltage, but would reduce the conductivity during the closed state of the switch.

Acoustic Waves and Flow Interactions in High Repetition Rate Plasma Switches -  
A. E. Hill

All plasma switches undergo sudden changes in temperature which produce shock waves. These shocks eventually degenerate into sound waves of  $\approx 190$  DB intensity, and carry up to 40% of the entire waste energy deposited in the gap. The resulting disturbance can initially modulate the mean density value by  $\pm 50\%$ ! If we allow these waves to arbitrarily bounce around inside of the device, they will not die out in a 100  $\mu s$  inter-pulse period, to the point of not affecting the next pulse. Furthermore, acoustically resonant cavity modes will develop which distribute complex but reproducible standing waves over the surface of the electrodes. In turn, the spatially modulated  $E/n$  will affect initial breakdown homogeneity and quickly drive a variety of ionization, attachment and thermal instabilities.

Although high velocity gas flow can help to sweep out acoustic disturbances, it should also be noted that further complications result from this flow. If the flow is subsonic and lies in the compressible range, Rayleigh heating effects will enhance and spatially grade the magnitude of the density disturbances. If the flow is supersonic, things get much better because:

a) the magnitude of the Rayleigh heating density interaction is much lower; b) the sign of the density change is opposite which tends to promote stability in a negative feedback fashion; and c) acoustic waves, once swept out cannot be reflected back into the gap against the supersonic flowstream. However, it is not likely we can count on the luxury of using supersonic flow for many applications, and therefore, we should plan on directing the waves out of the gap region and absorbing them. Very sophisticated acoustic design may be required.

#### CONCLUSIONS AND RECOMMENDATIONS

The group considerations of diffuse discharge switching highlights this area as an attractive direction for further research and development. While problem areas have been identified, no fundamental limits have been defined quantitatively. However, laser discharge experience suggests that the diffuse nature of a discharge cannot be sustained much beyond  $10^{-6}$  sec. If the diffuse phase duration against instability and filamentation carries over to the low impedance discharge visualized for the switch application, pulse widths may be limited to the above range.

Diffuse discharge switching, if feasible, yields relatively small perturbation of the gas and little electrode vaporization compared to effects noted in arc discharges. This opens up the possibility to utilize subtle (compared to gas flow) gaseous electronic processes such as those associated with Ramsauer minima in electron scattering cross-section. Thus, for example, gases may be found with abnormally high conductivity at low values of E/N to militate against the generally resistive nature of high pressure diffuse discharges. Similarly, gases exhibiting attachment rates which increase with E/N will also be in demand for diffuse discharges in order to achieve high critical values of E/N. Fluorocarbons have been identified already which possess both of the desired features. Research in this area is strongly recommended.

Underlining the above need, it was noted above that arc switches, designed to work at elevated temperature, might benefit from molecular gases whose attachment rate increased with temperature.

An area of critical concern is related to filamentation by any of several processes in diffuse discharges. Theoretical modeling and experimentation should be brought to bear on this question, particularly in regard to its duration. Some insights may be gained from the laser experience, although our requirements are divergent with respect to discharge impedance (energy absorption or dissipation) and degree of "diffuseness" required. Indeed, a middle ground might be found which advantageously compromises on multi-channeling or multi-filamentation. The latter might yield rapid recovery of dielectric strength while minimizing the energy density dissipated in the gas or at the electrode surface.

Arc discharges with multichanneling as well as diffuse discharges have numerous common problems to be addressed which are related to discharge initiation. These encompass both pre-ionization and triggering questions. The value in developing a better physical understanding of these features lies in its wide-based need and applicability.

APPENDICES

## APPENDIX A

SUMMARY OF THE CAPABILITIES OF  
REPETITIVE SPARK GAP SWITCHES

I. Smith, T. Burkes, A. Guenther,  
M. Kristiansen, G. Lauer, and W. Portnoy

1. Introduction:

We provide a brief summary and overview of the state-of-the-art of repetitive, high-pressure spark gap switches, their limitations, and the types of application in which their development will continue to be important, in comparison with other switch candidates.

We begin in Section 2 by broadly characterizing the capabilities of the high-pressure spark gap switch and those of other general types of switches used in repetitive pulse power systems; namely, low-pressure switches, magnetic switches, and solid-state, semiconductor switches. The intention here is to show where spark gaps fit into the general switching scheme and what operating parameter space they best fulfill. This assessment

was partly prompted by recent advances in magnetic switches, which can now perform fast, high-voltage switching functions previously possible only with spark gaps. This development is illustrated in the Appendix, which summarizes how magnetic switches are used to satisfy the ATA switch requirements (250 kV, 50 kA, 60 ns, 10 kpps, 10 pulse burst, a few pps average).

Section 3 illustrates the state-of-the-art of spark gaps by giving specific examples of the most powerful switches operating at various repetition rates. It also summarizes what appear to be the general limitations of spark gaps, as indicated by the examples, and introduces the general physical processes that are thought to give rise to these limitations.

Section 4 gives some general concluding thoughts.

## 2. A General Comparison of Repetitive Switches

The four main classes of switches that are important in high repetition rate, pulsed power applications are high-pressure spark gaps, low-pressure switches (thyatrons and low-pressure spark gaps), solid-state switches (semiconductors), and magnetic switches (saturable reactors). Here we illustrate the capabilities and disadvantages of each and show how these lead to the specific important roles each typically may play in future power systems.

Spark gap characteristics of import are listed in Table 1. Those capabilities that make spark gaps particularly useful are at the top of the list. The numbers refer to capabilities demonstrated in repetitive operation; spark gaps were mainly developed originally for single-pulse or low-repetition rate applications, and these low duty cycle switches have achieved even higher ratings (e.g., 6 MV, several MA). More recent, repetitive applications or tests, have not always pushed the parameters to their limits. Below the broken line in Table 1 are the disadvantages or more stringent limitations of spark gaps, principally repetition rate and lifetime. Note that Table 1 refers to the properties of single spark gaps. Operation of gaps in parallel or multichannel gaps might improve total current, current rise, and life characteristics but has not as yet been attempted to any significant degree, at least not near the limits of the repetition rate.

Table 1

High Voltage ( $> 1$  MV, scalable)

Current (~ 100 kA)

High  $di/dt$  (a few  $\times 10^{12}$  A/s)

Fast (~ 10 ns), low jitter (~ 1 ns) triggering

Cheap, easy to custom build

Modest auxilliary needs allow use in Marx  
generators

Limited repetition rate (up to a few kpps or less, depending on voltage and energy)

Limited life ( $\sim 10^5$  Coulombs);

### Maintenance needed

Need high gas flow for high repetition rate

Table 2 characterizes magnetic switches in the same format as Table 1. A magnetic switch is a ferromagnetic core inductor that is unsaturated during charge, and therefore has a large inductance; saturation brings a rapid change to low inductance. The switch is essentially self-closing when the  $\int V dt$  reaches the value for saturation; it cannot be command triggered, and the operating range is limited. Because the relative inductance change is also limited, the switch charging time can be no more than about ten times the output pulse duration, so that if a short output pulse is needed together with slow charging, several stages of time compression may be needed, each with its own switch and a capacitor that stores all the energy; this adds to the size and weight.

The repetition rate is limited only by the time needed to remagnetize the core between pulses; this may typically be done with up to one tenth the charging voltage, and thus requires a time of about ten charging pulse durations, since the  $\int V dt$  for reset is of the same magnitude but opposite sign as for the pulse charge. The  $di/dt$  may be arbitrarily increased by using a wider switch core, and lifetime has been described as essentially infinite, at least if electrical stresses can be kept below breakdown or corona levels. Very high power magnetic switching is a new and a rapidly developing technology and MV switching has recently been demonstrated at Sandia National Laboratories.

Table 2

## CHARACTERISTICS OF MAGNETIC SWITCHES

High repetition rates ( $\sim 10^{-2}$ /pulse duration)

High  $di/dt$  (a few  $\times 10^{12}$  A/s per meter of core)

Very long life

-----

Not triggerable

Limited operating range

Power gain  $\leq 10$ ; needs staging

Heavy

Table 3 summarizes the characteristics of low pressure switches such as hot cathode thyratrons and the low pressure spark gap recently developed at LLNL (see Appendix). These use diffuse discharges, and have long life because the electrode heating is greatly reduced, at least if the current and  $di/dt$  are kept below limits that lead to arcing. Their rapid recovery (deionization) after each pulse allows repetition rates of more than 10 kpps. Thyratrons were developed specifically for repetitive operation, and their manufacturing technology is mature; however, it is specialized, and complicated research is needed to advance the state-or-the-art. Voltage is limited to a few hundred kV, but more usually less than 100 kV.

Solid state switches are little used at present for very high peak power, but SCR's might be used in place of low pressure switches as the first switch in a magnetic modulator. In the future, however, silicon semiconductor switches may be developed with high peak power and  $di/dt$  capabilities, e.g. photo-conductive and avalanche devices. There are essentially two types of construction; intrinsic material switched by applying photons of energy greater than the band gap and four layer devices utilizing either avalanche processes or photons for discharge control. In the 4-layer construction, 7 kV/chip has been demonstrated with 10 kV/chip thought to be a reasonable extension. Stacking of these devices is required to achieve high voltages. For avalanche devices,  $di/dt$  is probably limited to about  $10^{12}$  A/s with a few times  $10^{11}$  A/s already demonstrated.

Table 3

## CHARACTERISTICS OF LOW PRESSURE SWITCHES

High repetition rate (a few  $\times 10^4$  pps)

### Very long life

Low jitter ( $\leq 1$  ns)

— —

Limited current (~ 10 kA)

Limited  $di/dt$  (a few  $\times 10^{11}$  A/s)

Limited voltage (~100 kV)

Auxiliary needs (heater, pumping) prevent use in Marx generators.

Intrinsic material made conductive by photon irradiation is not obviously limited in voltage capability, with switching of > 100 kV having been demonstrated. The optical energy required to control this switch is greater than that for four-layer devices because of several factors. However, the simplicity, flexibility, etc. for this switch make it a very attractive candidate for high power applications. Table 4 summarizes some general solid state switch characteristics whereas Table 5 gives more specific characteristics.

The characteristics described above and summarized in Tables 1-5 lead to different roles for the four classes of switches. The low pressure and solid state switches (apart from the newly-developing intrinsic silicon and avalanche switches) can generate short pulses only at low voltage and very low energies per pulse; their roles in high energy devices are in providing long pulses, typically tens of microseconds in duration. These pulses may be used directly where the requirement is for a long pulses, typically tens of microseconds in duration, either at relatively low voltage or stepped up to as much as 1-2 MV by a transformer; or they may be used to charge pulse forming networks or transmission lines that are in turn switched by spark gaps or magnetic switches to produce shorter pulses.

Table 4

## General Characteristics of Solid State Switches

High repetition rate ( $> 10^5$  pps)

Very long life

Potential for high voltage (~1 MV (intrinsic))

## High current

Can be easily arrayed due to advanced manufacturing technology

Triggerable with low jitter

#### Potential limitation in $dV/dt$ for avalanche devices

## Insufficient reproducibility

## Thermal management

## Packaging and low impedance connections

Table 5 Characteristics of Solid State Switches

**General:** Very high pulsed power switching applications require arrays of discrete elements. Mismatch between elements of the array must be compensated, resulting in array performance which is degraded from the performance of a single element. However, the inherent reliability of most semiconductor switches make them attractive, and enhanced array performance is possible, in principle at least, with better manufacturing technology and selection of individual elements. All solid state devices require good thermal management for optimum performance; this issue has not been addressed in a pulsed power context.

Comments	Type	Current Density (A/cm <sup>2</sup> )	Blocking Voltage (kV)	Turn-on Time (μ s)	Opening Time (μ s)	Forward Drop (V)
Mature technology; high voltage and current arrays possible	Thyristor LASS	100-300	1.5	50-100	50-100	1-2
Possible problem with turn-off dV/dt	GTO	100	2.5		1-2	2-3
Filamenting current, reliability problem	Avalanche Transistor		Filamentary	0.25	10 <sup>-3</sup>	
Turn-off limited by gate and depletion capacitance	MOSFET	50 10		0.5 1.0	0.1	2-3
Under development	JFET (GaAs)	100		1000	0.1	0.1
Under study to determine scalability	(DI) <sup>2</sup>	500		1.0	0.1	1-10
Scalable, but low gain	Bulk (optically activated)	1000		5.0	10 (Silicon) 10 <sup>-2</sup> (GaAs)	100

Magnetic switches on the other hand can be used to generate pulses of durations down to tens of nanoseconds. They must be driven by an initial switch from one of the other three classes; this may be a low pressure or solid state switch where the voltage is within the range of these switches or can be stepped up by pulse transformers, while spark gaps will be used in the multimegavolt range. Magnetic switches will be preferred over spark gaps when the repetition rate is very high (1 kpps and above), the lifetime must be long, and weight and size are not major considerations.

Spark gaps can also be used to generate pulses of any duration down to tens of nanoseconds. They may be directly dc charged, and can produce very short pulses with few or no additional stages of energy storage and power gain; thus they can lead to simpler, smaller, and lighter circuits than magnetic switches, and will often be preferred for this reason. In the megavolt range and above they are at present the only switch in use. Their disadvantages appear at high repetition rates (where for example gas flow may become inconveniently large) and where long life is required. In Marx generators, which are at present the only way of achieving pulsed voltages in the 10 MV range and above, spark gaps are again the only candidate switch.

### 3.State-of-the-Art of Repetitive Spark Gaps

Table 6 lists the parameter of the most powerful or advanced repetitive spark gaps in the 100 kV range at repetition rates of 100 pps and upwards. The first item in Table 6, the AVCO/PI switch, is a single switch that was tested for 10 seconds at 120 pps; the duration was limited by the power source. The energy per pulse is about 20 kJ. The electrodes of the switch were roughly toroidal, and gas was injected from the outside with a helical motion, leaving along the switch axis through the center of each electrode. The flow rate was 100 SCF/min. The MLI switch was synthetically tested at the equivalent of 3 MW and 250 pps; again a radially inward gas flow as used, this time leaving through only one electrode.

The 250 kV LLNL switch was developed for 1 kpps burst duty in ETA. In this case the electrodes were coaxial, with a nonrotating axial flow of gas moving at 50 m/s through the 1.5 cm electrode gap. The lifetime is about  $10^7$  shots. At a lower voltage (50 kV) it was possible to operate with the same charge transfer in a continuous mode at 1-2 kpps (PI switch for LIS); the electrodes were again toroidal with an inward rotating gas flow. The lifetime is  $\sim 10^8$  shots.

Still higher rates are reported for a 40 kV Soviet switch with rather less energy and charge transfer; 4 kpps continuous operation and in some modes up to 9 kpps.

TABLE 6

## STATE-OF-THE-ART SPARK GAPS AT DIFFERENT REPETITION RATES

1. 100 pps: 125 kV, 20 kJ/pulse, a few  $\mu$ s pulses,  
continuous for 10 sec (AVCO/PI)
2. 250 pps: 100 kV, 10 kJ/pulse, few tens  $\mu$ s pulses,  
continuous for minutes (MLI)
3. 1 kpps: 250 kV, 300 J/pulse, 50 ns pulses,  
10-pulse burst, a few pps average,  
 $10^7$  shot life (LLNL)
4. 2 kpps: 50 kV, 50 J/pulse, 100 ns pulses,  
continuous  $10^8$  shot life (PI)
5. 4-9 kpps: 40 kV, 20 J/pulse, 100 ns - 1  $\mu$ s pulses  
continuous (Baranov, USSR)

There is less experience with repetitive spark gaps in the megavolt range, but Sandia has tested a 1.5 MV switch at 30 pps, 1 kJ/pulse. The electrodes can be described as toroidal or as opposing hemispheres with holes on axis, with gas flowed in through one electrode and out through the other setting up a flow pattern that sweeps over the electrode surfaces.

The state-of-the-art of repetitive spark gaps shows two major limitations, repetition rate and lifetime. The examples show a trend that illustrates that the repetition rate can be increased only at the expense of reducing voltage and energy per pulse. This limitation is thought to arise because hot gas from the arc produced by each shot has a low density and hence low breakdown strength. It must either be removed from the high field region before voltage can be reapplied, or cooled by mixing in cold gas; hence the need for gas flow (without flow, in the standard operating mode\* mixing takes a time of the order 10 ms and repetition rates cannot exceed about 100 pps). The larger the voltage, the larger the electrodes and the gap between them, and the further the gas must be moved; this requires a longer time before re-application of voltage and hence the repetition rate is lower. Also, high energy discharges create more hot gas, so that its removal takes longer.

---

\* Some possible, new methods for operating sealed, gas spark gaps at higher repetition rates are discussed briefly in the working group reports.

Rapid gas flow is thus characteristic of higher repetition rate gaps and the blower supplies needed are often substantial. However, optimum design criteria are not established; different gaps use different types of flow (straight or helical for example) and no systematic comparisons have been made. Nor is the role of pressure well understood; higher pressure means smaller gaps and hence probably reduced flow distances, so that a lower velocity is needed, albeit of a higher pressure, dense gas; but the trade-offs have not been studied. Only recently have the exact nature and paths of breakdowns in a degraded repetitive gap begun to be studied, and much more work is clearly needed along these lines to optimize design and performance and establish real limits.

Gap lifetime is largely set by erosion of the electrodes by the discharges. Each Coulomb passed removes very roughly  $10^{-5}$  to  $10^{-4}$  g of material of specific density 10, or a volume of  $10^{-4}$  to  $10^{-3}$  cm<sup>3</sup>. A typical switch lifetime is usually  $10^5$  Coulombs, with tens of cm<sup>3</sup> of material removed. Provided this material is kept from forming a conducting deposit on the insulator (by gas flow, shielding, or chemical change), the gap life can be prolonged by readjusting the electrodes to keep the spacing constant or by lowering the pressure to keep the breakdown voltage constant (though erosion of the trigger electrode may change its shape and affect triggering).

The above discussion of life and erosion in terms of Coulomb transfer is a simplification, since current, waveform pulse duration and rate, and many other parameters all affect erosion in ways not understood or well characterized. Work is needed to characterize and minimize erosion (e.g. by better choice of materials combination), after which engineering can minimize its effects.

#### 4. Concluding Remarks

Relatively speaking, magnetic switching is "the new kid on the block". We do not know all that may be wrong with magnetic switches yet. Some things are of obvious concern - they are heavy and they are not-triggerable with low jitter. These characteristics may be the 'kiss of death' for some applications. Magnetic switches will, however, probably be used in conjunction with other switches.

Solid state switched look great, probably because we have no real experience with their use in high-power, high rep-rate operation; however, they hold great promise, and we do feel somewhat comfortable with their future, generated by the proven state-of-the-art in manufacturing technology. Developments most likely will be along the lines of arrays or optically triggered, photo-conductive devices, intrinsic or otherwise.

Low-pressure or even vacuum spark gaps, although thought to be good candidates for rep-rate applications, based upon our greater physical understanding of their operation, suffer from limited  $di/dt$  and peak current capability, as well as fairly high jitter.

The high-power capability in thyratron diffuse discharges, in moderately long pulse switching, is limited because of their tendency to transition to an arc. These types of switches are the perennial bridesmaids of the high-power, high-voltage, high rep-rate switch community.

Finally, on the other hand, high-pressure spark gaps suffer from the fact that we have lots of experience and it is not all that good, plus it has the image of simplicity "If I want one, I'll build one." But there are no design data, no acceptable guidelines, save Paschen's Law, no real physical understanding of their operation compared to the other candidates (nobody has paid enough for the necessary basic R & D). Spark gap development has been project or specific-system related. Yet we keep coming back to high pressure spark gaps as the probable choice, if not the work horse, of most of today's high-power, high-voltage, rep-rate applications.

## APPENDIX

Considerations for Choice of Switches for ~10 kpps Repetition  
Rate with a 250 kV, 50 kA Pulse with a Rise Time  $\approx$  20 ns  
(Gene Lauer)

I. Introduction

A pulsed power train for this purpose contains at least two switches. There is a first switch which closes the circuit between a capacitor charged to, e.g., 25 kV and a 10:1 step up transformer. Next there may be one or more stages of pulse sharpening using lumped capacitors and saturating-core inductors. Next, a transmission line is charged. Finally there is a closing switch with 20 ns rise time at the output of the line.

II. Characteristics of Three Types of SwitchesA. High Pressure Spark Gaps

In principle, it would be possible to increase the repetition rate of the ATA high pressure spark gap switches to 10 kpps by blowing the gas at a higher velocity. The size of the required blowers is presently unreasonable; therefore, high pressure spark gaps are not attractive for any of the switches in the pulse train.

### B. Low Pressure Switches

This includes any switch with a pressure of ~ 0.1 torr, e.g. cold cathode, triggered, low pressure switches and hot cathode thyratrons. A low pressure switch is predicted to have a short voltage recovery time because the ionization products have a relatively long mean-free-path through the gas, so that they quickly reach the walls and recombine.

Tests (1) have shown that there is a severe problem when low pressure switches are used at the output of a transmission line to produce a short (~ 20 ns) rise time pulse. The nearly collision-free electrons are accelerated in the E-field between the electrodes to form a magnetically pinched electron beam. Typically one third of the energy originally stored in the line is given to the beam. Spots of mm diameter are vaporized where the beam hits the anode. The anode is damaged and, more important, the voltage recovery time is long and nonreproduceable, shot-to-shot. This may be because chunks of anode material deposit on the cathode with a sufficient temperature for thermionic electron emission.

---

1. E.J. Lauer and D.L. Birx, "Tests of a low Pressure Switch Protect by a Saturating Inductor", UCID 19230, 20 October, 1981.

357

On the other hand, when low pressure switches are tested (1) for the role of the first switch in the pulsed power train (with a rise time of a few microseconds), they work very well. The energy deposited in the switch is typically  $10^{-3}$  of the energy originally stored in the capacitor. There is no damage and the voltage holding recovery time is short, ( $\sim 100 \mu s$  when switching 10 kJ).

### C. Magnetic Switches

Preliminary tests are sufficiently encouraging that it is clear that they can play the role of the final line switch at 10 kpps. More testing is needed, e.g. good voltage regulation is necessary to avoid time jitter. Also, core resetting can be a problem.

## III. Optimized Pulsed Power Train

- 1) The first switch is some form of low pressure switch connecting the first capacitor to the step-up transformer. This is the only gas switch. Solid state switches may also be suitable for this purpose.
- 2) Next comes the step-up transformer.
- 3) This is followed by one or two stages of pulse time compression using lumped capacitors and saturating core inductors.
- 4) Next the transmission line is charged.
- 5) Finally there is a single turn, saturating core, coaxial, magnetic switch at the output of the line.

358  
APPENDIX B

List of Participants

Barry Ballard  
Foreign Technology Div.  
Wright-Patterson AFB  
Dayton, OH 45433  
513/257-3158

Herbert J. Carper  
Dept. Mechanical Engineering  
Texas Tech University  
P.O. Box 4289  
Lubbock, TX 79409  
806/742-3563

J. Norman Bardsley  
Department of Physics  
& Astromony  
University of Pittsburgh  
Pittsburgh, PA 15260  
412/624-4359

Lucas Christophorou  
Oak Ridge National Laboratory  
Building 4500-S, H-158  
P.O. Box X  
Oak Ridge, TN 37830  
615/574-6199

M.A. Biondi  
Department of Physics  
& Astromony  
University of Pittsburgh  
Pittsburgh, PA 15260  
412/624-4354

Robert N. DeWitt  
Code F-12  
Naval Surface Weapons Center  
Dahlgren, VA 22448  
703/663-8026

T.R. Burkes  
T.R. Burkes, Inc.  
P.O. Box 16577  
Lubbock, TX 79490  
806/885-4887

Anthony L. Donaldson  
Dept. Electrical Engineering  
Texas Tech University  
P.O. Box 4439  
Lubbock, TX 79409  
806/742-3507

Malcolm Buttram  
Org. 4253  
Sandia Nation Laboratories  
Albuquerque, NM 87185  
505/844-8659

J.J. Ewing  
Mathematical Sciences N.W., Inc.  
2755 Northup Way  
Bellevue, WA 98004  
206/827-0460

Stanley Byron  
Mathematical Sciences N.W., Inc.  
2755 Northup Way  
Bellevue, WA 98004  
206/827-0460

David Fenneman  
Code F-132  
Naval Surface Weapons Center  
Dahlgren, VA 22448  
703/663-8057

Karl Freytag  
 L-469  
 Lawrence Livermore National Lab.  
 P.O. Box 808  
 Livermore, CA 94550  
 415/422-5418

Lloyd Gordon  
 L-153  
 Lawrence Livermore National Lab  
 P.O. Box 808  
 Livermore, CA 94550  
 415/423-2838

Ron Gripshover  
 F-12  
 Naval Surface Weapons Center  
 Dahlgren, VA 22448  
 703/663-8057

A.H. Guenther  
 AFWL/CA  
 Kirtland AFB, NM 87117  
 505/844-9856

John C. Gustafson  
 Precision Materials Technology  
 GTE Laboratories, Inc.  
 40 Sylvan Road  
 Waltham, MA 02154  
 617/890-8460

Marion O. Hagler  
 Dept. Electrical Engineering  
 Texas Tech University  
 P.O. Box 4439  
 Lubbock, TX 79409  
 806/742 2212

R.B. Hammond  
 2700 Merced Street  
 San Leandro, CA 94577  
 415/357-4610

Lynn L. Hatfield  
 Physics Department  
 Texas Tech University  
 P.O. Box 4180  
 Lubbock, TX 79409  
 806/742-3783

Alan Hill  
 Plasmtronics  
 2460 Alamo S.E.  
 Albuquerque, NM 87106  
 505/843-9430

A.K. Hyder, Jr.  
 Office of the Vice  
 President for Research  
 Auburn University, AL 36849  
 205/826-5313

Bob Junker  
 Office of Naval Research  
 Code 421  
 800 N. Quincy  
 Arlington, VA 22217  
 202/696-4220

M. Kristiansen  
 Dept. Electrical Engineering  
 Texas Tech University  
 P.O. Box 4439  
 Lubbock, Texas 79409  
 806/742-2224

John M. Kuhlman  
Mechanical Engineering  
and Mechanics Dept.  
Old Dominion University  
Norfolk, VA 23508  
804/440-3727

Erich E. Kunhardt  
Electrical Engineering  
& Physics Depts.  
Texas Tech University  
P.O. Box 4439  
Lubbock, TX 79409  
806/742/3545

Gene Lauer  
L-436  
Lawrence Livermore National Lab  
P.O. Box 808  
Livermore, CA 94550  
415/422-7885

Lawrence H. Luessen  
Code F-12  
Naval Surface Weapons Center  
Dahlgren, VA 22448  
703/663-8057

John Marx  
Chemistry Department  
Texas Tech University  
P.O. Box 4260  
Lubbock, TX 79409  
806/742-3091

William M. Moeny,  
Tetra Corporation  
1325 San Mateo S.E.  
Albuquerque, NM 87108  
505/256-3595

Marshall Molen  
Dept. Electrical Engineering  
Old Dominion University  
Norfolk, VA 23508  
804/440-3750

James Mote  
Chemical & Material  
Sciences Div.  
University of Denver  
Denver, CO 80208  
303/753-1964

L.E. Murr  
Oregon Graduate Center  
19600 N.W. Walker Road  
Beaverton, OR 97005  
503/645-1121

William C. Nunnally  
Los Alamos National Lab.  
E 11, MS 429  
Los Alamos, NM 87544  
505/667-1360

Emil Pfender  
University of Minnesota  
242 Mechanical Engineering  
111 Church Street S.E.  
Minneapolis, MN 55455  
612/373-3907

Paul Predecki  
 University of Denver  
 Metallurgy & Materials Bldg.  
 Room 104  
 2450 South Gaylord  
 Denver, CO 80208  
 303/753-2141

Joseph M. Proud, Jr.  
 GTE Laboratories, Inc.  
 40 Sylvan Road  
 Waltham, MA 02154  
 617/890-8460, ext. 2539

Henry Pugh  
 Directorate of Physics  
 Air Force Office  
 of Scientific Research  
 Building 410  
 Room C 225  
 Bolling Air Force Base  
 Washington, D.C. 20332  
 202/767-4906

Gerald J. Rohwein  
 Sandia National Laboratory  
 Org. 4253  
 Albuquerque, NM 87185  
 505/844-6058

Gerhard Schaefer  
 Dept. Electrical Engineering  
 Texas Tech University  
 P.O. Box 4439  
 Lubbock, TX 79409  
 806/742-3501

Karl H. Schoenbach  
 Dept. Electrical Engineering  
 Texas Tech University  
 P.O. Box 4439  
 Lubbock, TX 79409  
 806/742-3595

Ian Smith  
 Pulsed Sciences, Inc.  
 14796 Wicks Blvd.  
 San Leandro, CA 94577  
 416/895-2984

Richard Sojka  
 Maxwell Laboratories  
 8835 Balboa Avenue  
 San Diego, CA 92123  
 619/279-5100, ext. 151

James Thompson  
 College of Engineering  
 University of South Carolina  
 Columbia, S.C. 29208  
 803/777-7304

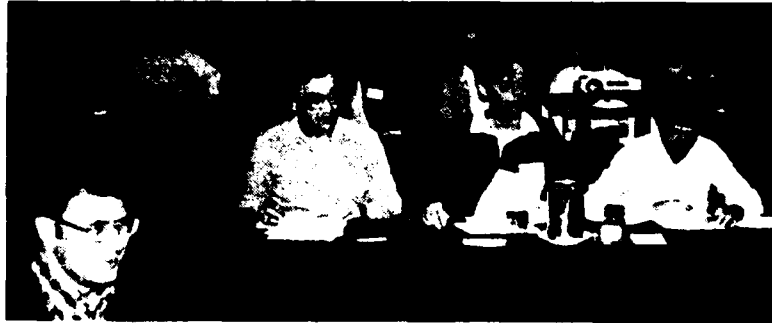
Larry Turner  
 U.S. Army Foreign Science &  
 Technology Center  
 220 7th Street N.E.  
 Charlottesville, VA 22901  
 804/296-5171, ext. 591

P. Frazer Williams  
 Electrical Engineering  
 & Physics Depts.  
 Texas Tech University  
 P.O. Box 4439  
 Lubbock, TX 79409  
 806/742-1399

Bill Wright  
 U.S. Army Electronics Technology  
 & Device Laboratory [ERADCOM]  
 Attn: DELET-PL-  
 Fort Monmouth, NJ 07703  
 201/544-5404



**TAMARRON**  
**JANUARY**  
**1983**





**WORKSHOP  
ON  
REPETITIVE  
SPARK GAP  
OPERATION**



DAT  
FILM